The Role of Transient Receptor Potential Melastatin 2 (TRPM2) Channel in Parkinson's Disease During Oxidative Stress: Interplay Between Calcium and Zinc Ions

Maali Lafi Alahmad

Submitted in accordance with the requirements for the degree of

Doctor of Philosophy

The University of Leeds

School of Biomedical Sciences

Supervisor: Professor Asipu Sivaprasadarao

October, 2022

INTELLECTUAL PROPERTY STATMENT

The candidate confirms that the work submitted is her own and the appropriate credit has been given where reference has been made to the work of others.

Acknowledgement

I want to express my sincere appreciation to my supervisor, Professor Asipu Sivaprasadarao, for his continuous support and guidance. I am deeply indebted to him for the invaluable knowledge that he has imparted. I am grateful to the University of Leeds for the opportunity and experience I have gained. I would like to sincerely thank Kuwait University for funding this research; this endeavour would not have been possible without their financial support. I would also like to extend thanks to the bioimaging facilities department at the University of Leeds, especially Dr Ruth Hughes, for their assistance.

I had the pleasure of working with staff members, colleagues and friends who have supported me both morally and academically. Thank you to Dr Sreenivasan Ponnambalam, Dr Beatrice Filippi, Dr Faheem Shaik, Dr Joanna Mitchell, Dr Barney Roper, Dr William Critchley, Queen Saikia, Dhananjay Jade, Dr Catherine Hodgson, Philippa Malko. I thank them dearly for their time and advice.

My deepest gratitude to my cousin, Dr Shrouq Bouskandre, and my friends, Dr Areej Alzahrani, Dr Fatema Mousawi, Abdulellah Alabdulsalam, Wafa'a Bahbahani, Dr Hala Ahmed, Hala Isbea, Esra Shitaw, Dr Nada Abuarab, Arwa alfailakawi, Dr Basmah Alsayegh, and Najoud Alsayegh, for their continuous friendship, support, advice, and encouragement, and mostly, for the joy that they brought into my journey.

Finally, massive thanks to my family, who have provided me with constant strength and motivation throughout my PhD study here in the UK. Thank you, my beloved parents (Lafi and Maryam), sisters (Mashael, Amthal, Shaikha and Bashayer), nieces (Ghayda'a, Maryam and Lulwa) and nephews (Yousef and Rakan).

Abstract

Parkinson disease (PD) is a progressive neurodegenerative disorder characterized by the selective death of dopaminergic neurons in the brain. Excess production of reactive oxygen species (ROS) and Ca^{2+} dyshomeostasis are strongly implicated in dopaminergic cell death. Genetic and toxin-based studies, as well as post-mortem analysis of the brains of PD patients, indicated a strong association between the dysfunction of mitochondria and lysosomes with PD. How ROS and Ca^{2+} affect these organelles is not fully understood. Previous studies reported that the ROS-sensitive transient receptor potential melastatin 2 (TRPM2) Ca^{2+} channel plays a role in neurotoxin-induced cell death. In this thesis, I hypothesized that TRPM2-mediated Ca^{2+} entry affects the dynamics of ROS and the intracellular organelles to cause neuronal cell death.

I have tested the hypothesis using 1-methyl-4-phenylpyridinium (MPP^+), a potent PD-inducing agent, and the SH-SY5Y human neuroblastoma cell line. Results presented in Chapter 3 show that MPP^+ stimulates ROS production leading to neuronal cell death by stimulating TRPM2 dependent rise in cytosolic Ca^{2+} and the Ca^{2+} dependent NADPH oxidase 2 (NOX2). Inhibition of either NOX2, or the TRPM2 channel, prevented MPP^+ induced ROS production and cell death, indicating potential functional crosstalk between NOX2 and TRPM2. Inhibition of NOX2 alone was able to prevent mitochondrial ROS (mtROS) production, indicating NOX2-derived ROS stimulates mtROS generation. Quenching of mtROS was sufficient to prevent cell death, indicating that NOX2-derived ROS amplify mtROS to cause cell death. Interestingly, Zn^{2+} mediates Ca^{2+} induced mtROS amplification.

In Chapter 4, I have studied the effect of MPP^+ on lysosomes and mitochondria, and asked whether NOX2 and TRPM2 channels play roles. The results showed MPP^+ treatment caused a decline in lysosomal numbers and increased mitochondrial fragmentation. TRPM2 inhibition as well as NOX2 inhibition prevented both these effects. I found Ca^{2+} and Zn^{2+} have distinct roles in organelle dynamics. Ca^{2+} caused loss of lysosomes whereas its effect on

mitochondrial fragmentation is mediated by Zn^{2+} induced recruitment of fission inducing Drp-1 protein to mitochondria. Zn^{2+} caused the mitochondrial effects by inhibiting complex I and III.

Finally, an antibody capable of blocking TRPM2 mediated Ca^{2+} entry was able to rescue the neurotoxin-induced cell biological effects and neuronal cell death (Chapter 5). In conclusion, studies presented in this thesis reveal new insights into the cell biological mechanisms underlying PD-toxin induced neuronal cell death.

Table of Contents

Table of Figures

Table of Tables

List of Abbreviations

°C	Degrees Celsius
µg	Microgram
µl	Microliter
µM	Micromolar
$^1O_2$	Singlet oxygen
2-APB	2-aminoethoxydiphenyl borate
2D	Two-dimensional
3D	Three-dimensional
3-MFA	2-(3-methylphenyl) aminobenzoic acid
ACA	Anthranilic acid
AD	Alzheimer's disease
ADP	Adenosine diphosphate
ADPD	Rare autosomal dominant trait
ADPR	Adenosine diphosphate ribose
AIF	Apoptotic-inducing factor
Apaf-1	Apoptotic protease activating factor 1
APS	Ammonium persulphate
AQP	Aquaporin channel
ARE	Antioxidant response element
ATCC	American Type Culture Collection
ATP	Adenosine triphosphate
ATPase	Adenosine triphosphatase
BAPTA-AM	1,2-bis-(aminophenoxy)-ethane-N,N,N',N'-tetra-acetic acid-acetoxymethyl ester
Bcl-2	B-cell lymphoma 2
BSA	Bovine serum albumin
Ca^{2+}	Calcium ion

cADPR	Cyclic adenosine diphosphate ribose
ChEMBL	European molecular biology laboratory
CI	Mitochondrial complex I
CIC3	Chloride channel-3
CIII	Mitochondrial complex III
CoQ10	CoenzymeQ10
Cryo-EM	Cryo-electron microscopy
CTRL	Control
Cu^{+}	Copper ion
CypD	Cyclophilin D
Cyt *c*	Cytochrome c or Cytochrome complex
DAPI	4′,6-diamidino-2-phenylindole
DAT	Dopamine transporter
dATP	Deoxyadenosine triphosphate
ddH_2O	Double-distilled water
DHE	Dihyroethidium
DIC	Differential interference contrast
DISC	Death-inducible signaling complex
DMEM®	Dulbecco's Modified Eagle Medium
DMSO	Dimethyl sulfoxide
DNA	Deoxyribonucleic acid
Dnm2	Dynamin2
DOPAL	3,4-dihydroxyphenylacetaldehyde
DRG	Dorsal root ganglion
Drp1	Dynamin-related protein 1
DTPA	Diethylenetriaminepentaacetic acid
ECE	Extracellular epitope
EDTA	Ethylenediamine tetraacetic acid
EndG	Endonuclease G

ER	Endoplasmic reticulum
ERK	Extracellular signal-regulated kinase
ETC	Electron transport chain
FAD	Flavin adenine dinucleotide
$FADH_2$	Flavin adenine dinucleotide
FDA	Food and drug administration
Fe^{2+}	Ferrous ion
Fe^{3+}	Ferric ion
FFA	Free fatty acids
FFA	Flufenamic acid
Fis1	Fission protein
GCase	β-glucocerebrosidase
GFP	Green fluorescent protein
GPXs	Glutathione peroxidases
GSH	Glutathione
GSPx	Glutathione peroxidase
GTPase	Guanosine Triphosphatase
H2DCF-DA	2',7'-Dichlorodihydrofluorescein diacetate
H_2O_2	Hydrogen peroxide
HBSS	Hank’s Balanced Salt Solution
HEK cells	Human embryonic kidney cells
HEPES	Hydroxyethyl piperazineethanesulfonic acid
HUVECs	Human umbilical venous cord cells
IMM	Inner mitochondrial membrane
IP_3	Inositol 1,4,5-triphosphate
IP_3R	Inositol 1,4,5-triphosphate receptors
KDa	Kilodaltons
Keap1	Kelch-like ECH-associated protein 1
LAMP-1	Lysosomal-associated membrane protein 1

LAMP-2	Lysosomal-associated membrane protein
LBs	Lewy bodies
LDL	Low density lipoprotein
LMP	Lysosomal membrane permeabilization
mAbs	Monoclonal antibodies
MAMs	Mitochondria-associated membranes
MAO-b	Monoamine oxidase-b
MAPK	Mitogen-activated protein kinase
MCU	Mitochondrial calcium uniporter
mdivi1	Mitochondrial division inhibitor 1
MERCs	Mitochondria-endoplasmic reticulum contacts
MFF	Mitochondrial fission factor
Mfn1	Mitofusin 1
Mfn2	Mitofusin2
MHRs	TRPM-homology regions
MICU1	Mitochondrial Ca^{2+} uptake 1
MICU2	Mitochondrial Ca^{2+} uptake 2
MiD	Mitochondrial dynamics proteins
MitoQ	Mitoquinone mesylate
Mito-TEMPO	(2-(2,2,6,6-Tetramethylpiperidin-1-oxyl-4-ylamino)-2-oxoethyl)triphenylphosphonium chloride
ml	Milliliter
Mn^{2+}	Manganese
MOMP	Mitochondrial outer membrane permeabilization
MPP^{+}	1-methyl-4-phenylpyridinium
MPPP	1-methyl-4-phenyl-4-propionoxy-piperidine
MPRs	Mannose-6-phosphate receptors
mPTP	Mitochondrial permeability transition pore
MPTP	1-methyl-4-phenyl tetrahydropyridine
MRE	Metal response element

MT	Metallothionein
MTF-1	Metal transcription factor 1
mtROS	Mitochondrial reactive oxygen species
NAAD	Nicotinic acid adenine dinucleotide
NAADP	Nicotinic acid adenine dinucleotide phosphate
NAC	N-acetyl cysteine
NaCNBH3	Cyanoborohydride solution
NAD	Nicotinamide-adenine dinucleotide
NADPH	Nicotinamide adenine dinucleotide phosphate
Ni^{2+}	Nickel ion
nM	Nanomolar
NM	Neuromelanin
NMDA	N-methyl-D-aspartate
NMS	Non-motor symptoms
NO	Nitric oxide
NOX	NADPH oxidase
Nrf2	Nuclear factor erythroid 2-related factor 2
NS	Not significant
NUDT9H	Nudix-type motif 9 homology domain
O_2	Oxygen
O_2^-	Superoxide anion
OH^-	Hydroxyl ion
$OH^\bullet$	Hydroxyl radical
OMM	Outer mitochondrial membrane
OPA1	Optic atrophy 1
Opti-MEM®	Opti-Minimal Essential Medium
OXPHOS	Oxidative phosphorylation
Pak	p21-activated kinase
PARG	Poly-ADPR-glycohydrolases

PARP	Poly-ADPR-polymerases
PBS	Phosphate buffered saline
PBS-T	Phosphate buffered saline -Tween
PD	Parkinson’s disease
PFA	Paraformaldehyde
pH	Potential hydrogen
PI	Propidium iodide
PJ34	N-(5,6-Dihydro-6-oxo-2-phenanthridinyl)-2-acetamide hydrochloride
PKC	Protein kinase C
PMCA	Plasma membrane Ca^{2+} activated ATPase
PRXs	Peroxiredoxins
P-value	Probability value
Redox	Oxidation-reduction
RFP	Red fluorescent protein
RIRP	ROS-induced ROS production
RNA	Ribonucleic acid
ROS	Reactive oxygen species
RyR	Ryanodine receptors
S1QEL	Suppressor of complex I site Q electron leak
S3QEL	Suppressor of complex III site Q electron leak
SBS	Standard buffer solution
Scr-siRNA	Scramble siRNA
SDS	Sodium dodecyl sulfate
SDS-PAGE	Sodium dodecyl sulfate – polyacrylamide gel electrophoresis
SEM	Standard error of the mean
SERCA	Sarco/endoplasmic reticulum Ca^{2+} activated ATPase
SH-SY5Y	Human neuroblastoma cell line
siRNA	Small interfering RNA
SNpc	Substantia nigra pars compacta

SOCE	Store-operated Ca^{2+}-entry
SOD1	Superoxide dismutase 1
SOD2	Superoxide dismutase
STIM1	Stromal interaction molecule 1
STIM2	Stromal interaction molecule 2
TCA	Tricarboxylic acid
TEMED	Tetramethylethylenediamine
TEMPO	2,2,6,6-tetramethylpiperidinyl-1-oxyl
TM	Transmembrane
TMRE	Tetramethylrhodamine, ethyl ester
TNFα	Tumor necrosis factor alpha
TPEN	N,N,N’,N’-tetrakis(2-pyridinylmethyl)-1,2-ethanediamine
TRAIL	Tumor necrosis factor-related apoptosis-inducing ligand
TRP	Transient receptor potential
TRPC5	Transient receptor potential canonical 5
TRPM2	Transient receptor potential melastatin 2
VDAC	Voltage-dependent anion channels
VDCC	Voltage dependent Ca^{2+} channels
VSLD	Voltage sensor-like domain
Zip1	Zinc transporter 1
ZIPs	Zrt, irt-related proteins
Zn^{2+}	Zinc ion
Zn-PTO	Zinc pyrithione
Znt	Zn^{2+} transporter
α-Syn	α-Synuclein
ΔpH	Electrochemical proton gradient
ΔΨm	Mitochondrial membrane potential

Chapter 1
Introduction

1.1 Parkinson's disease

1.1.1 Parkinson's disease overview

Parkinson's disease (PD) is the second most common neurodegenerative movement disorder after Alzheimer's disease. PD was originally described by James Parkinson in 1817. It is highly associated with a partial loss of dopaminergic neurons in the brain (Alexander, 2004). The cause of PD is still unclear. However, both genetic and environmental factors are suggested to be involved (Dickson, 2018). Age, heredity, gender, and exposure to exogenous toxins are some of the factors thought to be associated with PD. Although several drugs are available to improve the disease's symptoms, current therapies fail to slow down or stop the progression of dopaminergic neuronal loss.

1.1.2 Epidemiology

It is generally accepted that the prevalence of PD in industrialized countries is around 0.3% of the general population. The disease affects 1% of the population above the age of 60 (de Rijk et al., 1995), and 3% in people aged above 80 years. The mean duration of the disease from diagnosis to death is around 15 years (Katzenschlager et al., 2008). More recent data suggests that the incidence rate of the disease ranges from 8 to 18 per 100,000 persons per year (Lee and Gilbert, 2016).

Age is the major risk factor for PD. However, sex also appears to play a role as it has been noticed that men are about 1.5 times greater risk than women in

developing PD. However, gender-association of the disease remains controversial (Twelves et al., 2003). Furthermore, recent studies support an increased risk of PD in the later years of life that could be attributed, at least in part, to traffic-related air pollution (Lee et al., 2016b). The prevalence of PD is predicted to double by year 2060 (Savica et al., 2018), which entails the need to better understand of the pathophysiology of the disease and to develop new therapeutic strategies.

1.1.3 Symptoms, causes and pathophysiology

PD is characterized by the gradual and selective loss of dopaminergic neurons and the consequent decline in dopamine secretion in the substantia nigra pars compacta (SNpc) (Kinoshita et al., 2015). By the time the patient is diagnosed with PD, up to 60% of dopaminergic neurons are already lost (Balestrino and Schapira, 2020). The symptoms of the disease start gradually. The primary motor symptoms of PD include bradykinesia (slowed movement), tremor (involuntary shaking of certain parts of the body), rigidity (muscle stiffness), and postural instability (balance problem) and difficulty in walking (Moustafa et al., 2016, Rodriguez-Oroz et al., 2009). The decreased dopamine level is the major reason for developing these symptoms. The severity of symptoms increases as the disease progresses over time. Non-motor symptoms (NMS) are also common in PD patients, including sensory abnormalities, sleep disturbances, gastrointestinal dysfunction, bladder dysfunction and fatigue (Pfeiffer, 2016). It is, however, known that NMS can also occur normally in elderly without PD. Studies suggested that 68-88% of normal people will show at least one NMS with aging. However, in PD patients the NMS tends to be more frequent and severe (Pfeiffer, 2016).

The aetiology of PD is still unclear. Most of the PD cases (85-90%) are sporadic and are attributed to the environment, such as industrial pollution and exposure to certain pesticides (e.g., paraquat). The neurotoxin 1-methyl-4-phenyl

tetrahydropyridine (MPTP), a by-product produced during the manufacturing of the synthetic opioid 1-methyl-4-phenyl-4-propionoxy-piperidine (MPPP) (Langston et al., 1983, Ballard et al., 1985), could cause selective destruction of dopaminergic neurons (Kopin, 1987). Exposure to toxic levels of manganese, carbon monoxide and trichloroethylene could also result in a kind of parkinsonism. Also, it has been reported that use of β2-adrenoreceptor antagonists can increase the risk of the disease in contrast to β2-adrenoreceptor agonists (Mittal et al., 2017). On other hand, an inverse association has been reported in users of calcium channel blockers (Gudala et al., 2015) and statins (Bai et al., 2016); these drugs appear to lower the risk of PD.

It is believed that family history is an important risk factor of PD. 5-15% of the PD causes are familial in origin, where the disease is linked to mutations in a number of genes (Balestrino and Schapira, 2020). Examples of these genes including *SNCA*, *PRKN*, *PINK1*, *DJ-1*, *PARK8*, *PARK9* and *GBA* (Balestrino and Schapira, 2020).

Another hallmark pathological feature of PD is the accumulation of misfolded protein known as α-synuclein (α-Syn) found as cytoplasmic inclusions in the brains of affected individuals; these are called Lewy bodies. (Braak et al., 2003). Lewy bodies are composed of a mixture of more than 90 proteins, including PD associated gene products (such as α-Syn, PARKIN, DJ-1, LRRK2 and PINK1), ubiquitin, mitochondria-related protein and autophagy proteins (Wakabayashi et al., 2013). α-synuclein is a soluble protein that is abundantly found in the brain especially concentrated in the presynaptic nerve terminal (Wakabayashi et al., 2013). The normal function of α-synuclein is poorly understood, but a study on Zebrafish suggested a role in the regulation of vertebrate neuronal plasticity (George et al., 1995). It was originally described as a precursor of the non-Aβ component of Alzheimer's disease amyloid (Iwai et al., 1995). α-Synuclein plays a direct role in the pathophysiology of PD, and this had been proven by genetic evidence. PD can be inherited as a rare autosomal dominant trait (ADPD). α-Synuclein is encoded by *SNCA*, a gene mapped to human chromosome 4q21-22. A53T is a mutation identified in α-Synuclein gene in Italian kindred and

unrelated Greek families (Polymeropoulos et al., 1997). Other missense mutations (A30P and E46K) of α-Synuclein gene are also thought to be associated with the development of PD (Krüger et al., 1998, Zarranz et al., 2004). E46K mutation was found in all affected family members and in some asymptomatic individuals, but not in the healthy controls. This mutation (substitution of glutamic acid for lysine) occurs in the conserved area of α-synuclein protein that could severely affect the protein function. The A30P mutation is an alanine to proline exchange at position 30, but how this mutation affects α-synuclein protein function is unknown. However, the mutation is in the highly conserved region of α-synuclein protein where it is thought to be involved in interactions with the membrane cytosolic surface and, therefore, interfere with its binding to synaptic vesicles. It has been suggested that proline substitution affects the secondary structure of the protein and increases its ability to aggregate leading Lewy bodies formation (Krüger et al., 1998).

Abnormal aggregation of α-synuclein results in intermediate toxic oligomeric and fibrillar forms that have detrimental effects on the cell, including impairment of mitochondrial, lysosomal and proteasomal function, and damage to membranes and cytoskeleton. These damages, in turn, impair synaptic function leading to neuronal degeneration (Balestrino and Schapira, 2020). A major target of dysfunctional α-synuclein is the mitochondrion. α-Synuclein-induced effects on mitochondria result in oxidative stress and neuronal cell death. Thus, abnormal forms of α-synuclein play an important role in mitochondrial dysfunction and may contribute to PD pathogenesis.

The basis for selective death of specific neuronal populations in neurodegenerative diseases remains unclear. The SNpc dopamine neurons appear to produce a large amount of ROS due to high metabolic activity and have low levels of antioxidant defences, such as glutathione. Furthermore, they contain high concentrations of dopamine, which is a highly reactive molecule capable of generating ROS through autooxidation (Surmeier et al., 2011). Furthermore, SNpc neurons have high levels of neuromelanin (NM) pigment. NM is a derivative of oxidized catecholamine that reacts with lipids and proteins, and acts as a

reservoir that traps iron, metals, and other toxic substances. Lewy pathology which is a major hallmark of PD is nearly always found in the NM neurons in the SNpc and the loss of NM is seen in all PD patients (Sulzer and Surmeier, 2013). Thus the combination of excess ROS production from high metabolic activity, metabolism of dopamine and neuromelanin, and low antioxidant defences leads to a net increase in ROS levels in these cells making them especially vulnerable to oxidative damage (Carrasco and Werner, 2002).

1.1.4 Prevention and management

To date, PD is considered as an incurable disorder since no treatment has yet been found to either arrest or reverse the progression of the disease. The currently available therapies aim to improve the symptoms of the disease. Most of the treatments aim to restore the levels of dopamine either by enhancing the levels of dopamine in the brain or by reducing its metabolism (Singh et al., 2007). They include Levodopa, which is a precursor of dopamine, and MAO-b (monoamine oxidase-b) inhibitor (e.g., rasagiline, selegine, safinamide), which prevents oxidative degradation of dopamine. Levodopa is converted to dopamine by dopa decarboxylase. It is often administered in combination with Carbidopa. Carbidopa does not cross the blood brain barrier and inhibits dopa decarboxylase in the peripheral tissues, thereby increasing its availability to the brain. It also helps prevent the side effects of Levodopa (nausea and vomiting), resulting from the actions of dopamine in peripheral tissues. However, these therapies failed to modify the progression of neurodegeneration. Other pharmacological drugs include dopamine receptor agonists, and the newly researched neuroprotective agents such as nicotine, melatonin, selenium, Iron-chelators, vitamins (A, C, E), and anti-inflammatory agents. Finally, there are non-pharmacological therapies involving gene therapy, cell transplantation, immunotherapies and surgical interventions which are currently under investigation. (Singh et al., 2007, Balestrino and Schapira, 2020). Recent phase 2 clinical trials, using monoclonal

antibodies targeted against pathologically aggregated form of α -synuclein, which engendered much hope, have unfortunately proven unsuccessful (Whone, 2022).

1.1.5 MPTP as a model of Parkinson's disease

The role of neurotoxins in the aetiology of PD has been of interest for many researchers. 1-methyl-4-phenyl tetrahydropyridine (MPTP) is a potent neurotoxin that selectively damages dopaminergic neurons and has been linked to PD (Langston et al., 1983). MPTP is commonly used as an experimental model of PD because it can induce Parkinsonian syndrome in humans and primates (Jenner, 2003). It is a highly lipophilic molecule and can easily cross the blood-brain barrier. In neuronal cells, MPTP is oxidized to 1-methyl-4-phenylpyridinium (MPP^+) by the enzyme monoamine oxidase b (MAO-b) that is found at high levels in mitochondria, especially in glial cells. MPP^+ is an active metabolite that inhibits the mitochondrial electron transport chain (ETC) by inhibiting the NADH-quinone oxidoreductase (Complex 1), causing an increase in mitochondrial ROS production, thereby affecting many cellular events (Langston et al., 1987). MPP^+ is structurally similar to dopamine and can therefore be readily taken up by cells expressing dopamine transporters (DAT). Dopamine neurons of SNpc express high levels of DAT compared to other cell types and are therefore capable of accumulating toxic levels of MPP^+. In dopamine neurons, MPP^+ is thought to inhibit mitochondrial complexes to increase ROS production and thereby damage these neurons. In support of this, Mazindol, a selective DA-uptake inhibitor, was shown to provide a neuroprotective effect against the MPP^+-induced loss of DA neurons (Javitch and Snyder, 1984, Sanchez-Ramos et al., 1986). Furthermore, MPP^+ generates reactive oxygen species (ROS) when it is reduced to MPP by cytochrome P-450 reductase, generating oxygen radicals (Yoshikawa, 1993). These findings together imply a close association between oxidative stress and MPP^+ toxicity in neuronal cells.

MPP-based studies, thus support a role for mitochondrial dysfunction and the associated oxidative stress in the pathogenesis of sporadic PD.

1.2 Oxidative stress

1.2.1 Roles of ROS: Physiology and pathophysiology

Oxidative stress results from an imbalance between the production of prooxidants and antioxidants (Takahashi et al., 2011). Prooxidants are mainly represented by ROS; when their levels exceed the control by antioxidants, they result in an oxidative stress. ROS are chemical species that are highly reactive and are formed due to partial reduction of oxygen (O_2). The term ROS refer to the oxygen free radicals, including superoxide anion (O_2^-) and hydroxyl radical ($OH^\bullet$), and nonradical oxidants such as hydrogen peroxide (H_2O_2) and singlet oxygen ($^1O_2$) (Zorov et al., 2014). Although H_2O_2 does not have unpaired electrons, it is highly effective as an oxidant and it could be reduced to $OH^\bullet$, the most reactive oxygen radical (Tarafdar and Pula, 2018). O_2^- is short lived and has limited ability to diffuse cross cellular membranes when compared with H_2O_2. However, O_2^- can react with nitric oxide (NO) resulting in highly reactive peroxynitrite ($ONOO^-$).

ROS are natural by-products of various cellular processes, such as cellular respiration, protein folding, and end-products of some metabolic reactions (Reczek and Chandel, 2015). ROS play vital roles in intracellular signaling regulating several physiological and cellular processes. For instance, they are involved in growth factor signaling, host defence, autophagy, and proliferation and differentiation of stem cells (Reczek and Chandel, 2015). ROS are involved directly and indirectly in the defence against invading microorganisms. In cell signaling, ROS could modify redox-sensitive amino acids in many proteins, such as ion channels, phosphatases and transcription factors. Many biosynthetic processes, such as iodination of thyroid hormones and crosslinking of matrix proteins, are ROS-dependent. However, excess ROS have a damaging effect on macro-molecules, including DNA, proteins, and lipids. DNA oxidation could result in mutations and affect gene expression (Brieger et al., 2012, Dröge, 2002). These damaging effects lead to pathological changes that trigger ROS-related

diseases. For this reason, it is critical for the cell to manage these conflicting dual functions of ROS.

Mitochondrial DNA is more sensitive to oxidative damage because of lack of DNA repair enzymes in mitochondria. Furthermore, protein oxidation by ROS could result in insoluble protein aggregation which is considered as one of the pathological features found in many diseases, including neurodegenerative disorders. (Brieger et al., 2012).

1.2.2 Sites of ROS production

ROS could originate from both exogenous and endogenous sources. Examples of exogenous sources include radiation and drugs, while endogenous sources of ROS include various cellular compartments such as the cell membrane, cytoplasm, endoplasmic reticulum (ER), mitochondria, and peroxisomes (Forrester et al., 2018, Rastogi et al., 2017). However, about 90% of ROS are produced by the mitochondria, named mtROS, as a by-product during electron transport via the electron transport chain (Zorov et al., 2014). mtROS will be discussed later in (section 1.2.3.2).

In the cytoplasm, O_2 is reduced to O_2^- through the nicotinamide adenine dinucleotide phosphate (NADPH) oxidase (NOX) enzymes. There are several isoforms of NOX (1-7), of which NOX2 is found at the plasma membrane where it catalyses the generation of O_2^- in the extracellular space (Fisher, 2009). Extracellular O_2^- can enter the cytosol through chloride channel-3 (CIC3) (Fisher, 2009). O_2^- can also be dismutated to H_2O_2 in the extracellular space which can then diffuse into the cell through aquaporin channel (AQP) (Figure 1.1). All cytosolic O_2^- is rapidly converted to H_2O_2 by the enzymatic activity of superoxide dismutase 1 (SOD1). Also, significant amount of ROS is generated from the ER (Tu and Weissman, 2004). The ER releases H_2O_2 as a by-product during oxidative protein folding (Reczek and Chandel, 2015). The accumulation of

unfolded and/or misfolded proteins elevates the ER ROS level and induces ER stress which promotes Ca^{2+} leak from the ER stores. The released H_2O_2 can be converted to water by the antioxidant enzymes including glutathione peroxidases (GPXs), peroxiredoxins (PRXs), and catalase (Reczek and Chandel, 2015). GPXs and PRXs are present in the cytosol, mitochondria, and the ER, whereas catalase is restricted to the peroxisomes (Reczek and Chandel, 2015). In addition, H_2O_2 can react with the reduced form of metal cations (Fe^{2+} and Cu^{+}) to produce the $OH^{\bullet}$, which has irreversible oxidative damaging effect on the DNA, proteins, and lipids (Reczek and Chandel, 2015). Finally, another source of H_2O_2 is the oxidation of long-chain fatty acids in the peroxisomes (Figure 1.1).

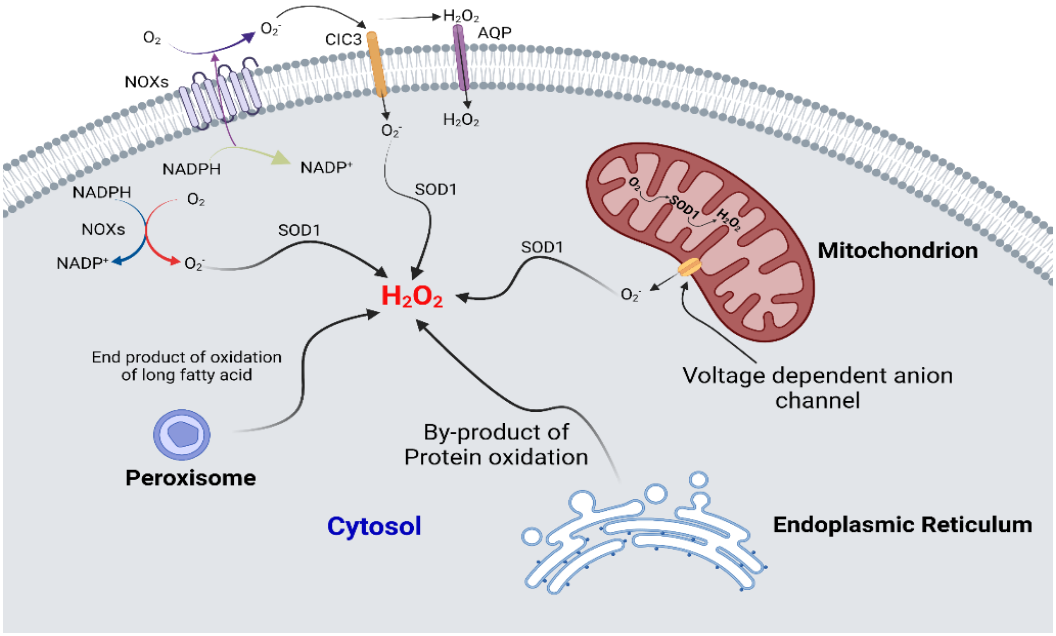

Figure 1.1 Endogenous sources of ROS.

Intracellular ROS are primarily produced by cytosolic NADPH oxidase enzymes (NOXs), the mitochondria, the endoplasmic reticulum, and the peroxisome. NOX found in the plasma membrane generates superoxide (O_2^-) in extracellular space. The extracellular O_2^- can be dismutated to hydrogen peroxide (H_2O_2) which can diffuse into the cell through aquaporin channel (AQP). Also, extracellular O_2^- can penetrate the plasma membrane to the cytosol through chloride channel-3 (ClC3). In the cytosol, O_2^- is rapidly converted into hydrogen peroxide (H_2O_2) by the action of superoxide dismutase 1 (SOD1). Figure adapted from (Reczek and Chandel, 2015), and created with BioRender.com

1.2.3 Mechanism of ROS production

1.2.3.1 NADPH oxidase (NOX)

The NADPH oxidase (NOX) is a family of multi-subunit enzyme complexes that are expressed throughout the body. NOXs are membrane-associated proteins, and their function is to transfer electrons from NADPH to O_2 resulting in superoxide anion (O_2^-) generation and subsequently other forms of ROS (Bedard and Krause, 2007, Tarafdar and Pula, 2018). NOX enzymes play important roles in many biological processes, such as in cellular signaling, stress response, cellular defence, and regulation of transcription and translation (Tarafdar and Pula, 2018, Bedard and Krause, 2007, Sorce and Krause, 2009). The first NOX enzyme discovered was the NOX2, and it was initially named g92phox, as an enzyme responsible for respiratory burst in neutrophils (Rossi and Zatti, 1964, Tarafdar and Pula, 2018). Later, six members of NOX family were added, including NOX1, NOX3, NOX4, NOX5, DUOX1 and DUOX2. All NOX isoforms share conserved functional and structural characteristics (Magnani et al., 2017, Bedard and Krause, 2007). The dual oxidases (DUOX1 and DUOX2) contain both a NOX domain and a peroxidase-like domain, and they are also called NOX6 and NOX7, respectively (Altenhöfer et al., 2015, Bedard and Krause, 2007).

The NOX domain comprises at least six membrane-spanning alpha helical domains harbouring two hemes, and at the cytosolic C-terminus there is a flavin adenine dinucleotide (FAD) and NADPH binding site (Kawahara et al., 2007, Bedard and Krause, 2007). However, there are minor structural differences between the members of NOX family. The catalytic subunits of some NOXs require association with other functional protein subunits. For example, NOX1 requires p22phox and NoxA1 for activation. NOX2 associates with p22phox and needs other cytosolic subunits, including p40phox, p47phox, p67phox and the small GTPase Rac1 or Rac2, for its activation and assembly in the plasma membrane. In some cells, such as microglia, phosphorylation of the p47phox subunit appears to play a major role in controlling NOX2 activation. Phosphorylation of p47phox could be catalysed by various kinases, such as

protein kinase C (PKC), Akt, p21-activated kinase (Pak), mitogen-activated protein kinase (MAPK), and extracellular signal-regulated kinase (ERK). For NOX3, the protein subunits p22phox, NoxO1, NoxA1 and Rac are needed for enzyme activity. On other hand, NOX4 does not contain cytosolic subunits, and only p22phox appears to be required for its activation. Finally, activation of NOX5, NOX6 and NOX7 depends directly on increased cytosolic Ca^{2+} concentration and none of the protein subunits which have been mentioned earlier are thought to be involved. (Belarbi et al., 2017)

All NOX enzymes catalyse a reaction that involves the transfer of two electrons from NADPH, through the FAD and the two hemes, to molecular oxygen. NOX1, NOX2, NOX3 and NOX5 produce superoxide (O_2^-), whereas NOX4, NOX6 and NOX7 generate hydrogen peroxide (H_2O_2). Several factors are thought to activate ROS production by NOX enzymes, including mechanical forces, environmental factors such as hypoxia, and hormones such as angiotensin II and aldosterone, and the cytokine tumor necrosis factor α (TNFα). (Tarafdar and Pula, 2018, Sahoo et al., 2016)

The expression levels of NOX enzymes vary among different tissues in the body. For example, NOX 1 is highly expressed in the colon, NOX2 in phagocytes, NOX3 in the ear, NOX4 in blood vessels and kidney, NOX5 in the lymphoid and testis, NOX6 and NOX7 are expressed more in the thyroid (Tarafdar and Pula, 2018). It has been shown that within the human brain, NOX2 is the predominant NOX, and traces of NOX4 and NOX5 were also detected (Cheng et al., 2001, Belarbi et al., 2017). In neurons, NOX4 is found to be associated with the internal membranes such as ER, endosomes, and mitochondrial membranes (Case et al., 2013, Martyn et al., 2006, Belarbi et al., 2017). Dopaminergic neuron samples from PD patients showed NOX1 (Choi et al., 2012) and NOX4 (Zawada et al., 2015) expression in the nucleus and are involved in oxidative stress induced neuronal cell death in PD.

It is believed that NOX enzymes are major generators of ROS in the brain (Belarbi et al., 2017). The reported physiological functions of NOXs in the central nervous

system include host defence, debris removal, and the regulation of neuronal function and synaptic plasticity (Belarbi et al., 2017). However, overproduction of ROS by NOXs could be harmful and lead to neuronal degeneration.

1.2.3.2 Mitochondrial ROS

Mitochondria are the major source of cellular ROS. Approximately 90% of ROS are generated from the mitochondria (Balaban et al., 2005). Mitochondrial ROS are produced mainly from ETC during the process of oxidative phosphorylation, where O_2 is reduced to H_2O. The most abundant form of ROS in the mitochondria is the superoxide anion (O_2^-) (Zorov et al., 2014). 0.2-2% of oxygen consumed by the mitochondria is reduced to O_2^-, which can be converted to other ROS, for example, hydrogen peroxide (H_2O_2) and hydroxyl ions (OH^-). (Balaban et al., 2005)

During electron transport, electrons could leak from the ETC complexes and interact with O_2 resulting in O_2^- formation. This takes place mainly at the flavin mononucleotide (FMN) site of complex I and the Q cycle of complex III. Therefore, complex I and III are considered as the major sources of O_2^- and H_2O_2 in mitochondria (Nickel et al., 2014). Also, under normal conditions, low levels of O_2^- are produced at II_F site of complex II, which is associated with succinate dehydrogenase (Zhao et al., 2019), and complex IV appears to be not involved in ROS production. However, there appear to be 11 ROS-producing sites in total in mammalian mitochondria (Zhao et al., 2019).

Several pathologies associated with excess mitochondrial ROS production have been reported. mtROS are involved in atherosclerotic lesion progression and plaque erosion and rupture (Hulsmans et al., 2012, Kattoor et al., 2017). A study on cellular and animal models of cardiovascular diseases showed that mitochondrial-targeted antioxidants reduced ROS-induced apoptosis and enhanced cardiac function (Hulsmans et al., 2012). In hypertension, oxidative

stress induces endothelial dysfunction, remodelling and inflammation leading to vascular damage (Montezano et al., 2015). Furthermore, it has been found that mtROS are involved in the initiation of cancer, amplification of tumour cells, and could stimulate additional mutations that lead to metastatic behaviour (Sabharwal and Schumacker, 2014, Sosa et al., 2013). Moreover, there is emerging evidence that mitochondria are the main source of excess mtROS production in Type 2 Diabetes Mellitus, where they play a major role in disease onset and complications (Ceriello, 2006, Erejuwa, 2012, Ahmad et al., 2017). Similarly, a strong association between mtROS and Alzheimer's and Parkinson's disease has been reported (Dias et al., 2013, Manczak et al., 2004, Angelova and Abramov, 2018).

mtROS were reported to be associated with numerous other disorders including obesity (Ghosh et al., 2011), cardiomyopathy (Lorenzo et al., 2013), Ischemia-reperfusion injury (Chouchani et al., 2016), pulmonary arterial hypertension (Fulton et al., 2017), schizophrenia (Nagano et al., 2015), non-alcoholic liver disease (Dias et al., 2013), and age-related macular degeneration (Marazita et al., 2016). Thus, understanding of how excess mtROS production leads to the onset or progression of diseases is fundamental to the development of mitochondria-targeted therapies.

1.2.4 Roles of metal ions in ROS production

Metal ions, especially $Ca^{2+,}$ Zn^{2+} and Fe^{2+} have been shown to play key roles in the generation of ROS and ROS associated disease (Gulcin and Alwasel, 2022).

1.2.4.1 Calcium ions

Calcium ions (Ca^{2+}) play a vital role in many physiological processes and in maintaining cellular homeostasis. Ca^{2+} acts as a second messenger in signal

transduction pathways that control a wide range of cellular processes such as gene transcription, muscle cell contraction and cell proliferation (Bootman et al., 2003). Ca^{2+} is also involved in activating neurotransmitter release to modulate neuronal function (Burgoyne, 2007), and is an important cofactor of many enzymes. In eukaryotic cells, Ca^{2+} concentration gradients are maintained across the cellular membrane (~ 100 nM inside, and ~ 1-2 mM outside) (Berridge et al., 2003). Intracellular Ca^{2+} homeostasis and signaling are mainly regulated through Ca^{2+} entry into the cells through channels and transporters, and by Ca^{2+} release from intracellular stores such lysosomes, Golgi apparatus, ER and mitochondria. Ca^{2+} could be pumped out the cell against its concentration gradient by several mechanisms, the most important one being through plasma membrane Ca^{2+} activated ATPase (PMCA) (Brini and Carafoli, 2011). Membrane Ca^{2+} transporters are shown in Figure 1.2. Defects in intracellular Ca^{2+} homeostasis are associated with multiple pathophysiological conditions and have been linked to many age-related diseases (LaFerla, 2002, Ermak and Davies, 2002, Berridge et al., 2003, Marambaud et al., 2009).

The largest intracellular Ca^{2+} storage site is the ER. Ca^{2+} release from the ER can increase the cytosolic Ca^{2+} concentration from 100 nM (at rest) to 1 mM (Berridge et al., 2003, Jin et al., 2021). The ER releases Ca^{2+} in response to the activation of specific Ca^{2+} channels found on its membrane, such as inositol 1,4,5-triphosphate receptors (IP_3R) and ryanodine receptors (RyR). Ca^{2+} can then be transferred to other cellular organelles including mitochondria (Jin et al., 2021). In the mitochondria, Ca^{2+} homeostasis has a vital role in the physiology and pathophysiology of the cell. Ca^{2+} also plays a critical role in determining the morphology of mitochondria; this will be discussed later under the mitochondrial dynamics section (section 1.3.3).

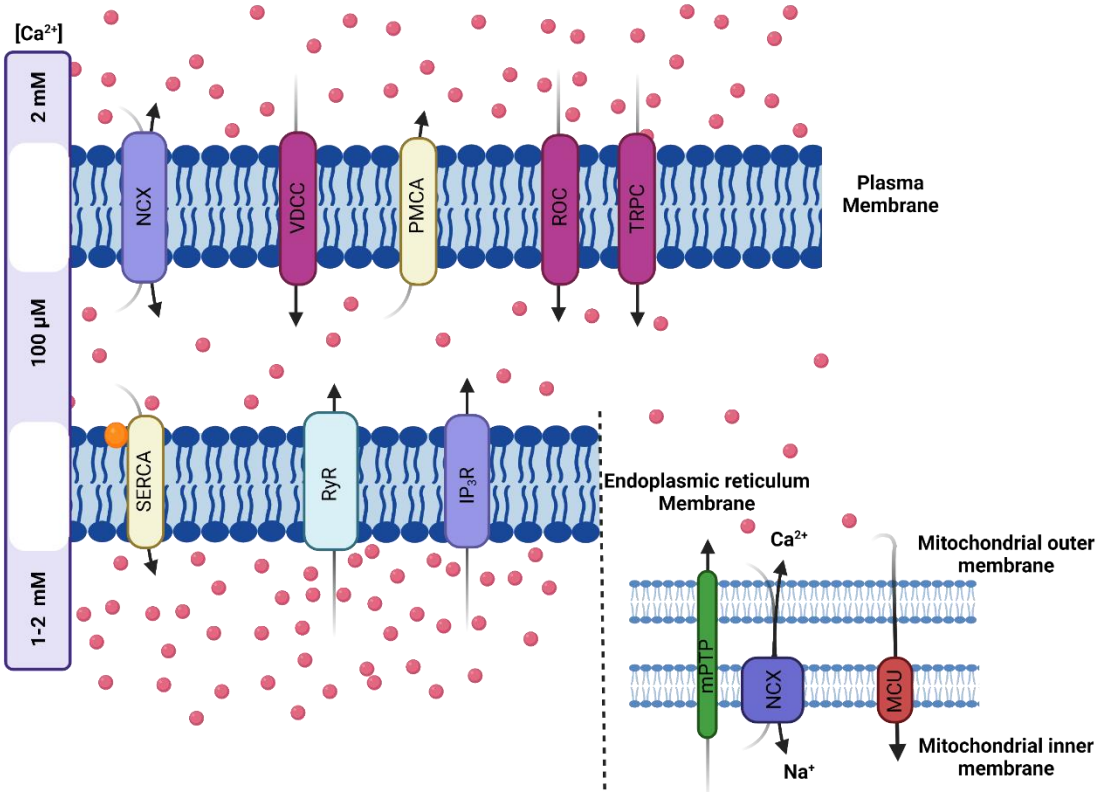

Figure 1.2 Membrane transporters of calcium ions.

Illustration showing the calcium ions transporters that are found in the cell membrane, endoplasmic reticulum (ER) and mitochondrial membranes. The voltage dependent Ca^{2+} channel (VDCC), receptor operated channel (ROC) and transient receptor potential channel (TRPC) are calcium channels that transport calcium ions into the cytosol. The plasma membrane Ca^{2+} activated ATPase (PMCA) and the sarco/endoplasmic reticulum Ca^{2+} activated ATPase (SERCA) are energy-dependent calcium pumps that transport calcium ions from the cytosol or into the endoplasmic reticulum. NOX, the sodium-calcium exchanger. In the ER, two receptors (Ryanodine receptor; RyR and Inositol 1,4,5-triphosphate receptor; IP_3R) mediate the release of calcium from the ER store. The mitochondrial permeability transition pore (mPTP), mitochondrial uniporter (MCU), and mitochondrial sodium-calcium exchanger (NCX) are all involved in calcium transport in mitochondrial. Figure adapted from (Görlach et al., 2015), and created with BioRender.com

Studies suggest an interplay between calcium signaling pathways and other signaling systems, such as ROS, (Görlach et al., 2015) which in turn seems to control cellular physiology. As mentioned earlier (section 1.2.3.1), the activation of most NOX enzymes involves Ca^{2+}, either by directly binding the enzyme or through phosphorylation of the regulatory proteins by calcium dependent kinases such as PKC. Thus, increased cytosolic Ca^{2+} levels promote ROS generation as a result of Ca^{2+}-induced NOX activation. Ca^{2+} also plays a role in mitochondrial ROS production (section 1.3.3). Thus, Ca^{2+} regulates intracellular ROS generation from multiple sources.

Conversely, Ca^{2+} homeostasis can be regulated by ROS. Various Ca^{2+} channels, pumps and exchangers are regulated by ROS (Görlach et al., 2015). Ca^{2+} permeable channels such as, voltage dependent Ca^{2+} channels (VDCC) and some members of transient receptor potential (TRP) channels, have been shown to be sensitive to ROS. The TRPM2 channel was the first identified TRP channel that is ROS sensitive. This channel was found to be activated by H_2O_2 and adenosine diphosphate ribose (ADPR). The activation mechanism of TRPM2 will be described in (section 1.6.3). Other TRP members including TRPC1, TRPC3, TRPC4, TRPC6, are also sensitive to ROS (Görlach et al., 2015).

Furthermore, the store-operated Ca^{2+}-entry (SOCE) is controlled by two Ca^{2+} sensor molecules, STIM1 and STIM2 (stromal interaction molecule 1 and 2), which translocate from the ER to the plasma membrane to bind and stimulate the Ca^{2+}- permeable Orai channels, thereby promoting Ca^{2+} influx and refilling intracellular Ca^{2+} stores (Bogeski et al., 2012, Görlach et al., 2015). It has been shown that H_2O_2 induces STIM1 stimulation of SOCE through interaction with its cysteine residue at position 56 (Grupe et al., 2010, Görlach et al., 2015). Also, the activity of Orai channels was found to be modulated in response to extracellular oxidative stress (Bogeski et al., 2010, Görlach et al., 2015). Another study suggested an association between NOX2-derived ROS and the activity of STMI and Orai1 (Bréchard et al., 2008).

In addition, ROS can also modulate the ER Ca^{2+} channels, RyR and IP_3R. The RyR has many cysteine residues making the protein an excellent target for redox regulation (Meissner, 2010, Görlach et al., 2015). Studies have shown that RyR activity can be directly regulated by ROS though oxidation of thiol group leading to Ca^{2+} leak from the ER (Zima and Blatter, 2006, Görlach et al., 2015). It has been shown that ROS generation from NOX2 can stimulate RYR1 activity in skeletal muscle cells (Hidalgo et al., 2006). Furthermore, an association between mtROS and RyR activation has been reported (Bovo et al., 2012). It has been shown that the sensitivity of IP3R to IP3 is enhanced by ROS (Bánsághi et al., 2014).

ROS also affect Ca^{2+} homeostasis by modulating the activity of PMCA and SERCA by disrupting ATP binding and hydrolysis required for the activity of these Ca^{2+} pumps (Zaidi, 2010). ROS regulation of Ca^{2+} pumps plays major role in neuronal function in the aging brain and increase the susceptibility to neurodegenerative diseases including AD, PD and stroke (Zaidi, 2010). Taken together, many channels and transporters are modulated by oxidative stress to affect Ca^{2+} homeostasis.

1.2.4.2 Zinc ions

Zinc is the second most abundant trace element in human body (2-3 g) after iron (Hübner and Haase, 2021). Zn^{2+} is essential for all living organisms and plays an important role in many cellular processes such as development, protein metabolism, DNA synthesis and gene expression (Colvin et al., 2010, Ma et al., 2022). In humans, Zn^{2+} binds around 10% of total proteins either to support the protein structure (such as the Zn^{2+} finger), or serve as a cofactor required for enzyme activity (such as in oxidoreductases, hydrolases, isomerases, transferases, and ligases) (Ma et al., 2022, Colvin et al., 2010). Zn^{2+} that is loosely bound to proteins is known as labile Zn^{2+}. In humans, the total cellular concentration of Zn^{2+} is in the range of 200-300 µM (Maret, 2014), while the

concentration of free cytosolic Zn^{2+} is ~100 pM, although these values vary among different cell types and fluctuate in response to certain extracellular stimuli (Pratt et al., 2021). Experimentally, it is quite challenging to distinguish between protein-bound Zn^{2+} and free Zn^{2+} (Maret, 2014). Zn^{2+} deficiency has been shown to be linked to abnormal growth and development, congenital neuronal and immune disorders (Sensi et al., 2009). However, excess Zn^{2+}, like Ca^{2+}, is cytotoxic. Accumulation of Zn^{2+} has been shown to induce neuronal cell death and is associated with neurodegenerative diseases such as Alzheimer's and PD (Sensi et al., 2009). Therefore, both excess and shortage of Zn^{2+} are detrimental to the cell. Intracellular Zn^{2+} levels are controlled by two families of Zn^{2+} transporters, Zrt-, Irt-related proteins (ZIPs) and Zn^{2+} transporters (Znt), and by metallothioneins (MTs), which collectively regulate cellular homeostasis of Zn^{2+} (Maret, 2014). The ZIP family (14 members) is responsible for Zn^{2+} influx into the cytosol, whereas the Znt family (9 members) mediates Zn^{2+} efflux (Sensi et al., 2009, Ma et al., 2022). In addition to the cell membrane, these Zn^{2+} transporter proteins are also found in some subcellular organelles including the nucleus, lysosomes, ER, Golgi, endosomes, and mitochondria (Colvin et al., 2010, Ma et al., 2022).

Like Ca^{2+}, Zn^{2+} dyshomeostasis is closely linked with oxidative stress. MT has 20 cysteine residues which contribute to Zn^{2+} binding. Under normal conditions, the majority of intracellular Zn^{2+} is bound to MT, but during severe oxidative stress, ROS can oxidize the thiol groups of MT resulting in the release of free Zn^{2+} (Marreiro et al., 2017). Although MT is mostly located in the cytosol, it can be translocated to the nucleus to protect against DNA damage (Hübner and Haase, 2021). Elevation of Zn^{2+} stimulates two key transcription factors to induce the expression of Zn^{2+} binding proteins, transporters as well as antioxidants to restore Zn^{2+} and ROS homeostasis. Binding of Zn^{2+} to the metal transcription factor 1 (MTF-1) enables its binding to metal response element (MRE) promoter of target genes to induce the expression of MTs and ZnTs (Colvin et al., 2010, Hübner and Haase, 2021). Another zinc-dependent transcription factor, called nuclear factor erythroid 2-related factor 2 (Nrf2), induces the expression of the antioxidant proteins in response to elevation of ROS and Zn^{2+}. In normal conditions, Nrf2 is inactive because it is bound to the suppressor protein, Kelch-like ECH-associated

protein 1 (Keap1). Elevation of ROS and Zn^{2+} induces the degradation Keap1, enabling Nrf2 translocation to the nucleus. In the nucleus, Nrf2 binds the antioxidant response element (ARE) promoter to induce the expression of antioxidants proteins (Hübner and Haase, 2021)

Excess Zn^{2+} is harmful and can be cytotoxic. It has been shown that besides releasing Zn^{2+} from MT, ROS can also induce lysosomal Zn^{2+} release. Zn^{2+} released from the lysosomes has been shown to specifically affect mitochondrial dynamics and function in endothelial and pancreatic-β cells (Abuarab et al., 2017, Li et al., 2017a). These aspects will be elaborated in section 1.3.3.

Given these reports, it is important to better understand the mechanistic relationship between Ca^{2+}, Zn^{2+} and ROS and how this relationship is affected in numerous oxidative stress associated diseases, including PD.

1.2.5 ROS in human diseases

Excess ROS production is deleterious to cells and tissues leading to pathological changes associated with several diseases, including cardiovascular diseases, diabetes, cancer, and neurodegenerative diseases.

ROS play an important role in atherogenesis, endothelial dysfunction, low density lipoprotein (LDL) oxidation, and inflammation leading to the initiation and development of atherosclerosis (Negre-Salvayre et al., 2020). A recent study has reported a role for excess mtROS in early and advanced atherosclerosis lesions. The study showed that low levels of mitochondrial superoxide dismutase (SOD2), an enzyme that neutralizes ROS, can increase mitochondrial ROS levels and the consequent endothelial dysfunction in ApoE-deficient mice, leading to the development of atherosclerosis (Vendrov et al., 2017).

Oxidative stress caused by hyperglycaemia-induced ROS generation contributes to the development and progression of diabetes and the associated vascular complications (Gao and Mann, 2009). NOX is the main source of ROS in the vasculature in hyperglycaemia (Gao and Mann, 2009). Prolonged NOX activation in diabetes diminishes NADPH levels, which is an essential cofactor for endothelial antioxidant systems (Gao and Mann, 2009). Moreover, ROS overproduction by NOX leads to mitochondrial dysfunction. Studies have reported that diabetes induces defects in the mitochondrial ETC and promotes increased ROS production (Bugger and Abel, 2010, Yuan et al., 2010). Pancreatic β-cell dysfunction is a major pathological feature of type 2 diabetes. These cells are vulnerable to oxidative stress and hence to apoptosis because of their relatively poor ROS-detoxifying mechanisms (Lenzen et al., 1996). Another main feature of type 2 diabetes is insulin resistance. Studies have shown that insulin resistance occurs before the development of hyperglycaemia. It has been suggested that increased ROS levels are an important trigger for insulin resistance (Houstis et al., 2006). H_2O_2, for example, induces insulin resistance by inhibiting insulin-stimulated tyrosine phosphorylation of insulin receptors (Hansen et al., 1999). It is also becoming clear that diabetes is associated with obesity. Obesity is characterized by elevated plasma free fatty acids (FFA) concentrations. FFAs induce β-cell dysfunction and cell death, but the underlying mechanisms are still unclear (Yuan et al., 2010). Inhibition of NOX2 activity has been shown to rescue β-cells from FFA-induced cell death (Yuan et al., 2010, Li et al., 2017a). All these findings suggest that excess ROS generation might contribute to the pathogenesis of diabetes by affecting both β-cell function and insulin sensitivity.

Recent studies have shown a role for oxidative stress in cancer (Franco et al., 2008). Excess ROS can lead to inflammation and induce somatic mutations and neoplastic transformation (Khandrika et al., 2009). Oxidative stress has been linked to prostate cancer (Khandrika et al., 2009), and breast and ovarian cancers (Desouki et al., 2005). Studies have shown crosstalk between mtROS and NOX redox signaling (Desouki et al., 2005, Dikalov, 2011), and that abnormal crosstalk contributes to breast and ovarian cancer (Desouki et al., 2005). Interestingly, inhibition of NOX enzymes was found to reduce malignant melanoma

proliferation (Brar et al., 2002). Excess ROS also promotes cancer cell migration by remodelling the actin cytoskeleton (Li et al., 2016).

Finally, studies have shown a role for ROS in neurodegenerative diseases. In neuronal cells of the brain, ROS generating mechanisms are not fully understood. Normal level of ROS is required for brain function. However, increased ROS concentrations in the brain lead to neurotoxicity which, in turn, contributes to neuronal diseases. For example, in Alzheimer's disease, amyloid induces microglia activation and long-lasting ROS generation leading to neuronal cell damage and dementia (Elfawy and Das, 2019, Barnham et al., 2004, Gibson, 2002). The role of ROS in PD will be discussed next.

1.2.5.1 Oxidative stress in Parkinson's disease

The mechanisms by which ROS cause PD is not completely understood. It has been suggested that NOX-derived ROS is a major factor for dopaminergic neuronal loss in PD. Knockout of NOX2 protected mice from MPTP-induced loss of dopaminergic neurons (Brieger et al., 2012). Neuronal cells are especially vulnerable to oxidative stress damage because of their high oxygen consumption, high content of polyunsaturated fatty acids in their cell membranes and poor antioxidant mechanisms (Liu et al., 2017). As mentioned earlier, ROS can affect the structure and function of many macromolecules such as DNA and proteins. ROS can promote α-synuclein and parkin aggregation. These changes are thought to lead to the selective apoptotic death of dopaminergic neurons (Naoi and Maruyama, 1999). Such apoptosis could be suppressed by antioxidants, confirming the role of ROS in neuronal cell death in PD. Moreover, heavy metal ions such as iron , copper and cobalt are highly associated with oxidative stress and are implicated in the aetiology of PD (Lan et al., 2016). Patients with PD have higher levels of ferric (Fe^{3+}) and ferrous (Fe^{2+}) ions in the midbrain (SN) in comparison to healthy individuals (Dexter et al., 1989), and show increased ROS generation in the brain (Halliwell, 1989). The Fe^{3+} and Fe^{2+} ions can react with

O_2^- and H_2O_2, respectively, producing the highly reactive $OH^\bullet$ (Núñez et al., 2012). Furthermore, patients with PD have decreased glutathione levels, decreased mitochondrial complex I and increased dopamine turnover (Yoshikawa, 1993), all of which increase ROS generation and lead to neuronal cell damage.

Dopamine is an unstable molecule and can undergo auto-oxidation to produce dopamine quinones and free radicals in a reaction catalysed by oxygen, metals, or enzymes such as tyrosinase (Dias et al., 2013). These products of dopamine oxidation can contribute to mitochondrial dysfunction and neurodegeneration in PD (Hastings, 2009). Dopamine can also be oxidized by MAO-a and MAO-b enzymes which are located in the outer mitochondrial membrane. Under normal conditions, dopamine level is regulated mainly by MAO-A. However, in PD and during aging, MAO-b levels increase and it becomes the major regulator of dopamine metabolism producing 3,4-dihydroxyphenylacetaldehyde (DOPAL) and H_2O_2 (Dias et al., 2013). Taken together, there is considerable evidence supporting a link between oxidative stress and PD.

1.2.6 Targeting ROS in human diseases

As mentioned in the previous sections, oxidative stress results from an imbalance between antioxidants and free radicles generated in the cell (Mazo et al., 2017). Therefore, antioxidants have been considered an attractive approach to counteract ROS-mediated diseases. However, antioxidant treatment strategies have yielded disappointing results, especially in neurodegenerative diseases, because of the lack of understanding of the underlying mechanisms (Liu et al., 2017). It is also important to recognize the fact that for any therapeutic chemical to be successful in the treatment of PD, it must be able to cross the blood-brain barrier and reduce oxidative stress (Neves Carvalho et al., 2017). Instead of antioxidants, recent approaches have selectively targeted ROS-generating enzymes, such as NOX (Casas et al., 2015).

NOX inhibition is a promising pharmacological approach in ROS-associated diseases. NOX2 is highly expressed in the brain and dopaminergic neurons. Apocynin, 4-hydrozy-3-methoxy acetophenone, is one of the promising NOX inhibitors. It blocks p47phox translocation to the cell membrane and prevents NOX assembly thus inhibiting the enzyme activity (Rastogi et al., 2017, Wang et al., 2006). However, it is not specific. It acts on NOX1 and NOX2, the most active forms, more than other NOX enzymes. Apocynin has protective effects against ischemic injury, lipid peroxidation, and neuronal cell death. In a rat model of PD, apocynin was able to suppress α-Syn aggregation, α-Syn-mediated NOX activation, and ROS generation (Sharma et al., 2016). Furthermore, the gp91-ds-tat is another promising drug which is specific to NOX2 (Williams and Griendling, 2007). This inhibitor prevents p47phox binding to gp91phox through emulating the binding site of pg91phox. It has been shown that gp91-ds-tat reduced ROS generation and cerebrovascular alterations associated with Alzheimer disease (Park et al., 2008), and also attenuated angiotensin II-induced hypertension (Rey et al., 2001) in a mouse model. Finally, some drugs can act indirectly on NOX. For example, angiotensin converting enzyme (ACE) inhibitors and angiotensin receptor antagonists can reduce NOX activation that is stimulated by angiotensin II/PKC pathway. (Rastogi et al., 2017)

1.3 Mitochondria

1.3.1 Mitochondria structure and function

Mitochondria are well known for their role in ATP production. However, mitochondria are also involved in numerous other physiological processes, such as apoptosis, innate immunity, Ca^{2+} homeostasis and ROS generation (Tilokani et al., 2018, Camello-Almaraz et al., 2006). Mitochondria are enclosed by two membranes, an outer membrane and an inner membrane separated by the intermembrane space. The inner mitochondrial membrane (IMM) surrounds a matrix. The IMM contains the electron transport chain (ETC) which comprises

four protein complexes: complex I, II, III, and IV, and ATP synthase (Figure 1.3). Complex I (NADH dehydrogenase) accepts electrons from NADH that are generated from tricarboxylic acid (TCA) cycle and passes these electrons to coenzyme Q (ubiquinone). Complex II (succinate dehydrogenase) transfers electrons from succinate to coenzyme Q as well. Electrons are then transferred to complex III (cytochrome *c* reductase), which passes them to cytochrome *c* (Cyt *c*). Cyt *c* is a small protein that mediates the transfer of electrons from complex III to complex IV (cytochrome *c* oxidase) which finally uses the electrons and H^+ ions to reduce O_2 to H_2O. (Harvey, 2011, Dudkina et al., 2010). The pumping of H^+ ions from the matrix into the intermembrane space creates an electrochemical proton gradient (ΔpH) across the IMM and mitochondrial membrane potential (ΔΨm). The protons are pumped back into the matrix by ATP synthase (complex V) and, in doing so, phosphorylates ADP to ATP. This process is known as oxidative phosphorylation (OXPHOS) because ADP phosphorylation is coupled to the oxidative reactions in ETC (Jonckheere et al., 2012). ETC in mitochondria is considered as the major site of intracellular ROS production. This is due to the premature electron leakage to O_2 causing its reduction to O_2^-. Complex I, II, and III release O_2^- into the matrix as a side product of ETC (Figure 1.3) (Camello-Almaraz et al., 2006). In the matrix, O_2^- is rapidly converted to H_2O_2 by the enzyme superoxide dismutase 2 (SOD2) (Murphy, 2009b). The only scavenger enzyme found in mitochondria is the glutathione peroxidase (GSPx) that uses reduced glutathione (GSH) as coenzyme to convert H_2O_2 to H_2O (Kirkinezos and Moraes, 2001). O_2^- released from complex III into the intermembrane space can be transported to the cytosol through voltage-dependent anion channels (Reczek and Chandel, 2015). In the cytosol, O_2^- is dismutated to H_2O_2 by SOD1. Under normal conditions, the rates of O_2^- production is less than 1% of the total rate of electron transport from NADH to O_2, and the effects of ROS are counteracted by antioxidants. However, the rate of ROS production by mitochondria is increased in several pathological conditions such as hypoxia, ischemia, and aging (Kirkinezos and Moraes, 2001). Accumulation of ROS in mitochondria can lead to several adverse effects including damage to mitochondrial proteins, membranes, and DNA, and to impaired ATP synthesis (Murphy, 2009b). Moreover, mitochondrial oxidative damage induces the release of intermembrane space proteins such as cytochrome c (Cyt *c*) by the outer membrane

permeabilization to the cytoplasm which activates cell apoptosis (Murphy, 2009b). ROS production by mitochondria can be stimulated by ER stress. Ca^{2+} released from the ER stores enters mitochondria causing depolarization of mitochondrial membrane leading to further production of mitochondrial ROS.

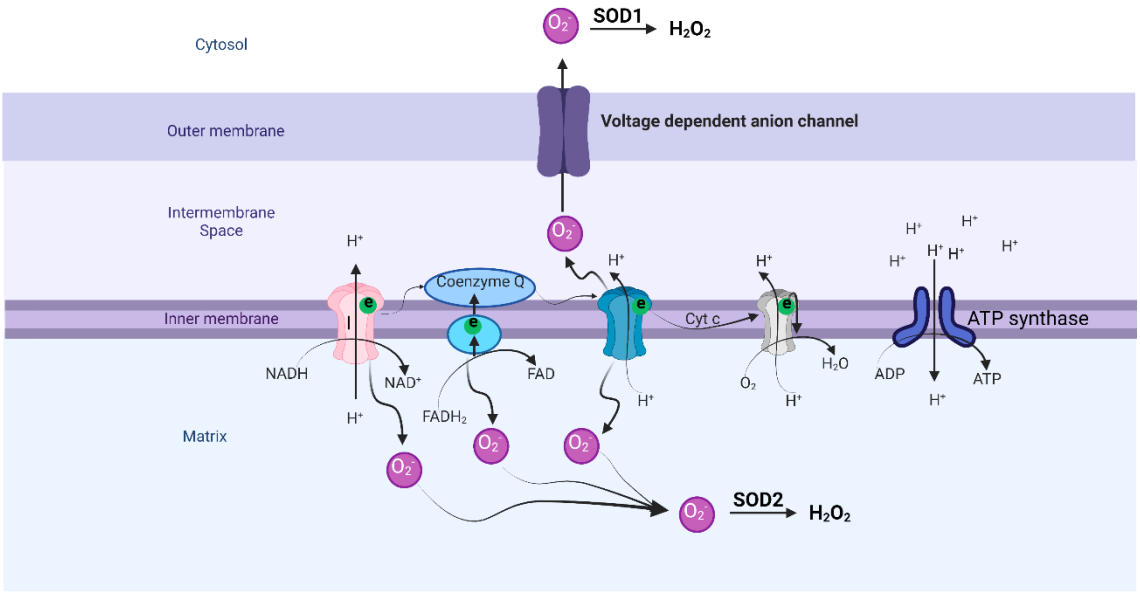

Figure 1.3 Mitochondrial respiratory chain (electron transport chain, ETC) showing the flow of electrons, and the production of ATP and ROS.

ROS can be produced from the respiratory chain. Superoxide **(**O_2^-) generated from complexes I, II and III is released into the matrix where it could be dismutated into H_2O_2 by mitochondrial superoxide dismutase (SOD2). O_2^- released from complex III into the intermembrane space can be transported to the cytosol through voltage-dependent anion channels where it can be converted to H_2O_2 by superoxide dismutase 1 (SOD1). Figure created by BioRender.com

1.3.2 Mitochondrial dynamics

Mitochondria are mobile organelles that exist as tubular branched networks. The network undergoes continuous fusion and fission to maintain a healthy structure, function, and distribution (Archer, 2013, Friedman and Nunnari, 2014). Fission helps to promote the dysfunctional parts of the mitochondrial network to undergo mitophagy. Fission also has a role in tissue development and function, as a study showed that defective fission in animals is embryonically lethal (Ishihara et al., 2009). On other hand, fusion enables the functional parts of the network to merge with and extend the healthy mitochondria network. Fusion is important for extending and interconnecting mitochondrial network which, in turn, allows mitochondria to mix and redistribute their contents (Favaro et al., 2019). These two processes are collectively known as “mitochondrial dynamics”. Mitochondrial dynamics are affected by various metabolic stimuli, including excess nutrients, environmental toxins, and cellular dysfunction. In many disorders, such as diabetes, cancer, obesity, and cardiovascular and neurodegenerative diseases, there is increased mitochondrial fission (Wai and Langer, 2016). ROS are major stimulants of mitochondrial fission.

The core components of fission and fusion machinery are the GTPase proteins belonging to the dynamin family. In the fission process, mitochondrial constriction and scission are carried out mainly by Drp1 (dynamin related protein-1) and Dynamin2 (Dnm2) (Lee et al., 2016a, Tilokani et al., 2018). Drp1 mediates outer membrane fission in response to specific cellular signals that cause its translocation from the cytosol to the outer membrane of mitochondria causing constriction of the membrane. Wakabayashi *et al*., (2009) have shown that genetic loss of Drp1 leads to a drastic elongation of mitochondrial tubules that could be rescued by Drp1 re-expression (Wakabayashi et al., 2009).

During mitochondrial fission, Drp1 forms a ring-like structure around the mitochondria promoting the narrowing of the outer mitochondrial membrane (OMM), following by GTP hydrolysis leading to membrane constriction which specify the site of mitochondrial scission. Drp1 assembles at OMM as Drp1-

oligomeric helices. (Friedman and Nunnari, 2014, Fröhlich et al., 2013, Tilokani et al., 2018)

Drp1 recruitment to OMM requires other adaptor proteins. These are Drp1 receptors at the OMM, including fission protein (Fis1), mitochondrial fission factor (MFF), and mitochondrial dynamics proteins (MiD49 and MiD51), which facilitate Drp1 recruitment. (Wai and Langer, 2016). The activity of Drp1 and its association with mitochondria are controlled by phosphorylation, ubiquitination and sumoylation (Santel and Frank, 2008).

Experiments using live-cell imaging reported that Dnm2 works downstream to Drp1 recruitment and action (Lee et al., 2016a). Dnm2 gathers as a collar-like structure around the constricting site catalysing the final step of mitochondria fission. Furthermore, ER is involved in the initial step of mitochondrial fission. It has been shown that ER tubules not only contact mitochondria but are also able to wrap around the mitochondria causing the constriction of mitochondria (Friedman et al., 2011). This could reduce the average mitochondrial diameter from 300-500 nm to around 150 nm, that not only specify the recruitment site for Drp1 and its adaptor proteins, but also facilitates the formation of Drp1-oligomeric ring structure (Friedman et al., 2011, Tilokani et al., 2018).

The molecular machinery responsible for the IMM fission is less well understood. However, it has been suggested that Drp1-mediated constriction of the OMM is sufficient to drive IMM scission (Wai and Langer, 2016). IMM constriction takes place at mitochondria-ER contact site, and it is a Ca^{2+}-dependent step (Chakrabarti et al., 2018, Cho et al., 2017). ER stimulation causes Ca^{2+} mobilization from the ER to mitochondria leading to constriction and scission of IMM before Drp1 recruitment and activity, suggesting that the IMM and OMM constriction events are independent (Chakrabarti et al., 2018, Cho et al., 2017, Tilokani et al., 2018). Inhibition of the mitochondrial calcium uniporter (MCU) prevents this fission process (Hom et al., 2007), supporting the idea that mitochondrial Ca^{2+} influx is required for mitochondrial fission. (Tilokani et al., 2018)

Mitochondrial fusion is an important process that allows cooperation between mitochondria, thereby maintaining an efficient respiratory function (Chen et al., 2003). The fusion mechanism is controlled by two other GTPases called Mitofusin 1 (Mfn1) and mitofusin2 (Mfn2) which mediate OMM fusion. Studies showed that Mfn1 or Mfn2 overexpression or deficiency affect mitochondrial morphology (Chen et al., 2003, Santel and Fuller, 2001). Overexpression of Mfn1 and Mfn2 induces mitochondrial aggregation around the nucleus (Eura et al., 2003, Tilokani et al., 2018). In a study using mouse embryonic fibroblasts, Chen *et al*., (2003) revealed that Mfn1 mutant cells display severely fragmented mitochondria. Similarly, Mfn2 mutant cells showed shorter swollen rounded mitochondria in contrast to wild-type cells which displayed long extended mitochondrial network (Chen et al., 2003). During fusion, these proteins accumulate between adjacent mitochondria forming complexes that initiate the fusion process (Brandt et al., 2016).

Mitochondrial fusion consists of three main steps. First, the tethering of the outer membranes of two attached mitochondria to a distance approaching 6 nm, followed by GTP hydrolysis to induce the fusion. In the second step, characterized by a docking ring of protein density surrounding the extended areas of outer membranes, the distance between the OMM decreases to less than 3 nm, and thereby, increasing their contact surface area. Finally, fusion of OMM of the tethered mitochondria occurs as a result of conformational changes stimulated by GTP hydrolysis. (Brandt et al., 2016, Tilokani et al., 2018)

IMM fusion is mediated by optic atrophy 1 (OPA1) and specific lipid components. OPA1 is localized in the intermembrane space bound firmly to the outer surface of the inner membrane (Griparic et al., 2004). Overexpression of OPA1 causes mitochondrial elongation, whereas genetic depletion of the protein by siRNA leads to mitochondrial fragmentation (Griparic et al., 2004). Different isoforms of OPA1 protein exist, two of which play a major role in mitochondrial dynamics, the long-form (L-OPA1) and the short-form (S-OPA1). Both OPA1 isoforms are required for IMMs fusion, and they work together to mediate efficient fusion

process; however, a recent study showed that L-OPA1 alone is sufficient to induce fusion. (Tilokani et al., 2018)

1.3.3 Role of calcium and zinc ions in mitochondrial dynamics

Several studies have shown that a rise in intracellular Ca^{2+} and the consequent increase in mitochondrial Ca^{2+} affects mitochondrial dynamics and promotes the fission process (Camello-Almaraz et al., 2006, Pinton et al., 2008). Mitochondria can take up the Ca^{2+} from several sources including cytoplasm and intracellular organelles, such as the ER and lysosomes (Lange et al., 2009). Excess ROS in the cell could cause ER stress resulting in Ca^{2+} release from ER and its uptake by mitochondria. There is evidence for physical interaction between the ER and mitochondria. Known as mitochondria-endoplasmic reticulum contacts (MERCs), these sites facilitate Ca^{2+} transfer from the ER to the mitochondria. The isolated MERCs, called mitochondria-associated membranes (MAMs), contain parts of both OMM and smooth ER. Both MAMs and IMM participate in Ca^{2+} signaling, cell death and autophagy (Gomez-Suaga et al., 2017, Rizzuto et al., 1998, Jin et al., 2021).

Ca^{2+} enters the mitochondria through voltage-dependent anion channels (VDAC) which are components of mitochondrial permeability transition pore (mPTP). These channels are regulated by two proteins: Mfn2, which tethers ER to mitochondria for efficient Ca^{2+} transfer, and by cyclophilin D (CypD) which serves as a sensitizer controlling the opening of the mPTP (de Brito and Scorrano, 2008). However, data on the molecular structure of mPTP and whether the VDAC channel is a part of it, remain unclear. After Ca^{2+} entry through the OMM, it crosses the IMM. The large negative $\Delta\Psi m$ (~-140 mV) serves as a driver for Ca^{2+} entry. Ca^{2+} entry into the matrix is regulated by mitochondrial calcium uniporter (MCU) and its regulators, including mitochondrial Ca^{2+} uptake 1 (MICU1) and mitochondrial Ca^{2+} uptake 2 (MICU2) (Jin et al., 2021). Chemical inhibition of mPTP using cyclosporine, prevents Ca^{2+}-induced mitochondrial fragmentation

(Cereghetti et al., 2010). Together, these lines of evidence suggest a key role for Ca^{2+} in mitochondrial dynamics.

Baumgartner *et al*., (2009) reported that increased mitochondrial Ca^{2+} uptake stimulates loss of ΔΨm and subsequent mitochondrial ROS production (Baumgartner et al., 2009). However, other studies showed that Ca^{2+} signaling and ΔΨm are independent (Chalmers and McCarron, 2008, Collins et al., 2001), and may depend on cell type. Ca^{2+} accumulation induces mitochondrial superoxide generation leading to mitochondrial damage and subsequent cell death (Nicholls, 2005) by promoting mPTP opening and release of Cyt *c* and apoptotic-inducing factor (AIF) (Duchen, 2000a).

Mitochondrial dynamics and function are also modulated by Zn^{2+}. Impairment of Zn^{2+} homeostasis has been reported to lead to mitochondrial dysfunction, increased fission and consequently cell death. Zn^{2+} can be taken up by mitochondria through MCU. Although mitochondrial Zn^{2+} uptake provides a way of excess Zn^{2+} clearance from the cytosol of neurons undergoing excitotoxicity (Dineley et al., 2005, Sensi et al., 2009), increased mitochondrial Zn^{2+} can induce loss of ΔΨm and ROS generation leading to cell death (Dineley et al., 2005). It is thought that there is an overlap or cross-talk between Ca^{2+} and Zn^{2+} pathways in cell death (Sensi et al., 2009); however, the mechanism of cross-talk is unclear.

Zn^{2+} can stimulate mitochondrial ROS production by inhibiting complex III of ETC, or by interfering with complex I and α-ketoglutarate dehydrogenase (Sensi et al., 2009). Like Ca^{2+}, Zn^{2+} can induce mPTP opening leading to release of apoptotic factors, Cyt *c* and AIF, from mitochondria leading to neuronal cell death (Jiang et al., 2001).

While it is clear that Zn^{2+} plays an important role in mitochondrial homeostasis, how mitochondrial Zn^{2+} is controlled is poorly understood. The role of Zn^{2+} in mitochondrial fission is still unclear. However, recent studies have shown that increased mitochondrial Zn^{2+} leads to mitochondrial fragmentation which is

associated with loss of ΔΨm (Abuarab et al., 2017, Li et al., 2017a). These events have been shown to be linked to TRPM2 channel activation by oxidative stress. But, how TRPM2 activation triggers the rise in mitochondrial Zn^{2+} and then mitochondrial fission remain to be investigated. These studies also have investigated the role of Zn^{2+} in Drp1 recruitment, and the authors found that Zn^{2+} chelation prevents Drp1 recruitment to mitochondria in pancreatic β-cells (Li et al., 2017a) and in endothelial cells (Abuarab et al., 2017). These data suggest a role for Zn^{2+} in Drp1-mediated mitochondrial fission.

The newly identified Drp1-interacting protein Zip1, a Zn^{2+} transporter that is localized with Drp1 and MFF at mitochondrial division sites (Bowers and Srai, 2018) has provided additional evidence supporting the role of Zn^{2+} in mitochondrial fission. The authors proposed that Drp1 is recruited from the cytosol to the OMM by binding to MFF. Then, at the OMM, Drp1 associates with Zip1 promoting Zn^{2+} influx into the mitochondrial matrix via MCU causing inhibition of ETC components and loss of ΔΨm. The mechanism by which Drp1 stimulates Zip1 for Zn^{2+} entry into the mitochondria remains unclear (Cho et al., 2019)

Furthermore, it has been demonstrated that the loss of function of SLC-30A9/ZnTP9, the mitochondrial Zn^{2+} exporter, leads to mitochondrial Zn^{2+} accumulation and the consequent damage to mitochondrial structure and function. This impairs development in animals and shortens their life span (Ma et al., 2022).

Taken together, studies indicate important roles for both Ca^{2+} and Zn^{2+} in mitochondrial dynamics, function, and cell viability. However, the underlying molecular mechanisms and the interplay between Ca^{2+} and Zn^{2+} in mitochondrial dysfunction need further investigation.

1.3.4 Mitochondrial membrane potential (ΔΨm)

ΔΨm is the most reliable indicator of mitochondrial function (Bagkos et al., 2014). Its value ranges between -136 to -140 for optimal ATP production. Any deviation from that range could result in a significant drop in ATP production and a large increase in mitochondrial ROS production (Bagkos et al., 2014). Mitochondria use oxidizable substrates such as NADH and $FADH_2$ generated during glycolysis and the Krebs cycle to produce ΔΨm. Deficiency of oxidizable substrates available to the mitochondria and blockage of respiration could result in a decrease in ΔΨm (Gottlieb et al., 2003). Assessment of the ΔΨm in living cells is taken as a proxy for mitochondrial activity. Loss of ΔΨm results in mitochondrial dysfunction and reduced ATP production. Impaired ATP generation coupled with increased ROS production, have adverse effects on cellular function and underlie various pathologies.

Loss of ΔΨm marks mitochondria for selective elimination, and thus, plays a role in mitochondrial homeostasis. Furthermore, ΔΨm influences mitochondrial dynamics. Studies have shown that mitochondrial membrane fusion depends on healthy ΔΨm across the membrane, whereas loss of ΔΨm shifts the mitochondrial dynamics toward fission (Ishihara et al., 2003, Legros et al., 2002).

Loss of ΔΨm leads to Cyt *c* translocation from the matrix to the intermembrane space facilitating its release from the mitochondria into the cytosol. In the cytosol, Cyt *c* induces the assembly of the apoptosome, apoptotic protease activating factor 1 (Apaf-1), and caspase-9 that initiate pathways leading to cell death (Adrain and Martin, 2001, Gottlieb et al., 2003, Hengartner, 2000). Thus, loss of ΔΨm is closely associated with bioenergetic failure, increased ROS production, increased mitochondrial fission and apoptotic cell death.

1.3.5 Mitochondrial fission and neuronal cell death in Parkinson's disease

The human brain may only make up 2% of total body mass, yet it consumes around 20% of the body's resting energy (Harris and Attwell, 2012). Each neuron utilizes ~ 4.7 million ATP molecules per second. ATP production supports the synapse assembly, generation of action potentials and synaptic transmission. Also, in the presynaptic terminals, mitochondria maintain and regulate neurotransmission (Islam, 2017). Therefore, neurons require high amount of energy to maintain their biological functions (Naoi and Maruyama, 1999). Furthermore, it is known that neurons are postmitotic cells that do not exhibit cell division after fetal development is completed and they remain alive and function for decades. Therefore, aged or dysfunctional mitochondria in these cells will have a negative impact on cell function. Thus, the mitochondria play an important role in age-related diseases such as PD (Federico et al., 2012).

Several studies have reported an association between abnormal mitochondrial fission and neuronal diseases such as Parkinson's (Rappold et al., 2014), Huntington's (Guo et al., 2013), and Alzheimer's disease (Reddy et al., 2017). The interaction between genetic predisposition and environment is thought to induce mitochondrial ETC failure and oxidative stress in Substantia nigra neurons leading to neuronal cell death (Schapira et al., 1992). Selective damage of brain dopaminergic neurons in PD has been suggested to be due to impaired mitochondria respiration as a result of complex I dysfunction following MPP^+ uptake through dopamine transporters (Langston and Ballard Jr, 1983). Furthermore, complex I impairment was also found in cybrid cells isolated from patients with PD (Swerdlow et al., 1996). The defect in complex I in PD seems to be related to genetics, and may have a vital role in the neurodegeneration in PD by catalysing ROS generation and increasing the neuronal susceptibility to mitochondrial toxins (Swerdlow et al., 1996). Another study also showed that the level of ROS production in isolated brain cell mitochondria treated with MPP^+ is proportionally associated with the degree of damage to complex I (Perier et al., 2005). MPP^+-induced complex I defect can eventually cause impaired respiration

and ATP production. In vivo studies reported that MPP^+ treatment causes significant reduction in ATP level in whole brain tissue from mouse (Chan et al., 1991). Studies reported that restoration of mitochondrial function can slow down disease progression as well as the neuronal function loss in PD and Alzheimer disease (Onyango et al., 2017).

Abnormal mitochondrial fission and its association with PD has been well documented (Van Laar and Berman, 2009, Nakamura et al., 2011, Feng et al., 2020, Wang et al., 2012, Deng et al., 2008). Oxidative stress induces mitochondrial fragmentation that in turn leads to apoptosis. Studies have shown that MPP^+ induces Drp1 hyperactivity, mitochondrial fragmentation, and dopaminergic neuronal cell death (Barsoum et al., 2006, Meuer et al., 2007). This was further supported by studies which demonstrated that mitochondrial fission and neuronal cell death can be prevented through Drp1 inhibition or mitofusin 1 (Mfn1) overexpression (Gomez-Lazaro et al., 2008). A recent study also supported the link between increased Drp1 levels and neurotoxin (rotenone)-induced PD (Rahimmi et al., 2015). Furthermore, it has been shown that Drp1 inhibition by mitochondrial division inhibitor (Mdivi1) reduces MPP^+-induced neurotoxicity and restored dopamine release in mice (Rappold et al., 2014). All these findings suggest that the inhibition of mitochondrial fission has a protective effect against dopaminergic neuronal death in PD.

Genetic evidence has shown that abnormal mitochondrial dynamics and impaired mitochondrial function are key features of PD. Genes, such as *PINK1*, *Parkin* and *PARK7* regulate mitochondrial structure and function. The *PINK1* gene encodes for PTEN-induced kinase 1, a protein located in the mitochondria. It has a protective effect on the cell by tagging damaged mitochondria and activating the mitophagy pathway through Parkin recruitment (Valente et al., 2004). *PARKIN* is a gene responsible for the pathogenesis of autosomal recessive juvenile parkinsonism (AR-JP) found in patients of different ethnic origins (Kitada et al., 1998). Parkin protein is a ubiquitin protein ligase (E3), involved in the pathway that attaches ubiquitin to certain proteins marking them for degradation by proteasome (Fishman and Oyler, 2002). Mutations in the *Parkin* gene affect the

function of Parkin protein causing selective damage of nigral neurons in the brains of AR-JP patients (Kitada et al., 1998, Shimizu et al., 2000). *PARK7* is another gene which plays a role in the pathology of PD. It encodes DJ-1, a ubiquitous highly conserved protein, but its exact function is still unknown. However, evidence suggests its involvement in regulating calcium influx in mitochondria, and in protecting the cell from the damaging effect of oxidative stress. A study showed that loss of DJ-1 function leads to neurodegeneration (Bonifati et al., 2003)

1.4 Lysosomes

1.4.1 Structure and function

Emerging evidence indicates that lysosomal dysfunction is associated with PD. Lysosomes are specialized single membrane-bound organelles containing a variety of hydrolase enzymes that are responsible for the degradation of macromolecules, entering the cells by endocytosis or intracellular components delivered by autophagy; thus, they play a key role in maintaining cellular homoeostasis (Wang et al., 2018a, Nagakannan et al., 2020). Lysosomes are also involved in other cellular processes such as in immune defence and cell death. In cells of the immune system, lysosomes play an important role in phagocytosis, processing and secretion of cytokines, and antigen presentation (Ge et al., 2015, Udayar et al., 2022). Furthermore, they serve as storage organelles for nutrients and metal ions such as calcium, iron, copper, and zinc (Nagakannan et al., 2020).

There are over 60 different hydrolase enzymes in the lysosomal lumen, including proteases, nucleases, lipases, phosphatases, and glycosidases, which are highly active at the acidic pH (4.5-5) inside the lysosomes and are inactivated at the neutral pH (7.4) of the cytosol (Nagakannan et al., 2020). The low pH is

maintained by the proton pumping v-ATPase, chloride channels and ion transporters that are located in the lysosomal membrane. Other proteins including lysosomal-associated membrane protein 1 and 2 (LAMP-1 and LAMP-2) are thought to protect the lysosomal membrane from degradation by hydrolase enzymes (Wang et al., 2018a).

1.4.2 Lysosomal membrane permeabilization and cell death

Lysosomal membrane permeabilization (LMP) is caused by the damage of lysosomal membranes. Partial LMP results in selective leakage of lysosomal contents such as cathepsins (for example, cathepsin B and D), which activates a cascade of events leading to apoptotic cell death (Wang et al., 2018a, Nagakannan et al., 2020). Complete LMP, on the other hand, results in massive leakage of lysosomal contents causing loss of lysosomal proton gradient, an increase in cytosolic acidity, breakdown of cellular components, and cell death (Wang et al., 2018a). Moreover, increased intracellular acidity can cause mitochondrial acidification leading to loss of $\Delta\Psi m$ and impaired Ca^{2+} homeostasis and apoptotic cell death. The acidic cytosol also provides optimal environment for the activity of released lysosomal hydrolases causing proteolytic degradation of cytosolic proteins contributing to cell death. (Nagakannan et al., 2020)

Several intracellular and extracellular factors can stimulate LMP; they include ROS, proteases, and B-cell lymphoma 2 (Bcl-2) family of proteins which regulate cell death. Excessive ROS production could lead to loss of lysosomal membrane integrity by peroxidation of lysosomal membrane lipids (Fong et al., 1973, Nagakannan et al., 2020). Studies have shown that ROS scavengers can reduce LMP-induced cell death. For instance, the N-acetylcysteine has been shown to have a protective effect against apoptosis and lysosomal damage in the SH-SY5Y cell line (Nagakannan et al., 2016). Lysosomes contain labile redox-active iron resulting from the digestion of many iron-containing macromolecules, such as MT (Nagakannan et al., 2020). In the acidic lumen of lysosomes, the free ferric

iron (Fe^{3+}) is reduced to ferrous state (Fe^{2+}) which reacts with H_2O_2 to form the highly active $OH^{\bullet}$ causing peroxidation of lysosomal membrane lipids and lysosomal damage (Kurz et al., 2008b, Johansson et al., 2010).

As mentioned earlier, proteases such as cathepsins induce apoptotic cell death. Leakage of cysteine cathepsins, mainly cathepsin B, into the cytosol has been shown to cause LMP through degradation of lysosomal membrane proteins LAMP-1 and LAMP-2 (Nagakannan et al., 2020). Also, the Ca^{2+}-dependent cytosolic cysteine proteinase, called calpain, was found to be responsible for LMP by cleavage of LAMP-2 (Rodriguez and Torriglia, 2013, Khorchid and Ikura, 2002). Increased cytosolic Ca^{2+} concentrations can activate calpain and subsequently induce LMP.

1.4.3 Lysosomes in Parkinson's disease

Studies have shown that lysosomal dysfunction in glial and neuronal cells is a pathological hallmark of neurodegenerative diseases, such as Alzheimer's and Parkinson's diseases (Udayar et al., 2022). It has been shown that autophagy plays a role in PD. Lysosomal dysfunction leads to reduced clearance of toxic protein aggregates such as α-synuclein and dysfunctional intracellular organelles such as depolarized mitochondria. Samples from PD patients showed accumulation of autophagosomes in the brain, indicating failure of lysosomal fusion of autophagosomes (Dehay et al., 2010). Furthermore, depletion of lysosomal numbers precedes the autophagosome accumulation in MPP^+-treated dopaminergic neurons. Lysosomal depletion results from LMP caused by excess ROS production (Dehay et al., 2010). Induced permeabilization of lysosomal membrane causes release of hydrolase enzymes into the cytosol which could directly contribute to neurodegenerative diseases, besides affecting the autophagic clearance process. Genetic and pharmacological stimulation of lysosomal biogenesis can restore the lysosomal levels and attenuate MPP^+-induced cell death (Dehay et al., 2010).

Recent studies have provided a better understanding of both physiological and pathophysiological functions of neurodegeneration-related lysosomal genes such as *GBA1*, *LRRK2*, *ATP13A2*, *ATP10B*, *VPS13C*, *C9orf72*, *GRN*, *TMEM175*, *TMEM106B*, and *CHMP2B* (Udayar et al., 2022) many of which have been shown to be associated with PD. Mutations in *GBA1*, *LRRK2* and *ATP13A2* associated with PD will be explained below.

Loss of function mutations in *GBA1* have been shown to trigger PD. The *GBA1* gene encodes β-glucocerebrosidase (GCase). GCase is a lysosomal hydrolase capable of cleaving glucocerebroside and glucosylsphingosine. The mechanism by which mutations in *GBA1* leads to PD remains unclear, however, GCase dysfunction can result in accumulation of lipid in the lysosomes leading to undetectable structural and functional changes at organelle level (Udayar et al., 2022). It has been shown that GCase activation within lysosomes can reduce α-synuclein levels in the midbrain neurons of patients with PD (Mazzulli et al., 2016b). A study using neuronal cells from patients with PD carrying mutations in *GBA1* revealed prolonged mitochondria-lysosome contacts affecting mitochondrial function. These effects could be prevented by enhancing GCase activity, thus suggesting the role of mitochondria-lysosome contacts as an upstream regulator of mitochondrial function in *GBA1*-linked PD (Kim et al., 2021).

Mutations in the *LRRK2* gene, which codes for leucine-rich repeat kinases, also contribute to the pathology of PD. Gain of function mutations in *LRRK2* increase the risk of both familial and sporadic PD (Bonet-Ponce et al., 2020). The PD-linked *LRRK2* mutations promote the recruitment of LRRK2 to damage lysosomes (Bonet-Ponce et al., 2020). Although the underlying mechanism of the role of LRRK2 in PD is poorly understood, it has been reported that *LRRK2* mutations contribute to aggregation of α-synuclein protein because of lysosomal damage (Udayar et al., 2022).

Another important gene, *ATP13A2* (*PARK9*), is associated with autosomal recessive early-onset PD (Park et al., 2014), and encodes a lysosomal ATPase cation transporting ATP13A2. The ATP13A2 protein is located in acidic vesicles, including lysosomes and autophagosomes, suggesting a role in autophagy-lysosomal pathway (ALP) (Park et al., 2014). ATP13A2 is a cation pump for several metal ions, mainly Ca^{2+} Mn^{2+} and Zn^{2+}. Studies have shown that Mn^{2+} is one of the environmental risk factors of PD, and Mn^{2+} cytotoxicity has been linked with ATP13A2 knockout in various cell models (Tan et al., 2011, Gitler et al., 2009). ATP13A2 can prevent Mn^{2+} cytotoxicity by reducing intracellular Mn^{2+} levels and Cyt *c* released from mitochondria (Tan et al., 2011). Zn^{2+} is another environmental risk factor for PD. Although Zn^{2+} dyshomeostasis has a major pathological influence in PD, the underlying cell biological mechanisms are unclear.

However, it has been reported that mutations in ATP13A2 caused not only loss of lysosomal function, but also mitochondrial dysfunction (Park et al., 2011, Grünewald et al., 2012). Furthermore, using patient-derived human olfactory neurosphere (hON) with ATP13A2 deficiency, Park et al. (2014) demonstrated that loss of ATPA13A2 caused an increase in cytosolic Zn^{2+} because of impaired cellular buffering capacity of cytosolic Zn^{2+} resulting from poor Zn^{2+} sequestration by lysosomes (Park et al., 2014). Increased cytosolic Zn^{2+} induces mtROS production leading to loss of $\Delta\Psi m$, mitochondrial dysfunction and oxidative stress. Prolonged mitochondrial dysfunction is accompanied by mitochondrial fission leading to ATP depletion and cell death (Park et al., 2014).

Thus, studies on *PARK9* mutations support a role for Zn^{2+} dyshomeostasis in dysfunction of lysosomes and mitochondria in the context of PD.

1.5 Cell death

1.5.1 Physiological and pathophysiological roles of cell death

Cell death is an essential biological process required for the elimination of cells that are harmful or no longer needed (Kaiser et al., 2020). It is a vital process in normal physiology, that together with cell proliferation, helps to maintain the homeostasis in human body (Elmore, 2007). Cell death is important during developmental processes. For example, the nervous and immune systems develop through overproduction of cells, however, overproduction of cells is followed by the death of unwanted cells that failed to establish functional synaptic connections or produce antigen specificities, respectively (Elmore, 2007). This process of programmed cell death is commonly known as apoptosis.

Dysregulation of cell death may lead to pathophysiology such as developmental defects, autoimmune disorders, cancer, ischemia and neurodegenerative diseases (Elmore, 2007). Excessive apoptosis is thought to be involved in autoimmune diseases such as, the autoimmune deficiency syndrome (AIDS) (Li et al., 1995). Much of our understanding of apoptosis comes from studies of cancer cells. Tumour cells use different mechanisms to suppress apoptosis including the downregulation of pro-apoptotic proteins, such as Bax. (Kerr et al., 1994, Elmore, 2007). Also, a role for the pro-apoptotic *Bax* gene in myocardial ischemia injury has also been reported (Hochhauser et al., 2003). Overexpression of Bax has been detected in ischemic myocardial tissue, and Bax-deficient mice showed reduced damage to mitochondria and the nuclear chromatin morphology, indicating reduced apoptosis. Therefore, it is suggested that Bax might be considered as a potential therapeutic target in myocardial ischemia (Hochhauser et al., 2003). The role of apoptosis in neurodegenerative diseases will be discussed in section 1.5.3.

1.5.2 Mechanism of cell death

Historically, three types of cell death have been identified: apoptosis, autophagy, and necrosis. However, as this field is still developing, an updated classification focussing on the mechanistic and fundamental aspects of this process has been proposed. These include intrinsic apoptosis, extrinsic apoptosis, mitochondrial permeability transition-driven necrosis, necroptosis, ferroptosis, pyroptosis, parthanatos, entotic cell death, lysosome-dependent cell death, autophagy-dependent cell death, immunogenic cell death, cellular senescence, and mitotic catastrophe (Galluzzi et al., 2018).

Whether a cell dies by apoptosis, autophagy or necrosis is determined mainly by the nature and severity of the cell death insult and the biochemical pathways involved. Autophagy manifests a substantial cytoplasmic vacuolization and culminates in phagocytic uptake and subsequent lysosomal degradation (Galluzzi et al., 2018). On the other hand, apoptosis and necrosis exhibit different morphological features which will be discussed in the next section.

1.5.2.1 Apoptosis

Apoptosis is characterized by specific morphological changes including cell shrinkage, chromatin condensation, nuclear fragmentation, a reduction of cellular volume, and plasma membrane blebbing but without affecting its integrity until the final stages of apoptosis (Kroemer et al., 2009). During apoptosis, the cell breaks up into fragments called apoptotic bodies. These cell fragments are engulfed by neighbouring cells and phagocytes where they are degraded into small molecules and reused to build new cells. Since the plasma membrane is intact and does not rupture during this process, there is no leakage of cellular contents and therefore apoptosis is not associated with an inflammatory immune response (Kaiser et al., 2020).

In apoptotic cells, many of the morphological changes are thought to be derived from activation of one or more specific proteases known as caspases. Caspases are present in their inactive forms. They are divided into two types: initiator caspases, including caspase-2, -8, -9, and -10, and the effector caspases that include caspase-3, -6, and -7. The caspases-dependent apoptosis could be triggered by either extrinsic (cell surface receptor-linked, caspase 8) or intrinsic (mitochondrial depolarization-linked, caspase 9) pathways (Lockshin and Zakeri, 2004). Caspases are responsible for some of the morphological changes seen in apoptotic cells. They cleave intracellular proteins, such as nuclear and cytoskeletal proteins which precede the nuclear condensation and the plasma membrane blebbing. Caspases are also involved in phosphatidylserine exposure which is a signal for phagocytosis and clearance of apoptotic cells (Orrenius et al., 2003). Bcl-2 family is a group of proteins that work in conjunction with caspases to regulate cell death. They are divided into two types, anti-apoptotic (e.g., BCL-X_L, BCL-2, MCL-1) and pro-apoptotic (e.g., Bax and BAK) proteins. These proteins are translocated from the cytosol to the mitochondria to regulate apoptotic events (Orrenius et al., 2003).

Extrinsic (receptor-linked) pathway

This pathway is mediated by pro-apoptotic ligands such as tumor necrosis factor-related apoptosis-inducing ligand (TRAIL), that interacts with specific cell surface death receptors to form the death-inducible signaling complex (DISC) (Elmore, 2007). DISC activates the initiator caspase-8 which, in turn, activates the effector caspase-3 leading to apoptosis. Caspase-8 can also cleave Bid (a pro-apoptotic protein) which induces the translocation and insertion of Bax and Bak into the outer mitochondrial membrane to form a pore (mitochondrial outer membrane permeabilization, MOMP) through which Cyt *c* is released into the cytosol. In the cytosol, Cyt *c* associates with apoptotic activating factor-1 (Apaf-1) and pro-caspase-9 in the presence of dATP to form an apoptosome complex. This complex activates pro-caspase-9 that, in turn, activates caspase-3, leading to nuclear condensation and fragmentation (Figure 1.4). (Orrenius et al., 2003).

Intrinsic (mitochondria-linked) pathway

In the intrinsic pathway, the death stimulus acts directly or indirectly on mitochondria leading to cell death. In the early stages of apoptosis, death signals induce certain intracellular events including increased Ca^{2+} and ROS levels, and translocation of the pro-apoptotic Bax and Bak to the mitochondrial outer membrane to form MOMP (Mattson, 2000). The later stages of apoptosis include the formation of a pore in the inner mitochondrial membrane, referred to as mPTP (mitochondrial permeability transition pore). Although the structural basis for mPTP formation is unclear, by increasing the permeability of the inner membrane, mPTP promotes nonselective diffusion of ions and other small molecules, including H^+ ions, Ca^{2+} and ROS. This results in bioenergetic failure (due to collapse of H^+ gradient, required for ATP synthesis), increased oxidative stress and release of Cyt *c* into the cytoplasm. The intrinsic pathway also promotes translocation of apoptosis inducing factor (AIF) and endonuclease G (EndG) from mitochondria to the nucleus where they cause chromatin condensation and fragmentation. All these events collectively contribute to apoptotic cell death (Orrenius et al., 2003) (Figure 1.4).

1.5.2.2 Necrosis

Necrosis is another form of cell death that occurs when cells are exposed to injury or extreme stress, such as heat, lack of oxygen, or infection by pathogens. The morphological characteristics of cells undergoing necrosis include gain in cell volume (oncosis), swelling of organelles, rupture of plasma membrane and subsequent loss of intracellular contents (Kroemer et al., 2009). These changes lead to inflammatory responses including temperature, pain, swelling and phagocytic removal of necrotic cells, and initiate repair of damaged tissue (Kaiser et al., 2020). Unlike apoptosis, necrosis is an accidental uncontrolled form of cell death (Kroemer et al., 2009). Furthermore, necrosis could activate another mechanism of cellular suicide, known as necroptosis, which is often initiated by

extracellular cytokines such as the tumor necrosis factor alpha (TNFα). This form of cell death usually causes inflammation and is associated with several diseases including neurodegeneration and atherosclerosis (Kaiser et al., 2020).

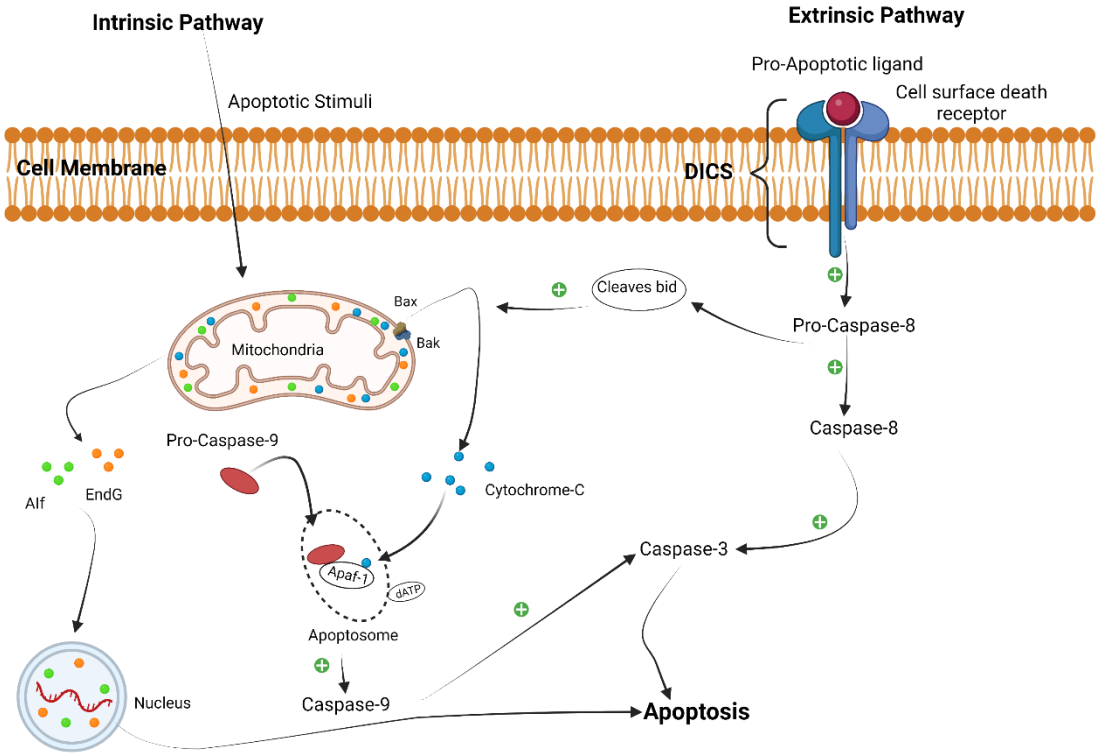

Figure 1.4 Signaling pathways that induce cell death (apoptosis).

A schematic diagram showing the intrinsic and extrinsic pathways of apoptosis. In the intrinsic pathway, the death stimulus acts on mitochondria leading to the assembly of the apoptosome complex. It involves the translocation of the pro-apoptotic members of Bcl-2 family, Bax, and Bak to the outer mitochondrial membrane which promotes cytochrome *c* (Cyt *c*) release from the mitochondria to the cytosol. It also involves the translocation of apoptosis inducing factor (AIF) and endonuclease G (EndG) from mitochondria to the nucleus where they cause chromatin condensation and fragmentation. In the extrinsic pathway, pro-apoptotic ligands, such as tumour necrosis factor-related apoptosis-inducing ligand (TRAIL), bind the conjugate cell surface death receptors to form the death-inducible signaling complex (DISC). DISC activates caspase-8 which in turn

stimulates the effector caspase-3 leading to apoptosis. Caspase-8 can also cleave Bid (a pro-apoptotic protein) which induces the translocation and insertion of Bax and Bak into the outer mitochondrial membrane to from MOMP through which Cyt *c* is released. In the cytosol, Cyt *c* forms an apoptosome complex of apoptotic activating factor-1 (Apaf-1) and pro-caspase-9 in the presence of dATP. The apoptosome complex activates pro-caspase-9 and then caspase-3, leading to apoptosis. Figure adapted from (Orrenius et al., 2003), and created with BioRender.com

1.5.3 Apoptosis in neurodegenerative diseases

Neurodegenerative diseases are complex disorders where both genetic and environmental factors are thought to be involved. However, it is believed that these diseases share a common signaling pathway leading to neuronal cell death. The pathway involves ROS, disturbed calcium homeostasis, mitochondrial dysfunction, and activation of caspases (Mattson, 2000).

Apoptosis is the underlying cause of many neurological disorders in humans such as Alzheimer's, Parkinson's, and Huntington's disease (Ethell and Buhler, 2003). Alzheimer's disease is associated with the deposition of amyloid-*β* which is neurotoxic when in its aggregated form. Amyloid-*β* can induce apoptosis by causing oxidative stress or by activating TNFα secretion by microglia (Elmore, 2007). Huntington's disease is another neurodegenerative disorder that results from specific neuronal loss and dysfunction in the striatum and cortex regions of brain (Ona et al., 1999). A study has reported that caspase-1 is important in the pathogenesis of this disease. In the transgenic mouse model of Huntington's disease, reduced caspase-1 expression extends the survival, protects against cell death, and delays the appearance of neuronal inclusions and onset of symptoms (Ona et al., 1999). Another study using lymphoblasts from patients with Huntington's disease showed increased stress-induced apoptotic cell death associated with increased mitochondrial depolarization and caspase-3 activation (Mattson, 2000, Sawa et al., 1999).

Studies of neuronal cell death in PD suggest a central role for oxidative stress. Increased iron levels, low complex I activity, and a decrease in the reduced form of glutathione (GSH) levels are all detectable pathophysiological features in PD. Low GSH levels increase the oxidative stress leading to cell death. This occurs in the pre-symptomatic stage of PD and promotes neuronal degradation or make neurons more vulnerable to neurotoxins (Jenner and Olanow, 1998).

Investigation of brain tissue from patients with Parkinson's diseases showed a link between the apoptosis-related DNA damage and the death of dopaminergic neurons (Jenner and Olanow, 1998). A study reported that caspase-1 mediated mechanisms are shared in different chronic and neurodegenerative diseases such as, ischemia, PD, and Huntington's disease (Ona et al., 1999). Moreover, as mentioned earlier, one of the major hallmarks of PD is the formation of Lewy bodies in the substantia nigra which are formed by the aggregation of damaged or mutant α-synuclein. Experiments using human neuroblastoma SH-SY5Y cell-line has shown that expression of mutant α-synuclein can induce apoptotic cell death (El-Agnaf et al., 1998). Taken together, studies have supported a role for apoptotic cell death in the pathology of several neurodegenerative diseases.

1.6 Human TRPM2 (*hs*TRPM2) channels

The Transient receptor potential (TRP) channel was originally identified from genetic studies on visual transduction in photoreceptors of the fruit fly (*Drosophila Melanogaster*) (Minke et al., 1975). The TRP family consists of six subfamilies. They mainly conduct Ca^{2+}, but some members of the TRP family are capable of conducting other cations including Na^{+}, K^{+}, Mg^{2+}, and Zn^{2+}. The transient receptor potential melastatin (TRPM) subfamily consists of eight members that are divided into four groups. These are TRPM1 – TRPM3, TRPM4 – TRPM5, TRPM6 – TRPM7, and TRPM2 – TRPM8. This classification is based on their sequence homology. Of these, TRPM2 and TRPM8 have been widely studied (Naziroglu, 2011). TRPM2 is a non-selective cation channel (PCa/PNa = 0.5-5) (Owsianik et al., 2006) that allows Ca^{2+} influx across the plasma membrane (Nagamine et al., 1998, Sano et al., 2001, Perraud et al., 2001, Hara et al., 2002, Sumoza-Toledo and Penner, 2011).

1.6.1 *hs*TRPM2 structure

TRPM2, formerly known as TRPC7 or LTRPC2, was first described in 1998 (Nagamine et al., 1998). The structure of human (*homo sapiens*) TRPM2 (*hs*TRPM2) is recently described (Wang et al., 2018b). It is a tetramer; each subunit consists of 1503 amino acids (~171 kDa). The Cryo-electron microscopy (Cryo-EM) structure of TRPM2 showed an umbrella shaped architecture with dimensions of approximately 100 Å by 100 Å by 150 Å (Figure 1.5). Each monomer comprises six transmembrane segments (S1-S6) with N- and C-termini facing the cytosol. The N-terminal domain consists of four TRPM-homology regions (MHRs), MHR 1/2, MHR 3, and MHR 4 domains, followed by the six transmembrane (TM) regions. The TM region is composed of a voltage sensor-like domain (VSLD) (S1-S4), and a pore domain (S5-S6). The C-terminal contains the TRP helices (H1 and H2), rib helix, and pole helix, followed by the unique Nudix-type motif 9 homology domain (NUDT9H) (Figure 1.5) (Xia et al., 2019, Perraud et al., 2001, Sumoza-Toledo and Penner, 2011). NUDT9H was predicted to hydrolyse ADPR in 2003 (Perraud et al., 2003). The activity of NUDT9H in TRPM2 varies in different species. For example, in *nv*TRPM2 of sea anemone, NUDT9H hydrolyses ADPR. While in human *hs*TRPM2, the domain binds ADPR but does not cause hydrolysis as it lacks the enzymatic activity because of the absence of key glutamate residues (Shen et al., 2003, Xia et al., 2019). The significance of these differences between the domains of NUDT9H of different species is not fully understood but suggests complexity of channel activation and gating.

The high-resolution structure of *hs*TRPM2 revealed an overall three-tiered architecture (Figure1.5 C), and between them there is a Ca^{2+} binding site in the VSLD, and an ADPR binding site in the NUDT9H domain. The bottom tier comprises the C-terminal NUDT9H and the pole helix, and the N-terminal MHR1/2 and MHR 3. The middle tier comprises the MHR 4 domain and the rib helix. Finally the top tier includes the TM domain and the TRP helices (Wang et al., 2018b).

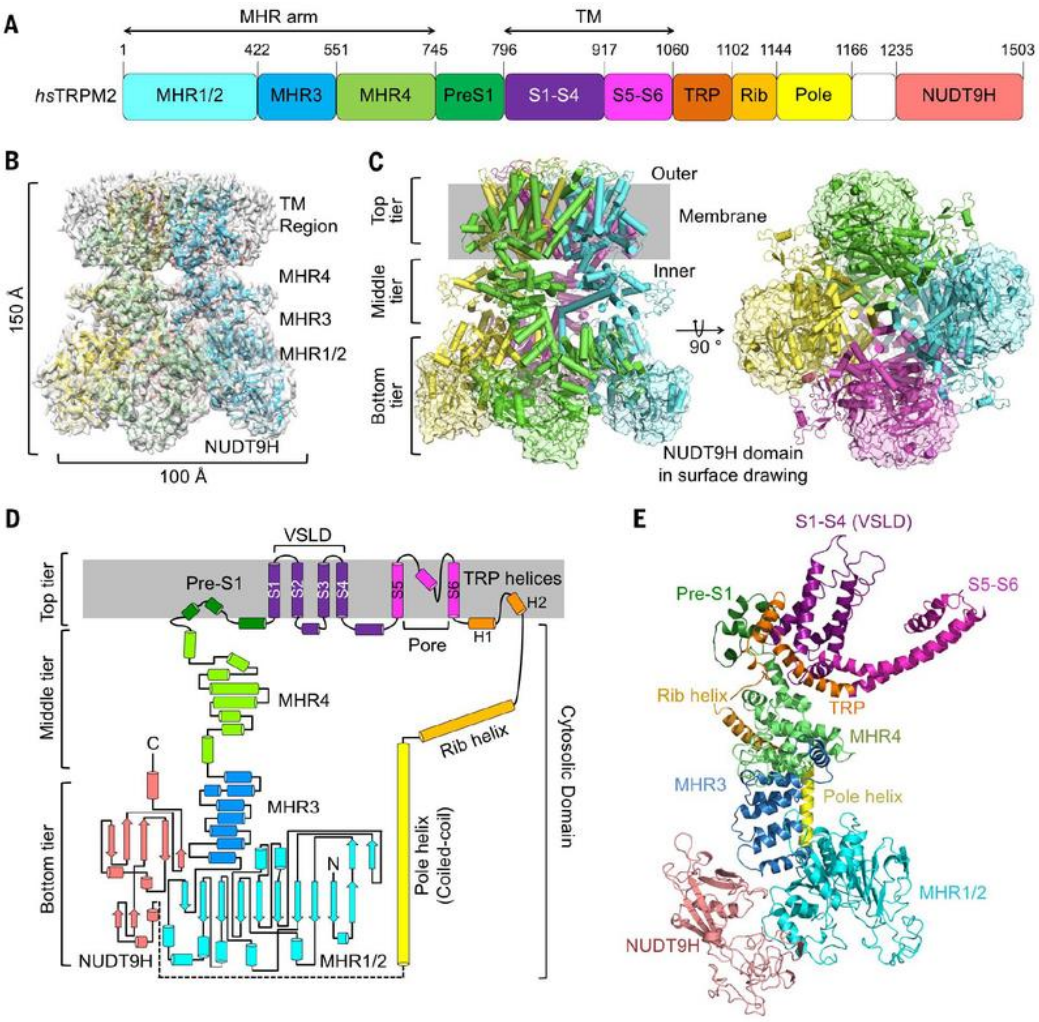

Figure 1.5 The structure of Human TRPM2 (*hs*TRPM2).

The diagram shows the structure of *hs*TRPM2 structure in its apo-state. (A) The arrangement of domains composing *hs*TRPM2, with residue numbers being shown above. (B) Side view of a 3D cryo-EM image. The estimated dimension of the tetramer is 100 Å by 100 Å by 150 Å. (C) Ribbon diagram of the three-tier architecture of the *hs*TRPM2 showing the four differently coloured subunits in two orthogonal views. (D) Schematic of single subunit with its main structural components and their arrangement, using the same colour scheme as in (A). (E) A ribbon diagram of (D). (Wang et al., 2018b)

This structure provides a better understanding of the gating mechanism of the TRPM2 channel. NUDT9H, which is responsible for sensing ADPR, is located in close proximity to MHR1/2 and MHR3 in the same subunit. Three contact areas were identified: interface I, II, and III. Interface I and II of NUDT9H interact with MHR1/2 and MHR3, respectively, of its own subunit (*cis*-interaction). Interface III mediates intersubunit interactions with the neighbouring subunit (*trans*-interaction) at the bottom tier (Figure 1.6) (Wang et al., 2018b, Xia et al., 2019). In the apo (closed-inactive) state, *trans*-interaction occurs causing the channel closure by limiting the movements of the subunits in the absence of ligands (Xia et al., 2019). When ADPR binds to NUDT9H (primed state), the NUDT9H and MHR 1/2 undergo a large 27° rotation (counter clockwise), causing disruption of *trans*-interaction to prime the channel for further conformational changes upon Ca^{2+} binding. Next, when both ADPR and Ca^{2+} are bound (open state) to TRPM2, it induces 15° rotation in the cytoplasmic domain, a tilt at the TRP H1 to drag the S6 helix leading to enlargement of the pore, opening the channel and allowing Ca^{2+} influx (Figure 1.6). (Xia et al., 2019)

1.6.2 Cellular distribution

TRPM2 channels are expressed in several tissues including the brain, liver, spleen, heart, vasculature, pancreas, and immune cells (Jang et al., 2014, Hecquet et al., 2010, Lange et al., 2009). At the cellular level, they are expressed at the plasma membrane as well as in the lysosomes (Lange et al., 2009)

In the central nervous system (CNS), TRPM2 mRNA is most prevalent among transient receptor potential (TRP) channels (Fonfria et al., 2006). Quantitative real-time polymerase chain reaction (qRT-PCR) analysis of TRPM2 mRNA expression found that it is most abundant in the brain, where they contribute to CNS physiology and pathophysiology (Belrose and Jackson, 2018). Within the CNS, microglia, astrocytes, and neuronal populations in the hippocampus, substantia nigra, striatum, and cortex, as well as dorsal root ganglion sensory

neurons, have all been shown to express TRPM2 (Belrose and Jackson, 2018, Fonfria et al., 2006, Hill et al., 2006). Exposure to ROS or intracellularly administered of ADPR can activate TRPM2 in these cells in the presence of Ca^{2+} (Belrose and Jackson, 2018, Olah et al., 2009).

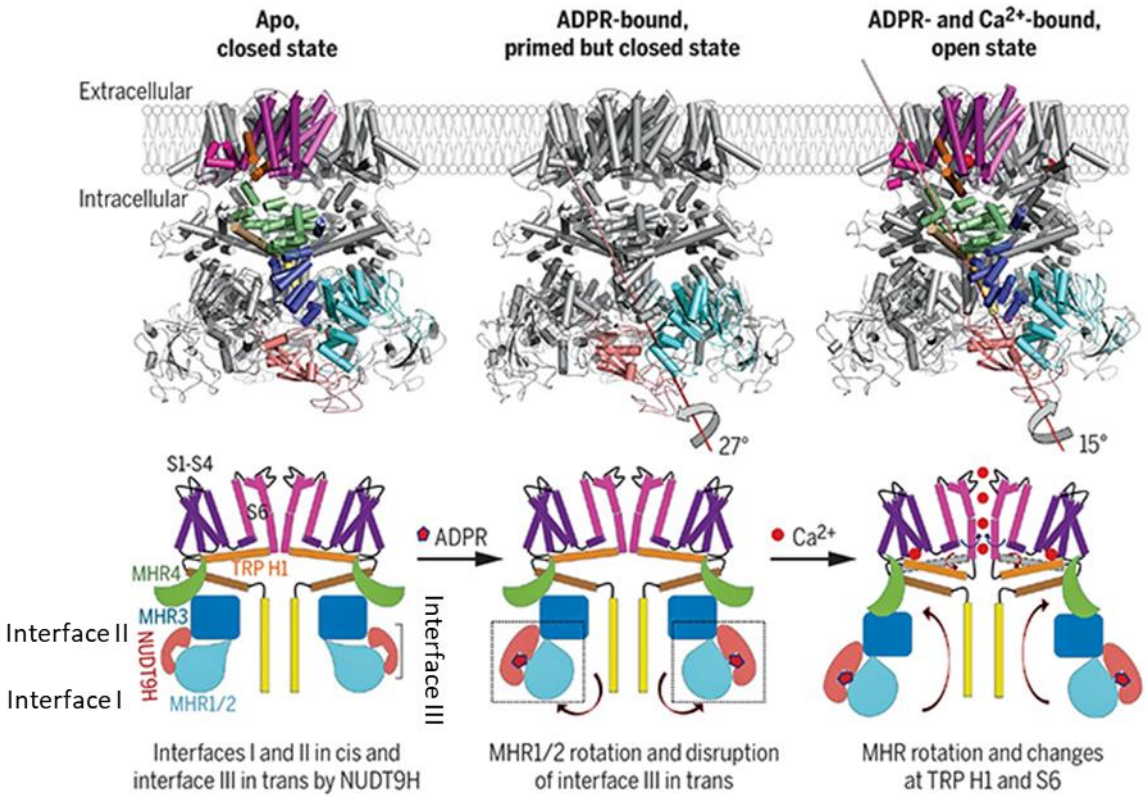

Figure 1.6 The gating mechanism of the human TRPM2 channel (*hs*TRPM2).

(*Top*) Cryo-EM of TRPM2 structure in apo (closed state), ADPR-bound (primed closed state), ADPR- and Ca^{2+}-bound (open state). (*Down*) corresponding drawing that demonstrate the process of gating TRPM2 channel. (Wang et al., 2018b)

1.6.3 TRPM2 function, activation, and disease association

The TRPM2 channel is a non-selective, voltage independent cation channel, capable of sensing oxidative stress (Jiang et al., 2010). By raising the cytoplasmic Ca^{2+} level, TRPM2 plays essential roles in cell death (Kaneko et al., 2006) and a number of other functions, including in immune responses (Massullo et al., Knowles et al., 2013), cell proliferation (Zeng et al., 2010a), and insulin secretion (Kashio and Tominaga, 2017). Furthermore, it is expressed in sensory neurons and mediates sensation of warmth. It has been reported that TRPM2 is expressed in warmth-sensitive neurons (WSNs) of the hypothalamus, where it serves as a thermosensitive channel (Song et al., 2016). At the subcellular level, TRPM2 regulates mitochondrial dynamics (Abuarab et al., 2017, Li et al., 2017a).

On the other hand, studies have shown that TRPM2 plays a role in oxidative stress-induced death of many types of cells including neuronal, cardiac endothelial and pancreatic-β cells (Abuarab et al., 2017, Li et al., 2017a, Manna et al., 2015, Kaneko et al., 2006) as a result of increased Ca^{2+} influx and Zn^{2+} dyshomeostasis. The death of pancreatic-β cells and neuronal cells could be prevented by small interfering RNA against TRPM2 or deletion of the TRPM2 gene in mice (Kaneko et al., 2006, Manna et al., 2015). In vivo mouse studies have shown that knock-out of TRPM2 channels prevents streptozotocin-induced type 1 diabetes (Manna et al., 2015) and development of post-ischemic brain injury (Ye et al., 2014). Knock-out of TRPM2 channel also prevents high fat diet induced insulin resistance in mice indicating a role for TRPM2 in type 2 diabetes (Zhang et al., 2012).

Moreover, a number of studies have reported an association of abnormal activation of TRPM2 with other diseases (Yamamoto and Shimizu, 2016) including stroke (Wang et al., 2021, Ye et al., 2014), vascular damage (Alves-Lopes et al., 2020), inflammation (Yamamoto and Shimizu, 2016), and cancer cell migration (Li et al., 2016). TRPM2 channels have also been implicated in neurodegenerative disorders such as Alzheimer's (Yamamoto et al., 2007) and PD (Hermosura and Garruto, 2007). Therefore, TRPM2 channels could be considered as a potential therapeutic target.

TRPM2 channel activation causes Ca^{2+} influx, leading to the elevation of cytosolic Ca^{2+}. Elevated cytosolic Ca^{2+} affects several intracellular signaling events, including mitochondrial fission (Abuarab et al., 2017, Li et al., 2017a). TRPM2 channels can be activated by different intracellular and extracellular factors. Intracellularly, it is activated by ADPR, Ca^{2+}, and H_2O_2. Cytosolic ADPR is the most potent TRPM2 activator since it binds to the NUDT9-H domain and gates the channel to allow Ca^{2+} influx (Launay et al., 2001). ADPR activation of TRPM2 requires Ca^{2+} binding to the TM domain, as without Ca^{2+} binding, the channel is inactive (closed). However, intracellular Ca^{2+} is capable of activating the TRPM2 channels independent of ADPR, the mechanism of which is not yet clear, but is thought to involve a calmodulin-binding IQ-motif which is identified between residues 404-416 and is thought to induce conformational changes in N-terminus of TRPM2 protein upon Ca^{2+} binding (Du et al., 2009a). TRPM2 can also be activated by other nucleotides including cyclic adenosine diphosphate ribose (cADPR), nicotinamide-adenine dinucleotide (NAD), nicotinic acid adenine dinucleotide (NAAD) and NAAD-phosphate (NAADP), but the mechanisms by which they activate the channel remains unclear (Rosenbaum, 2015).

ADPR is generated from the hydrolysis of NAD^+ and/or cADPR by glycohydrolases such as the ectoenzymes CD38 and CD157. Mitochondria are the major source of ADPR (Sumoza-Toledo and Penner, 2011). Mitochondrial membranes are impermeable to NAD^+ that is found in mitochondrial matrix, but the influx of Ca^{2+} into the mitochondria induces the mPTP to NAD^+ release. Then NAD^+ is converted into ADPR by the action of NADase that is found in the outer membrane of the mitochondria (Ayub and Hallett, 2004). Therefore, NAD^+ activates the TRPM2 channel indirectly through hydrolysis to ADPR; Ca^{2+} at high concentration is thought to stimulate ADPR production from mitochondria (Ayub and Hallett, 2004). ADPR can also be generated in the nucleus. This occurs by the combined action of poly-ADPR-polymerases (PARP) and poly-ADPR-glycohydrolases (PARG) in response to DNA damage (Sumoza-Toledo and Penner, 2011). In response to ROS-induced DNA damage, PARP breaks down NAD^+ to nicotinamide and ADPR. ADPR is then polymerized onto different

nuclear proteins that activate the DNA repair pathways. PARG degrades ADPR polymers generating free ADPR that subsequently activates TRPM2 channels (Sumoza-Toledo and Penner, 2011).

Furthermore, TRPM2 can be directly activated by H_2O_2, as revealed by the finding that a mutation in the N-terminal sequence between 307-316 residues can revoke TRPM2 response to H_2O_2 (Hara et al., 2002). Later, another study reported a role for methionine 214 in N-terminal domain in TRPM2 activation by H_2O_2, (Kashio et al., 2012).

Although these TRPM2 activators can independently activate the channel, they have synergistic effects with other influences such as temperature (Togashi et al., 2006, Kashio and Tominaga, 2017). It has been reported that H_2O_2-induced TRPM2 activation is promoted by temperature elevation (Kashio and Tominaga, 2017). TRPM2 activity is also influenced by cellular acidification. The function of TRPM2 channel is completely inhibited when the cells are exposed to external or internal pH between 5 and 6 (Du et al., 2009b).

To date, there are no pharmacological inhibitors that can specifically target the TRPM2 channel. However, there are some blockers that can effectively work on TRPM2, such as 2-aminoethoxydiphenyl borate (2-APB) (Togashi et al., 2008), N-(5,6-Dihydro-6-oxo-2-phenanthridinyl)-2-acetamide hydrochloride (PJ34) (Fonfria et al., 2004), *N*-(*p*-amylcinnamoyl)anthranilic acid (ACA) (Kraft et al., 2006), flufenamic acid (FFA) (Hill et al., 2004a), and antifungal imidazoles, such as, clotrimazole and econazole (Hill et al., 2004b). Genetic knockdown of TRPM2 or siRNA-based approaches, have been successfully used to underpin the cellular and physiological roles of TRPM2 channels.

Presently, there are no treatments that can modify the progression of PD. Dopaminergic drugs are mostly used to control the symptoms. However, because these drugs do not prevent disease progression and the underlying neurodegeneration, they lose their effectiveness in controlling disease symptoms

with time. Several ion channels have been implicated in the regulation of dopamine release, neuronal activity and neuronal viability in substantia nigra pars compacta (Duda et al., 2016). As such, dysregulation of these channels is thought to be associated with the degeneration of dopaminergic neurons in PD. Thus, targeting ion channels is a promising approach for prevention neurodegeneration (Daniel et al., 2021).

1.7 Therapeutic approaches to Parkinson's disease

Currently, there are no medicines that can cure or slow down the progression of PD. The main line of treatment involves administering a combination of Levodopa and Carbidopa. By replacing the dopamine lost due to dopaminergic neuronal death, these drugs reduce the symptoms in PD patients. However, new understanding of the genetic, cellular, and molecular mechanisms of dopaminergic cell death in PD is beginning to highlight new therapeutic opportunities.

1. *Therapeutics targeted to ROS*: As mentioned in section 1.2.5.1, increased ROS production is a characteristic feature of both genetic and sporadic forms of PD. Attempts were made to target the major sources of ROS, viz., NOX2 and mitochondria. Antioxidants such as CoQ10 (CoenzymeQ10) and mitochondria-targeted antioxidants such as MitoQ (mitoquinone mesylate) were found to be effective in animal studies and protected against mitochondrial damage-mediated neurotoxicity (Murphy and Hartley, 2018, Miquel et al., 2014, McManus et al., 2011). MitoQ prevented ROS overproduction and loss of ΔΨm in neurons which had a protective effect against the progression of AD-liked neuropathology, thus supporting the use of mitochondria-focused therapies for the treatment of oxidative stress-related disorders (McManus et al., 2011). Although CoQ10 and MitoQ data are promising in animal models, they had no effect in PD in clinical trials (Snow et al., 2010, Chaturvedi and Flint Beal, 2013). It is clear that targeting ROS is a useful therapeutic strategy for treating

many oxidative stress-related diseases such as PD; however, the lack of success of these drugs in clinical trials could be attributed to the fact that these drugs cannot distinguish between beneficial ROS and harmful ROS.

2. *Therapeutics targeted to Lysosomes*: As explained in sections 1.4.3, lysosomal dysfunction is a key feature of PD, and that GCase and LRRK2 play key roles (Udayar et al., 2022, Ysselstein et al., 2019a). Thus, attempts are being made to test the potential of activators of GCase and inhibitors of LRRK2 for PD treatment (Ysselstein et al., 2019b). Currently, phase 1b clinical studies of LRRK2 kinase inhibitors are in progress and target PD patients with and without *LRRK2* mutations (Ysselstein et al., 2019a). In addition, clinical studies of GCase activators in patients with *GBA1*-PD are also ongoing. It was shown that the GCase level is persistently low in LRRK2 mutant neurons, which suggests that activating GCase may also be beneficial for *LRRK2*-PD patients (Ysselstein et al., 2019a). Increased lysosomal GCase activity was sufficient to reduce the buildup of oxidised dopamine and α-syn in the neurons of PD patients (Ysselstein et al., 2019a).

3. *Therapeutics targeted to mitochondria*: Increased mitochondrial fission is a characteristic feature of neurons in PD (Van Laar and Berman, 2009). Targeting Drp-1, a key regulator of mitochondrial fission (see section 1.3.2), could be a novel approach to PD treatment. The mitochondrial division inhibitor 1 (mdivi1), a chemical that can cross the blood-brain barrier, is known to be a pharmacological Drp1 inhibitor (Feng et al., 2020). It is found that mdivi1 can inhibit the OMM's permeabilization and prevent the release of apoptotic proteins from the mitochondria to the cytosol (Grohm et al., 2012). Knocking-down Drp1 or treatment with mdivi1 reduces mitochondrial ROS in activated microglial cells (Park et al., 2013), preventing mitochondrial fission, loss of MPP, and the death of neurons (Grohm et al., 2012). Importantly, mdivi1 has been shown to have a neuroprotective effect against oxidative stress and mitochondrial

fragmentation associated with α-syn mutation (A53T) in a PD animal model (Bido et al., 2017). Despite these promising findings and the fact that Drp1 was first recognized as a potential target in diseases associated with mitochondrial dynamics, subsequent studies demonstrated that deletion of the Drp-1 gene is embryonically lethal (Ishihara et al., 2009, Wakabayashi et al., 2009). Also, the mdivi1 effect in human neurons was disappointing and failed to specifically inhibit Drp1, although it can suppress mitochondrial Complex I and modify mitochondrial ROS generation (Bordt et al., 2017). In addition, recent research in a pig model suggests that mdivi1 has no effect on mitochondrial morphology (Ong et al., 2019, Feng et al., 2020). Thus, it is essential to investigate further the mechanism through which mdivi1 targets Drp1 and mitochondria fission.

Clinical trials targeting mitochondrial dynamics in PD were faced with another obstacle. In animal studies, the intervention is administered in the presymptomatic stage, whereas, in humans, at the point of diagnosis of the neurodegenerative disease and recruitment into clinical trials, the implicated pathological features are underway and cannot be reversed (too late to interfere at the level of mitochondria). Hence, the therapeutic window had already passed by the time symptoms develop. (Murphy and Hartley, 2018)

4. *Therapeutics targeted to α-synuclein aggregates*: Since aggregated α-synuclein is a key pathological feature of PD (see Section 1.1.2), aggregates being found in Lewy bodies of patient brains, monoclonal antibodies have been developed against the aggregates. However, recent clinical trials using the antibody approach provided disappointing results (Whone, 2022). Therefore, it is crucial to pursue other PD-associated protein targets. For example, targeting ion channels, such as TRPM2, may provide a new therapeutic approach.

In light of the above, it is essential to understand how PD-causing agents affect the signalling mechanisms underlying ROS regulation and lysosomal and mitochondrial homeostasis associated with dopaminergic cell death.

1.8 Aim of the thesis

The overall aim of this thesis is to understand how the PD causing MPP^+ toxin affects ROS, the intracellular organelle dynamics, and cell survival in a cellular model of PD. Specific aims of the thesis are:

1. To investigate the role of the TRPM2 channel in MPP^+-induced oxidative stress and cell death through understanding the dynamics of three important players (ROS, Ca^{2+} and Zn^{2+}) in this process.
2. To study how TRPM2-Ca^{2+}-Zn^{2+} signaling impacts the function of intracellular organelles to cause dopaminergic neuronal cell death.
3. To test the ability of antibodies produced against an extracellular epitope of the TRPM2 channel to prevent MPP^+- induced intracellular cytotoxic events and neuronal cell death.

Chapter 2
Materials and Methods

2.1 Materials

2.1.1 Cell lines

- Human neuroblastoma cell line (SH-SY5Y) was from ATCC (CRL-2266)– Manassas, VA, USA.
- Human embryonic Kidney cells expressing TRPM2 (HEK-TRPM2^{tet} cells) was obtained from Dr A.M Scharenberg, University of Washington, Seattle, WA, USA.

2.1.2 Cell Culture medium

- DMEM (Dulbecco's Modified Eagle Medium) + GlutaMAX-1 was purchased from Invitrogen (Gibco Life Technologies, UK).
- Opti-MEM® (1x) from Gibco® Life Technologies, USA.
- 0.05% Trypsin-EDTA solution (1%) from Sigma-Aldrich.
- TrypLE™ Express enzyme (1x) was purchased from Thermo Fisher Scientific.
- (DPBS) Dulbecco's phosphate buffered saline from Sigma-Aldrich
- FBS (Fetal bovine serum) from Gibco® Life Technologies, USA.
- Antibiotics (10000 U/ml penicillin and 10000 µg/ml streptomycin) from Gibco® Life Technologies, USA.

2.1.3 For Transfection

- Lipofectamine® 2000 was purchased from Life technologies™.
- Lipofectamine® RNAiMAX was purchased from Invitrogen.

2.1.4 Molecular probes

- Hoechst 33342, Pluronic®F127, Fura-2-AM were purchased from Life Technologies™.
- Propidium iodide (PI), 2',7'-Dichlorodihydrofluorescein diacetate (H2DCF-DA), Dihyroethidium (DHE), MitoSOX™, Fluo4-AM and FluoZin™3-AM, MitoTracker™ Red, and MitoTracker™ Green were all purchased from Invitrogen.
- LysoBrite™ Deep Red from AAT Bioquest, Inc, US.
- Tetramethylrhodamine, ethyl ester (TMRE) was purchased from Sigma.
- Drp1-GFP was kindly provided by Dr. Stefan Strack (University of Iowa, US).

2.1.5 Pharmacological reagents

- Hydrogen peroxide (H_2O_2) from Sigma-Aldrich.
- 1-Methyl-4-phenylpyridinium (MPP^+) iodide, N-acetyl cysteine (NAC), 2,2,6,6-tetramethylpiperidinyl-1-oxyl (TEMPO), (2-(2,2,6,6-Tetramethylpiperidin-1-oxyl-4-ylamino)-2-oxoethyl)triphenylphosphonium chloride (Mito-TEMPO), N,N,N',N'-tetrakis(2-pyridinylmethyl)-1,2-ethanediamine (TPEN), 1,2-bis-(aminophenoxy)-ethane-N,N,N',N'-tetra-acetic acid- acetoxymethyl ester (BAPTA-AM) were purchased from Sigma-Aldrich.
- Apocynin was purchased from Abcam.

- Gp91ds-tat was purchased from (AnaSpec, Inc. Fremont, CA, USA).
- 2-Aminoethoxydiphenyl borate (2-APB) was purchased from Cayman Chemical Company-Ann Abor, MI, USA.
- N-(p-amylcinnamoyl) anthranilic acid (ACA) and PARP inhibitor VII, PJ34 were purchased from Sigma-Aldrich.
- Calcium ionophore (A23187) was purchased from Sigma - life Science.
- Zinc pyrithione (Zn-PTO) complex made by mixing stock solution of $ZnCl_2$ (0.7 µM) and pyrithione (PTO, 0.5 µM) purchased from Thermo Fisher Scientific, made up in ethanol in the desired ratio.
- Suppressor of complex I (S1QEL) and complex III (S3QEL) from Sigma-Aldrich.
- SiRNA (5´-GAAAGAAUGCGUGUAUUUUGUAA-3´) against human TRPM2 was designed using siDirect and custom made by Dharmacon (GE Healthcare, Chicago, USA).
- Control siRNA was from Ambion.

2.1.6 Antibodies

2.1.6.1 Primary antibodies

- Mouse monoclonal Anti-FLAG®M2 (1:5000 dilution) was purchased from Sigma-Aldrich®, F1804 - 1 mg/ml).
- Anti-TRPM2 antibodies (1:1000 dilution) against home-designed extracellular epitopes were custom generated in rabbit.

2.1.6.2 Secondary antibodies

- Goat anti-Mouse IgG HRP-conjugated antibody (1:10000) purchased from BIO-RAD.

- Goat anti-Rabbit IgG HRP-conjugated antibody (1:5000) from Sigma-Aldrich®.
- Cy3-conjugated anti-Rabbit IgG (1:500) from Jackson Immuno-Research.

2.1.7 Buffers and solutions

- Hank's Balanced Salt Solution (1x) (HBSS) was purchased from Gibco® by Life Technologies™.
- 10x standard buffer solution (SBS)

Ingredients	**Quantity**
NaCl	7.85 g
KCl	0.37 g
HEPES	2.38 g
Milli-Q water	100 ml
pH adjusted to 7.4 with 2 M NaOH	

- 1x SBS – supplemented with Ca^{2+}, Mg^{2+} and glucose

Ingredients	**Quantity**
10x SBS	5 ml
1 M $MgCl_2$	60 µl
1 M $CaCl_2$	75 µl
1 M glucose	400 µl
Milli-Q water	Up to 50 ml

- 10x sodium dodecyl sulphate (SDS) running buffer

Ingredients	Quantity
Glycine	144 g
Tris	30.3 g
SDS	10 g
Milli-Q water	Up to 1 L

- 1x SDS running buffer: diluted from 10x stock in Milli-Q water.
- 10x phosphate buffered saline (PBS)

Ingredients	Quantity
NaCl	80 g
KCl	2 g
$Na_2HPO_4.7H_2O$	26.8 g
KH_2PO_4	2.4 g
Milli-Q water	Up to 1 L

- 1x PBS diluted from 10x stock in Milli-Q water.
- 1x PBS/Tween (PBS-T) prepared by adding 250 µl of Tween20 into 500 ml of 1x PBS.
- Ice-cold transfer buffer (prepared and stored at 4 ºC)

Ingredients	Quantity
Glycine	14.4 g
Tris	3.03 g
SDS	1 g
Milli-Q water	800 ml
methanol	200 ml

- Blocking buffers: 5% Marvel milk in 1x PBS-T, or 5% Bovine serum albumin (BSA), or 5% goat serum.

- Fixative solution: 16% formaldehyde prepared in PBS purchased from Invitrogen.
- Lumigen PS-atto solution A and solution B purchased from Lumigen, U.S.A.

2.1.8 Tissue cultures materials

All tissue culture plates (6, 24 and 96 well plates) and flasks were purchased from Sarstedt. The 8-well ibiTreat slides were purchased from ibidi. The 35 mm fluoroDish™ glass bottomed tissue culture dishes were purchased from World Precision instruments.

2.2 Methods

2.2.1 Cells culture

SH-SY5Y and HEK-TRPM2^{tet} were cultured in DMEM+GlutaMAX-1 supplemented with 10% FBS and penicillin (100 U/ml) and streptomycin (100 µg/ml), referred to as complete medium. All cell lines were grown at 37ºC in a humidified 5% CO_2 incubator. Cells were sub-cultured in T-25 or T-75 flasks until they reached 70-80% confluency. For passaging the cells, growth medium was removed from the flask, and cells were washed with DPBS. Then, cells were detached from the flask by adding 1-2 ml (1 ml for T-25 and 2 ml for T-75 flasks) of TrypLE™ (for SHSY-5Y cells) or 0.05% trypsin-EDTA (for HEK-TRPM2^{tet} cells) solution and incubated in 37ºC for 2-5 minutes until complete cell detachment has been achieved. This was followed by resuspending the cells in 6-8 ml medium. Cell culture was continued by transferring 0.5-1.0 ml of cell suspension into a new flask containing pre-warmed fresh culture medium (e.g., 5-10 ml for T-25 flask,

or 10-20 ml for T-75 flask). For experiments, cells were seeded into multi-well plates, ibidi tissue culture slides or dishes and grown at 37ºC in 5% CO_2 incubator followed by treatments after 24-48 hours. HEK-TRPM2^{tet} cells were induced with tetracycline (1 µg/ml) for 48 hours before treatment to induce TRPM2 expression in these cells. Uninduced cells were used as controls.

2.2.2 Treatments

Cells were grown on multi-well plates, 35 mm FluoroDishes™ or 8 well ibiTreat slides for live cell imaging and maintained in DMEM+GlutaMAX-1 complete medium. For cell treatment, all stock chemical reagents and molecular probes were made up in sterile Milli-Q water, PBS or DMSO and, where appropriate, diluted in the media.

2.2.2.1 ROS production inducers

MPP^+ was used to induce ROS production in SH-SY5Y cells. MPP^+ was made up in sterile Milli-Q water at 100 mM. To determine the effect of MPP^+ on total cellular and mitochondrial ROS generation, SH-SY5Y cells were treated with different concentrations of MPP^+ (0, 0.5, 1 mM) diluted in DMEM medium. Then, they were incubated at 37 ºC in 5% CO_2 incubator for 24 hours. In HEK-TRM2^{tet} cells, ROS production was induced by treating the cells with 50 µM H_2O_2 for 2 hours at 37 ºC in a 5% CO_2 incubator. The final concentration of H_2O_2 was achieved by diluting the 9.8 M stock with DMEM medium. Following the treatments, cells were stained (see later and relevant figure legends), and washed with 1x HBSS before imaging.

2.2.2.2 ROS scavengers and NOX inhibitors

Three ROS scavengers (antioxidants) were tested on SH-SY5Y cells. Cells were treated with 1 mM MPP^+ with and without antioxidants; NAC (5 mM), TEMPO (10 µM) or Mito-TEMPO (10 µM). Then, they were incubated for 24 hours at 37 ºC. Co-treatments with the general NOX inhibitor, Apocynin (10 µM), or the NOX2 specific gp91ds-tat peptide inhibitor (5 µM) were also performed for 24 hours at 37 ºC in a 5% CO_2 incubator. Cells were stained (see relevant figure legends) after the treatments, rinsed, and washed with 1x HBSS before imaging.

2.2.2.3 Inhibition of TRPM2

To determine the role of TRPM2 channels in mediating MPP^+-induced ROS production, mitochondrial fragmentation, lysosomes depletion, and cell death, TRPM2 blockers (chemicals) or siRNA were used. In addition, to block the channel, anti-TRPM2 function blocking antibodies were used on SHSY5Y and HEK-$TRPM2^{tet}$ cells (see chapter 5).

TRPM2 blockers

For TRPM2 inhibition, SH-SY5Y cells were pre-treated for 1 hour with three different TRPM2 pharmacological blockers; ACA (10 µM), 2-APB (50 µM) and PJ34 (10 µM). Then, MPP^+ was added to a final concentration of 1 mM and the cells were incubated for 24 hours at 37 ºC. HEK-$TRM2^{tet}$ cells were incubated with 50 µM H_2O_2 for 2 hours after the pre-treatment.

siRNA-TRPM2 Transfection

Transfections were performed on SH-SY5Y cells grown in a 24-well plate at 60% confluency. 12.5 ng of small interfering RNA (siRNA) specific to TRPM2 (TRPM2-siRNA) or control scrambled siRNA (Scr-siRNA) were prepared in Opti-MEM® and incubated at room temperature for 5 minutes. In parallel, a second combination consisting of Lipofectamine® RNAiMAX and Opti-MEM® was also prepared and incubated at room temperature for 5 minutes. The two mixes were then combined and allowed to incubate at room temperature for 25 minutes before adding to the cells. After 6 hours, the medium was replaced with the complete medium and cells were allowed to grow for 24 hours. Transfected cells were exposed to 1 mM MPP^+ for 24 hours at 37 ºC. Then, depending on the aim of the experiment, cells were stained either with DHE (for total cellular ROS), MitoSOX (for mitochondrial ROS), MitoTracker™ Red (for mitochondria), or propidium iodide (for dead cells nuclei) and/or Hoechst (for nuclei) (see later and relevant figure legends). Finally, stain was replaced with 1XHBSS before imaging the stained cells.

Anti-TRPM2 antibodies

Cells were treated with anti-TRPM2 antibodies (1:100 dilution in DMEM), or with preimmune serum (1:100 dilution in DMEM) for 2 hours at 37 ºC prior to desired treatments (e.g., H_2O_2 or MPP^+). Depending on the aim of the experiment, cells were then stained for cell death (PI stain), calcium (Fura-2-AM or Fluo4-AM), cytosolic ROS (DHE), mitochondrial ROS (MitoSOX), lysosomes (LysoBrite Red), or mitochondria (MitoTracker™ Red) (see relevant figure legends). After washing with 1XHBSS, the cells were imaged.

2.2.2.4 Ca^{2+} and Zn^{2+} chelators

To understand the role of Ca^{2+} and Zn^{2+} in this study, two ion chelators were used. To determine the role of Ca^{2+}, SH-SY5Y cells were treated with 1 mM MPP^+ plus or minus the Ca^{2+} chelator, BAPTA-AM (5 µM) for 24 hours at 37 ºC. TPEN was used for quenching Zn^{2+}. Cells were treated with MPP^+ (1 mM) plus or minus TPEN (0.5 µM) for 24 hours at 37 ºC in a 5% CO_2 incubator. Cells were stained as required (see later and relevant figure legends) and washed with 1X HBSS before imaging.

2.2.2.5 Ca^{2+} and Zn^{2+} ionophores

To rise the intracellular Ca^{2+} and Zn^{2+} levels, the Ca^{2+} ionophore (A23187) and Zn^{2+} ionophore, Zn-pyrithione (Zn-PTO) were used. A23187 is not specific for Ca^{2+} and could allow Zn^{2+} entry, therefore, it was combined with the membrane impermeable Zn^{2+} chelator, DTPA (diethylenetriaminepentaacetic acid). The latter removes any Zn^{2+} present in the ambient medium. Cells were treated with 2 µM A23187 in the presence of 2 mM DTPA and incubated at 37ºC for 4 hours. For Zn^{2+} delivery into the cells, Zn-PTO (2 µM) was added to the cells in Ca^{2+} free medium and incubated for 2 hours at 37ºC. Then, depending on the aim of the experiment, cells were stained and imaged.

2.2.2.6 Suppressors of superoxide production from mitochondrial complexes

To determine the mitochondrial site of ROS production in MPP^+ treated SH-SY5Y cells, site-specific suppressors of electron leak from complex I (S1QEL) and complex III (S3QEL) were used. These selective chemicals suppress mitochondrial ROS generation at complex I/III without altering forward electron

transport (Wong et al., 2019a, Orr et al., 2015). SH-SY5Y cells were pre-treated with S1QEL (10 µM) or S3QEL (5 µM) for one hour. The cells were then incubated with 1 mM MPP^+ for 24 hours at 37 ºC. Following the treatments, they were stained for mitochondria (MitoTracker™ Red), mtROS (MitoSOX), or cell death (PI). The cells were washed with 1x HBSS before recording the images.

2.2.3 Immunoblotting

2.2.3.1 Sample Preparation

SH-SY5Y cells were cultured in T-25 flask to 80% confluency. HEK-$TRPM2^{tet}$ cells were cultured in two T-25 flasks to 50% confluency. One flask was treated with 1 µg/ml tetracycline for 48 hours, and the other flask was left untreated (uninduced). From all three flasks, medium was removed, and cells were washed with PBS. Cells were scraped in 3 ml PBS, transferred into tubes, and then centrifuged at 200 *g* for 5 minutes at 4ºC. Following centrifugation, supernatant was discarded, and the pellets were suspended 1x SDS sample buffer and incubated for five minutes at 95ºC before loading into SDS-PAGE gels (sodium dodecyl sulfate – polyacrylamide gel electrophoresis).

2.2.3.2 SDS-PAGE gel preparation

10% SDS – polyacrylamide gels were prepared as follows: the resolving gel was prepared by mixing 4 ml of ddH_2O, 3.33 ml 30% Bis/Acrylamide, 2.5 ml 1.5 M Tris (pH 8.8), 100 µl 10% SDS, 100 µl 10% APS (Ammonium persulphate) and 4 µl TEMED (Tetramethylethylenediamine). The stacking gel was prepared by mixing 2.73 ml ddH_2O, 680 µl 30% Bis/Acrylamide, 500 µl 1 M Tris (pH 6.8), 40 µl 10% SDS 40 µl 10% APS and 4 µl TEMED. The resolving gel mixture was loaded first into the casting cassette, allowed to polymerize, and then the stacking gel mixture

was overlaid. A comb was placed into the stacking gel and the gel was allowed to set for at least 1 hour before use.

2.2.3.3 Gel running, transferring and antibody incubation

Cell lysates were loaded onto the SDS-PAGE gel. 6 µl of protein marker and 10 µl of each sample were loaded into preformed wells. Gel was run at 200 volts until the required separation of the marker bands was achieved. Then, gel was removed from the tank and placed in ice-cold transfer buffer for 15 min. Stacking gel was removed and the running gel was placed on a 0.45 µm nitrocellulose membrane (BIO-RAD). The gel-membrane stack was then placed between two blotting papers that were pre-wetted with transfer buffer. The separated proteins were then transferred electrophoretically from the gel onto the nitrocellulose membrane using a semi-dry transfer apparatus (BIO-RAD) at 0.06 A for 90 minutes. The membrane was incubated with the blocking buffer on a shaker at 4ºC for 4 hours. After the blocking step, the membrane was incubated with the primary antibody (diluted in blocking buffer) on a shaker at 4ºC for overnight. The membrane was washed with PBS-T for 1 hour (changed every 20 minutes) on a shaker at room temperature. Following the wash, the membrane was incubated with the secondary antibody (diluted in blocking buffer) for two hours on a shaker at room temperature. Then, the washing step was repeated as described earlier after primary antibody incubation.

2.2.3.4 Developing

Lumigen PS-atto solution A and solution B were mixed in equal volumes (250 µl each) and left in dark for 5 minutes. The membrane was placed onto a clean glass back plate (side of membrane that faced gel upwards) then covered completely with the PS-atto mixture. The membrane was then incubated in dark

for two minutes. The excess reagent was then drained off and the membrane was covered with cling film. Finally, the membrane was imaged using the SYNGENE imager. A band of ~ 170 KDa corresponds to the size of TRPM2 subunit.

2.2.4 Immunostaining

To examine the ability of anti-TRPM2 antibodies to recognize native TRPM2, immunocytochemical surface staining was performed. HEK-TRPM2^{tet} cells (both tetracycline induced and non-induced cells) and SH-SY5Y cells grown on pre-treated glass coverslips in a 24-well plate were first fixed with 4% paraformaldehyde solution for 15 minutes at room temperature. After washing with 1x PBS (three times, five minutes each), non-specific binding sites were blocked with blocking buffer (5% goat serum in 1x PBS) for one hour at room temperature. Then, cells were incubated with anti-TRPM2 antibody (1:200 dilution in blocking buffer) for two hours followed by washing with 1x PBS (three times, five minutes each). After that, cells were stained with Cy3 conjugated donkey anti-rabbit IgG secondary antibody (1:500 dilution in blocking buffer) for one hour and washed with 1x PBS (three times, five minutes each). Cells were then rinsed with distilled water before mounting the coverslips onto a microscope slide using a small drop of DAPI Fluoromount-G mounting medium (purchased from SouthernBiotech). Coverslips edges were sealed with nail varnish, and cells were imaged using EVOS FL Auto 2 microscopes fitted with RFP filter and a 40x objective.

2.2.5 Intracellular Ca^{2+} measurement by Flexstation

Changes in intracellular Ca^{2+} in response to H_2O_2 stimulus was monitored by pre-loading the cells with Fura-2-AM, a fluorescent Ca^{2+} reporter. Fluorescence was recorded using FlexStation®III (Molecular Devices). FlexStation can perform

automated fluorescence measurements in multi-well plates, and report the activity of Ca^{2+} channels by measuring changes of intracellular free Ca^{2+} level in response to a stimulus (Marshall et al., 2005). For this, cells were grown in 0.001% poly-L-lysine coated 96-well plate, so the confluency reached 100% within 24 hours. Then medium was removed, and cells washed with SBS. Then, the cells were incubated in Fura-2-AM (2 µM) and 0.01% Pluronic®F127 diluted in SBS and incubated in the dark at 37°C for 1 hour. After incubation, Fura-2-AM solution was removed and replaced with 200 µl of SBS and further incubated in the dark for 30 minutes. After incubation, cells were washed 3 times with SBS. Following this dye loading step, appropriate treatment solutions were prepared and added to the cells; the plate was incubated in the dark for desired period of time (as shown in the relevant figure legends). During the incubation time, a round-bottom 96-well (compound) plate containing H_2O_2 solution was prepared (for concentrations see figure legends). Finally, both the plates (cells and the compound) were loaded into the FlexStation®III Multi-Mode Microplate Reader. Fluorescence was detected with excitation wavelength at 340 nm and 380 nm for Ca^{2+}-bound and Ca^{2+}-free Fura-2, respectively. In both states, the emission wavelength was 510 nm. The readings were taken for a total of 6 minutes at 5 seconds time intervals. At the 60 seconds time point, 20 µl of H_2O_2 (five-fold the required final concentration) was automatically injected into the wells. The fluorescence intensities were calculated from the ratios of 510 nm/340 nm and 510 nm/380 nm which are directly related to the concentration of intracellular Ca^{2+}. The statistical analysis was performed by calculating the mean ± S.E.M of fluorescence ratios that were calculated by taking the fluorescence intensities at the baseline (before the addition of H_2O_2) and subtracting the value from the last time point. Then the statistical differences between various treatments were compared using One-way Anova in Origin software (version 9.1.0).

2.2.6 Intracellular Ca^{2+} measurement by live cell imaging

Cells were grown in 8-well ibiTreat slides, 35 mm FluoroDish™, or 96-well plate to approximately 60% confluence. Cells were treated or not treated (control) with

the test chemicals (as shown in the relevant figure legends) for desired length of time. Cells were washed with 1x HBSS and loaded with Fluo4-AM as described above. After washing with 1XHBSS to remove the excess stain, cells stained with Hoechst 33342 (2 µM) in 1XHBSS for 30 minutes at 37 ºC. Finally, stain was replaced with 1x HBSS before recording the images using the inverted confocal microscope (see imaging details in section 2.2.16, table 2.2).

2.2.7 Intracellular Zn^{2+} measurement by live cell imaging

To detect intracellular free Zn^{2+}, cells were grown on a 8-well ibiTreat slides or 35 mm FluoroDish™ to about 50% confluency. After desired treatments, cells were washed with 1XHBSS and loaded with 2 µM FluoZin3-AM (prepared in 1x HBSS) in the presence of 0.01% pluronic acid for 1 hour at 37 ºC. Cells were then washed and incubated with Hoechst 33342 (2 µM) for 30 minutes. After washing with 1x HBSS to remove the excess stain, cells were imaged using the inverted confocal microscope (see imaging details in section 2.2.16, table 2.2).

2.2.8 Live cell imaging of mitochondria and lysosomes

Cells were grown in 8-well ibiTreat slides or 35 mm FluoroDish™ to ~50% confluency. After desired treatments, the chemicals/medium were removed. Cells were then loaded with 500 nM MitoTracker™ Red, 200 nM MitoTracker™ Green, or 200 nM LysoBrite™ Deep Red for 30 minutes at 37 ºC. Subsequently, cells were washed once with 1x HBSS and imaged using the inverted confocal microscope (see imaging details in section 2.2.16, table 2.2).

2.2.9 Mitochondrial morphology assessment

The imaging-based quantitative assessment of mitochondrial morphology was performed using the “Mitochondria Analyzer” as described by (Chaudhry et al., 2020). Mitochondria Analyzer is a plugin in Image J or Fiji software that enables quantitative analysis of mitochondrial morphology and network from photo-labelled mitochondria. It allows quantification of the morphological changes of mitochondria and to produce both two-dimensional (2D) analysis of the images and three-dimensional (3D) analysis of the entire mitochondrial network. For an accurate analysis, image acquisition was optimized for best resolution images. Single cross-section images were acquired for 2D analysis, whereas for 3D analysis, Z-stacks were acquired. Mitochondria Analyzer provides multiple parameters of analysis that allow identification of mitochondria morphologies (see section 2.2.20). In this study, two parameters (aspect ratio and form factor) have been selected from 2D data analysis. All other parameters that reflect the full mitochondrial network morphology were calculated using 3D data analysis. These parameters are volume, surface area, sphericity, number of branches, mean branch length, total branch length, number of branch junctions and branch end points (see details in table 2.1 and figure 2.1).

2.2.10 Mitochondrial membrane potential

To investigate the effect of specific chemical treatment on the inner mitochondrial membrane potential (ΔΨm), cells were grown in 96 well tissue culture plate at ~ 50% confluency. After treatment (see relevant figure legends), cells were stained for ΔΨm using 200 nM tetramethylrhodamine ethyl ester (TMRE) for 30 minutes at 37 ºC. Then, cells were washed once with 1x HBSS and recorded by using EVOS FL Auto 2 microscope (see imaging details in section 2.2.16, table 2.2). Strong red fluorescence indicates healthy mitochondria, whereas a reduction in fluorescence indicates loss of ΔΨm, an indicator of unhealthy mitochondria (Crowley et al., 2016). Thus, the intensity of TMRE fluorescence (analysis details

in section 2.2.20) was utilized to evaluate whether mitochondria in a stained cell have high (active mitochondria) or low (inactive mitochondria) ΔΨm (Crowley et al., 2016).

Table 2.1 Definitions of mitochondria parameters.

Definitions of parameters used in 2D and 3D analysis of mitochondrial morphology. Modified from (Chaudhry, 2019, Picard et al., 2013)

Parameter	Definition/ Description
2D parameters	
Aspect ratio	A shape measure given by: (major axis)/(minor axis). It reflects the length-to-width ratio.
Form factor	A shape measure given by: $(\text{perimeter}^2)/(4\pi)(\text{surface area})$ 1 indicates round mitochondrion and the value increases with elongation. It reflects the complexity and branching of mitochondria.
3D parameters	
Mean volume	Mean volume of mitochondrion
Mean Surface area	Mean surface area of mitochondria (mitochondria size)
Sphericity	A shape measure of sphericity. It reflects the circularity and roundness of mitochondria. The higher sphericity value, the more the sphericity of the mitochondrion.
Branches	Total number of branches in image.
Total branch length	Sum of length of all branches in image.
Mean branch length	Total branch length divided by number of branches.
Branch junctions	Number of junctions (points where two or more branches meet) within all skeletons in image.
Branch end points	Total number of end point, which are where the branches end without connecting to another branch.

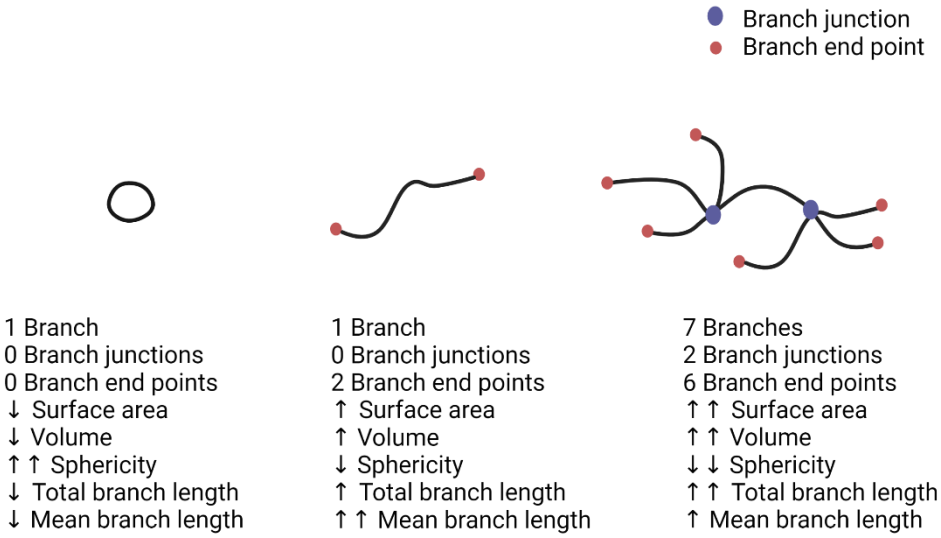

Figure 2.1 Schematic drawing summarized the various parameters used for describing the mitochondrial network connectivity in 3D analysis.

2.2.11 Assessment of lysosomes number and Lysosomal membrane permeabilization

To examine the lysosomal membrane permeabilization (LMP) in SH-SY5Y cells in normal and neurotoxic condition, they were grown in 8-well ibiTreat slide. Cells were treated with medium alone (CTRL) or 1 mM MPP^+ in the presence or absence of a TRPM2 inhibitor (2-APB, 50 µM) for 24 hours at 37 ºC. Also, the effect of elevated cytosolic Ca^{2+} on LMP was investigated by exposing the cells to the Ca^{2+} ionophore A23187 (2 µM plus 2 mM DTPA) for different incubation periods (0, 2, 4 hours) with and without the Ca^{2+} chelator (BAPTA, 5 µM). After treatment, cells were stained for lysosomes using 200 nM LysoBrite™ Deep Red for 30 minutes at 37 ºC. Cells were then washed once with 1x HBSS and imaged using the inverted confocal microscope (see imaging details in section 2.2.16, table 2.2)**.** The number of lysosomes and LMP were assessed through two methods: either by calculating the number of LysoBrite Red-positive lysosomes, or by measuring the intensity of LysoBrite fluorescence per cell (analysis details in section 2.2.20). LMP is indicated by the reduction in the number/intensity of positive-stained lysosomes (Abuarab et al., 2017, Li et al., 2017a).

2.2.12 Drp 1-GFP recruitment to mitochondria

To investigate MPP^+-induced Drp1 recruitment to mitochondrial, SH-SY5Y cells grown in 8-well ibiTreat slide at ~ 50% cells confluency were transfected with 0.3 µg of Drp1-GFP using Lipofectamine® 2000 in Opti-MEM medium. After 8 hours, equal volume of complete medium was added, and the incubation continued for 48 hours at 37 ºC. Then, cells were treated with either MPP^+ (1 mM) in present or absence of the TRPM2 blocker (2-APB, 50 µM) and incubated further for 24 hours, or treated with Ca^{2+} free medium containing the Zn^{2+} ionophore (Zn-PTO, 2µM) for 2 hours at 37 ºC. After treatment, cells were stained for mitochondria using MitoTracker™ Red for 30 minutes, washed with 1x HBSS, and cells were

imaged for Drp1-GFP and MitoTracker™ Red using confocal microscope (see imaging details in section 2.2.16, table 2.2).

2.2.13 Assessment of total cytosolic ROS production

Total intracellular ROS generation was determined by staining the cells either with DHE or H_2DCF-DA in cells grown in 96-well plates. Cells were treated or not treated (control) with the test chemicals (as shown in the relevant figure legends) for the desired incubation period. Medium was removed and the cells were stained with 100 µl of DHE (5 µM) or H_2DCF-DA (10 µM) and Hoechst 33342 (2 µM), diluted in 1x HBSS, for 30 minutes at 37°C. Following this, cells were washed with 1x HBSS and then imaged using EVOS FL Auto 2 microscope (see imaging details in section 2.2.16, table 2.2). The results were expressed as the mean of DHE (or H_2DCF-DA) fluorescence intensity per cell (see details in section 2.2.20).

2.2.14 Assessment of mitochondrial ROS production

Following the desired treatments, cells were tested for mitochondrial superoxide production using the MitoSOX Red stain. Staining was performed by incubating the cells, grown in 96-well plates with 100 µl of 2 µM MitoSOX and Hoechst 33342 (2 µM), diluted in 1x HBSS, for 30 minutes at 37°C. Following this, the stain was replaced with 1x HBSS and then cells were imaged using EVOS FL Auto 2, or a confocal microscope (see imaging details in section 2.2.16, table 2.2). The results were expressed as the mean of MitoSOX fluorescence intensity per cell (see details in section 2.2.20).

2.2.15 Cell death Assay

The cell viability was determined by co-staining the cells with Hoechst 33342 and propidium iodide (PI). Hoechst 33342 stained total nuclei of all cells whereas PI stained only the nuclei of dead cells. PI is commonly used as a good indicator of loss of cell viability. It is economical, stable and does not stain live or early apoptotic cells. In the experiment, PI stock (1 mg/ml) was prepared in water, and the working stain solution was made up by diluting the stock in DMEM medium to give 5 µg/ml final concentration. For Hoechst 33342, the final concentration used was 2 µM. Staining was performed at 37ºC for 20-30 minutes. Then, cells were imaged using EVOS FL Auto 2 microscope (see imaging details in section 2.2.16, table 2.2). The results are expressed as percentage of cell death; that is, the number of dead cells (PI positive - Red) out of total number of cells (Hoechst 33342 – blue).

2.2.16 Fluorescence Microscopy

Images of stained cells were captured using either an EVOS FL Auto 2 microscope (Invitrogen™, Thermo Fisher Scientific Waltham, MA, USA) with a 20x or 40x objective lens, or an inverted confocal microscope (LSM 880 + Airyscan, Carl Zeiss, Germany) with a 40x/1.4 Oil DIC M27 objective lens. Images were taken from at least three different fields of view per well. The microscope as well as the specific filter sets or wavelengths used to observe each fluorescent dye are listed in table 2.2.

Table 2.2 Shows the microscope and filter set used for the fluorescent dyes.

Fluorescent dye	Microscope	EVOS Filter	Excitation	Emission
Hoechst 33342	EVOS/ Confocal	DAPI	360 nm	460 nm
PI	EVOS	Texas Red	535 nm	617 nm
H2DCF-DA	EVOS	GFP	488 nm	510 nm
DHE	EVOS	RFP	510 nm	580 nm
MitoSOX™	EVOS/ Confocal	RFP	510 nm	580 nm
Fluo4-AM	EVOS/ Confocal	GFP	488 nm	510 nm
FluoZin™3-AM	Confocal	-	490 nm	520 nm
MitoTracker™ Red	Confocal	-	581 nm	644 nm
MitoTracker™ Green	Confocal	-	490 nm	516 nm
LysoBrite™ Deep Red	Confocal	-	581 nm	644 nm
TMRE	EVOS	RFP	550 nm	575 nm
Drp1-GFP	Confocal	-	488 nm	505 nm

2.2.17 Image and statistical analysis

2.2.17.1 Image analysis

Fiji/ImageJ (1.53c) were used for all analysis of total cellular and mitochondrial ROS fluorescent intensity, mitochondrial morphology, mitochondrial membrane permeabilization, lysosomes and dead cells counting.

For fluorescent intensity measurements, integrated density for the entire image (x) was measured. Background fluorescence intensity (y) was determined from the mean of multiple selected areas where cells were absent and subtracted from x. Number of cells (n) was counted from Hoechst stain and the following equation was used to determined fluorescent intensity per cell:

$$Fluorescent\ intensity\ per\ cell = \frac{x-y}{n}$$

For analysis of mitochondria morphology, images were acquired using inverted confocal microscope, with a 40x/1.4 Oil DIC M27 objective lens to best resolution. Single cross-section images were acquired for 2D analysis, whereas for 3D analysis, Z-stacks were acquired. The quantitative assessment of mitochondrial network was carried out using the “Mitochondrial Analyzer” plugin in Fiji/ImageJ 1.53c software that provides several analytical parameters allowing a quantitative description of mitochondria morphologies. The acquired images were first pre-processed and thresholded by selecting either “2D or 3D Threshold” command to obtain maximum mitochondrial structural details and minimizing any background signal. This command depends on the local threshold method which provides a threshold for each pixel in the image and normally requires two important parameters to be identified: the block size (The area around each pixel and which depends on the objects size) and the C value (signal to noise contrast) (Chaudhry et al., 2020). Therefore, different combination of block size and C value was tested to get the optimal one for the acquired mitochondrial images. For 3D analysis, the 3D construction of mitochondria was generated by merging

a stack of serial slices spanning the whole cell using the “stacks-Z project” command. Then, the threshold images converted into skeleton image using “skeletonize (2D/3D)” command following by skeleton analysis by applying “2D or 3D analysis” command. From 2D analysis, the aspect ratio and form factor were measured. 3D images were utilized to obtain the volume, surface area, sphericity, number of branches, mean branch length, total branch length, number of branch junctions and branch end points in mitochondria (table 2.1 and figure 2.1).

Finally, the number of lysosomes were determined either manually using the “cell counter” command or automatically by applying the “find Maxima” command on pre-processed (to reduce the background signals) images.

2.2.17.2 Statistical analysis

Statistical significance was determined using One-way ANOVA followed by Tukey post-hoc mean comparison test using OriginPro 9.1 (Seifert, 2014) and Jamovi stat 1.6.23 (Şahin and Aybek, 2019). All experiments were performed at least three times (n), and the number of cells (N) analyzed in each experiment was indicated in the figure legend. The values were presented as mean ± SEM. Probability (*P*) values; * Indicates $p < 0.05$; ** indicates $p < 0.01$; *** indicates $p < 0.001$.

Chapter 3
Neurotoxin-induced SH-SY5Y neuroblastoma cell death is mediated by TRPM2 stimulated ROS amplification

3.1 Introduction

Oxidative stress is intimately associated with neuronal cell death, which is an underlying cause of many neurodegenerative disease. Understanding the regulatory mechanisms underlying oxidative stress is therefore important for development of therapies for neuronal diseases. Oxidative stress results from an imbalance between the production of prooxidants and antioxidants (Takahashi et al., 2011). The prooxidants are mainly represented by the reactive oxygen species (ROS) and when their levels exceed the control by antioxidants, they result in oxidative stress. ROS are natural by-products of various cellular processes, such as cellular respiration, protein folding, and some metabolic reactions (Reczek and Chandel, 2015). They play vital roles in intracellular signaling in several physiological and cellular processes. For instance, they are involved in growth factor signaling, host defence, autophagy, and proliferation and differentiation of stem cells (Reczek and Chandel, 2015). In cell signaling, ROS can modify redox-sensitive amino acids in many proteins, such as ion channels, kinases, phosphatases, and transcription factors, thereby affecting their activities. However, over-production of ROS has damaging effects on biomolecules, including DNA, proteins, and lipids. DNA oxidation could result in mutations and impact gene expression (Brieger et al., 2012, Dröge, 2002). Oxidative damage compromises the function of a number of proteins essential for cellular health. ROS can also affect the integrity of the lipid bilayer of cell membranes through peroxidation of polyunsaturated fatty acids. These damaging effects collectively contribute to pathological changes characteristic of many ROS-related diseases. Indeed, overproduction of ROS is a defining feature of almost all late-age onset human diseases including diabetes (Gao and Mann, 2009, Houstis et al., 2006), cardiovascular diseases (Negre-Salvayre et al., 2020), cancer (Franco et al., 2008, Khandrika et al., 2009, Desouki et al., 2005)

and neurodegenerative diseases (such as, Parkinson's and Alzheimer's) (Tarafdar and Pula, 2018). Several *in vitro* and *in vivo* studies have shown that prevention of excess ROS production, as well as ROS scavengers (Hulsmans et al., 2012, Ceriello, 2006, Erejuwa, 2012, Yan, 2014, Calkins et al., 2012), reduce cell death and the severity of many diseases. The mechanisms underlying the generation of pathological concentration of ROS have been extensively investigated, but how ROS production is regulated is unclear. Addressing the latter question is important for developing safe and effective therapies targeted to ROS.

Excess ROS production in a cell is often trigged by exogenous agents such as different types of radiation, toxins, environmental pollutants including heavy metal ions such as Mn^{2+} and Zn^{2+}. These agents stimulate ROS production in various cellular compartments such as the cell membrane, cytoplasm, ER, mitochondria, and peroxisomes (Forrester et al., 2018, Rastogi et al., 2017). A major source of ROS, however, is mitochondria, where 90% of total cellular ROS is produced. Mitochondrial ROS (mtROS) are produced as a by-product during the transport of electrons from reduced nucleotides to molecular oxygen through the electron transport chain (ETC) (Zorov et al., 2014). Most exogenous agents target the protein complexes of ETC to generate toxic amounts of mtROS.

Recent studies have implicated TRPM2 channels in ROS regulation and cell death (Abuarab et al., 2017, Li et al., 2017a). ROS activation of TRPM2 channels affects intracellular Ca^{2+} and Zn^{2+} dynamics. Both ions are implicated in ROS production by affecting NADPH oxidase (NOX) enzymes and the mitochondrial ETC (Sensi et al., 2009, Dineley et al., 2005, Görlach et al., 2015, Nicholls, 2005, Marreiro et al., 2017). Studies have suggested an association between TRPM2 channel activation and a number of diseases (Yamamoto and Shimizu, 2016) including PD (Sun et al., 2018). Patients with PD have decreased glutathione levels, decreased mitochondrial complex I activity and increased dopamine turnover (Yoshikawa, 1993), all of which increase ROS formation and lead to neuronal cell damage. The aim of this study is to test the hypothesis that TRPM2 channel mediated changes in intracellular Ca^{2+} and Zn^{2+} trigger ROS

overproduction and neuronal cell death in PD. To test this hypothesis, human neuroblastoma SH-SY5Y cells were used. This cell line expresses tyrosine hydroxylase required for conversion of L-tyrosine to L-dihydroxyphenylalanine (L-DOPA), that is subsequently converted to dopamine by aromatic L-amino acid decarboxylase (Xicoy et al., 2017). Furthermore, they express dopamine transporters to facilitate uptake of dopamine as well as MPP^+ (Kovalevich and Langford, 2013, Knaryan et al., 2014). For these reasons, SH-SY5Y cells have widely been used in PD research (Xicoy et al., 2017). Expression of TRPM2 channels in SH-SY5Y cells has been demonstrated using western blotting and electrophysiology (Sun et al., 2018, Chen et al., 2013). For these reasons, in this study, this cell was used in conjunction with MPP^+ as a model to study the TRPM2 dependent intracellular events that lead to ROS dyshomeostasis and cell death.

In these models, MPP^+ has been shown to induce ROS generation and quenching of ROS protects DA neurons from toxin induced cell death (Wang et al., 2011, Fragkouli and Doxakis, 2014, Choi et al., 1999, Lotharius et al., 1999, Anantharam et al., 2007), however, the details of the underlying mechanisms are unclear. Thus, the aim of this chapter is to understand the molecular mechanism of oxidative stress induced neuronal cell death and the role that TRPM2 channels play using the *in vitro* model of PD. In this context, it is important to note that SH-SY5Y cells natively express TRPM2 channels (Chen et al., 2013, Sun et al., 2018).

3.2 Results

3.2.1 MPP^+ Promotes ROS production in SH-SY5Y cells

To determine the optimal MPP^+ concentration required for ROS production, SH-SY5Y cells were treated with various concentrations of MPP^+ (0, 0.5, 1, 2 and 5 mM) for 24 hours. The effect of MPP^+ on total (cytosolic plus mitochondrial) as

well as mitochondrial ROS was determined by co-staining the cells with the H_2DCF-DA (green) and MitoSOX (red) fluorescent dyes. At 0.5 mM concentration, MPP^+ caused a significant increase in both mitochondrial ($p < 0.01$) and total ROS ($p < 0.001$) production. Elevation of MPP^+ to 1 mM caused further increase in ROS levels (Figure 3.1). Concentrations above 1 mM caused marked cell death causing a reduction in ROS signals and were therefore avoided in all subsequent ROS experiments.

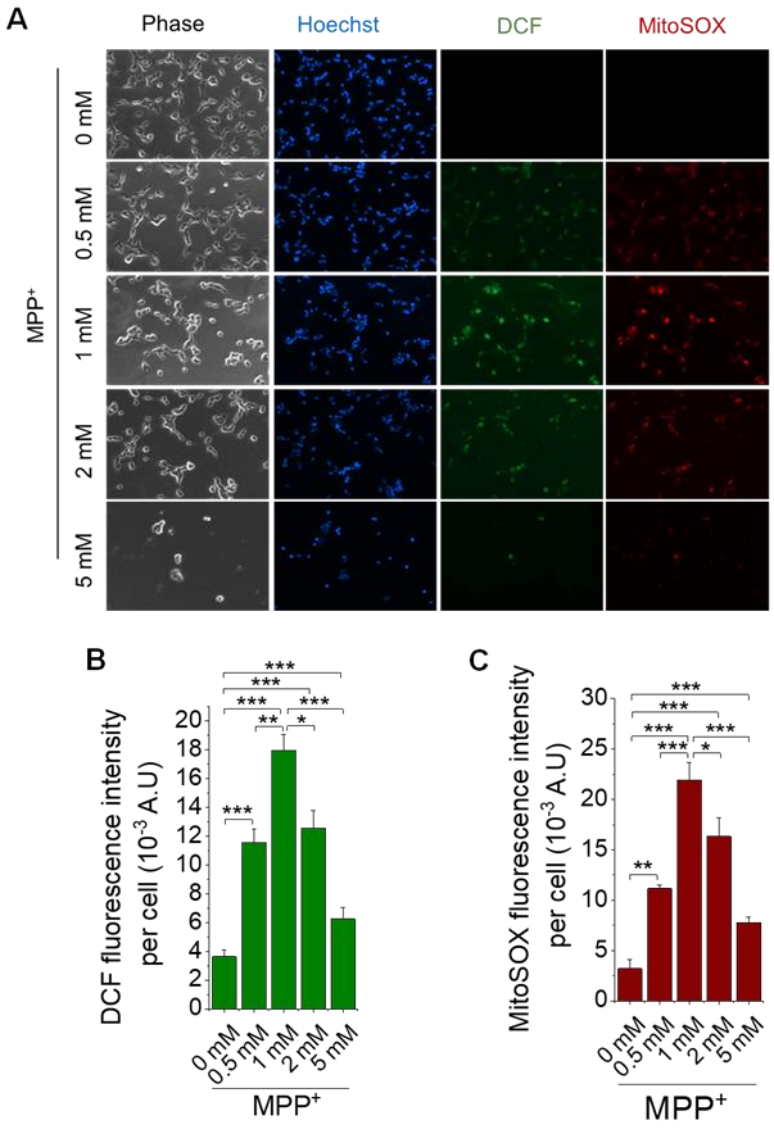

Figure 3.1 Dose dependent effect of MPP⁺ on total intracellular and mitochondrial ROS generation in SH-SY5Y cells.

SH-SY5Y cells were treated with the indicated concentrations of MPP⁺ for 24 h. Cells were then stained for nuclei (Hoechst 33342), total (H_2DCF-DA) and mitochondrial (MitoSOX) ROS. **(A)** Representative phase and fluorescent images of stained cells. **(B-C)** the corresponding mean ± SEM of data of DCF fluorescence **(B)** and MitoSOX fluorescence **(C)** per cell, from three independent experiments. ** indicates $p < 0.01$; *** indicates $p < 0.001$; one-way Anova with post-hoc Tukey Test.

3.2.2 MPP^+ induced ROS production in completely quenched by Mito-TEMPO

I next tested the ability of three antioxidants (NAC, TEMPO, and Mito-TEMPO) to prevent MPP^+-induced ROS production and to confirm that the increased fluorescence of the reporter chemicals is not an artefact but due to a rise in ROS production. The mitochondria-targeted antioxidant “Mito-TEMPO” is a specific scavenger of mitochondrial superoxide. It combines the antioxidant piperidine nitroxide “TEMPO” with the lipophilic cation triphenylphosphonium (TPP^+) that gives the ability of the compound to pass through the phospholipid bilayers and accumulates several hundred-fold within mitochondria where it can dismutate superoxide in the catalytic cycle (Trnka et al, 2008). Cells were treated with medium only (CTRL) or MPP^+ with or without antioxidants for 24 hours at 37ºC. Results showed that NAC (5 mM), TEMPO (10 µM) and Mito-TEMPO (10 µM) inhibited MPP^+-induced increase in cytosolic (DHE fluorescence) and mitochondrial (MitoSOX fluorescence) ROS level in the cells (Figure 3.2). Interestingly, Mito-TEMPO was able to quench ROS signals as effectively as the total ROS scavenger, NAC. These results suggest that the major site of ROS generation by MPP^+ is mitochondria.

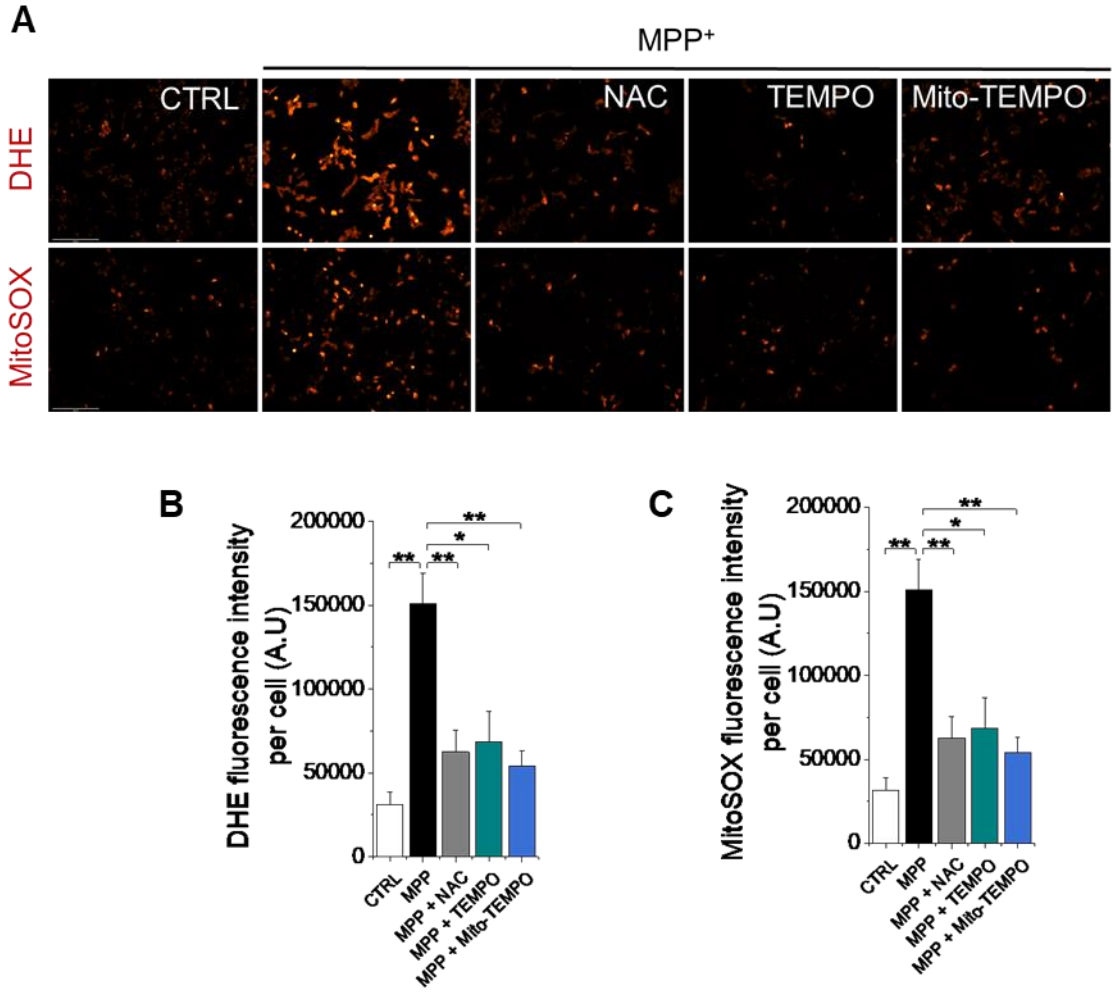

Figure 3.2 ROS quenchers attenuate MPP$^+$-induced total intracellular and mitochondrial ROS level in SH-SY5Y cells.

SH-SY5Y cells were treated with medium only (CTRL) or 1 mM MPP$^+$ with or without antioxidants (5 mM NAC, 10 µM TEMPO or 10 µM Mito-TEMPO) for 24 h at 37ºC. **(A)** Fluorescent images of SH-SY5Y cells stained for total cytosolic (DHE) and mitochondrial ROS (MitoSOX). Scale bar: 200 µM. **(B-C)** The corresponding mean ± SEM of data of DHE Fluorescence **(B)** and Mito-SOX Fluorescence **(C)** from three independent experiments. * indicates $p < 0.05$, ** indicates $p < 0.01$; *** indicates $p < 0.001$; one-way Anova with post-hoc Tukey test.

3.2.3 Inhibition of NADPH oxidase 2 (NOX2) prevents not only cytosolic ROS, but also mitochondria ROS production

Previous studies have reported that MPP^+ can also stimulate NOX2 (Zawada, 2011) to increase cytosolic ROS. To determine the relative contributions of both cytosolic and mitochondrial sources to MPP^+ induced increase in ROS level, I have first examined the effect of the general NOX inhibitor, apocynin (10 µM) on ROS production. The results show that apocynin attenuated DHE as well as, unexpectedly, the MitoSOX fluorescent signals (Figure 3.3). To exclude any non-specific effects of apocynin, I have used the NOX2 specific gp91ds-tat peptide inhibitor (5 µM) (Rey et al., 2001). The results were similar to those of apocynin (Figure 3.3). The ability of NOX inhibition to suppress MPP^+-induced mitochondrial ROS production raises questions on the previous reports (Yıldızhan and Nazıroğlu, 2020, Yang et al., 2018, Cleeter et al., 1992, Ramsay et al., 1991, Marambaud et al., 2009) that MPP^+ acts directly at Complex I of mitochondria to produce ROS. Instead, our results suggest that MPP^+ activates NOX2 and that NOX2-derived ROS, in turn, stimulate mitochondrial ROS production.

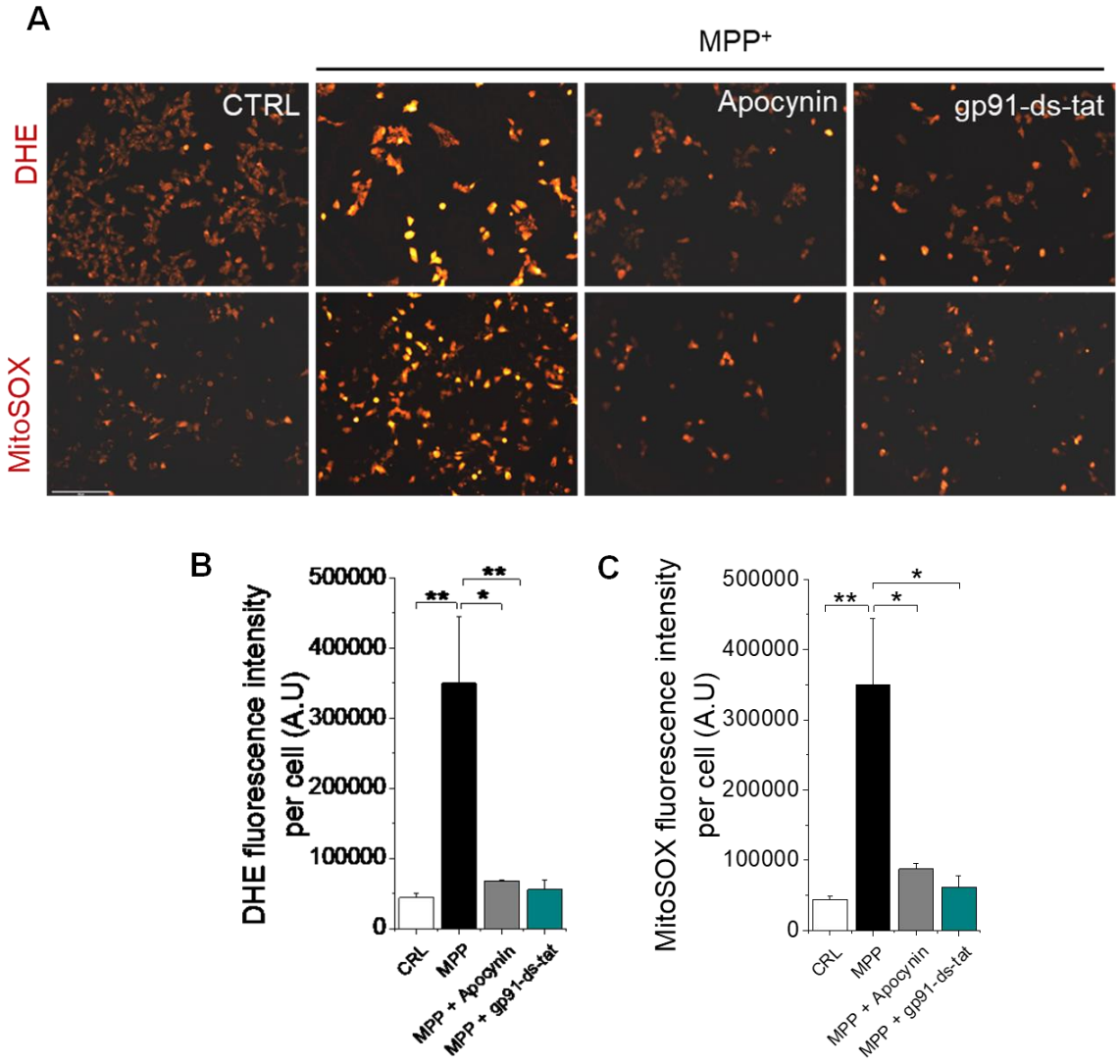

Figure 3.3 NOX2 inhibition prevents MPP$^+$ induced increase in total as well as mitochondrial ROS production.

(A) Fluorescent images of SH-SY5 cells treated with medium alone (CTRL), or medium containing 1 mM MPP$^+$ with and without NOX inhibitors (10 µM apocynin and 5 µM Gp91ds-tat). Then, cells were stained for total (DHE) and mitochondrial ROS (MitoSOX). Scale bar: 200 µM. **(B-C)** The corresponding mean ± SEM of data of DHE Fluorescence **(B)** and MitoSOX Fluorescence **(C)** from three independent experiments. ** indicates $p < 0.01$; *** indicates $p < 0.001$; NS, not significant; one-way Anova with post-hoc Tukey test.

3.2.4 ROS quenchers as well as NOX2 inhibitors prevent MPP^+-induced SH-SY5Y cell death

Given both ROS quenchers (Figure 3.2) and NOX2 inhibitors (Figure 3.3) attenuate the MPP^+-induced ROS increase, and ROS are known to trigger cell death, I have next examined the effect of these reagents on MPP^+-induced SH-SY5Y cell death. The results demonstrate that mitochondria targeted Mito-TEMPO is as effective as the general ROS quenchers, NAC and TEMPO, in preventing MPP^+-induced cell death (Figure 3.4). The ability of Mito-TEMPO to completely inhibit the cell death is consistent with the fact mitochondria are the major source of cytotoxic cytosolic ROS production.

I have next asked whether NOX2-derived ROS are the key drivers of cell death because inhibition of NOX2 was capable of preventing mitochondria ROS production. Both apocynin and gp91ds-tat treatments have resulted in a marked decrease in the percentage of cell death in MPP^+-treated SH-SY5Y cells (Figure 3.5). Therefore, these data reveal that inhibition of cytosolic ROS production through inhibition of NOX2 alone is enough to prevent mitochondrial ROS production as well as cell death.

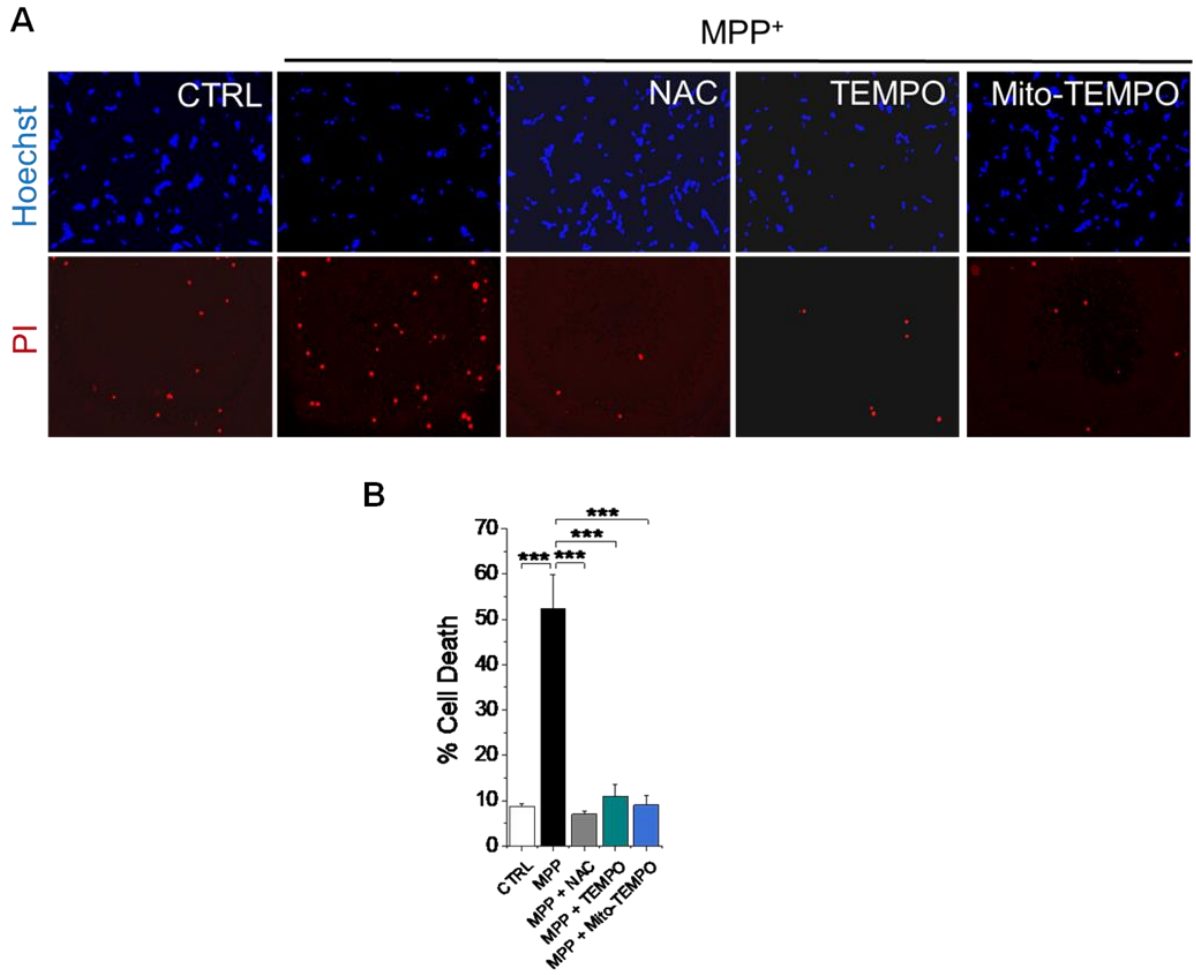

Figure 3.4 ROS quenchers have a protective effect against MPP^+ induced SH-SY5Y cell death.

SH-SY5Y cells were treated with medium only (CTRL) or 1 mM MPP^+ with and without antioxidants (5 mM NAC, 10 µM TEMPO or 10 µM Mito-TEMPO) for 24 h at 37ºC. **(A)** Fluorescent images of SH-SY5Y cells stained for nuclei of all (Hoechst) and dead (PI) cell nuclei. **(B)** Mean ± SEM of percent cell death from three independent experiments. *** indicates $p < 0.001$; one-way Anova with post-hoc Tukey test.

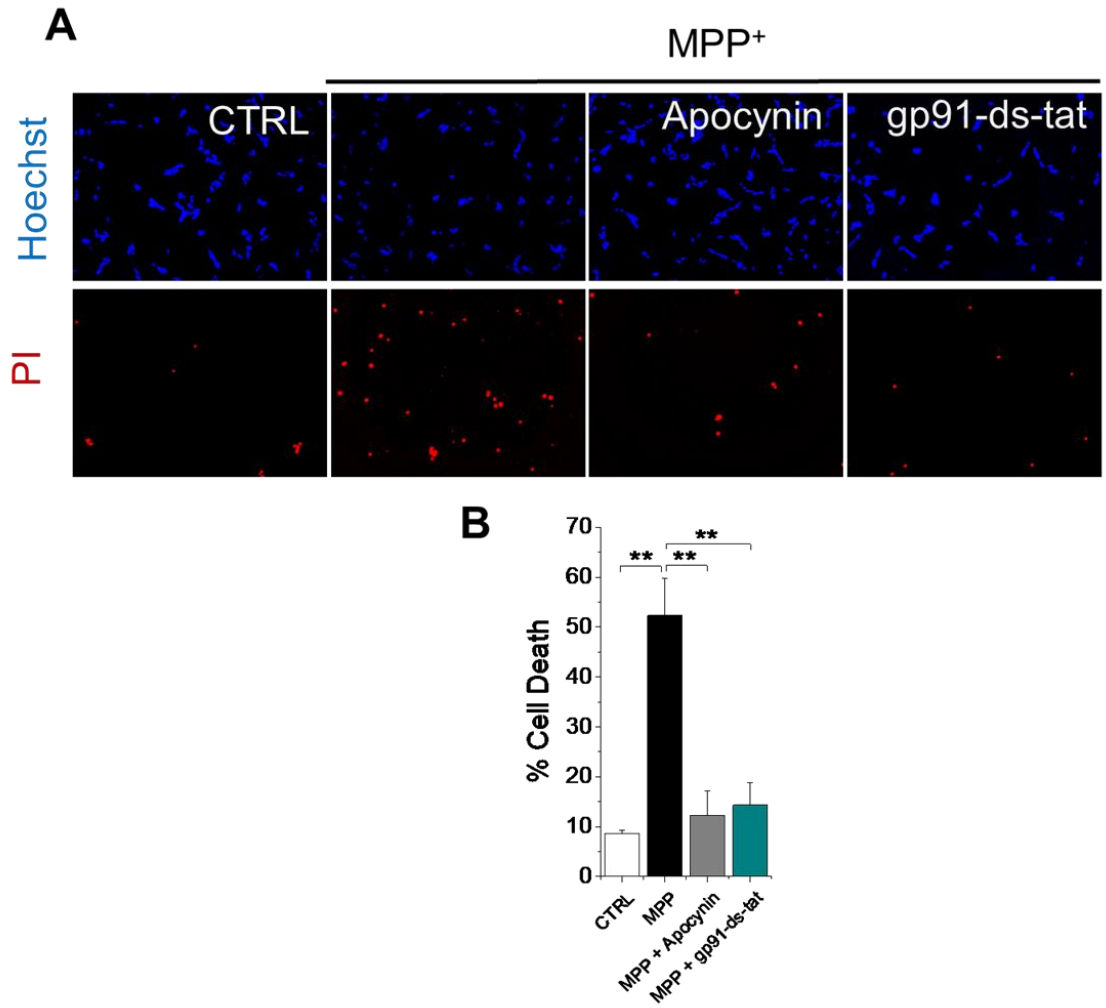

Figure 3.5 MPP$^+$ induces SH-SY5Y cell death through NOX2 activation.

NOX2 inhibitors attenuated MPP$^+$-induced SH-SY5Y cell death. **(A)** Fluorescent images of SH-SY5Y cells exposed to medium alone (CTRL), or medium containing 1 mM MPP$^+$ minus or plus NOX inhibitors (10 µM apocynin and 5 µM Gp91ds-tat). Cells were stained for nuclei of all (Hoechst) and dead (PI) cell nuclei. **(B)** Mean ± SEM of percent of cell death from three independent experiments. ** indicates $p < 0.01$; *** indicates $p < 0.001$; one-way Anova with post-hoc Tukey test.

3.2.5 TRPM2 channels mediate MPP^+-induced ROS production and cell death

Previous studies have shown that MPP^+ induces both TRPM2 expression and its activation, and that inhibition of TRPM2 channels prevents MPP^+-induced cell death (Sun et al., 2018) . Given the data that MPP^+ induces rise in both cytosolic and mitochondrial ROS in SH-SY5Y cells (Figure 3.1), as well as cell death (Figure 3.4). I asked whether TRPM2 channels mediate MPP^+-induced cell death by inducing ROS production.

SH-SY5Y cells were treated with MPP^+ (1 mM) in the absence or presence of three different pharmacological inhibitors of TRPM2 (10 µM ACA, 50 µM 2-APB and 10 µM PJ34) for 24 hours at 37ºC; the cells were then stained for cytosolic ROS as well as for mitochondrial ROS. Also, in a parallel experiment, PI staining was performed to measure the percentage of cell death. All the three inhibitors, ACA, 2-APB and PJ34 caused a significant reduction in MPP^+-induced cytosolic and mitochondrial ROS generation (Figure 3.6) as well as the accompanying cell death (Figure 3.7). Similar effects were seen when TRPM2 expression was suppressed using TRPM2-siRNA, but not with scrambled (Scr-) siRNA (Figure 3.8). These data support a role for TRPM2 channels in ROS overproduction and the consequent SHSY5Y cell death.

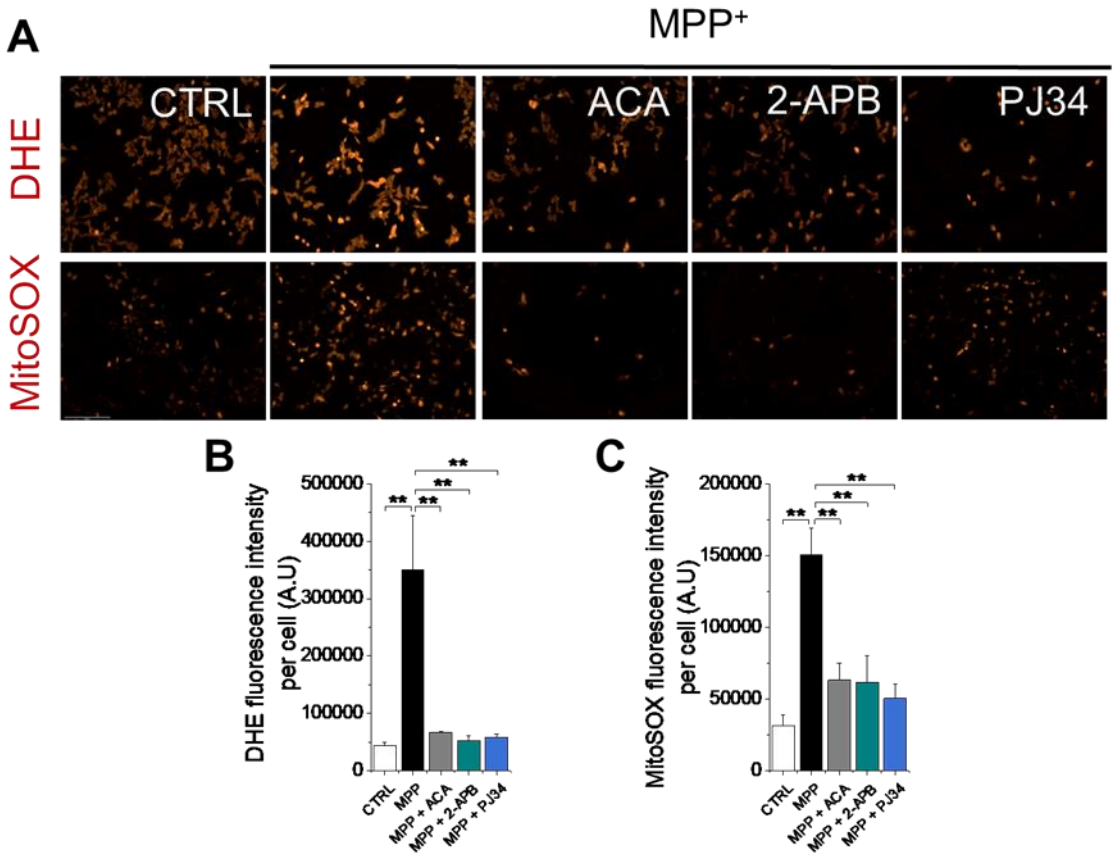

Figure 3.6 Inhibition of TRPM2 channels prevents MPP^+-induced ROS generation in SH-SY5Y cells.

Cells were treated with medium alone (CTRL) or medium containing 1 mM MPP^+ with and without TRPM2 inhibitors: ACA (10 µM), 2-APB (50 µM) and PJ34 (10 µM). **(A)** Fluorescent images of SHSY5Y cells stained for total cytosolic (DHE) and mitochondrial ROS (Mito-SOX). Scale bar: 200 µM. **(B-C)** The corresponding mean ± SEM of data of DHE Fluorescence **(B)** and Mito-SOX Fluorescence **(C)** from three independent experiments. ** indicates $p < 0.01$; *** indicates $p < 0.001$; one-way Anova with post-hoc Tukey test.

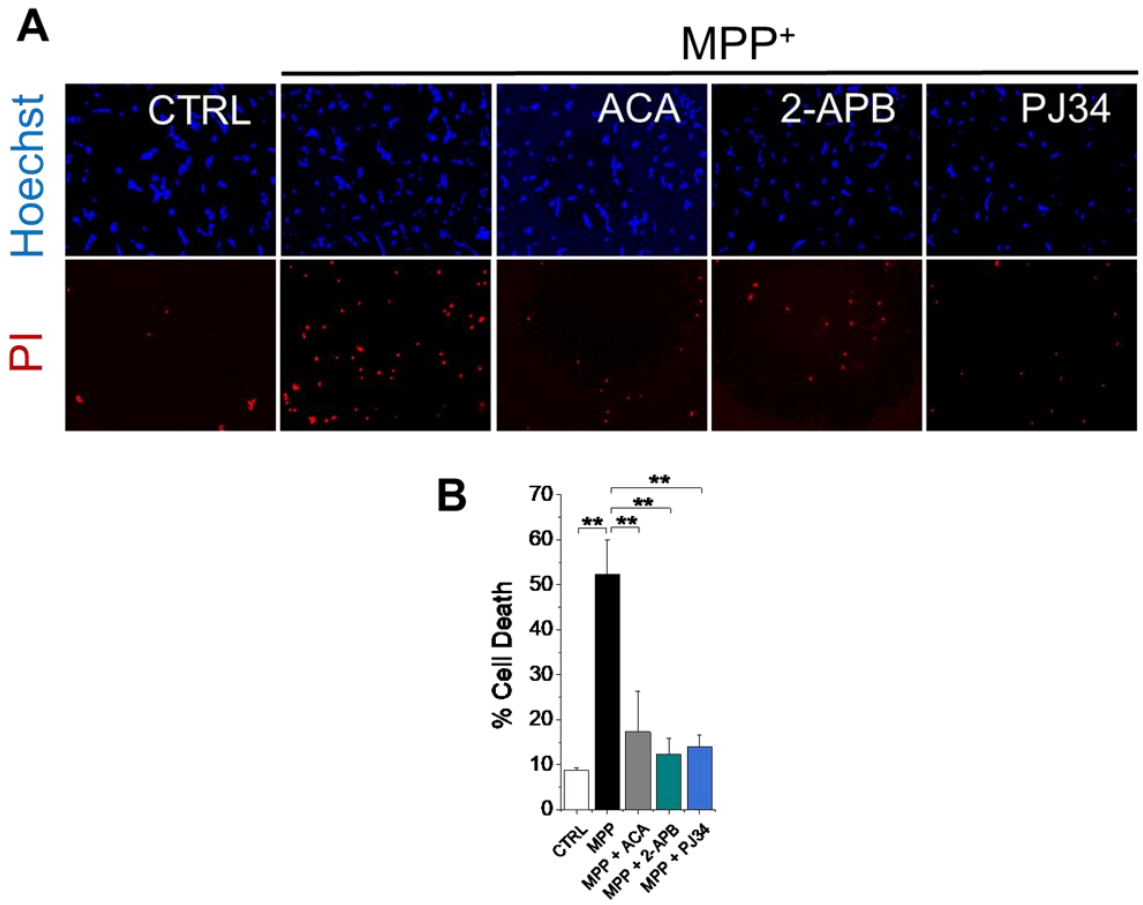

Figure 3.7 Inhibition of TRPM2 channels prevents MPP^+-induced SH-SY5Y cell death.

Inhibition of TRPM2 prevents MPP^+-induced SHSY5Y cell death. Cells were treated with medium alone (CTRL) or medium containing 1 mM MPP^+ with and without TRPM2 inhibitors: ACA (10 µM), 2-APB (50 µM) and PJ34 (10 µM). **(A)** Representative fluorescent images of SHSY5Y cells stained for all nuclei (Hoechst 33342) and nuclei of dead (PI) cells. **(B)** Mean ± SEM of percent cell death from three independent experiments. ** indicates $p < 0.01$; one-way Anova with post-hoc Tukey test.

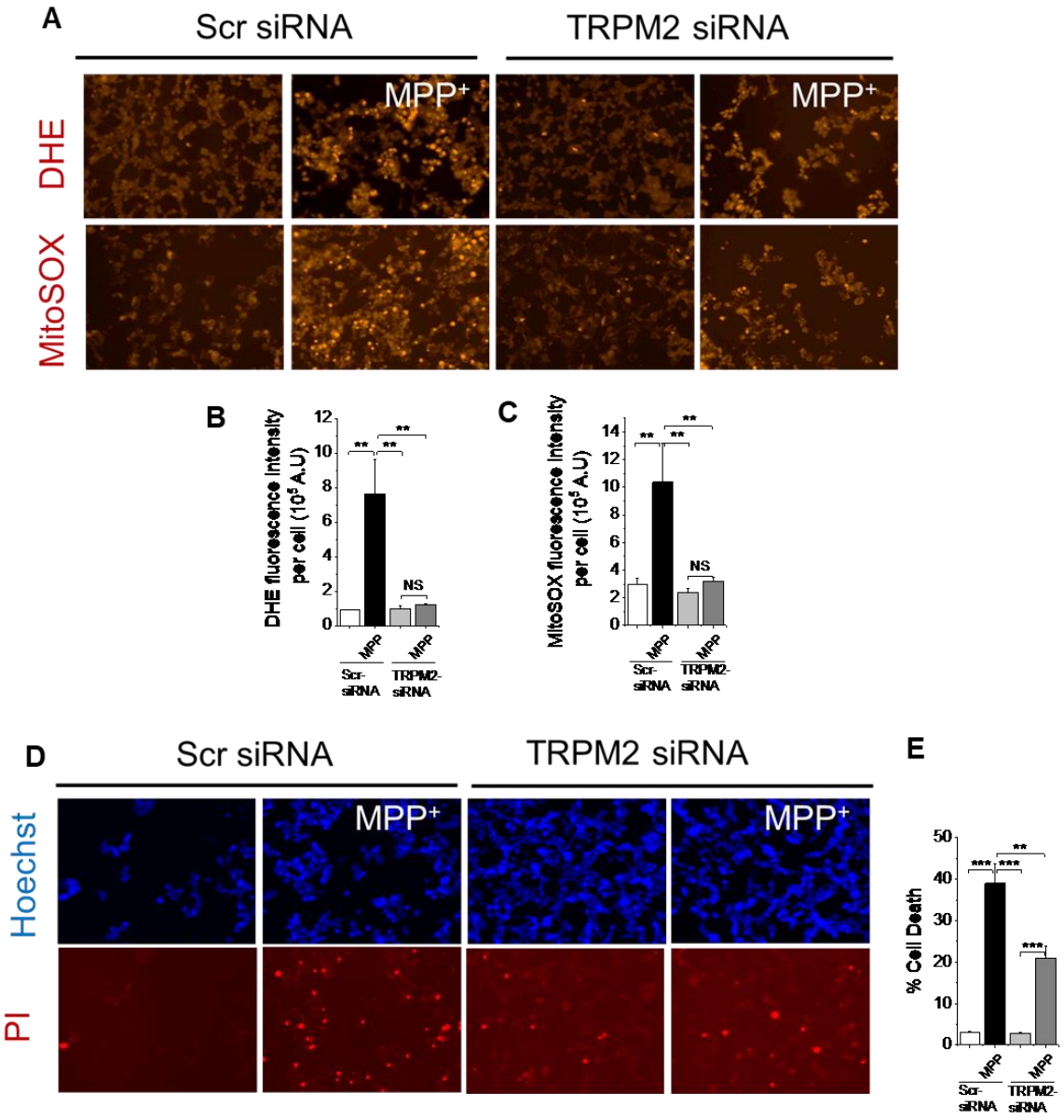

Figure 3.8 Inhibition of TRPM2 channels with siRNA prevents MPP$^+$-induced ROS production and cell death.

Cells were transfected with TRPM2-siRNA or scrambled (Scr)-siRNA and incubated with and without MPP$^+$ (1 mM) for 24 hours at 37ºC. **(A and D)** Fluorescent images of transfected SH-SY5Y cells stained for cytosolic ROS (DHE), mitochondrial ROS (MitoSOX), all nuclei (Hoechst 33342), and dead cell nuclei (PI). **(B,C,E)** The corresponding mean ± SEM of data of DHE Fluorescence **(B)** and MitoSOX Fluorescence **(C)** and percentage of cell death **(E)** from three independent experiments. ** indicates $p < 0.01$; *** indicates $p < 0.001$; one-way Anova with post-hoc Tukey test.

3.2.6 Use of a recombinant TRPM2 expression system to confirm the role of TRPM2 channels in ROS production

To confirm the role of TRPM2 channels in ROS generation, I have used HEK-293 cells (HEK-TRPM2^{tet}) transfected with TRPM2-FLAG gene that is controlled by a tetracycline-regulated promotor. Firstly, the effect of tetracycline on TRPM2-FLAG expression in HEK-TRPM2^{tet} cells was tested. Cells were treated with tetracycline (1 µg/ml, +tet) or vehicle (-tet) for 48 hours at 37ºC. The result of immunoblotting showed that cells treated with tetracycline display the TRPM2-FLAG band (~170 KDa); the band was absent in the control vehicle treated cells (Figure 3.9 A).

The function of expressed TRPM2 channel in HEK-TRPM2^{tet} cells was determined by measuring the Ca^{2+} influx using the Ca^{2+} imaging technique by Flexstation III. H_2O_2 (3 mM) treatment caused a marked increase in cytosolic Ca^{2+} signal (Figure 3.9 B) in tetracycline induced, but not uninduced cells. Furthermore, pre-treatment of the cells with the 2-APB (150 µM), an inhibitor of TRPM2, decreased the Ca^{2+} signal. These data indicate that TRPM2 expression was induced by tetracycline, and its activation by H_2O_2 stimulated extracellular Ca^{2+} entry in HEK-TRPM2^{tet} cells.

Using the inducible HEK-TRPM2^{tet} cell line, I sought supporting evidence for the role of TRPM2 channels in ROS production. Tetracycline-induced cells were treated with H_2O_2 (50 µM plus or minus 50 µM 2-APB) for 2 hours at 37°C; uninduced cells (minus tetracycline) were used as a control. After treatment, total and mitochondrial ROS generation was determined by staining the cells with DHE and MitoSOX, respectively. Results demonstrated that H_2O_2 caused some increase in total and mitochondrial ROS production in uninduced cells. In tetracycline induced cells, H_2O_2 caused further increase in both total and mitochondrial ROS production (Figure 3.9 C-E). Furthermore, 2-APB caused significant reduction in total and mitochondrial ROS generation in the induced cells (Figure 3.9 C-E). These data, together with the MPP^+ data on SH-SY5Y cells (Figures 3.6 and 3.8) support a role for TRPM2 channels in ROS production.

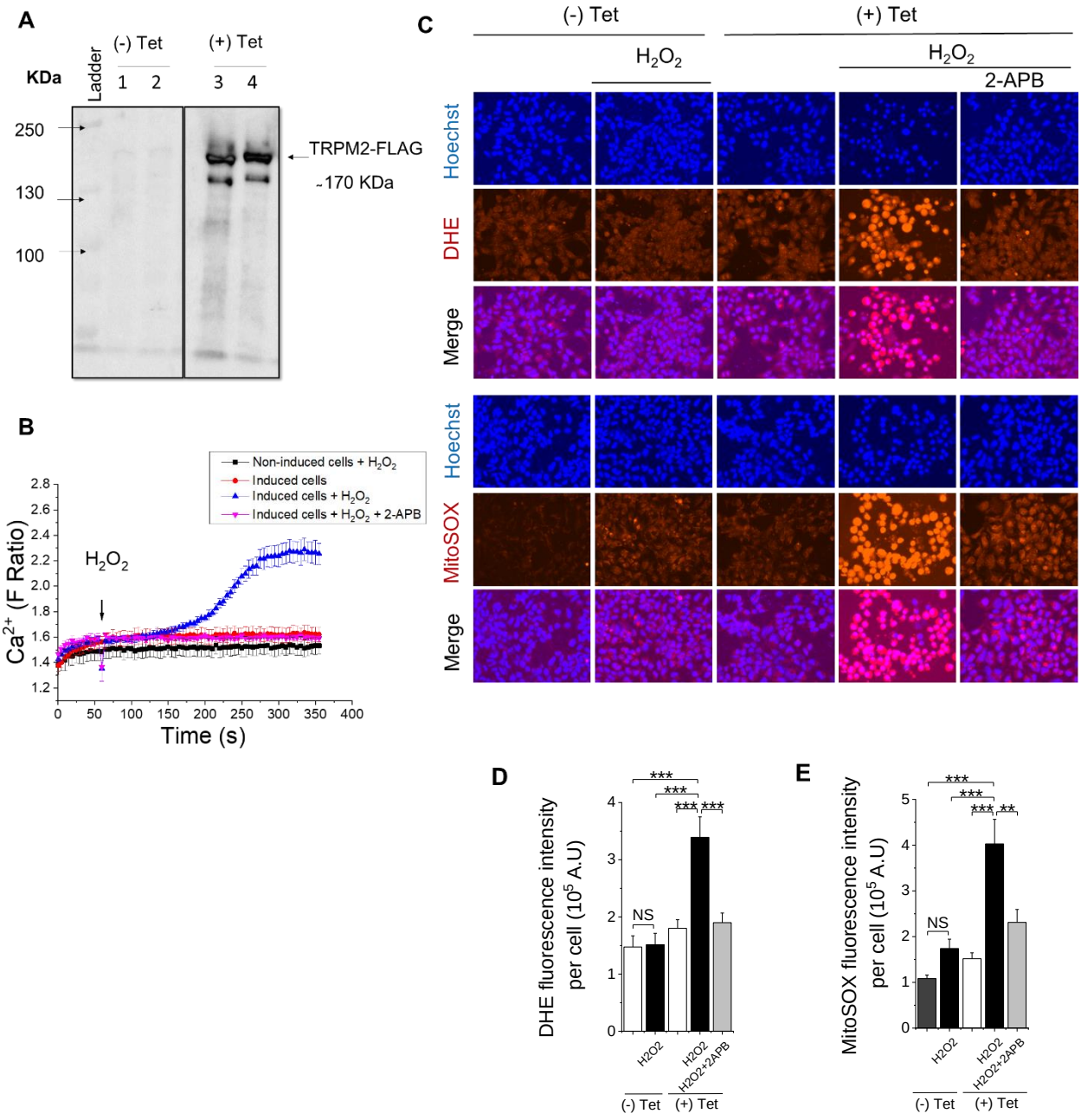

Figure 3.9 TRPM2 channels regulate ROS generation in HEK-TRPM2^{tet} cells.

(A-B) Tetracycline induction of TRPM2-FLAG expression in HEK-TRPM2^{tet} cells. **(A)** Western blot shows a ~170 KDa band corresponding to TRPM2-FLAG in HEK-TRPM2^{tet} cells induced with tetracycline (1 µg/ml). Duplicate samples were loaded; Samples 1 and 2 are non-induced (control), whereas samples 3 and 4 show the expression of TRPM2 in tetracycline-induced HEK-TRPM2^{tet} cells. **(B)** Functional analysis of TRPM2 expression in HEK-TRPM2^{tet} cells. Cells were loaded with Fura-2-AM for 1 hour followed by two times wash with SBS. They

were treated as follows: Control (non-induced cells treated with 3 mM H_2O_2), induced cells (tet) treated with 3 mM H_2O_2, and induced cells (tet) treated 3 mM H_2O_2 plus 150 µM 2-APB. Changes in cytosolic Ca^{2+} level were recorded using FlexStation III. H_2O_2 was applied at the time point shown with an arrow. Results show the F ratio (340 nm/ 380 nm), representing the Ca^{2+} level, at different time points. The symbols represent the treatment used on the cells. Results showed that when the expression of TRPM2 channel was induced by tetracycline (1 µg/ml), it stimulated marked Ca^{2+} influx into cells treated with H_2O_2 than non-induced cells. 2-APB inhibited the effect of H_2O_2 and reduced Ca^{2+} influx indicating the expression of TRPM2 in HEK-TRPM2^{tet} cells and its role in mediating the rise in intracellular Ca^{2+} level. **(C-E)** TRPM2 channels regulate ROS generation in HEK-TRPM2^{tet} cells. Cells either induced with tetracycline (+Tet) or left uninduced (-Tet) for 24 hours. One set of induced wells were pretreated with 2-APB (50 µM). Others were either left untreated or treated with H_2O_2 (50 µM) for 2 hours, as indicated. **(C)** Fluorescent images of cells in which Hoechst 33342 stained the cells nuclei, DHE and MitoSOX stained the cytosolic and mitochondrial ROS, respectively. **(D-E)** The corresponding mean ± SEM of data of DHE fluorescence **(D)** and MitoSOX fluorescence **(E)** per cell from three independent experiments. ** indicates $p < 0.01$; *** indicates $p < 0.001$; one-way Anova with post-hoc Tukey Test.

3.2.7 MPP^+ promotes ROS production by inducing intracellular Ca^{2+} increase through TRPM2 channels

The effect of MPP^+ in increasing cytosolic Ca^{2+} level has been previously reported (Chen et al., 1995, Kass et al., 1988, Marambaud et al., 2009). The results in this study thus suggest for the possibility that TRPM2 mediated rise in Ca^{2+} plays a role in MPP^+ induced ROS production and cell death.

To determine the effect of MPP^+ on intracellular Ca^{2+} level in SH-SY5Y cells, cells were exposed to medium only (CTRL) or medium containing MPP^+ (1 mM) for 24 hours at 37°C. The cells were then stained for Ca^{2+} using Fluo-4-AM, a Ca^{2+} fluorophore. Results showed that MPP^+ treatment caused a marked increase in intracellular Ca^{2+} level in SH-SY5Y cells (Figure 3.10).

Secondly, to support the fact that the increase in cytosolic Ca^{2+} level was due to the influx of Ca^{2+} through TRPM2 channels, TRPM2 blocker (2-APB) was used. SH-SY5Y cells were treated with medium only (CTRL) or medium containing MPP^+ (1 mM) plus or minus 2-APB (50 µM) for 24 hours at 37°C, followed by Fluo-4-AM staining. TRPM2-blocker has significantly reduced MPP^+-induced intracellular rise in Ca^{2+} level, indicating TRPM2 involvement in this process (Figure 3.10 A-B).

The expression of TRPM2 in SHSY-5Y cells was further tested by loading the cells with Fura-2-AM and measuring the Ca^{2+} signal using FlexStation. SH-SY5Y cells were exposed to MPP^+ (1 mM) for 24 hours. The rationale for exposing the cells to MPP^+ prior to measuring TRPM2 activity with FlexStation was the report that MPP^+ is capable of increasing the TRPM2 expression at the plasma membrane (Sun et al., 2018). Cells were then stimulated with H_2O_2 (2 mM) to reveal TRPM2 mediated Ca^{2+} influx. Cells that were stimulated with H_2O_2 showed higher intracellular Ca^{2+} signal compared to control (medium only). MPP^+ pre-treatment caused a further increase in Ca^{2+} signal (Figure 3.10 C-D), suggesting a role for MPP^+ in stimulating TRPM2 expression in SH-SY5Y cells.

Also, 2-APB attenuated H_2O_2-induced Ca^{2+} signal in MPP^+ pretreated cells (Figure 3.10 C-D), supporting the role of TRPM2 in mediating Ca^{2+} entry in SH-SY5Y cells during oxidative stress. Chelation of Ca^{2+} using BAPTA-AM was used to confirm that the rise in fluorescence of Ca^{2+} probe represents an increase in cytosolic Ca^{2+} levels. The data showed that BAPTA-AM pre-treatment was able to quench the rise in fluo-4 signal (Figure 3.10 A-B). Results of sections 3.2.5 to 3.2.7, taken together, suggest that TRPM2 is upregulated upon treatment with MPP^+, and the resultant increase in TRPM2 activity and cytosolic Ca^{2+} may cause the cells to become more vulnerable to apoptosis, mainly due to increased ROS level.

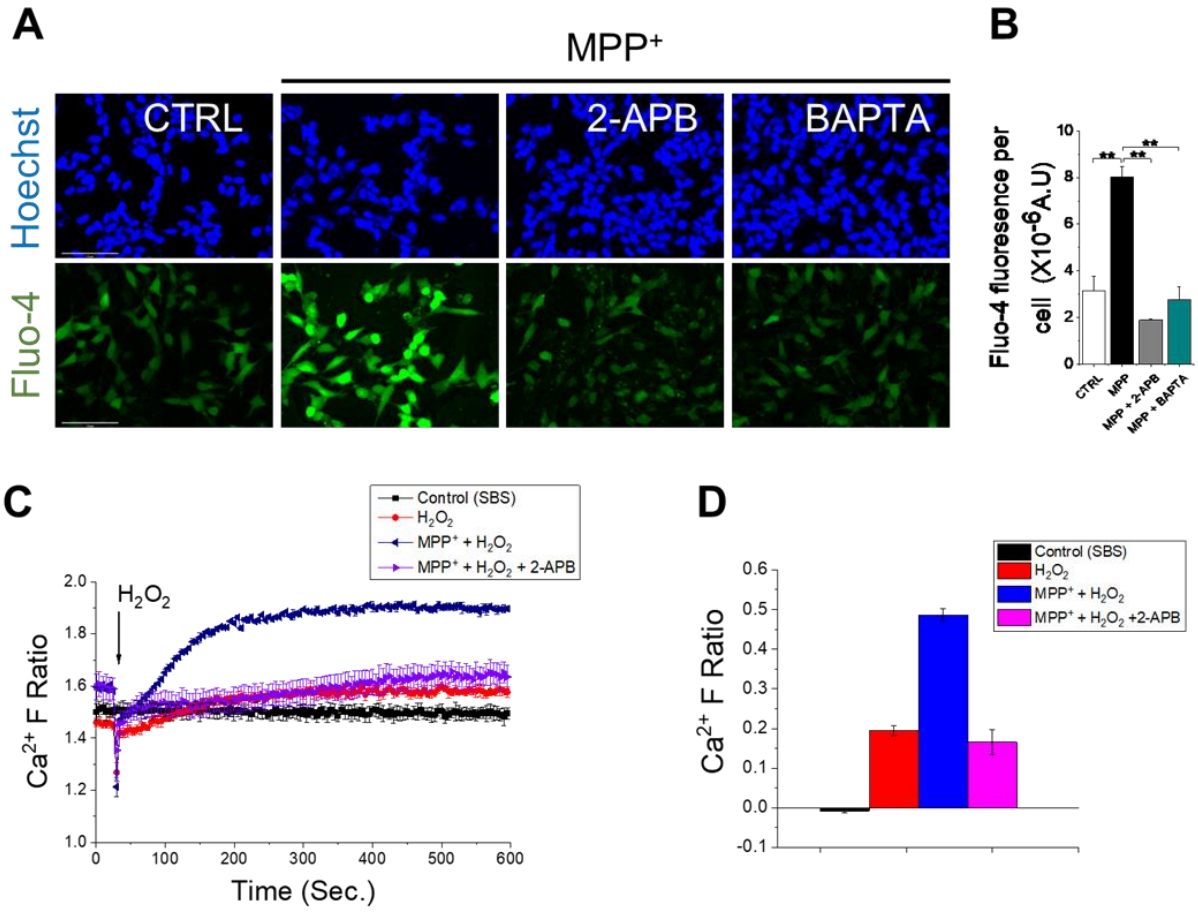

Figure 3.10 TRPM2 channels mediate MPP^+-induced rise in the intracellular Ca^{2+} level in SH-SY5Y cells.

(A) Fluorescent images of SH-SY5Y cells stained for Ca^{2+} using Fluo-4-AM and for all nuclei (Hoechst) after exposure to medium alone (CTRL) or medium containing 1 mM MPP^+ with and without the pretreatment (10 min) with TRPM2 blocker, 2-APB, or the Ca^{2+} chelator, BAPTA-AM. Scale bar: 75 µM. **(B)** Mean ± SEM of data from (A) expressed as mean of Fluo-4 fluorescence intensity per cell from three independent experiments. **(C)** Functional analysis of TRPM2 expression in SH-SY5Y cells. Cells were either untreated or pre-exposed for 24 h to 500 µM MPP^+ (MPP^+-pretreated). Cells were then loaded with Fura-2-AM for 1 h followed by two times wash with SBS. One group of MPP^+-pretreated cells were treated with 150 µM 2-APB for 15 min. Changes in cytosolic Ca^{2+} levels were recorded using FlexStation III, after addition of H_2O_2 or SBS (the time point shown with an arrow). Results show the F ratio (340 nm/ 380 nm), representing the Ca^{2+} level, at different time points. The symbols represent the treatment used

on the cells (see the key in **C**). **(D)** Mean ± SEM of peak fluorescence from **(C)**. * indicates $p < 0.5$ ** indicates $p < 0.01$; *** indicates $p < 0.001$; NS, not significant; one-way Anova with post-hoc Tukey test.

3.2.8 Chelation of Ca^{2+} and Zn^{2+} inhibits TRPM2-mediated ROS generation and SH-SY5Y cell death.

To understand the role of Ca^{2+} and Zn^{2+} in ROS production, first I examined the effect of Ca^{2+} and Zn^{2+} chelators on ROS production and cell death. As shown in the previous section, MPP^+ induced a rise in cytosolic Ca^{2+} that was inhibited by 2-APB (Figure 3.10). To determine the effect of Ca^{2+} on intracellular ROS generation and cell death, SH-SY5Y cells were co-treated with the Ca^{2+} chelator, BAPTA-AM (5 µM) and 1 mM MPP^+ for 24 hours at 37°C. Staining for total and mitochondrial ROS showed that cytosolic Ca^{2+} chelation by BAPTA-AM prevented MPP^+-induced ROS production in SH-SY5Y cells (Figure 3.11 A-C) as well as cell death (Figure 3.11 D-E). Taken together with the data presented in the previous section, these results support a role for TRPM2 mediated Ca^{2+} entry in ROS generation leading to SH-SY5Y cell death.

Next, the effect of Zn^{2+} chelation on MPP^+-induced ROS production and SH-SY5Y cell death was investigated. Previous studies with pancreatic β-cells have shown that TRPM2-mediated Ca^{2+} entry leads to rise in mitochondrial Zn^{2+} and this results in β-cells death (Li et al., 2017a). In this study, MPP^+ caused a similar rise in mitochondrial Zn^{2+} (will be discussed in chapter 4) resulting in an increase in ROS level and SH-SY5Y cell death that could be rescued with the Zn^{2+} chelator, TPEN (N,N,N',N'-tetrakis(2-pyridinylmethyl)-1,2-ethanediamine). In this experiment, cells were exposed to MPP^+ with and without TPEN (0.5 µM) for 24 hours at 37°C, following which cells were stained for cytosolic and mitochondrial ROS or for cell death. Chelation of intracellular Zn^{2+} by TPEN attenuated MPP^+-induced ROS production (Figure 3.12 A-C) as well as cell death (Figure 3.12 D-E) in SH-SY5Y cells. These data suggest that Ca^{2+} and Zn^{2+} both play a role in MPP^+-induced ROS overproduction leading to cell death.

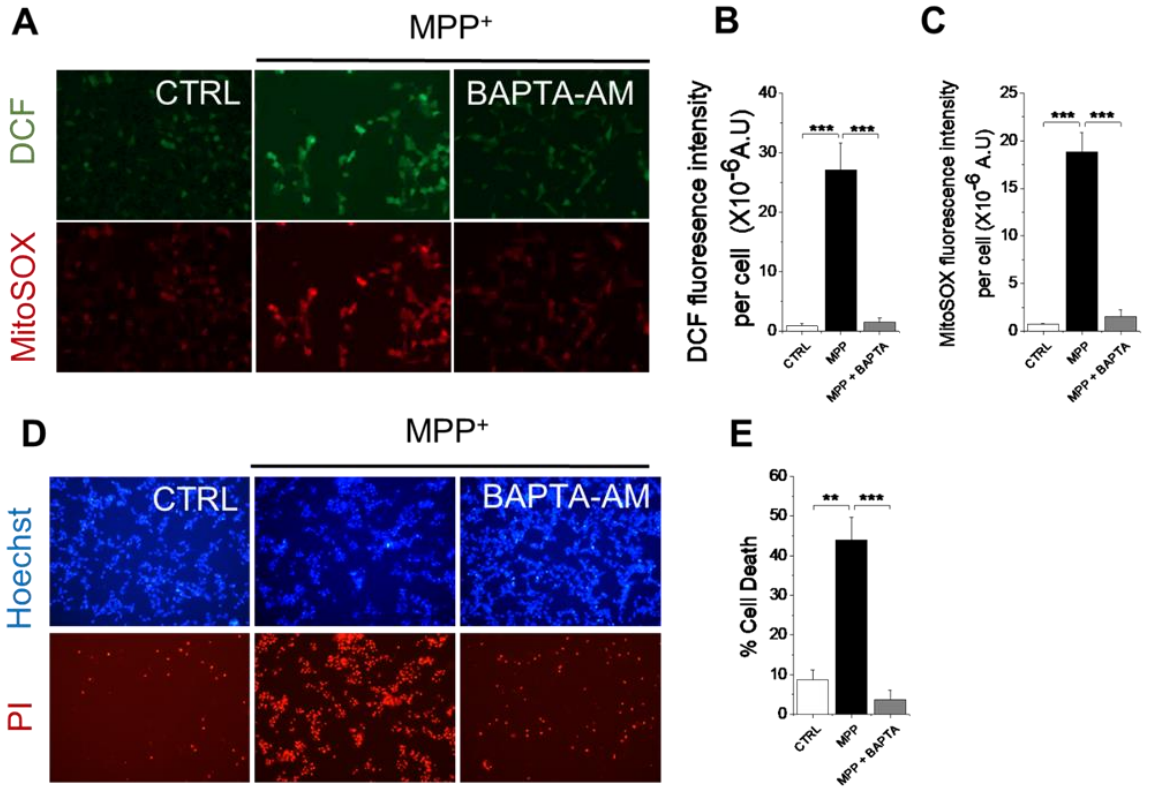

Figure 3.11 Chelation of Ca^{2+} prevents MPP^+-induced rise in ROS production and cell death.

(A-C) Chelation of Ca^{2+} prevented cytosolic and mitochondrial ROS production. SH-SY5Y cells were exposed to medium alone (CTRL), or medium containing 1 mM MPP^+ with and without the Ca^{2+} chelator, BAPTA-AM (5 µM), for 24 hours at 37ºC. **(A)** Fluorescent images of SH-SY5Y cells stained for total (DCF) and mitochondrial ROS (MitoSOX). **(B-C)** The corresponding mean ± SEM data for DCF Fluorescence **(B)** and MitoSOX Fluorescence **(C)** from three independent experiments. *** indicates $p < 0.001$; one-way Anova with post-hoc Tukey test. **(D-E)** Chelation of Ca^{2+} prevented cell death. Representative fluorescent images of SH-SY5Y cells stained for total nuclei (Hoechst 33342) and dead cell nuclei (PI) **(D)** and the corresponding mean ± SEM data for percentage cell death **(E)**. ** indicates $p < 0.01$; *** indicates $p < 0.001$ one-way Anova with post-hoc Tukey test.

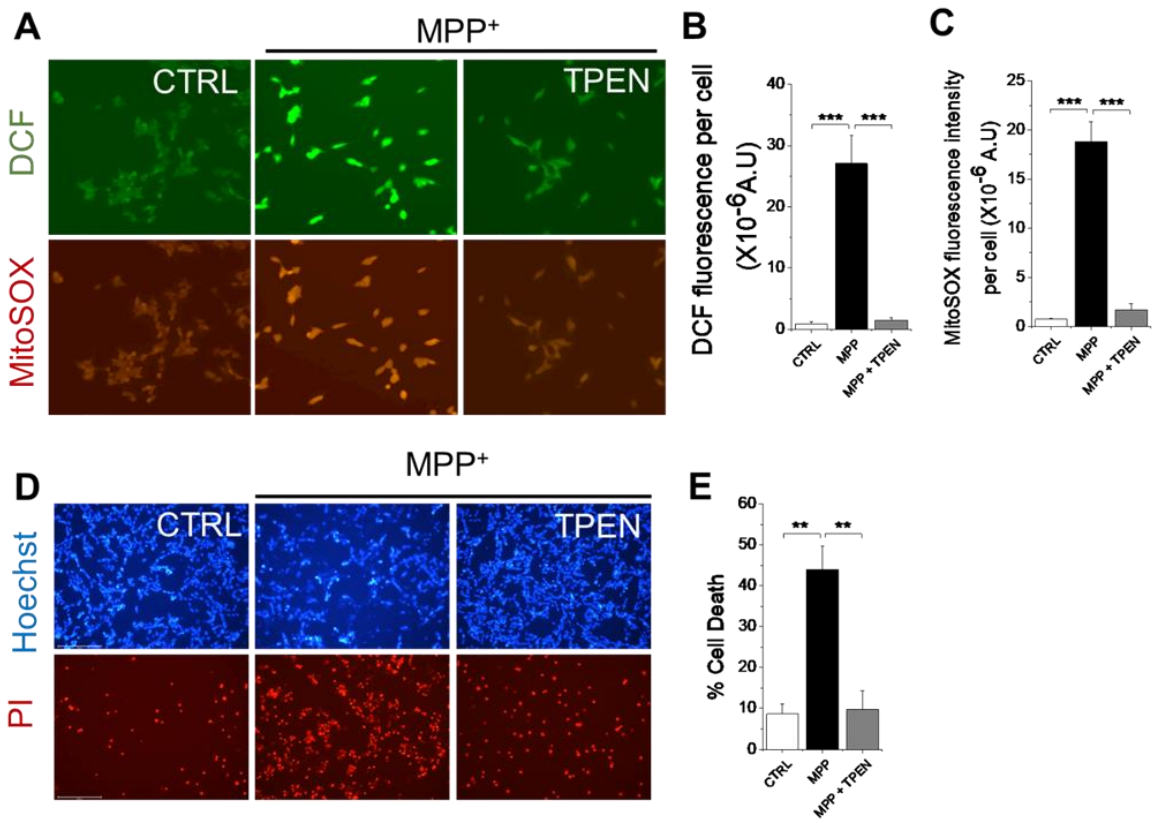

Figure 3.12 Chelation Zn^{2+} prevents MPP^+-induced rise in ROS production and cell death.

(A-C) Chelation of Zn^{2+} attenuated cytosolic and mitochondrial ROS production. SH-SY5Y cells were exposed to medium alone (CTRL), or medium containing 1 mM MPP^+ with and without Zn^{2+} chelator, TPEN (0.5 µM), for 24 hours at 37ºC. **(A)** Fluorescent images of SH-SY5Y cells stained for total (DCF) and mitochondrial ROS (MitoSOX). **(B-C)** The corresponding mean ± SEM data for DCF Fluorescence **(B)** and MitoSOX Fluorescence **(C)**. **(D-E)** Chelation of Zn^{2+} prevented cell death. Representative fluorescent images of cells stained for total nuclei (Hoechst 33342) and dead cell nuclei (PI). Scale bar: 125 µM. **(D)** and the corresponding mean ± SEM data for cell death **(E)**. All mean data are from three independent experiments; ** indicates $p < 0.01$; *** indicates $p < 0.001$; one-way Anova with post-hoc Tukey test.

3.2.9 Zn^{2+} acts downstream of Ca^{2+}

Since both Ca^{2+} and Zn^{2+} chelators were able to prevent ROS production and cell death, the possibility of an interplay between Ca^{2+} and Zn^{2+} in ROS production and cell death was next examined. For this, I used the calcium ionophore A23187 to raise intracellular Ca^{2+}. Cells were treated with A23187 for different time periods (0, 1, 2 and 4 hours) and the rise in intracellular Ca^{2+} recorded (Figure 3.13 A). The results showed time dependent increase in fluo-4 fluorescent intensity. Interestingly, longer exposure (2 hours and beyond) has resulted in Ca^{2+} accumulation in punctate structures. For subsequent experiments, I have used a 2 hours incubation period with A23187.

TRPM2 channels have been shown to promote Zn^{2+} release from intracellular sources and that the resultant increase in intracellular Zn^{2+} causes cellular damage (Manna et al., 2015, Abuarab et al., 2017, Li et al., 2017a, Li et al., 2017b). Since A23187 is not specific for Ca^{2+} and could allow Zn^{2+} entry, to eliminate the role for any extracellular Zn^{2+} entry, I combined A23187 with the membrane impermeable Zn^{2+} chelator, DTPA (diethylenetriaminepentaacetic acid). SH-SY5Y cells were treated with medium alone (CTRL) or medium containing A23187 (1 µM plus 1 mM DTPA) with and without the chelators, either BAPTA-AM (5 µM) or TPEN (0.5 µM). A23187 induced a rise ROS production (Figure 3.13 B-D) as well as cell death (Figure 3.13 E-F). Both ROS production and cell death were rescued by BAPTA-AM

Intriguingly, Zn^{2+} chelation with TPEN alone was sufficient to prevent the Ca^{2+} ionophore-induced ROS production (Figure 3.13 B-D) and cell death (Figure 3.13 E-F), indicating that Ca^{2+} entry affects Zn^{2+} dynamics and changes in intracellular Zn^{2+} homeostasis in turn affects ROS generation in the cell. Taken together, these results suggest that Ca^{2+} acts upstream of Zn^{2+} in a signaling pathway that leads to ROS overproduction and cell death.

To confirm and support this finding further, the intracellular concentration of Zn^{2+} was raised using a Zn^{2+} ionophore, Zn-pyrithione (PTO), in Ca^{2+} free medium to prevent Ca^{2+} entry. The results showed that Zn^{2+} delivery through Zn-PTO (2 µM) into SH-SY5Y cells caused a rise in cytosolic Zn^{2+}, detected using FluoZin-3 (Gee et al., 2002) (Figure 3.14 A) and mitochondrial ROS (Figure 3.14 B-C); Zn-PTO also significantly increased the cell death (Figure 3.14 D-E). Here I tested only for mitochondrial ROS as it is the major source of intracellular ROS and because mitochondrial Zn^{2+} has a vital role in this process, however, this will be investigated further in the following chapter. Moreover, TPEN (0.5 µM) was able to antagonize the effect of Zn-PTO (Figure 3.14). An important implication of these findings is that Zn^{2+}, rather than Ca^{2+}, plays a dominant role in ROS generation and cell death during MPP^{+}-induced oxidative stress in SH-SY5Y cells.

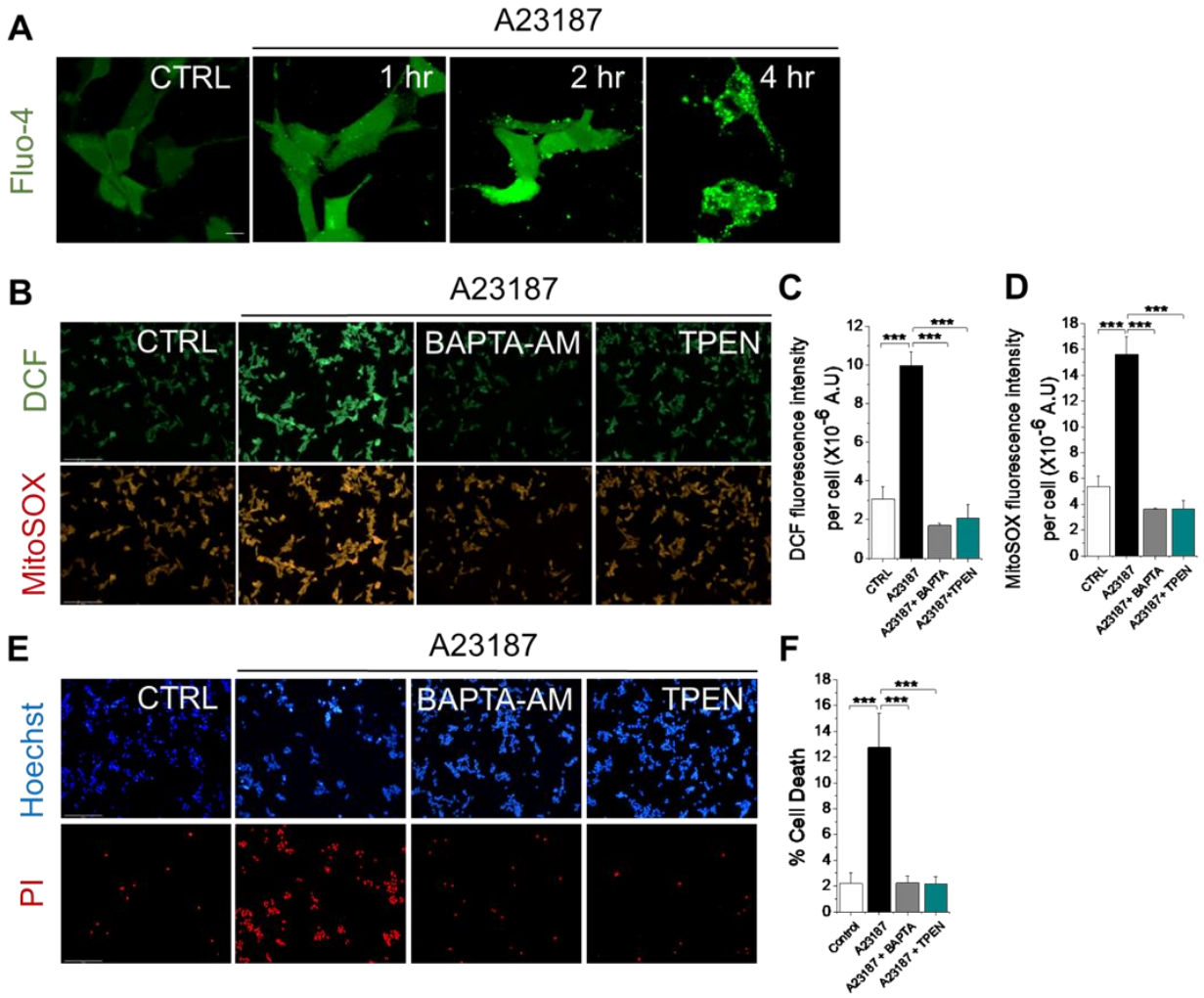

Figure 3.13 Ca^{2+} and Zn^{2+} chelators prevent A23187-induced ROS production and SH-SY5Y cell death.

(A) Confocal images of SH-SY5Y cells stained for Ca^{2+} using Fluo-4-AM after incubating the cells with the Ca^{2+}-ionophore, A23187 (1 µM, combined with 1 mM DTPA) for different time periods (0, 1, 2, 4 hours). A23187 increased the intracellular Ca^{2+}in a time-dependent manner. Scale bar: 10 µM. **(B-D)** Chelation of Ca^{2+} and Zn^{2+} prevented cytosolic and mitochondrial ROS production in A23187 treated cells. SH-SY5Y cells were exposed to medium alone (CTRL), or medium containing A23187 (1 µM, combined with 1 mM DTPA) with and without the Ca^{2+} chelator BAPTA-AM (5 µM) or Zn^{2+} chelator TPEN (0.5 µM) for 2 hours at 37ºC. **(B)** Fluorescent images of cells stained for total (DCF) and mitochondrial ROS (MitoSOX). Scale bar: 200 µM. **(C-D)** The corresponding mean ± SEM data of DCF Fluorescence **(C)** and MitoSOX Fluorescence **(D). (E-F)** Chelation of Ca^{2+}

and Zn^{2+} prevented A23187-induced cell death. Representative confocal images of SH-SY5Y cells stained for total cell nuclei (Hoechst 33342) and dead cell nuclei (PI) **(E)** and the corresponding mean ± SEM data for cell death **(F)**. Scale bar: 200 µM. All mean data are from three independent experiments; * indicates $p < 0.05$; ** indicates $p < 0.01$ one-way Anova with post-hoc Tukey test. *** indicates $p < 0.001$; one-way Anova with post-hoc Tukey test.

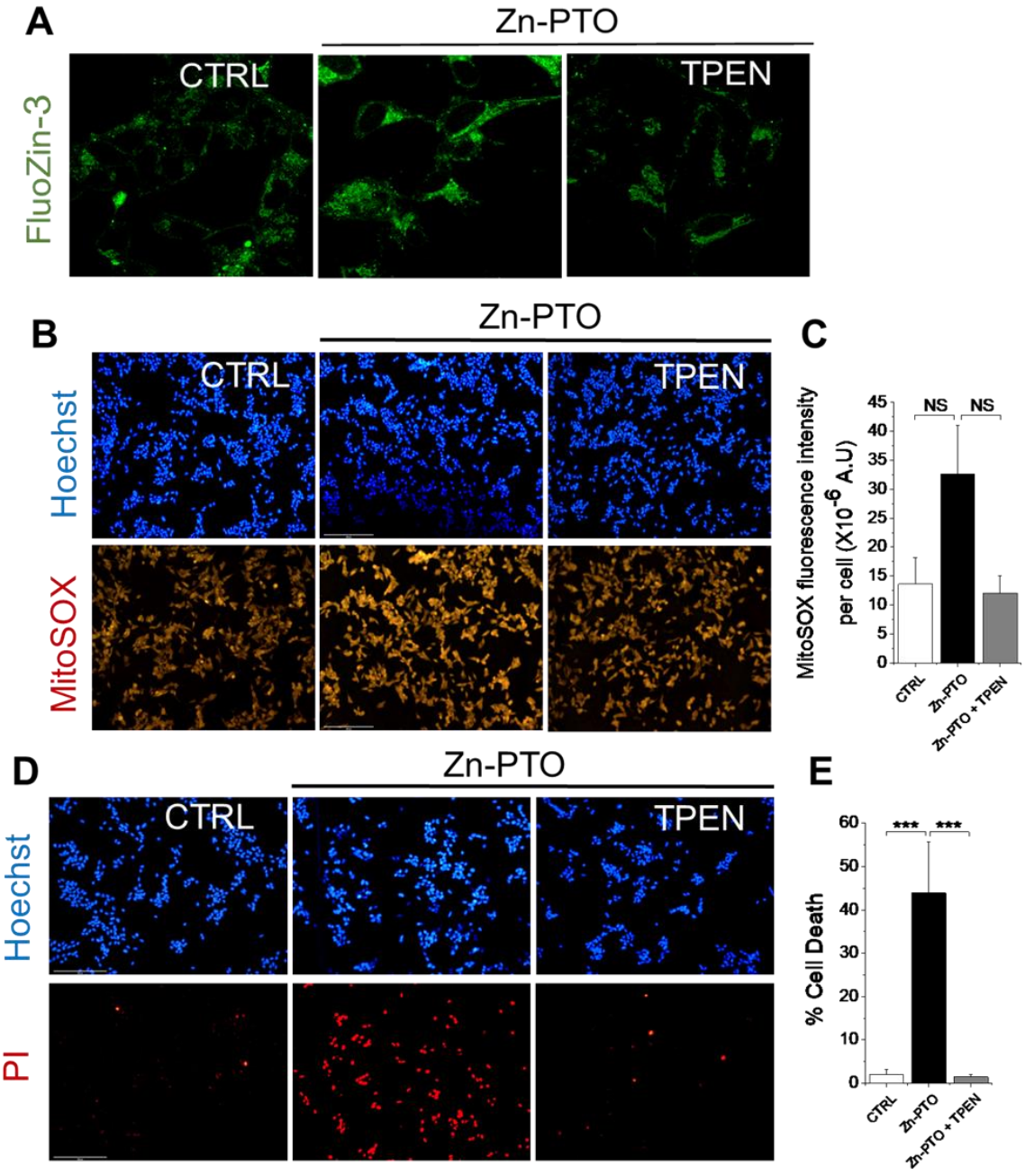

Figure 3.14 The Zn^{2+} ionophore (Zn-PTO) increases mitochondrial ROS production and cell death.

SH-SY5Y cells were exposed to Ca^{2+} free medium only (CTRL) or Ca^{2+} free medium containing Zn-PTO (2 µM) plus or minus the Zn^{2+} chelator, TPEN (0.5 µM), for 3 hours at 37ºC. **(A)** Confocal images of cells stained for intracellular Zn^{2+} using FluoZin-3 after Zn-PTO treatment. **(B-C)** Zn-PTO increases mitochondrial ROS production in SH-SY5Y cells that could be attenuated by TPEN. **(B)** Fluorescent images of cells stained for mitochondrial ROS (Mito-

SOX). Scale bar: 200 µM. **(C)** The corresponding mean ± SEM data for Mito-SOX fluorescence. NS, not significant; one-way Anova with post-hoc Tukey test. **(D-E)** TPEN prevented Zn-PTO -induced cell death. **(D)** Fluorescent images of SH-SY5Y cells stained for total (Hoechst 33342) and dead (PI) cell nuclei. Scale bar: 200 µM. **(E)** The corresponding mean ± SEM data for cell death. All mean date are from three independent experiments; *** indicates $p < 0.001$; one-way Anova with post-hoc Tukey test.

3.3 Discussion

Oxidative stress is a key pathogenic feature of many degenerative diseases, including PD (Metodiewa and Kośka, 1999, Beal, 2002, Dias et al., 2013). There is extensive genetic evidence as well as patient data to support a role for oxidative stress in the aetiology of PD. Post-mortem examination of the brains of PD patients displayed high levels of markers of peroxidation of lipids and proteins (Dias et al., 2013, Beal, 2002). The mechanisms of oxidative stress are highly complex involving a number of enzymes, regulatory molecules, and organelles. Added to this complexity is the evidence for extensive crosstalk between various mechanisms and organelles (Elfawy and Das, 2019, Castelli et al., 2019, Repnik and Turk, 2010, Camello-Almaraz et al., 2006, Feissner et al., 2009, Reczek and Chandel, 2015). This has presented enormous challenges to the development of therapies targeted to oxidative stress. Here I have focused on the role of the ROS-sensitive TRPM2 channel and the ions, Ca^{2+} and Zn^{2+}, it regulates. For this, an established cellular model of PD, where SH-SY5Y cells were challenged with a sub-lethal dose of MPP^+ to initiate oxidative changes that eventually lead to PD phenotype (Xicoy et al., 2017, Langston et al., 1983, Xie et al., 2010a, Vila and Przedborski, 2003), was used. The findings, summarized in the schematic (Figure 3.15), are as follows: 1. MPP^+ stimulates production of ROS via NOX2 and mitochondrial mechanisms. 2. The majority of cytotoxic ROS are produced at the mitochondria. 3. Inhibition of NOX2 was able to abolish MPP^+ induced mtROS production indicating NOX2 derived ROS drive mtROS production. 4. Inhibition of TRPM2-mediated Ca^{2+} entry abolishes the ability of MPP^+ to stimulate ROS production. 5. Chelation of intracellular Ca^{2+} rescued MPP^+ induced ROS production and cell death. 6. Importantly, Ca^{2+} induced ROS production and the consequent cell death were prevented by chelating Zn^{2+} alone, indicating a downstream role for Zn^{2+} in Ca^{2+}-induced ROS production. 7. Intracellular delivery of Zn^{2+} using an ionophore recapitulated the effect of MPP^+ on mtROS production. These findings (observations 3, 6 and 7) raise questions on the historically accepted view that MPP^+ generates cytotoxic mtROS by inhibiting mitochondrial complexes. I present an alternative mechanism whereby the neurotoxin, MPP^+ activates the TRPM2 channel to promote Ca^{2+} entry, that in

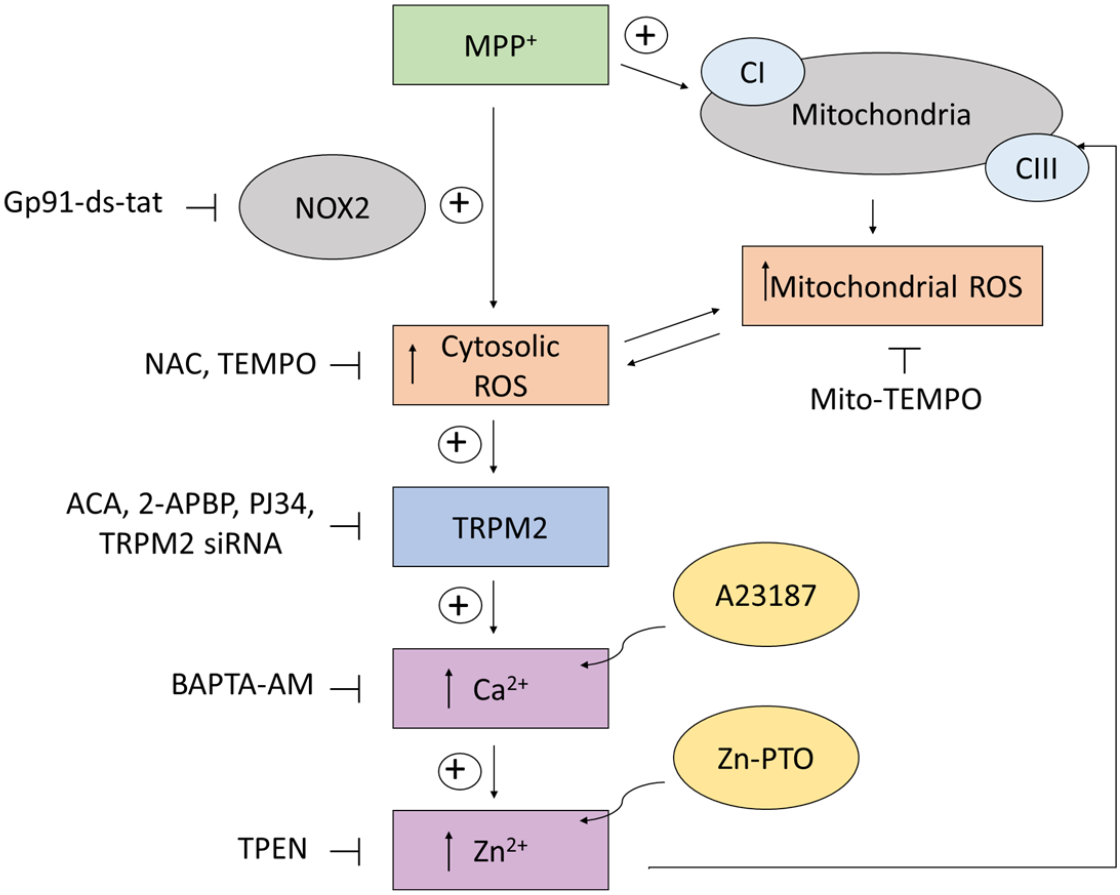

Figure 3.15 Schematic diagram summarized the findings.

In SH-SY5Y cells, MPP^+ induces ROS generation via NOX2 and mitochondrial pathways. The mitochondria generate the vast majority of harmful ROS. The inhibition of NOX2 by gp91-ds-tat was able to stop the generation of mtROS caused by MPP^+, which indicates that NOX-derived ROS are the likely major determinant of mtROS production. TRPM2, the Ca^{2+} permeable ion channel, is activated by ROS causing an increase in cytosolic Ca^{2+} and Zn^{2+} levels that subsequently stimulate mitochondrial ROS generation. Blocking the TRPM2 channel using pharmacological inhibitors (ACA, 2-APB, PJ34) or TRPM2 siRNA prevents MPP^+ induced ROS generation. Chelation of intracellular or Zn^{2+} alone was sufficient to prevent cytotoxic mtROS generation and cell death, indicating that Zn^{2+} plays a critical role in MPP^+ induced neuronal cell death. Figure created with BioRender.com

turn increases intracellular Zn^{2+} levels to cause mitochondrial complex inhibition and the cytotoxic mtROS production.

3.3.1 MPP^+ induced ROS amplification drives death of SH-SY5Y neuroblastoma cells

Numerous studies have demonstrated that MPP^+ induces ROS generation in SH-SY5Y cells (Yang et al., 2018, Yi et al., 2013, Lee et al., 2011, Wang and Liu, 2022). Various sources and mechanisms have been reported including dopamine metabolism (Wang et al., 2005, Feuerstein et al., 1988, Chang and Ramirez, 1987, Santiago et al., 1995), NADPH oxidases (Zawada et al., 2011, Gao et al., 2003, Wu et al., 2003) and mitochondria (Yi et al., 2013, Yang et al., 2018, Cleeter et al., 1992). MPP^+ can stimulate dopamine release from the storage vesicles into the cytosol (Rollema et al., 1988), which, in turn, can either be auto-oxidized leading to the formation of highly reactive intermediates and ROS or can be oxidized enzymatically by mitochondrial monoamine oxidase-b (MAO-b) producing 3,4-dihydroxyphenylacetaldehyde (DOPAL). During this process, H_2O_2 is produced as a by-product. One study has reported that DOPAL induces opening of the mitochondrial permeability transition pore (mPTP) thereby contributing to cell death (Kristal et al., 2001). Examination of post-mortem brains of PD patients revealed increased expression of NOX2 in both microglia and dopaminergic neurons in substantia nigra (Keeney et al., 2021) indicating a role for NOX2 in PD; however, the relative contributions of microglial NOX2 and neuronal NOX2 remains unclear. NOX2 upregulation and the resultant increase in ROS production has been reported in both animal models (Wu et al., 2003) and *in vitro* cellular models of PD (Keeney et al., 2021, Zawada et al., 2011). Furthermore, knock-out of NOX2 in mice reduces the loss of dopaminergic neurons (Brieger et al., 2012). An important source of ROS, however, is mitochondria where most neurotoxins are thought to inhibit mitochondrial complexes to produce mtROS (Cleeter et al., 1992, Przedborski et al., 2004). However, as will be discussed further, the underlying mechanisms are not

mutually exclusive, but significant positive feedback regulation seems to operate between NOX2 and mitochondria.

In this study, I found that MPP^+-induced ROS production and neuronal cell death could be prevented not only by quenching the total ROS with NAC and TEMPO, but by quenching the mitochondrial ROS alone with Mito-TEMPO (Figure 3.2 and 3.4). These results suggested that NOX2 derived ROS alone cannot cause SH-SY5Y cell death and may need to signal mitochondria to produce mtROS. Consistent with this possibility, I found inhibition of NOX2 prevented mtROS production (Figure 3.3) and cell death (Figure 3.5). These data provide support to the emerging concept whereby ROS generated at one source can serve as a positive feedback signal for ROS production at a different site - a pathway termed 'ROS-induced ROS production' (RIRP) (Daiber, 2010, Dikalov, 2011). While our results suggest that NOX2 derived ROS stimulate mtROS production in MPP^+ challenged neuronal cells, in the rotenone models, the toxin appears to stimulate mtROS first which in turn activate NOX2 (Keeney et al., 2021). Regardless of which way round RIRP occurs, RIRP appears to represent a key mechanism that enables amplification of intracellular ROS in order to raise the cytosolic concentration of ROS to toxic levels.

3.3.2 TRPM2 channels mediate MPP^+ induced ROS production and cell death

Ca^{2+} is a well-known regulator of ROS production (Görlach et al., 2015). Rise in intracellular Ca^{2+} is implicated in NOX2 activation (Brandes et al., 2014, Rada and Leto, 2008, Valentin et al., 2001, Bréchard et al., 2005, Schenten et al., 2008, Schenten et al., 2010) as well as mitochondrial ROS generation (Camello-Almaraz et al., 2006, Görlach et al., 2015, Feissner et al., 2009, Kowaltowski et al., 1998, Cadenas and Boveris, 1980). Thus, dyshomeostasis of Ca^{2+} is closely associated with ROS generation and the consequent cell death in degenerative diseases (Tan et al., 2001, Mattson, 2000, Jenner and Olanow, 1998, Cookson

and Shaw, 1999, Siklós et al., 1996, Barnham et al., 2004, Lewen et al., 2000, Ermak and Davies, 2002, LaFerla, 2002, Gibson, 2002). Furthermore, there is evidence for a significant interplay between Ca^{2+} and ROS: Ca^{2+} can stimulate ROS and ROS, in turn, can affect intracellular Ca^{2+} dynamics (Barnham et al., 2004, Suzuki et al., 1997, Neill et al., 2002). A number of calcium channels and transporters are ROS sensitive, and their activation can impact normal Ca^{2+}-ROS interplay, leading to cellular dysfunction or demise, and ultimately to disease states (Hempel and Trebak, 2017, Liu et al., 2022, Wang et al., 2017, Nilius, 2007, Ermak and Davies, 2002, Hool and Corry, 2007). The TRPM2 channel is one of the ROS-sensitive ion channels implicated in mitochondrial dysfunction and cell death (Fonfria et al., 2004, Takahashi et al., 2011, Abuarab et al., 2017, Li et al., 2017a). A role of TRPM2 channels in the regulation of Ca^{2+} as well as ROS has been reported (Fonfria et al., 2004, Li and Jiang, 2019, Takahashi et al., 2011, Abuarab et al., 2017, Li et al., 2017a). Also, recent studies suggest that TRPM2 channels might play important role in the pathology of neurodegenerative diseases (Sun et al., 2015, Xie et al., 2010b, Verma et al., 2012, Ye et al., 2014) because it is highly expressed in brain.

Thus, I hypothesized that TRPM2 channel plays a role in NOX2 activation and/or mitochondrial ROS generation. Consistent with this hypothesis, inhibition of TRPM2 channels with pharmacological agents or silencing RNA prevented MPP^+ induced ROS production (Figures 3.6, 3.7 and 3.8). Additional support for the role of TRPM2 was obtained using HEK-293 cells. HEK-293 cells lacking TRPM2 expression failed to generate ROS when challenged with an oxidant (H_2O_2). By contrast, when these cells were engineered to express TRPM2 channel, the cells responded to oxidant treatments and generated significant amounts of ROS (Figure 3.9). NOX2 is known to be activated by Ca^{2+}-dependent protein kinases (Fontayne et al., 2002, Belarbi et al., 2017). I asked whether TRPM2 activation provides the Ca^{2+} required for NOX2 activation. MPP^+ treatment of SH-SY5Y cells caused an increase in intracellular Ca^{2+} by activating the TRPM2 channels (Figure 3.10). Given the finding that NOX2 dependent ROS generation drives mitochondrial ROS production, these results suggest that TRPM2 activation promotes NOX2 activation by providing the Ca^{2+} required for the recruitment of $p47^{phox}$ and assembly of the functional NOX2 complex at the plasma membrane.

Previous studies have indeed reported that MPP^+ signals the translocation of $p47^{phox}$ to the plasma membrane (Zawada et al., 2011, Hernandes and Britto, 2012, Jackson-Lewis et al., 2002, Zhang et al., 2004); however the mechanism that ensures the Ca^{2+} supply, to the best of my knowledge, is unknown. Taken together, MPP^+ activation of the TRPM2 channel, by providing the Ca^{2+}, promotes activation of the plasma membrane NOX2 to stimulate ROS production that, in turn, stimulates mtROS generation. As NOX2 generates ROS at the plasma membrane it is conceivable that this would rise the local concentration of ROS to levels sufficient to activate the TRPM2 channel. Thus, I speculate that NOX2 and TRPM2 channels are functionally coupled at the plasma membrane to enable amplification of the two toxic signals, viz., Ca^{2+} and ROS.

These findings raise questions on the long-prevailing notion that MPP^+ acts primary on complex I of mitochondria directly to produce ROS and the subsequent cell death (Cleeter et al., 1992, Ramsay et al., 1991, Yang et al., 2018). However, it is difficult to conceive how TRPM2 inhibition can interfere with MPP^+ inhibition of Complex I. To address this, I have examined how the Ca^{2+} signals generated at the plasma membrane signal the mitochondria to stimulate ROS production. Chelation of cytosolic Ca^{2+} with BAPTA was sufficient to prevent MPP^+ induced ROS generation as well as cell death (Figure 3.11), a result that is consistent with several previous reports (Kass et al., 1988, Collatz et al., 1997, Tymianski et al., 1993, Togashi et al., 2008, Ichimiya et al., 1998, Annunziato et al., 2003, Norberg et al., 2010). Numerous studies have reported that a rise in intracellular Ca^{2+} is accompanied by an influx of Ca^{2+} into the mitochondria (Santo-Domingo and Demaurex, 2010, Rizzuto et al., 2008, Duchen, 2000b), and that the resulting rise of Ca^{2+} can impact mitochondrial complexes (Pandya et al., 2013, Sheehan et al., 1997, Pan et al., 2013, Bravo-Sagua et al., 2017). However, there are recent studies implicating Zn^{2+} in oxidative stress induced neuronal cell death (Li et al., 2017b, Kim et al., 1999). Furthermore, using endothelial (Abuarab et al., 2017) and pancreatic β-cells (Li et al., 2017a), recent studies have demonstrated that TRPM2-mediated Ca^{2+} influx can be accompanied by an elevation of mitochondrial Zn^{2+} to levels sufficient to cause significant mitochondrial fission and loss of function.

Consistent with a role for Zn^{2+}, the Zn^{2+} chelator (TPEN) prevented MPP^+ induced mtROS generation and cell death (Figure 3.12) (Sheline et al., 2013, Kim et al., 1999). TPEN is a cell permeable Zn^{2+} chelator that has high affinity to Zn^{2+} (K_d ~ 2.6 x 10^{-16} M^{-1}) (Sensi et al., 2009). However, it can also chelate Ca^{2+} but in low affinity (K_d ~ 1.3 x 10^{-4} M^{-1}), thus a low concentration of TPEN (0.5 µM) was used to exclude any Ca^{2+} binding.

Direct elevation of intracellular Ca^{2+} with the calcium ionophore, A23187 caused an increase in intracellular levels of Zn^{2+} and ROS production that was again suppressed by TPEN (Figure 3.13). Direct elevation of intracellular Zn^{2+} with the zinc ionophore, Zn-pyrithione, reproduced the effects of both MPP^+ and the intracellular Ca^{2+} rise on mtROS production and cell death (Figure 3.14). Together these results indicate that Ca^{2+} induced mtROS production is mediated by Zn^{2+}. It is likely that Zn^{2+} enters mitochondria through the mitochondrial uniporter (Malaiyandi et al., 2005) and other unidentified mechanisms and inhibit complexes I and III (Sensi et al., 2009) and thereby increase mtROS production. Studies with isolated mitochondria have shown inhibition of complexes I and III by Zn^{2+} (Sensi et al., 2009, Sharpley and Hirst, 2006, Kleiner, 1974, Skulachev et al., 1967, Kleiner and Von Jagow, 1972). Furthermore, a Zn^{2+} binding site was found in the crystal structure of Complex III (Giachini et al., 2007).

Although the ability of MPP^+ to induce mtROS production has been attributed to the ability of the drug to inhibit complex I, these results were obtained using isolated mitochondria (Mizuno et al., 1987, Suzuki et al., 1992, Cassarino et al., 1999, Przedborski et al., 2004, Hasegawa et al., 1990). In the intact cell, however, the situation appears to be different: the mtROS inducing effect of MPP^+ is more likely mediated by Zn^{2+} ions. Whether Zn^{2+} also mediates the mitochondrial effects of numerous other neurotoxins remains to be investigated. In support of a key role for Zn^{2+} in PD pathology is the evidence from post-mortem brains of PD patients where studies have shown high levels of free Zn^{2+} compared to healthy brains (Portbury and Adlard, 2017, Dexter et al., 1991).

In summary, results presented in this chapter reveal a novel signaling circuit, comprising NOX2, TRPM2, Ca^{2+}, and Zn^{2+}, that underlies neurotoxin-mediated dopaminergic cell death. Whether a similar mechanism occurs in other models of PD, including the genetic models remains to be determined. Given this pathway is associated with the generation of toxic levels of ROS, it could potentially be targeted to develop new drugs for PD.

3.3.3 Experimental limitations

This work has some limitations including the use of the small-molecule fluorescent probes for intracellular ROS assessment. Two fluorescent probes were used in studies presented in this chapter, DCFH-DA and DHE. Although in most experiments DHE was used, in some experiments DCFH-DA was used. DCFH is oxidized to the fluorescent product DCF by several ROS, so it is not specific for a particular ROS. Also, DCF is not oxidized directly by H_2O_2, but only after it is converted to more reactive species by peroxidases or redox-active metals (Murphy et al., 2022). The fluorescence of DCF is sensitive to local O_2 levels, pH (Murphy et al., 2022), and light. Thus, the fluorescent intensity might be affected by factors other than just ROS. It is therefore prudent to use other methods, such as mass spectrophotometry and genetic ROS sensors (Murphy et al., 2022).

It is known that BAPTA can bind divalent cations other than Ca^{2+}. However, BAPTA is routinely used in research based on the assumption that other divalent cations either have a significantly lower binding affinity for BAPTA than for Ca^{2+}, or their overall levels are too low to interfere with Ca^{2+}/BAPTA binding. It is common knowledge that Zn^{2+} competes with Ca^{2+} for binding to Ca^{2+} chelators and probes (such as Fluo-4 and Fura-2) (Qian and Colvin, 2016). For example, Zn^{2+} binds BAPTA with high affinity (K_d= 7.9 nM) (BENTERS et al., 1997) compared with Ca^{2+} (K_d= 110 nM) (Tsien, 1980), however, total intracellular Zn^{2+} levels range from one-tenth to one-third of total Ca^{2+} levels (Colvin et al., 2015). Furthermore, the majority of intracellular Zn^{2+} is protein bound. To eliminate Zn^{2+}

interference with Ca^{2+}/BAPTA binding, TPEN (Zn^{2+} chelator) was used in conjunction with BAPTA.

Furthermore, the ionophore A23187 is not specific for Ca^{2+} and could allow Zn^{2+} entry. To eliminate the role for any extracellular Zn^{2+} entry, I combined A23187 with the membrane impermeable Zn^{2+} chelator, DTPA. However, more specific delivery methods, for example, by modulating Ca^{2+} channels and transporters, could be used.

Chapter 4

TRPM2- mediated ionic signals promote lysosomal dysfunction and mitochondrial fragmentation in a cellular model of Parkinson's disease

4.1 Introduction

Parkinson's disease (PD) is the second most prevalent neurological movement disorder, characterized by the death of dopaminergic neurons in the brain (Balestrino and Schapira, 2020). To date, the molecular basis of PD is not completely understood, however, genetic and environmental factors are thought to play key roles (Dickson, 2018). The majority of PD cases (85-90%) are sporadic and are associated with environmental factors, such as industrial pollutants and pesticides (Breckenridge et al., 2016, Balestrino and Schapira, 2020). 1-methyl-4-phenyl tetrahydropyridine (MPTP) is one example of a neurotoxin that has the potential to destroy dopaminergic neurons selectively (Kopin, 1987). Exposure to hazardous levels of manganese, carbon monoxide and trichloroethylene could also result in a kind of Parkinsonism (Balestrino and Schapira, 2020). The remaining 5-15% of the PD causes are familial in nature, with mutations in a number of genes linked to disease development (Balestrino and Schapira, 2020). According to genetic studies, mitochondrial dysfunction is an important factor in PD. Genes such as *PINK1*, *PARKIN*, and *DJ-1* have been shown to influence mitochondrial function and are implicated in familial risk factors for PD (Valente et al., 2004, Kitada et al., 1998, Bonifati et al., 2003). Additionally, neuronal cells are vulnerable to lysosomal dysfunction (Feng and Yang, 2016). Importantly, lysosomal abnormities have been observed in the brains of PD patients (Dehay et al., 2010). Several studies indicated that oxidative stress due to excessive ROS production is the primary cause of dopaminergic cell death (Choi et al., 2012). Given ROS affects Ca^{2+} homeostasis (Suzuki et al., 1997, Neill et al., 2002, Camello-Almaraz et al., 2006, Ermak and Davies, 2002), it would seem that dysregulation of organelle homeostasis in dopaminergic neurons of individuals with PD is driven by abnormal ROS and Ca^{2+} signaling.

It has also been suggested that besides Ca^{2+}, Zn^{2+} plays a role in mitochondrial homeostasis (Ma et al., 2022, Dineley et al., 2005, Sensi et al., 2009); nevertheless, the mechanism by which mitochondrial Zn^{2+} is controlled is not well understood. In addition, it is unknown how Zn^{2+} contributes to the process of mitochondrial fission. Recent studies, however, have found that elevated mitochondrial Zn^{2+} leads to mitochondrial fragmentation which is linked to a loss of the mitochondrial membrane potential ($\Delta\Psi m$) (Abuarab et al., 2017, Li et al., 2017a). Furthermore, activation of TRPM2 channels is thought to be associated to these events. It was noted that most studies published up until this point have concentrated on one or two specific signals and/or organelles. Consequently, there is a significant gap in our understanding of how the ROS, Ca^{2+} and Zn^{2+} signals affect the communication between the various organelles, and how that results in organelle dysfunction and cell survival.

In this chapter, using the MPP^+-based cellular model of PD, I have investigated the mechanism by which ROS and Ca^{2+} signals generated at the plasma membrane are transmitted to lysosomes and mitochondria to cause mitochondrial fragmentation and cell death.

4.2 Results

4.2.1 MPP^+ causes mitochondrial fragmentation in SH-SY5Y cells

MPP^+ has been reported to induce extensive mitochondrial fragmentation in SH-SY5Y cells (Zhu et al., 2012). The effect of MPP^+ on mitochondrial structure in SH-SY5Y cells was first examined. To determine the optimal concentration to be used in subsequent experiments, cells were treated with different concentrations of MPP^+ (0, 1 and 2 mM) for 24 hours. Mitochondria were then stained with MitoTracker™ Red, a red-fluorescent dye used for labelling mitochondria in live

cells where its accumulation is dependent upon the mitochondria membrane potential.

In control cells (CTRL), mitochondria were seen as long, branched networks. Following the MPP^+ treatment, however, the tubular network disappeared and turned into shorter, rounded structures, representing fragmented mitochondria (Figure 4.1). Results showed that 1 mM MPP^+ caused significant fragmentation of the mitochondrial network, and a similar, but more pronounced effect was seen with 2 mM concentration (Figure 4.1). Thus, a concentration of 1 mM was selected for all subsequent experiments on mitochondrial fission.

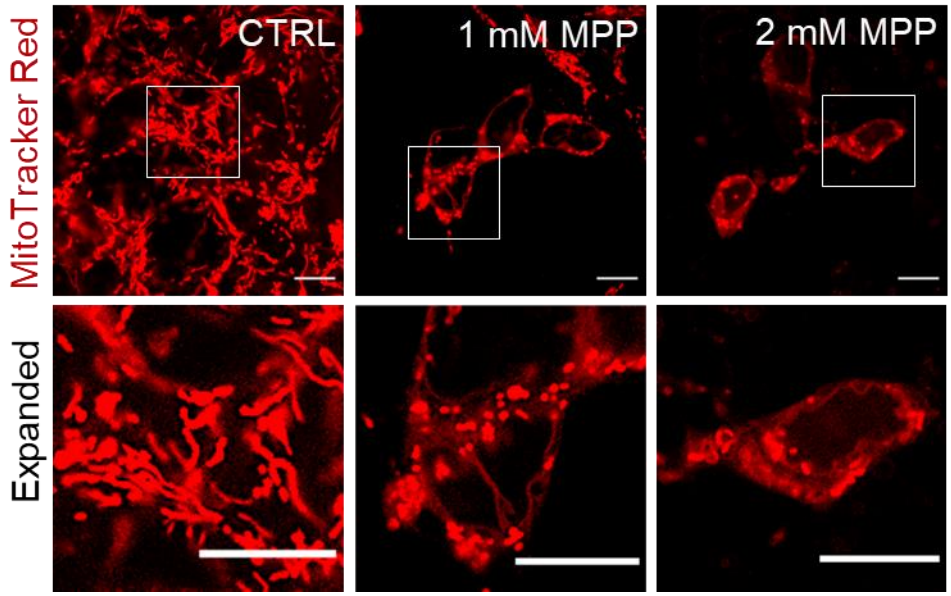

Figure 4.1 MPP^+ causes mitochondrial fragmentation in SH-SY5Y cells.

SH-SY5Y cells were incubated with medium alone (CTRL) or medium containing 1 or 2 mM MPP^+ for 24 hours at 37 ºC and stained for mitochondria (MitoTracker™ Red). Confocal images show that 1 mM MPP^+ is sufficient to cause mitochondrial fragmentation. Scale bar: 10 µm, and 5 µm for expanded images.

4.2.2 MPP^+ induces ROS production and mitochondrial fragmentation through NOX2 activation

Several studies have reported that mitochondrial structure is vulnerable to oxidative stress and the associated pathologies of many aging and metabolic diseases including the neurodegenerative disorders, especially PD (Roberts and Sindhu, 2009, Nojiri et al., 2006, Manczak et al., 2006, Blake and Trounce, 2014, Lin and Beal, 2006, Lee et al., 2011, Tsutsui et al., 2011). Studies, including the data in Chapter 3 of this thesis, also suggest that MPP^+ induces ROS production by activating NOX2 (Zawada et al., 2011, Di et al., 2012, Li et al., 2021), as well as through inhibition of mitochondrial electron transport (Nakamura et al., 2000, Choi et al., 2008, Cleeter et al., 1992). The mechanism by which ROS signals generated by the plasma membrane NOX2 leads to mitochondrial fragmentation was examined next.

SH-SY5Y cells were treated with 1 mM MPP^+ with and without NOX inhibitors (apocynin and gp91ds-tat) for 24 hours at 37 °C and the mitochondrial morphology were observed by staining the cells with MitoTracker™ Red. Apocynin is a general inhibitor of all NOX isoforms, whereas gp91ds-tat is a specific inhibitor of NOX2 (Williams and Griendling, 2007). Images were taken using a confocal microscope, followed by the analysis of mitochondrial morphology from 2D and 3D images using the 'Mitochondria Analyzer" plugin in image J as described by (Chaudhry et al., 2020). The data (Figure 4.2) show that MPP^+ induced a significant decrease in mean volume, surface area, total and mean branch length per mitochondrion. Also, MPP^+ significantly increased mitochondria sphericity and reduced the number of branches, branch junctions and branch end points per mitochondrion. These findings suggest that MPP^+ caused significant mitochondrial fragmentation in SH-SY5Y cells, and that Mitochondria Analyzer can be used to provide a quantitative description of the various parameters defining the mitochondrial morphology from the 2D and 3D sets of images acquired from a confocal microscope (Table 2.1). The analysis also revealed that quenching of ROS using the general NOX inhibitor, apocynin (10 µM), and NOX2 specific gp91ds-tat peptide inhibitor (5 µM) significantly

prevented MPP^+-induced mitochondrial fragmentation (Figure 4.2 D-M). These findings indicate that MPP^+ causes mitochondrial fragmentation in SH-SY5Y cells through a pathway that involves NOX2 activation and cytosolic ROS generation.

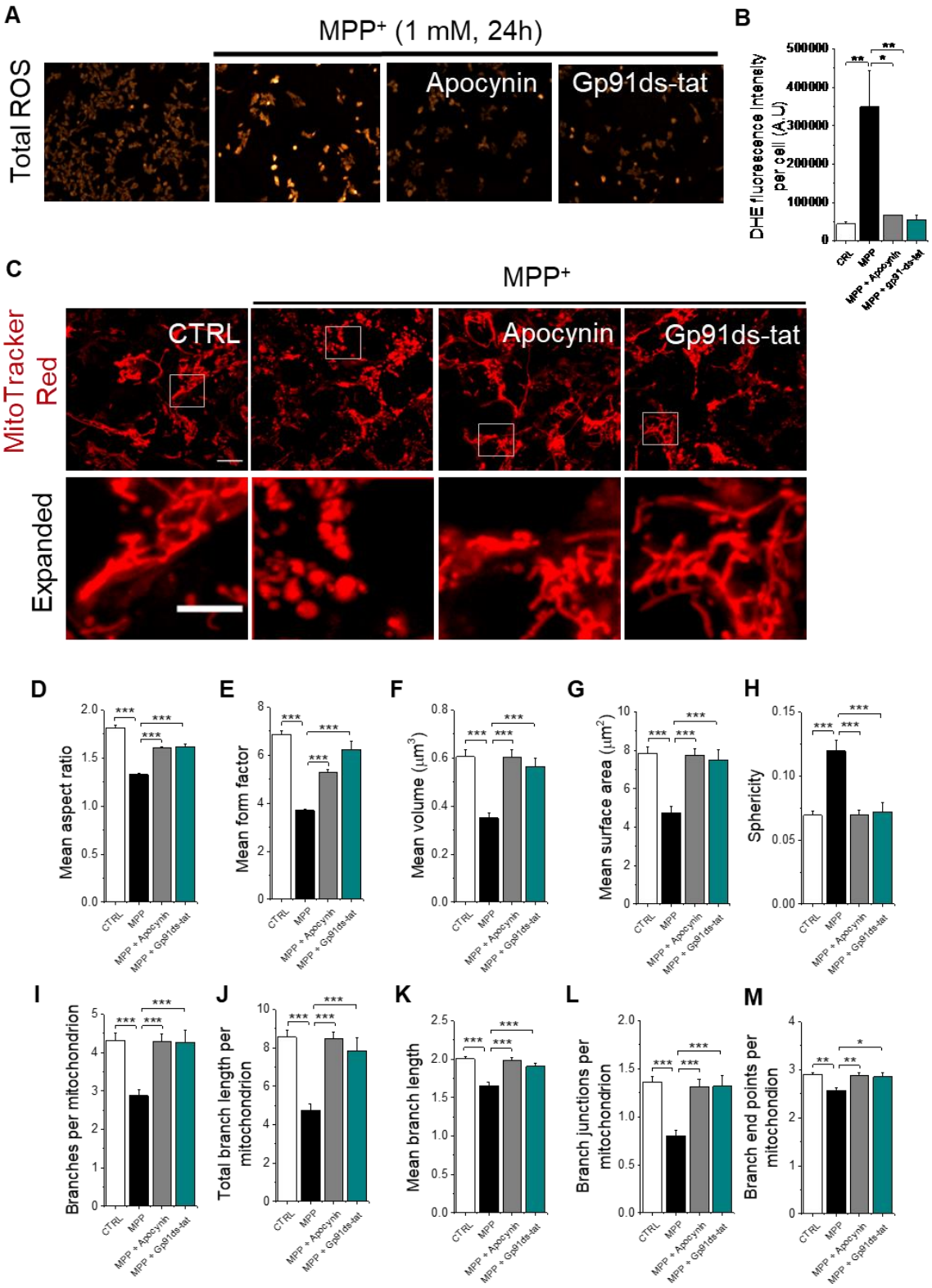
A
MPP+ (1 mM, 24h)
Total ROS
Apocynin
Gp91ds-tat
B
DHE fluorescence Intensity per cell (A.U)
CTRL
MPP
MPP + Apocynin
MPP + Gp91ds-tat
C
MPP+
MitoTracker Red
CTRL
Apocynin
Gp91ds-tat
Expanded
D
Mean aspect ratio
E
Mean fom factor
F
Mean volume (µm3)
G
Mean surface area (µm2)
H
Sphericity
I
Branches per mitochondrion
J
Total branch length per mitochondrion
K
Mean branch length
L
Branch junctions per mitochondrion
M
Branch end points per mitochondion

Figure 4.2 MPP^+ induces cytosolic ROS production and mitochondrial fragmentation in SH-SY5Y cells through NOX2 activation.

Inhibition of NOX2 prevented MPP^+-induced cellular ROS production and mitochondrial fragmentation. Cells were treated for 24 hours with medium alone (CTRL), or medium containing 1 mM MPP^+ with and without the general NOX inhibitor (10 µM apocynin) or NOX2 inhibitor (5 µM gp91ds-tat). **(A-B)** MPP^+ increases cellular ROS production by stimulating NOX2. **(A)** Fluorescent images of SH-SY5Y cells stained for total (DHE). **(B)** The corresponding mean ± SEM of DHE fluorescence intensity from three independent experiments. **(C-M)** MPP^+-induces mitochondrial fragmentation is dependent on NOX2. **(C)** Representative confocal images of SH-SY5Y cells stained for mitochondria (MitoTracker™ Red). Scale bars: 10 µm, and 5 µm for expanded images. **(D-M)** Quantification of changes in mitochondrial morphology through estimation of mean aspect ratio **(D)** mean form factor **(E)**, mean volume **(F)**, mean surface area **(G)**, sphericity **(H)**, branches per mitochondrion **(I)**, total branch length per mitochondrion **(J)**, mean branch length **(K)**, branch junctions per mitochondrion **(L)**, branch end points per mitochondrion **(M)**. Data presented as normalized mean ± SEM of mitochondrial parameters from three independent experiments, n = 3; N = 56 cells in total. * indicates $p < 0.05$; ** indicates $p < 0.01$; *** indicates $p < 0.001$; NS, not significant; one-way Anova with post-hoc Tukey test.

4.2.3 TRPM2 channels mediate MPP^+-induced mitochondrial fragmentation.

Many studies have shown a vital role for Ca^{2+} in mitochondrial fission (Slupe et al., 2013, Cereghetti et al., 2008, Abuarab et al., 2017, Liu and Hajnóczky, 2009, Calvo-Rodriguez and Bacskai, 2021, Clapham, 2007, Srinivasan et al., 2017). Data of the previous chapter also support the effect of Ca^{2+} on ROS levels in SH-SY5Y cells as well as on cell death. TRPM2 channels have been first demonstrated to play a role in mitochondrial fission in pancreatic β-cells (Li et al., 2017a) and human umbilical venous cord cells (HUVECs) (Abuarab et al., 2017) subjected to oxidative stress, but it is not clear whether they play a similar role in neuronal cells.

SH-SY5Y cells were treated with MPP^+ (1 mM) in the absence or presence of pharmacological inhibitors of TRPM2 (10 µM ACA, 50 µM 2-APB and 10 µM PJ34). After 24 hours of incubation at 37 ºC, cells were stained and imaged. Findings showed that inhibition of TRPM2 channels with ACA, 2-APB and PJ34 had significant rescue effect on MPP^+-induced mitochondrial fragmentation (Figure 4.3). 2-APB and PJ34 rescued all parameters of mitochondrial morphology. ACA rescued 7 out of 10 parameters examined but showed no significant rescue of three parameters (number of branches, branch junctions, and branch end points per mitochondrion) (Figure 4.3 G, J, K). Furthermore, similar rescue effects were observed when the SH-SY5Y cells were transfected with siRNA targeted to TRPM2, but not with Scr-siRNA (Figure 4.4). Interestingly, the mitochondrial morphology of cells treated with TRPM2-siRNA shows better network than the controls, however this was not quantified. Thus, suppression of TRPM2 expression or function attenuates MPP^+-induced mitochondrial fragmentation in SH-SY5Y cells.

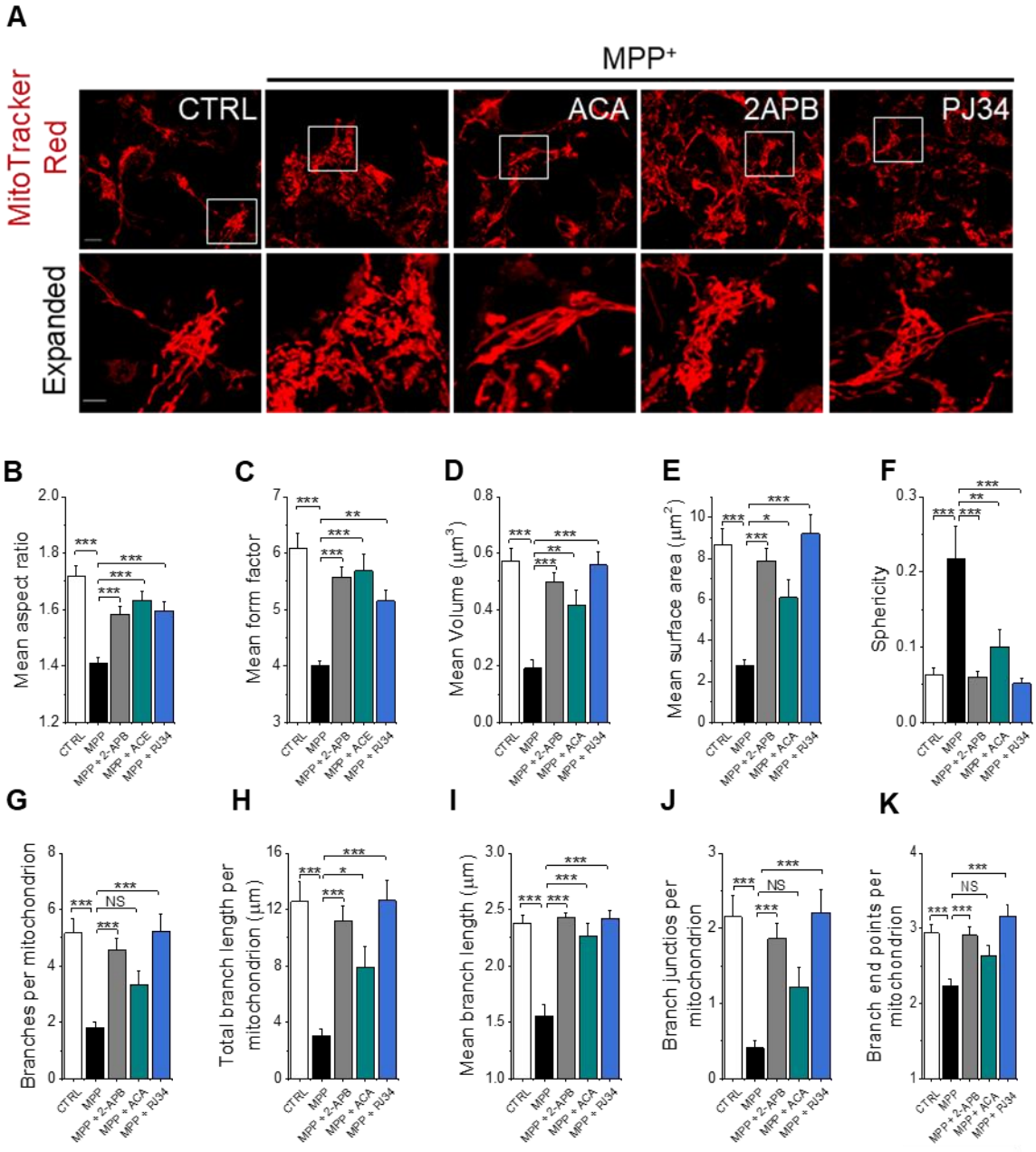

Figure 4.3 Inhibition of TRPM2 channels prevents MPP$^+$-induced mitochondrial fragmentation in SHSY5Y cells.

Pharmacological inhibition of TRPM2 prevents mitochondrial fragmentation. Cells were treated with medium alone (CTRL) or medium containing 1 mM MPP$^+$ with and without TRPM2 inhibitors; ACA (10 µM), 2-APB (50 µM) and PJ34 (10 µM) for 24 hours at 37 ºC. **(A)** Representative confocal images of SH-SY5Y cells stained for mitochondria (MitoTracker^{TM} Red). Scale bars: 10 µm, and 5 µm for

expanded images. **(B-K)** Quantification of changes in mitochondrial morphology through estimation of mean aspect ratio **(B)**, mean form factor **(C)**, mean volume **(D)**, mean surface area **(E)**, sphericity **(F)**, branches per mitochondrion **(G)**, total branch length per mitochondrion **(H)**, mean branch length **(I)**, branch junctions per mitochondrion **(J)**, branch end points per mitochondrion **(K)**. Data presented as normalized mean ± SEM of mitochondrial parameters from three independent experiments n =3; * indicates $p < 0.05$; ** indicates $p < 0.01$; *** indicates $p < 0.001$; NS, not significant; one-way Anova with post-hoc Tukey test.

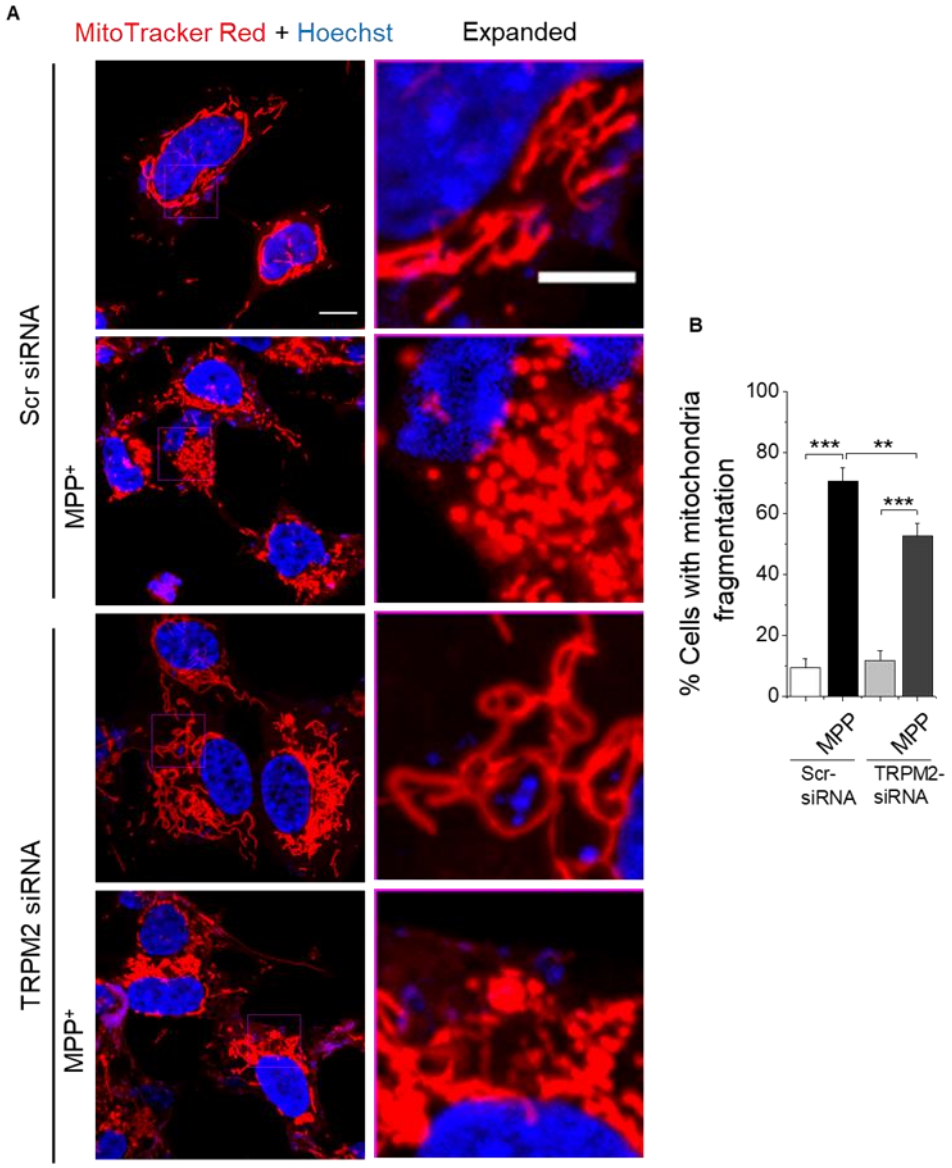

Figure 4.4 Inhibition of TRPM2 by siRNA prevents MPP⁺-induced mitochondrial fission.

(A) Fluorescent images of SH-SY5Y cells transfected with TRPM2-siRNA or Scr-siRNA for 48 hours and incubated with and without 1mM MPP^+ for 24 hours at 37 ºC and stained for mitochondria using MitoTracker Red and then recorded using a confocal microscope. Scale bars: 10 µm, and 5 µm for expanded images. **(B)** The corresponding mean ± SEM of percentage of cells with mitochondrial fission; data from three independent experiments performed as in (A) ** indicates $p < 0.01$; *** indicates $p < 0.001$; one-way Anova with post-hoc Tukey test.

4.2.4 The role of Ca^{2+} and Zn^{2+} in MPP^{+}-induced mitochondrial fragmentation

As mentioned earlier, activation of TRPM2 channels not only increases cytosolic Ca^{2+} levels, but also Zn^{2+} levels (Manna et al., 2015, Abuarab et al., 2017, Li et al., 2017a). It has been previously shown that Zn^{2+} chelation alone can prevent TRPM2-mediated excessive mitochondrial fission and β-cell death (Li et al., 2017a).

Accordingly, the role of Ca^{2+} and Zn^{2+} in MPP^{+} induced mitochondrial fission was examined. To achieve that, two ion chelators were used: BAPTA (Ca^{2+} chelator) and TPEN (Zn^{2+} chelator). SH-SY5Y cell were treated with MPP^{+} (1 mM) in the presence or absence of BAPTA-AM (5 µM) or TPEN (0.5 µM) and, after 24 hours of incubation at 37 °C, stained and imaged to assess changes in mitochondrial morphology. Results showed that both Ca^{2+} and Zn^{2+} chelation rescued mitochondrial fission (Figure 4.5). However, the latter showed a stronger rescue effect in most measured parameters indicating the critical role of Zn^{2+} in MPP^{+}-induced mitochondrial fragmentation in SH-SY5Y cells.

To understand and support the individual roles of Ca^{2+} and Zn^{2+} in mitochondrial dynamics, we used the Ca^{2+} ionophore (A23187) and the Zn^{2+} ionophore (Zn-PTO) to raise the intracellular levels of these two ions. First, to optimize the time, cells were treated with 2 µM A23187 for different time periods (0, 1, 2 and 4 hours). Diethylenetriaminepentaacetic acid (DTPA, 2 mM), a membrane-impermeable Zn^{2+}chelator, was included with A23187 to chelate Zn^{2+} in the extracellular medium and thereby ensure any changes in the levels of free Zn^{2+} is due to intracellular Zn^{2+} release. Then, the rise of intracellular Ca^{2+} and the morphology of mitochondria were monitored by co-staining the cells with Fluo-4 AM and MitoTracker™ Red. Results showed time dependent increase in Fluo-4 fluorescence intensity indicating increased intracellular Ca^{2+} concentration. A23187 caused a raise in intracellular Ca^{2+}, which initially appears as diffuse Fluo-4 stain in the cytoplasm (in the first 2 h), but longer exposure (4 hours) has resulted in Ca^{2+} accumulation in punctate structures. The nature of these puncta

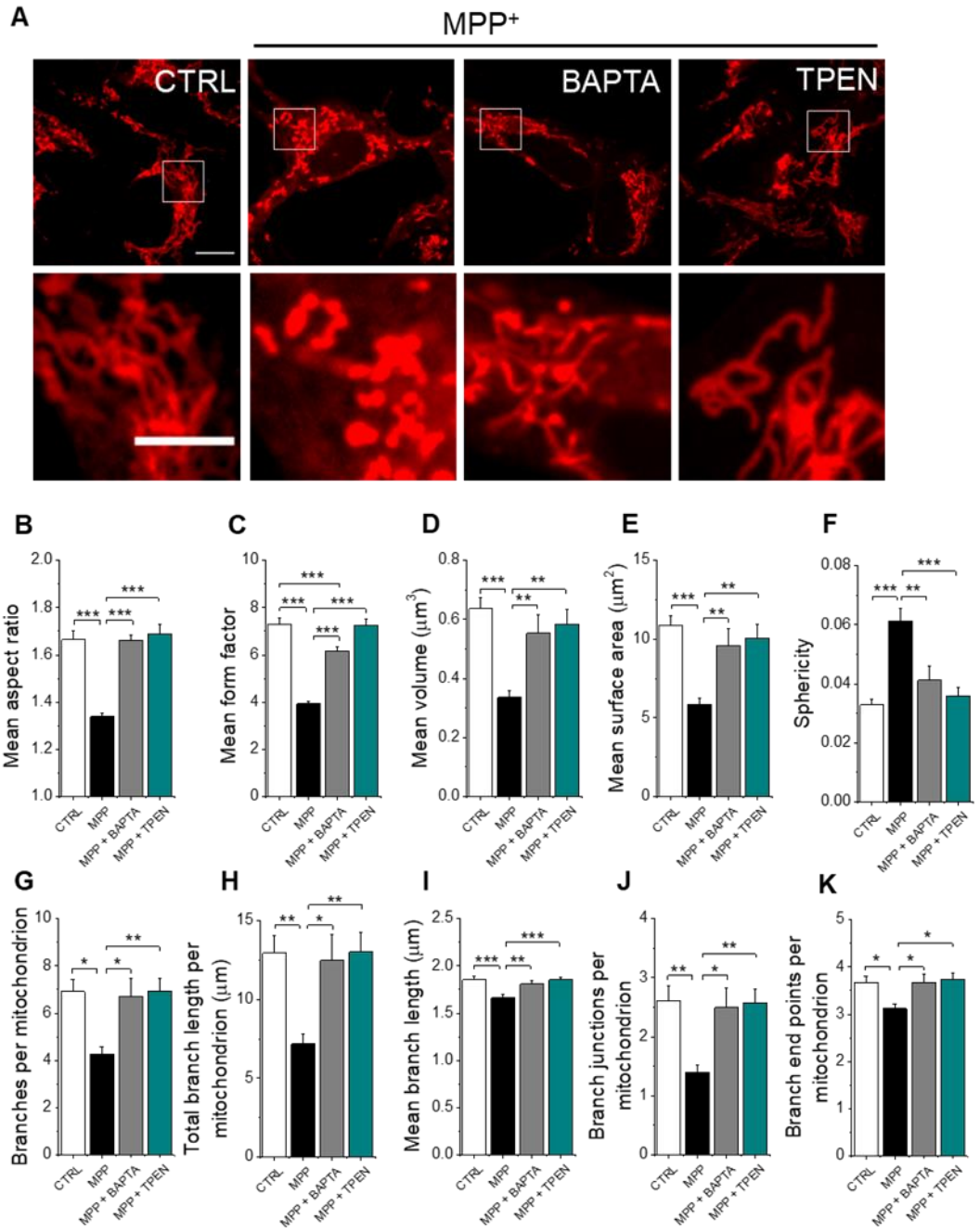

Figure 4.5 Ca^{2+} and Zn^{2+} chelation prevents MPP^+ induced mitochondrial fission.

(A) Fluorescent images of SH-SY5Y cells exposed to medium alone (CTRL) or medium containing 1 mM MPP^+ with and without the Ca^{2+} chelator BAPTA-AM (5 µM) or Zn^{2+} chelator TPEN (0.5 µM) for 24 hours at 37 ºC and stained for mitochondria using MitoTracker™ Red and the images were captured using confocal microscope. Scale bars: 10 µm, and 5 µm for expanded images. **(B-K)**

Quantification of changes in mitochondrial morphology through estimation of mean aspect ratio **(B)**, mean form factor **(C)**, mean volume **(D)**, mean surface area **(E)**, sphericity **(F)**, branches per mitochondrion **(G)**, total branch length per mitochondrion **(H)**, mean branch length **(I)**, branch junctions per mitochondrion **(J)**, branch end points per mitochondrion **(K)**. Data presented as normalized mean ± SEM of mitochondrial parameters from three independent experiments n =3; N = 176 cells in total. * indicates $p < 0.05$; ** indicates $p < 0.01$; *** indicates $p < 0.001$; NS, not significant; one-way Anova with post-hoc Tukey test.

remains to be determined. As for the mitochondrial morphology, delivery of Ca^{2+} through A23187 led to a progressive loss of the long-branched mitochondrial network with time, with excessive mitochondrial fragmentation being detected after 4 hours of treatment (Figure 4.6).

Moreover, co-staining the cells with FluoZin-3 and MitoTracker™ Red revealed that the A23187 induced cytosolic Ca^{2+} rise led to increased mitochondrial Zn^{2+} (Figure 4.7). The data also showed that longer incubation with the Ca^{2+} ionophore caused further increase in mitochondrial Zn^{2+} (shown as yellow puncta representing the co-localization of the green FluoZin-3 stain of Zn^{2+} with the red MitoTracker stain) and mitochondrial fragmentation. In the untreated cells (CTRL), there was less detectable Zn^{2+} in the mitochondria compared with cells after 2 or 4 hours incubation with A23187 which showed a marked rise in mitochondrial Zn^{2+} (Figure 4.7). These results suggest a correlation between cytosolic Ca^{2+} rise, intracellular Zn^{2+} redistribution and mitochondrial fission.

The roles for both Ca^{2+} and Zn^{2+} was further supported by the fact that both BAPTA and TPEN significantly rescued ($p < 0.001$) A23187-induced mitochondrial fragmentation (Figure 4.8).

Finally, the direct and independent effect of increasing the free intracellular Zn^{2+} on mitochondrial fragmentation was assessed. Cells were treated with 2 µM Zn-PTO in Ca^{2+} free medium for 2 hours at 37 °C before staining for mitochondria. Data showed that delivery of Zn^{2+} through Zn-PTO into SH-SY5Y cells resulted in excessive mitochondrial fragmentation, and that co-treatment with TPEN (0.5 µM) was able to antagonize the effect of Zn-PTO (Figure 4.9 A). The effects were apparent in all measured parameters of mitochondrial fission (Figure 4.9 B-K). The fact that Zn^{2+} chelation alone was sufficient to prevent mitochondrial fission suggests that Zn^{2+}, rather than Ca^{2+}, plays a dominant role in oxidative stress induced mitochondrial fragmentation. The data also suggest that Zn^{2+} likely acts downstream of Ca^{2+}.

Collectively, these findings support coordinated signaling roles for both Ca^{2+} and Zn^{2+} in MPP^{+}-induced mitochondrial fragmentation in SH-SY5Y cells.

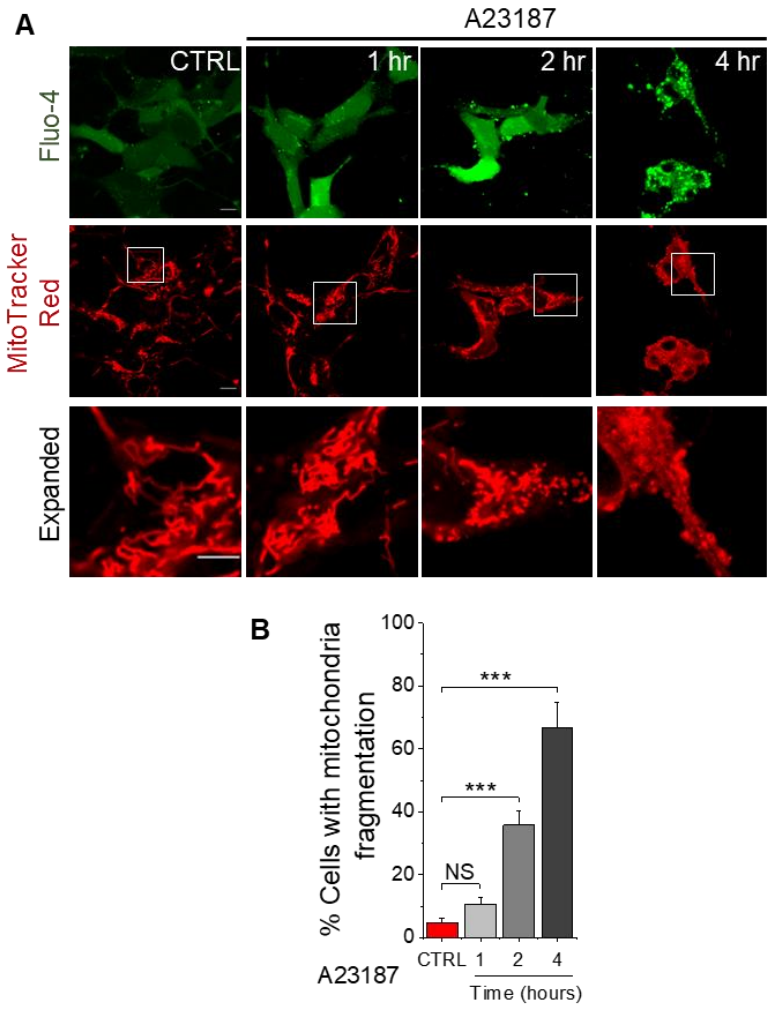

Figure 4.6 Rising cytosolic Ca^{2+} with Ca^{2+}-ionophore (A23187) causes mitochondrial fission.

(A) Fluorescent images of SH-SY5Y cells stained for Ca^{2+} (Fluo4-AM) and mitochondria (MitoTracker™ Red) following A23187 treatment. Cells were incubated at 37 ºC with A23187 (2 µM plus 2 mM DTPA) for different time periods (0, 1, 2, 4 hours). Representative confocal images show that A23187 induced rise in intracellular Ca^{2+} (top panel), and mitochondrial fission (bottom panels) in a time-dependent manner. Scale bars: 10 µm, and 5 µm for expanded images. **(B)** Mean ± SEM of percent cells displaying mitochondrial fragmentation in A23187 treated cells. Statistical analysis was performed from three independent experiments n = 3; N = 754 cells in total. *** indicates $p < 0.001$; NS, not significant; one-way Anova with post-hoc Tukey test.

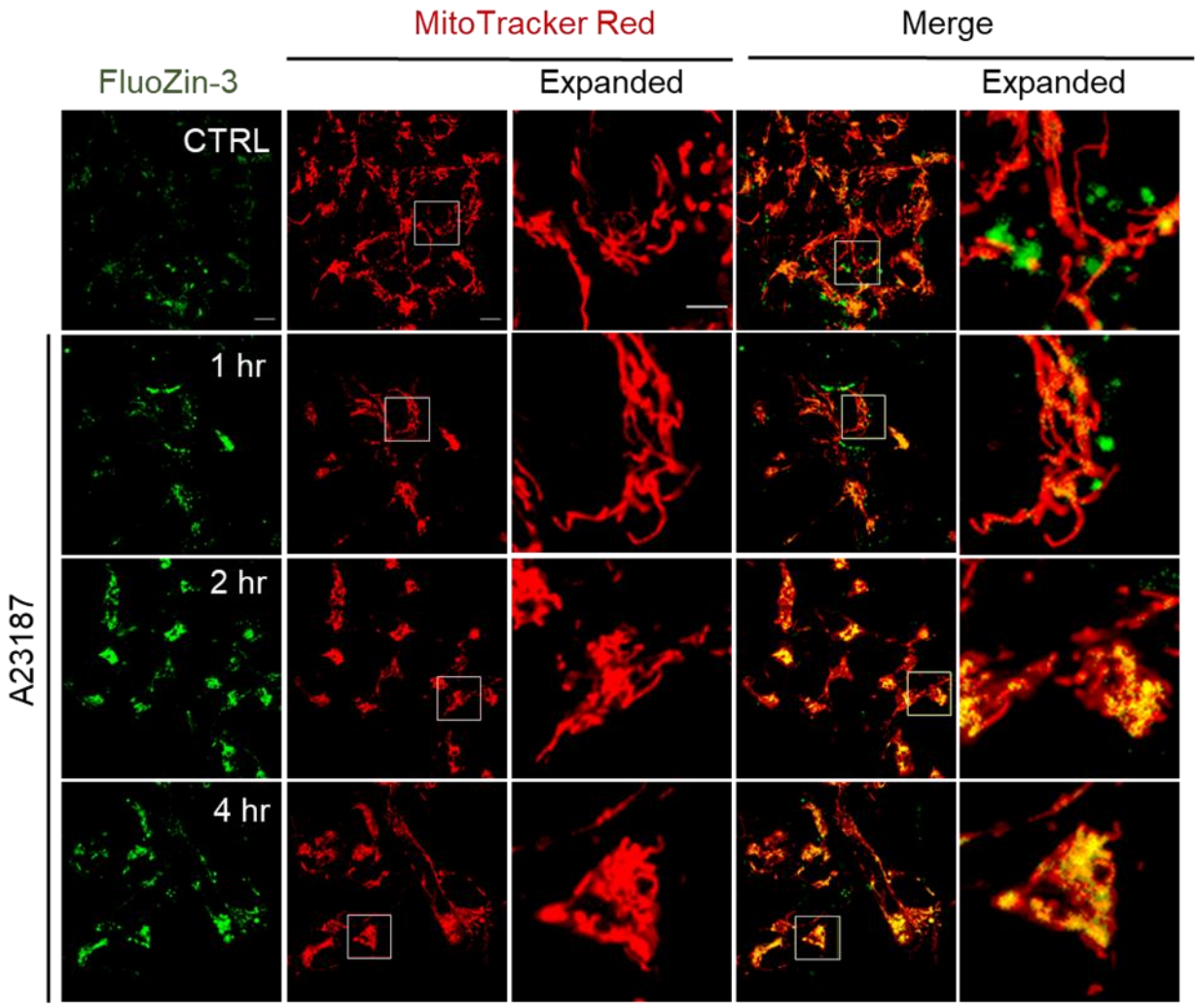

Figure 4.7 Cytosolic Ca^{2+} rise by A23187 increases mitochondrial Zn^{2+} and mitochondrial fission.

Fluorescent images of SH-SY5Y cells co-stained for Zn^{2+} (FluoZin-3) and mitochondria (MitoTracker™ Red). Images were taken using confocal microscopy of cells exposed to medium (CTRL) or A23187 (2 µM plus 2 mM DTPA) for the indicated times (0, 1, 2, 4 hours). Yellow puncta represent the co-localization of the green FluoZin-3 stain with the MitoTracker™ Red. The data show that longer incubation with A23187 caused increased Zn^{2+} mobilization to mitochondria and mitochondrial fragmentation. Scale bars: 10 µm, and 5 µm for expanded images.

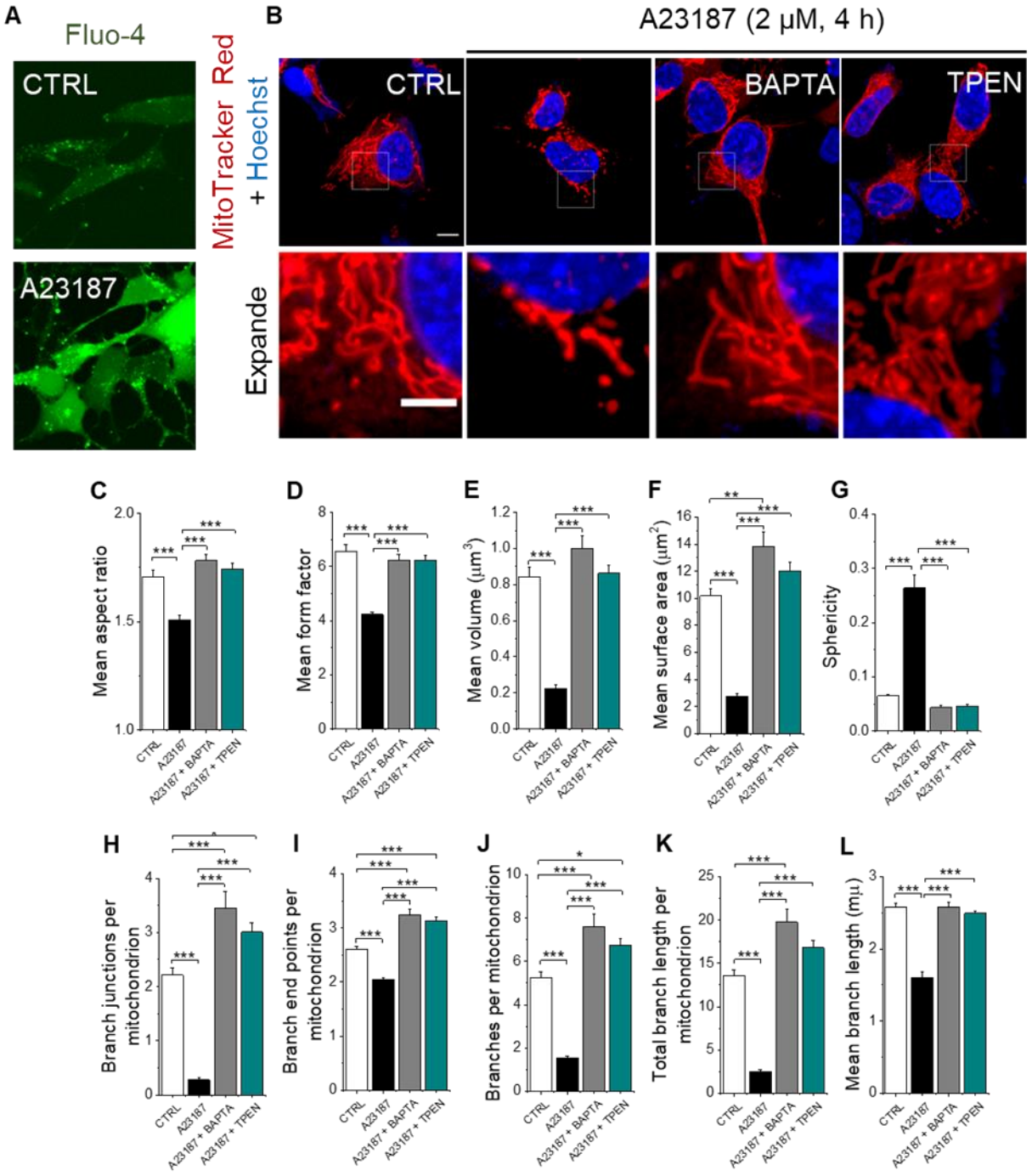

Figure 4.8 Ca^{2+}-induced mitochondrial fragmentation is mediated by Zn^{2+}.

(A) Representative confocal images of SH-SY5Y cells treated with medium alone (CTRL) or with A23187 (2 μM plus 2 mM DTPA) for 4 hours at 37 ºC and stained for Ca^{2+} using Fluo4-AM. **(B)** Fluorescent images of SH-SY5Y cells exposed to medium alone (CTRL) or A23187 (2 μM plus 2 mM DTPA) with and without the Ca^{2+} chelator (5 μM BAPTA) or the Zn^{2+} chelator (0.5 μM TPEN) for 2 hours at 37 ºC; cells were then stained for mitochondria using MitoTracker™ Red. Scale

bars: 10 µm, and 5 µm for expanded images. Data show that chelation of Ca^{2+} and Zn^{2+} prevents mitochondrial fragmentation. **(C-L)** Quantification of changes in mitochondrial morphology through estimation of mean aspect ratio **(C)**, mean form factor **(D)**, mean volume **(E)**, mean surface area **(F)**, sphericity **(G)**, branches per mitochondrion **(H)**, total branch length per mitochondrion **(I)**, mean branch length **(j)**, branch junctions per mitochondrion **(K)**, branch end points per mitochondrion **(L)**. Data presented as normalized mean ± SEM of mitochondrial parameters from three independent experiments n =3; N = 295 cells in total. * indicates $p < 0.05$; ** indicates $p < 0.01$; *** indicates $p < 0.001$; NS, not significant; one-way Anova with post-hoc Tukey test.

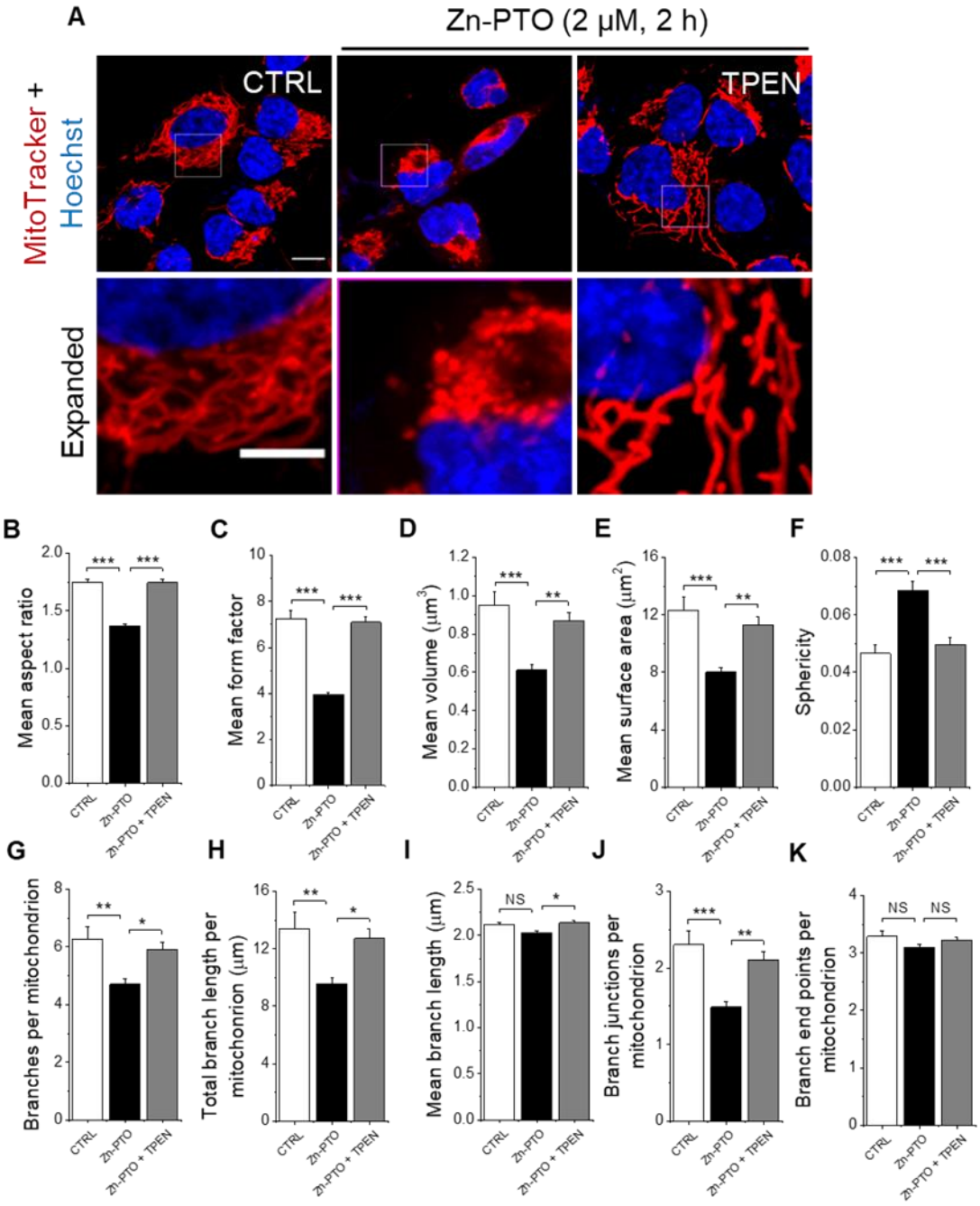

Figure 4.9 Zn^{2+} ionophore, Zn^{2+}-pyrithione (Zn-PTO) increases mitochondrial fragmentation in the absence of extracellular Ca^{2+}.

(A) Representative confocal images of SH-SY5Y cells exposed to Ca^{2+} free medium alone (CTRL) or Ca^{2+} free medium containing the Zn^{2+} ionophore (2 µM Zn^{2+}-pyrithione, Zn-PTO) in the absence or presence of the Zn^{2+} chelator (0.5 µM TPEN) for 2 hours at 37 ºC. Next, cells were stained for mitochondria using MitoTracker™ Red. Scale bars: 10 µm, and 5 µm for expanded images. **(B-K)** Quantification of changes in mitochondrial morphology through estimation of

mean aspect ratio **(B)**, mean form factor **(C)**, mean volume **(D)**, mean surface area **(E)**, sphericity **(F)**, branches per mitochondrion **(G)**, total branch length per mitochondrion **(H)**, mean branch length **(I)**, branch junctions per mitochondrion **(J)**, branch end points per mitochondrion **(K)**. Data presented as normalized mean ± SEM of mitochondrial parameters from three independent experiments n =3; N = 218 cells in total. * indicates $p < 0.05$; ** indicates $p < 0.01$; *** indicates $p < 0.001$; NS, not significant; one-way Anova with post-hoc Tukey test.

4.2.5 Zn^{2+} localization in intracellular organelles

Zinc (Zn^{2+}) is important for many cellular functions and its intracellular distribution can influence cellular metabolism and signaling (Lu et al., 2016). The exact distribution of free Zn^{2+} in subcellular organelles remains elusive. Studies have shown that lysosomes serve as Zn^{2+} storage organelle and protects the cells from excess intracellular Zn^{2+} toxicity (Roh et al., 2012, Kukic et al., 2014, Han et al., 2018, Abuarab et al., 2017, Li et al., 2017a).

In this study, to determine the source of intracellular Zn^{2+}, SH-SY5Y cells were grown in normal conditions, and were co-stained with FluoZin-3 and different organelle-specific fluorescent dyes (MitoTracker™ Red: for mitochondria, and LysoBrite Red: for Lysosomes). Results showed remarkable localization of Zn^{2+} to lysosomes, indicating that free Zn^{2+} is more likely to be found in lysosomes in healthy SH-SY5Y cells (Figure 4.10 A). On the other hand, FluoZin-3 - MitoTracker™ colocalization is less obvious (Figure 4.10 B), suggesting absence of Zn^{2+} in mitochondria in detectable amounts.

These results suggest that lysosome is a potential free Zn^{2+} storing organelle during cellular Zn^{2+} homeostasis under normal conditions.

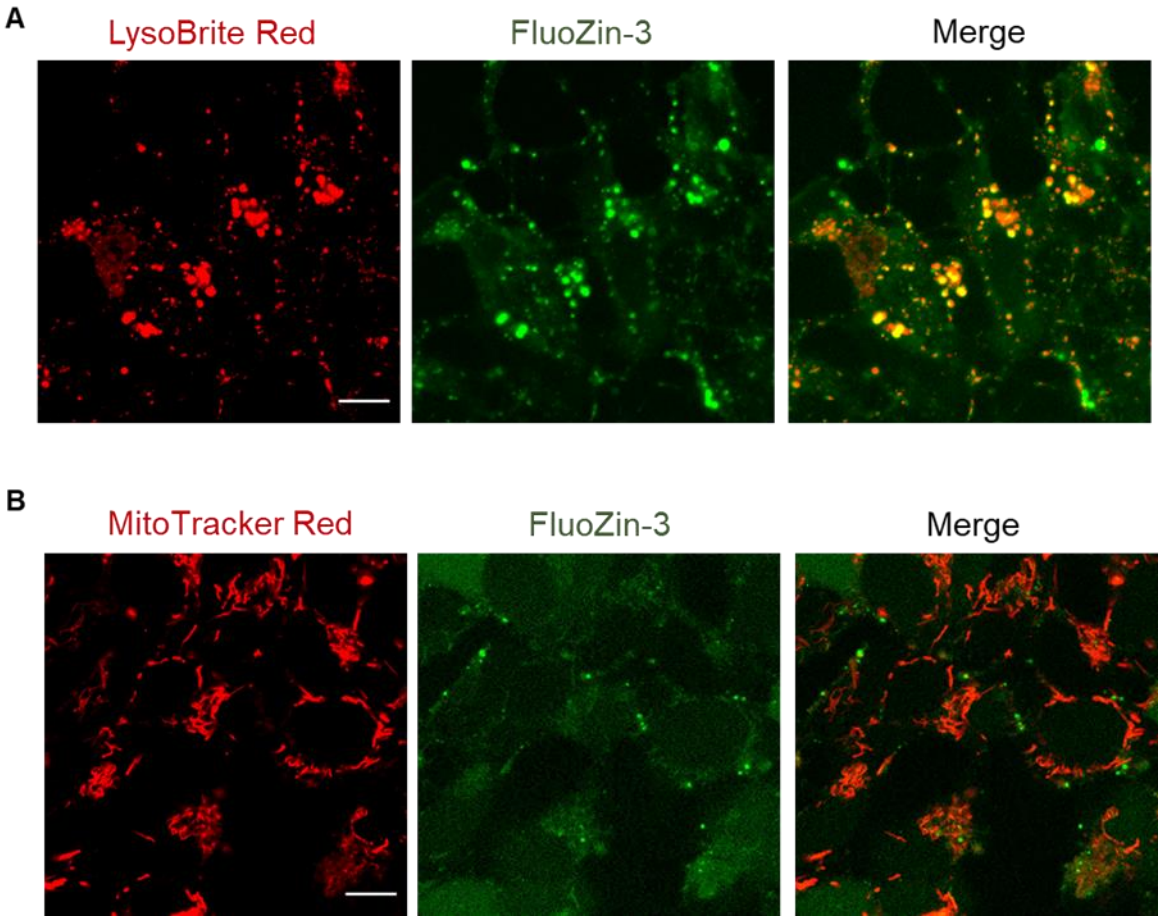

Figure 4.10 Zn^{2+} is stored in lysosomes of SH-SY5Y cells.

Fluorescent images taken of SH-SY5Y cells grown in medium alone and co-stained for Zn^{2+} using FluoZin 3-AM and lysosomes using LysoBrite Red **(A)**, or mitochondria using MitoTracker™ Red **(B)**. Results show that Zn^{2+} is localized mostly (indicated by yellow vesicles) to lysosomes rather than to mitochondria in SH-SY5Y cells. Scale bars: 10 µm.

4.2.6 TRPM2 activation mediates MPP^+-induced lysosomal membrane permeabilization

As shown in the previous section (Figure 4.10 A), free Zn^{2+} in SH-SY5Y cells is largely stored in the lysosomes. It has been reported that oxidative stress can alter intracellular Zn^{2+} dynamics and its distribution among subcellular compartments in a TRPM2-dependent manner (Abuarab et al., 2017).

To understand whether MPP^+-induced oxidative stress influences intracellular Zn^{2+} distribution in SH-SY5Y cells, the effect of MPP^+ on lysosomal Zn^{2+} was first examined. Cells were incubated with 1 mM MPP^+ for 24 hours at 37° C, and then co-stained with FluoZin-3 and LysoBrite Red. Results revealed that when cells were exposed to MPP^+, the overlap between FluoZin-3 green and LysoBrite Red dyes (represented by yellow particles) has declined, indicating loss of Zn^{2+} from lysosomes or a loss of LysoBrite Red from lysosomes (Figure 4.11 A). Results also showed a significant decrease in the number of LysoBrite Red-positive lysosomes per cell (Figure 4.11 B). These findings suggest that MPP^+ induced lysosomal membrane permeabilization leading to a loss of lysosomal Zn^{2+}.

We next asked whether TRPM2 channels are involved in MPP^+-induced lysosomal Zn^{2+} release in SH-SY5Y cells. To answer this question, cells were co-treated with MPP^+ and the TRPM2 blocker, 2-APB, following by staining for Zn^{2+} and lysosomes. The data showed that 2-APB rescued FluoZin-3 – LysoBrite overlap (yellow) as well as the number of LysoBrite Red- positive vesicles per cell (Figure 4.11), providing evidence that TRPM2 channels could mediate MPP^+-induced loss of lysosomal number and loss of Zn^{2+}.

Therefore, these data indicate that MPP^+ induces lysosomal membrane permeabilization and lysosomal Zn^{2+} loss through a pathway mediated by TRPM2 activation.

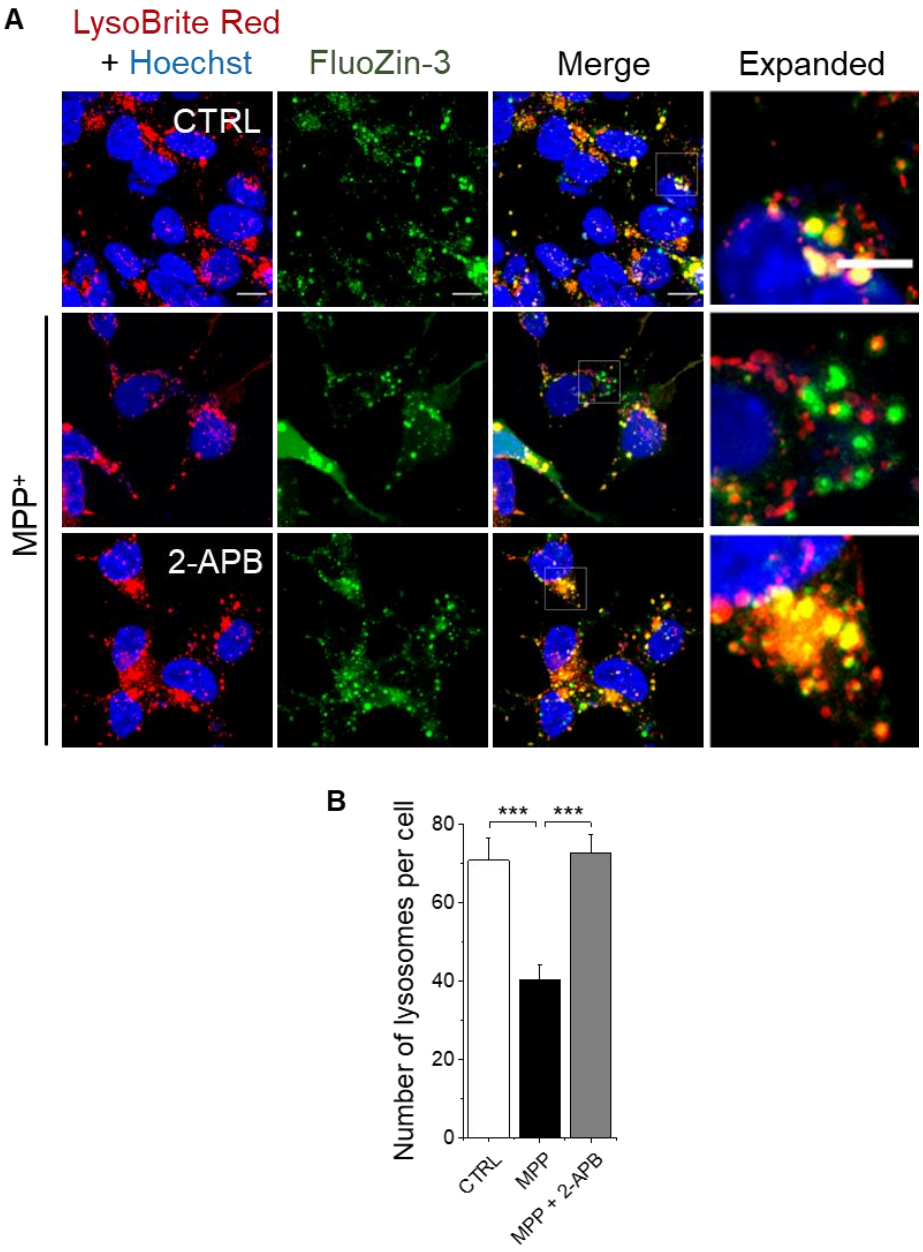

Figure 4.11 TRPM2 channels mediate MPP^+-induced lysosomal membrane permeabilization in SH-SY5Y cells.

(A) Representative fluorescent images of SH-SY5Y cells treated with medium alone (CTRL) or 1 mM MPP^+ in the presence or absence of a TRPM2 inhibitor (50 µM 2-APB) for 24 hours at 37 ºC and stained for Lysosomes using LysoBrite Red and for Zn^{2+} using FluoZin-3. **(B)** Mean ± SEM of data from (A) expressed as number of lysosomes per cell, n =3; The yellow spots represent the overlap of Zn^{2+} staining (FluoZin-3) with lysosomal staining (LysoBrite Red), indicating the localization of Zn^{2+} in lysosomes. Scale bars: 10 µm, and 5 µm for expanded images. *** indicates $p < 0.001$; one-way Anova with post-hoc Tukey test.

4.2.7 Increased Ca^{2+} uptake causes lysosomal membrane permeabilization

Since it has been previously shown that TRPM2-mediated Ca^{2+} influx induces intracellular Zn^{2+} release in pancreatic β-cells (Li et al., 2017a), the role of rise in intracellular Ca^{2+} in Zn^{2+} mobilization and redistribution within the SH-SY5Y cells was examined.

To determine the effect of Ca^{2+} entry on lysosomal membrane permeabilization and Zn^{2+} release in SH-SY5Y cells, they were treated with the calcium ionophore, A23187, and co-stained with FluoZin-3 and LysoBrite Red, then the changes recorded using a confocal microscope. When SH-SY5Y cells were incubated with A23187 (2 µM combined with 2 mM DTPA) for different periods of times (0, 2 and 4 hours), changes in intracellular Zn^{2+} distribution was observed (Figure 4.12 A). In control cells (CTRL), there was a noticeable overlap (yellow) of Zn^{2+} and lysosomal staining suggesting Zn^{2+} localization to lysosomes. However, the association of FluoZin-3 green with LysoBrite Red was diminished with an accompanied decline in the percentage of LysoBrite Red-positive lysosomes per cell when intracellular Ca^{2+} was raised using A23187 (Figure 4.12 B). The longer incubation time resulted in reduced Zn^{2+} localization to lysosomes. However, there was no significant increase in the number of Zn^{2+} positive puncta (Figure 4.12 C), suggesting that Zn^{2+} has been redistributed to other cellular organelles. These results indicate that increased Ca^{2+} entry causes lysosomal membrane permeabilization and redistribution of Zn^{2+} to other organelles in SH-SY5Y cells.

Moreover, results showed that Ca^{2+} chelation by BAPTA inhibited A23187-induced lysosomal membrane permeabilization and the loss of lysosomal Zn^{2+}, as shown by the restoration of yellow puncta, representing FluoZin-3 – LysoBrite Red signals (Figure 4.12 A). Also, I found that Ca^{2+} chelation prevented loss of LysoBrite Red positive-lysosomes caused by Ca^{2+} entry via A23187.

Although the exact mechanisms by which Ca^{2+} influx promotes lysosomal membrane permeabilization remains to be determined, these findings indicate that rise in intracellular Ca^{2+} triggers lysosomal membrane permeabilization leading to redistribution of lysosomal Zn^{2+} to other intracellular structures. The data suggest that Ca^{2+} channels might play critical roles in controlling intracellular Zn^{2+} dynamics.

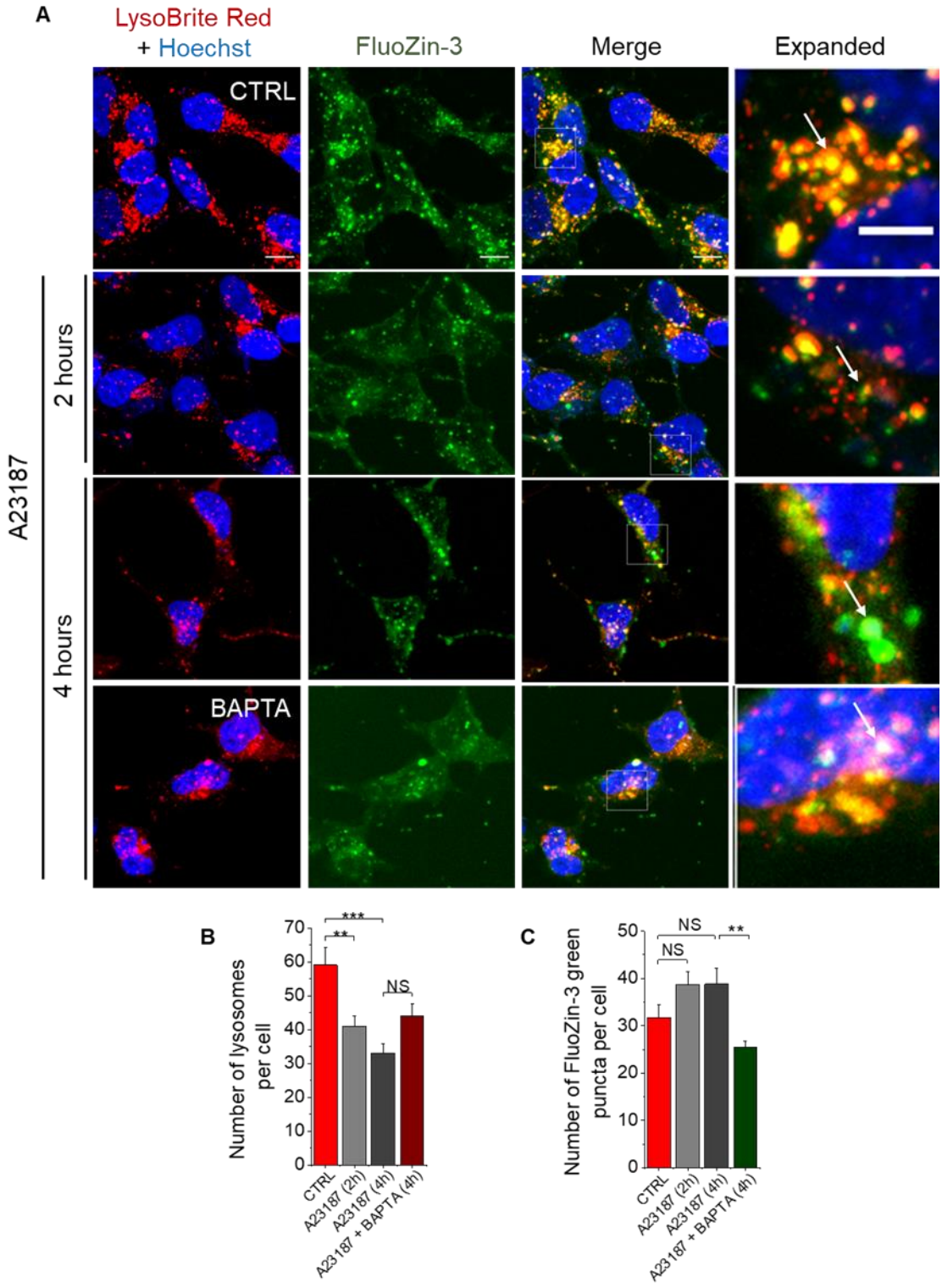

Figure 4.12 Ca^{2+} ionophore induces lysosomal membrane permeabilization.

(A) Representative confocal images of SH-SY5Y cells exposed to medium (CTRL) or A23187 (2 µM plus 2 mM DTPA) for the indicated times (0, 2 and 4 hours) and stained for Lysosomes using LysoBrite Red and for Zn^{2+} using FluoZin-3. **(B-C)** Mean ± SEM of percentage of LysoBrite Red-positive lysosomes per cell **(B)** and the number of FluoZin-3 positive puncta **(C)** analyzed from three

independent experiments performed as in (A). The yellow spots represent the overlap of Zn^{2+} staining (FluoZin-3) with lysosomes staining (LysoBrite), indicating the localization of Zn^{2+} in lysosomes. Scale bars: 10 μm, and 5 μm for expanded images. ** indicates $p < 0.01$; *** indicates $p < 0.001$; NS, not significant; one-way Anova with post-hoc Tukey test.

4.2.8 TRPM2 channels and Zn^{2+} mediate MPP^{+}-induced loss of mitochondrial membrane potential (ΔΨm)

In previous research, the loss of mitochondrial membrane potential (ΔΨm) has been correlated with changes in mitochondria network structure (Ishihara et al., 2003, Legros et al., 2002). Since MPP^{+} has been shown influence the mitochondrial dysfunction and fragmentation (Przedborski et al., 2004), the effect of MPP^{+} on ΔΨm was examined next. Additionally, it is important to determine whether TRPM2 channels and Zn^{2+} are involved in this mitochondrial dysfunction in the cellular model of PD, as was the case with pancreatic β-cells (Li et al., 2017a) and endothelial cells (Abuarab et al., 2017).

To investigate that, SH-SY5Y cells were treated with 1 mM MPP^{+} either without or in the presence of the TRPM2 inhibitor (50 µM 2-APB), or the Zn^{2+} chelator (0.5 µM TPEN), and after 24 hours incubation at 37 °C, cells were stained for ΔΨm using 200 nM tetramethylrhodamine ethyl ester (TMRE). Staining SH-SY5Y cells with TMRE allows for the detection of the negative charge that is present across the membrane of healthy mitochondria (Crowley et al., 2016). The intensity of TMRE fluorescence detected by confocal microscopy can be unitized to evaluate whether mitochondria in a stained cell have high (active mitochondria) or low (inactive mitochondria) ΔΨm (Crowley et al., 2016). Notably, cells exposed to MPP^{+} showed significant loss of ΔΨm (Figure 4.13). This effect was prevented by blocking TRPM2 channels with 2-APB (Figure 4.13). The results also showed that Zn^{2+} chelation with TPEN markedly reduced ΔΨm loss, demonstrating that Zn^{2+} plays an important role in MPP^{+}-induced ΔΨm loss (Figure 4.14).

These findings suggest that TRPM2 channels and Zn^{2+} play a critical role in the MPP^{+}-induced dissipation of ΔΨm.

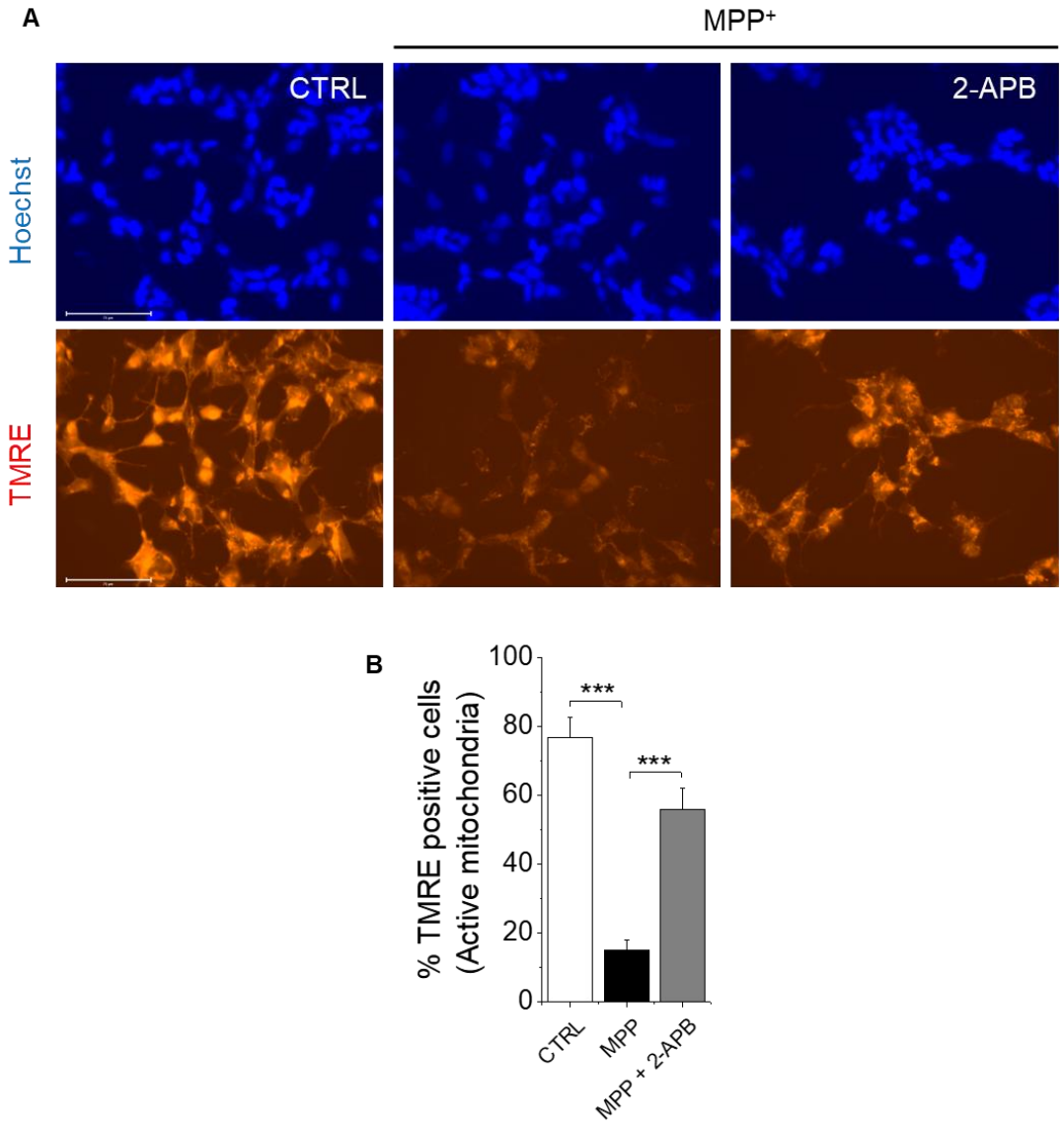

Figure 4.13 TRPM2 channels mediates MPP^+-induced loss of mitochondrial membrane potential (ΔΨm)

(A) Fluorescent images of SH-SY5Y cells co-stained for nuclei (Hoechst) and mitochondria membrane potential (TMRE) following of 1 mM MPP^+ treatment with and without the TRPM2 inhibitors, 2-APB (50 μM) for 24 hours at 37 ºC. Scale bar: 75 μM. **(B)** Mean ± SEM of percent cells displaying active mitochondria (TMRE-positive cells). Statistical analysis was performed from three independent experiments. *** indicates $p < 0.001$; one-way Anova with post-hoc Tukey test.

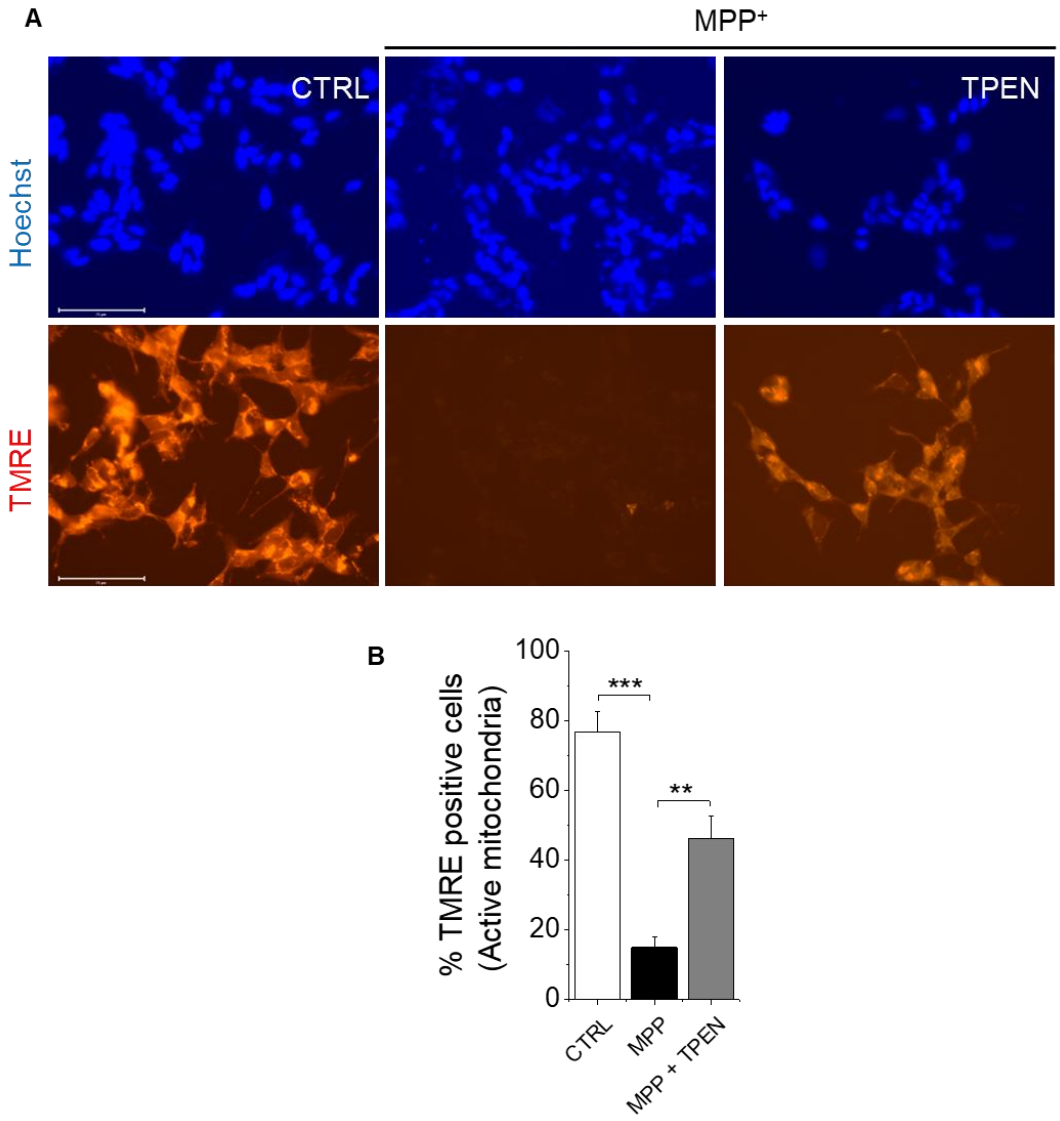

Figure 4.14 Zn^{2+} chelation reduces mitochondrial membrane potential (ΔΨm) loss caused by MPP^+.

(A) Fluorescent images of SH-SY5Y cells co-stained for nuclei (Hoechst) and mitochondria membrane potential (TMRE) following of 1 mM MPP^+ treatment with and without the Zn^{2+} chelator TPEN (0.5 μM) for 24 hours at 37 ºC. Scale bar: 75 μM. **(B)** Mean ± SEM of percent cells displaying active mitochondria (TMRE-positive cells). Statistical analysis was performed from three independent experiments. ** indicates $p < 0.01$; *** indicates $p < 0.001$; one-way Anova with post-hoc Tukey test.

4.2.9 Mitochondrial ROS stimulates MPP^+-induced mitochondrial fragmentation

It has previously been reported that the mitochondrial-targeted antioxidants can significantly rescue mitochondrial fragmentation caused by oxidative stress (Plotnikov et al., 2008) implicating a role for mitochondrial ROS (mtROS) in mitofission. Therefore, the effect of mitochondrial-targeted antioxidant Mito-Tempo, a specific scavenger of mitochondrial superoxide, was used to assess its ability to rescue mitochondrial fission in SH-SY5Y cells.

As shown in the previous chapter, MPP^+ induces mtROS generation (Figure 3.2) and the consequent cells death (Figure 3.4). In this section, I asked whether MPP^+-induced mtROS production is linked to mitochondrial fission. The association of mitochondrial fragmentation and the rise of mtROS was first examined. SH-SY5Y cells were treated with medium only (CTRL) or with 1 mM MPP^+ for 24 hours at 37 °C, before co-staining for mitochondria using MitoTracker™ green and for mtROS using MitoSOX Red. Images taken by the confocal microscope showed that MPP^+ treatment stimulated mtROS production, represented by an increase in MitoSOX fluorescent intensity, as well as an increase in mitochondrial fragmentation (Figure 4.15). Cells with little or no mtROS showed near normal mitochondrial morphology. These data could suggest that MPP^+ induced excessive mtROS generation is closely associated with mitochondrial fission.

Next, the effect of the mitochondrial-targeted antioxidant Mito-TEMPO on MPP^+-induced mitochondrial fission was investigated. SH-SY5Y cells were treated with medium only (CTRL) or 1 mM MPP^+ with and without Mito-TEMPO (10 µM) for 24 hours at 37 °C. Then, the mitochondrial morphology was observed by staining the cells with MitoTracker™ Red. Results showed that control cells have long, branched mitochondrial network, whereas following the MPP^+ treatment, the tubular network shape broke down into shorter, rounded structures, representing fragmented mitochondria. Regarding cells treated with Mito-TEMPO, they produced similar results as the control (Figure 4.16). Moreover, co-staining with

MitoTracker™ green and MitoSOX revealed the protective effect of Mito-TEMPO on SH-SY5Y cells against both mitochondrial fission and mtROS overproduction (Figure 4.17). Notably, the data clearly showed that only cells with high MitoSOX fluorescent intensity displayed discernible mitochondria fragmentation (Figure 4.17).

All the assessed parameters of mitochondrial fragmentation have shown that Mito-TEMPO prevented mitochondrial fragmentation in MPP^+-treated SHSY5Y cells (4.16 B-K). These findings suggest that mitochondrial fragmentation occurs in parallel with mtROS generation that serves as a trigger for mitochondrial dysfunction during neurotoxin (MPP^+)-induced oxidative stress.

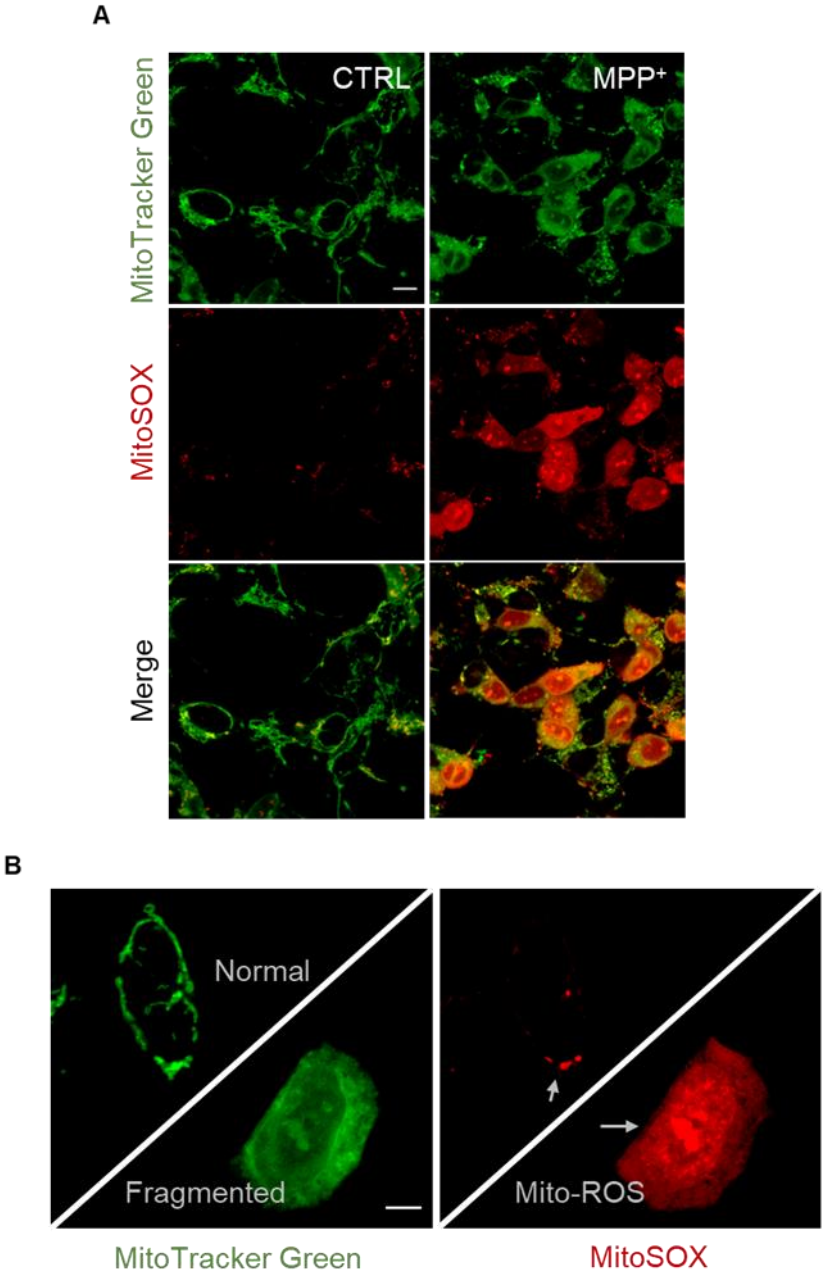

Figure 4.15 Mitochondrial ROS production is associated with mitochondrial fragmentation in MPP^+-treated SH-SY5Y cells.

SH-SY5Y cells were treated with medium alone (CTRL) or with 1 mM MPP^+ for 24 hours at 37 ºC and co-stained with MitoTracker™ green (for mitochondria) and MitoSOX (for mitochondrial ROS). **(A)** Representative confocal images show that MPP^+ treatment caused increased MitoSOX fluorescent intensity as well as the associated mitochondrial fragmentation. Scale bar: 10 µM. **(B)** Expanded images. Scale bar: 5 µM.

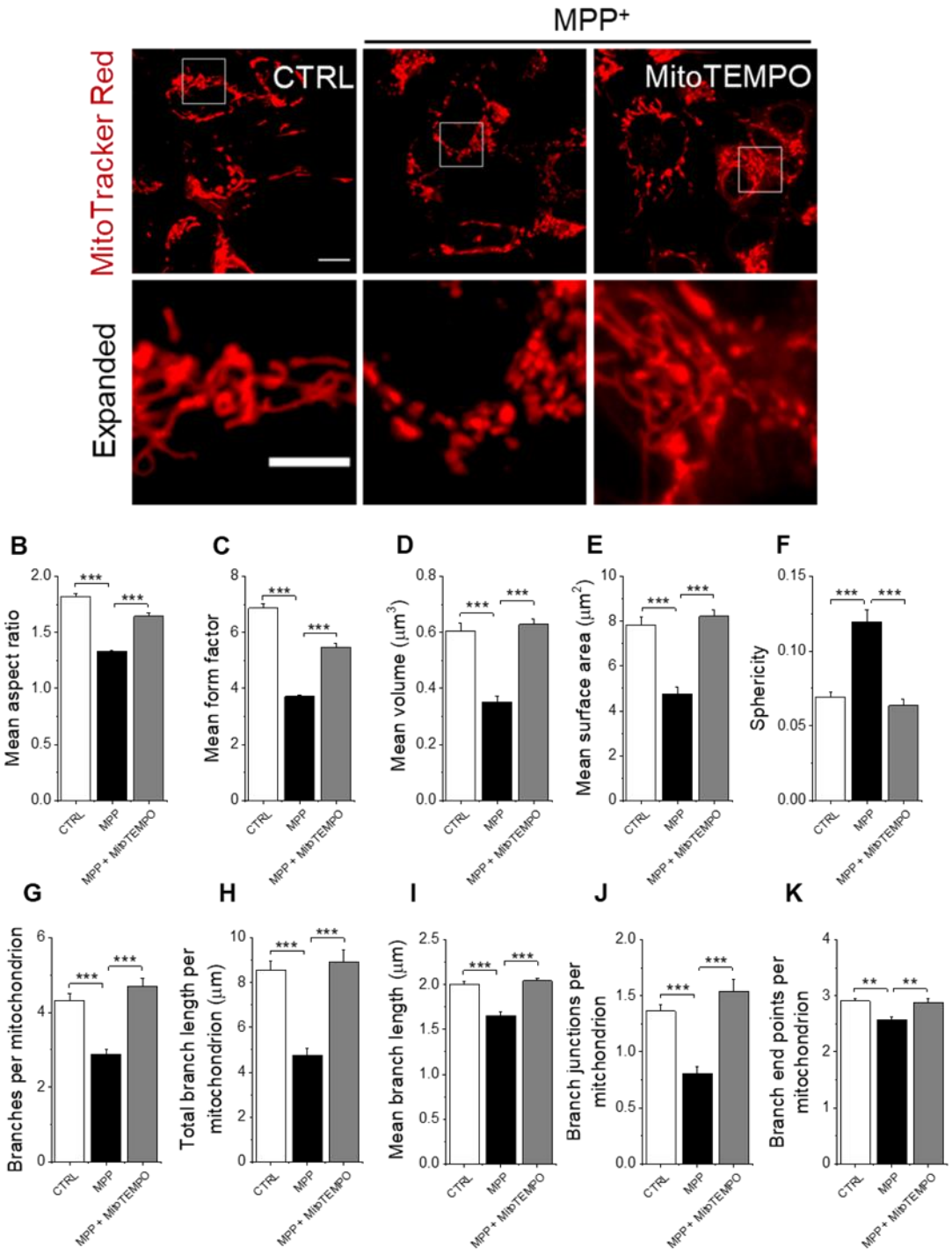

Figure 4.16 Quenching of mitochondrial ROS rescues mitochondrial fission in SH-SY5Y cells exposed to MPP⁺.

SH-SY5Y cells were treated with medium only (CTRL) or 1 mM MPP⁺ with and without the mitochondrial-targeted antioxidant (10 µM Mito-TEMPO) for 24 hours at 37 ºC. **(A)** Fluorescent images of SH-SY5Y stained for MitoTracker™ Red. Scale bars: 10 µm, and 5 µm for expanded images. **(B-K)** Quantification of

changes in mitochondrial morphology through estimation of mean aspect ratio **(B)**, mean form factor **(C)**, mean volume **(D)**, mean surface area **(E)**, sphericity **(F)**, branches per mitochondrion **(G)**, total branch length per mitochondrion **(H)**, mean branch length **(I)**, branch junctions per mitochondrion **(J)**, branch end points per mitochondrion **(K)**. Data presented as normalized mean ± SEM of mitochondrial parameters from three independent experiments n = 3; ** indicates $p < 0.01$; *** indicates $p < 0.001$; NS, not significant; one-way Anova with post-hoc Tukey test.

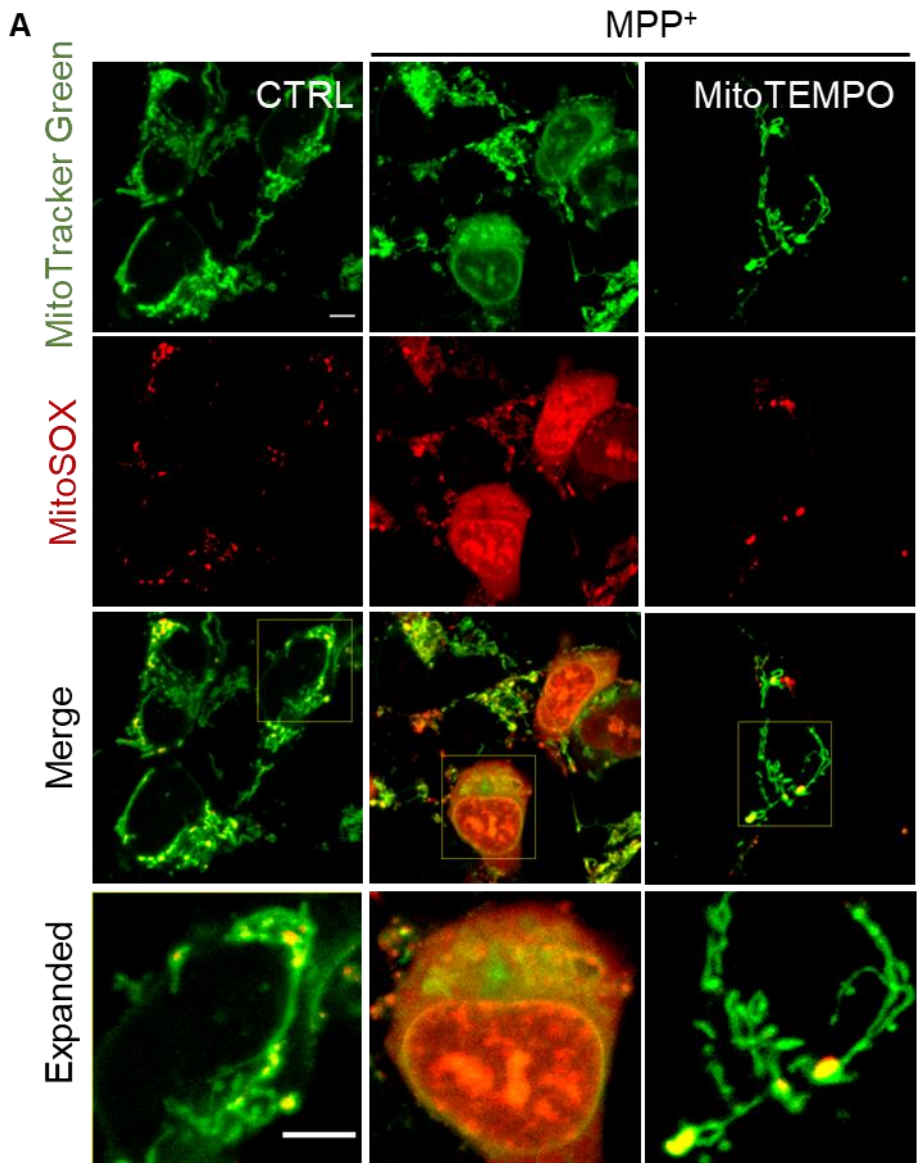

Figure 4.17 Mito-TEMPO protects SH-SY5Y cells from mitochondrial fission.

(A) Fluorescent images taken by confocal microscope of SH-SY5Y cells exposed to medium alone (CTRL) or 1 mM MPP^+ with and without the mitochondrial-targeted antioxidant (Mito-TEMPO, 10 µM) for 24 hours at 37 ºC. To determine the association between mitochondrial fragmentation and excessive mitochondrial ROS production, cells were co-stained with MitoTracker™ Green (for mitochondria) and MitoSOX (for mitochondrial ROS) for 30 minutes prior to the recording. Scale bars: 10 µm, and 5 µm for expanded images.

4.2.10 Inhibition of mitochondrial complexes I and III rescues MPP^+-induced mitochondrial fragmentation and cell death

In cellular signaling and pathology, mitochondria are key producers of ROS. Mitochondrial complex I and complex III are the primary contributors of mtROS production, in particular, superoxide/ hydrogen peroxide during reverse electron transport (Wong et al., 2019a, Brand, 2010, Murphy, 2009a). Deficits in complex I have been linked with PD and a number of other neurological diseases (Zorov et al., 2014). On the other hand, ROS from complex III has been linked to myocardial infraction, which has been shown to induce oxidative damage and impair mitochondrial function (Heather et al., 2010). Also, a recent study showed that genetically determined dysfunction in complex III may lead to a distinct neurodegenerative phenotype (Cerri and Valente, 2020).

To determine the source of ROS in MPP^+-induced oxidative stress in SH-SY5Y cells, the electron leak site-specific suppressors of complex I (S1QEL) and complex III (S3QEL) were used. These selective chemicals suppress mtROS generation at complex I or III without altering forward electron transport (Wong et al., 2019a, Orr et al., 2015). Thus, these chemicals allow assessment of the relative contribution of complex I and III to the overall mtROS signal by comparing the amount of inhibition caused by these two site-specific suppressors. Furthermore, the involvement of complexes I and III to mitochondrial fragmentation and cell death could also be examined.

To identify the contribution of mitochondrial complex I and complex III, SH-SY5Y cells were pretreated with S1QEL (10 µM) or S3QEL (5 µM) for one hour. The cells were then co-incubated with 1 mM MPP^+ for 24 hours at 37 °C. Following the treatment, they were stained for mitochondria, mtROS, and cell death (propidium Iodide). The results show that both S1QEL and S3QEL suppressed mitochondrial fission, mtROS generation and cell death indicating roles for both Complex I and III (Figures 4.18 and 4.19). However, their relative contribution to these effects was different. Results showed that both S1QEL and S3QEL lowered the overall mtROS production, however, the decreases were not statistically

significant (Figure 4.18 A-B). Of the two, S3QEL caused a greater decrease in mtROS levels compared to S1QEL, which suggests that the contribution of Complex III is greater than that of Complex I in terms of its contribution to MPP^+ induced mtROS production. Therefore, the subsequent question is whether ROS generated by mitochondria complex I and/or complex III, upon MPP^+ treatment, are involved in mitochondrial fission and cell death. Analyzing the mitochondrial morphology showed that S1QEL and S3QEL attenuated MPP^+-induced mitochondria fragmentation (Figure 4.19). In particular, S3QEL demonstrated a highly significant rescuing effect on mitochondrial fission (Figure 4.19). Moreover, when their effects on cell viability were investigated, data revealed that both the mtROS suppressors had significant effect (S1QEL, $p < 0.01$; S3QEL $p < 0.001$) against SH-SY5Y cell death caused by MPP^+ (Figure 4.18 C-D), suggesting a role of mitochondria-generated ROS from complex I and III in MPP^+-induced mitochondrial fragmentation and subsequent cell death.

Collectively, these findings indicate that Complexes I and III, mainly Complex III, represent the mitochondrial sites of ROS generation that impact mitochondrial fragmentation and neuronal cell death.

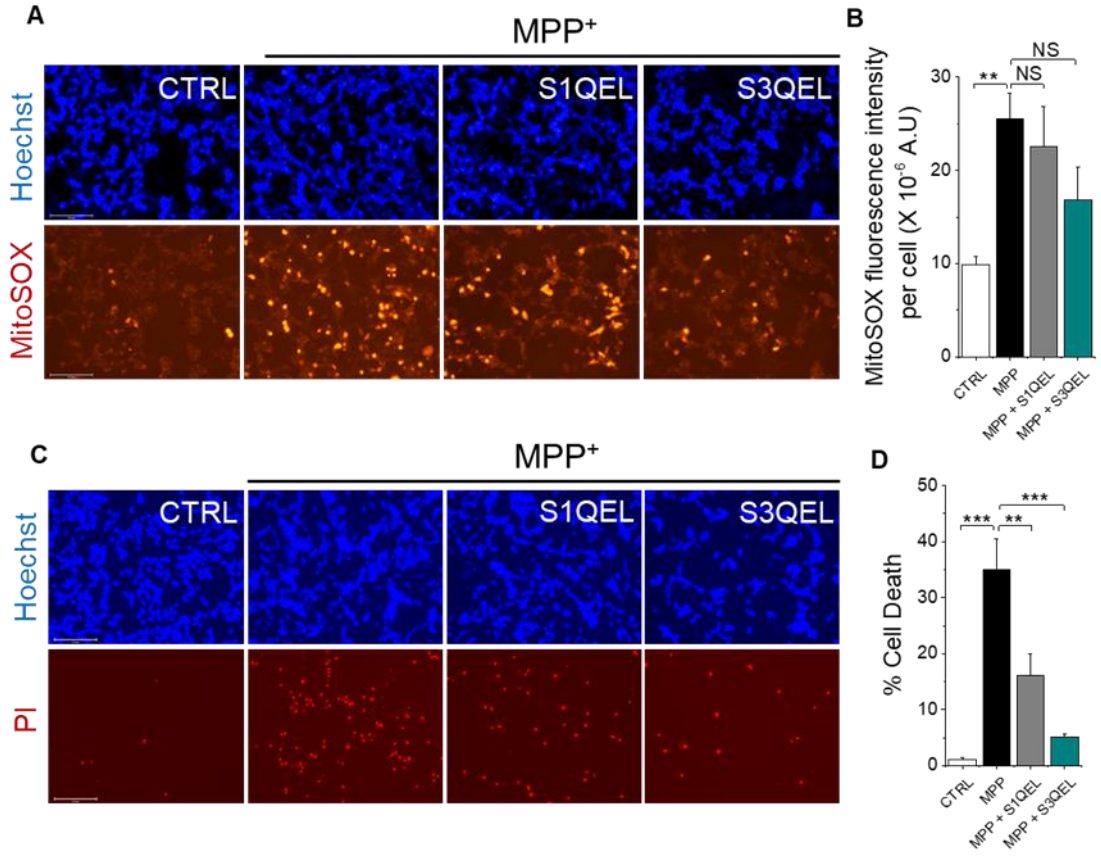

Figure 4.18 Effects of S1QEL and S3QEL on mitochondria ROS generation and SH-SY5Y cell death.

SH-SY5Y cells were pretreated with either S1QEL (10 µM) or S3QEL (5 µM) for 1 hour, then they were incubated with 1 mM MPP^+ for 24 hours at 37 ºC. **(A)** Fluorescent images of SH-SY5Y cells stained for mitochondrial ROS using MitoSOX and for cells nuclei using Hoechst. Scale bar: 125 µM. **(B)** Mean ± SEM of data of MitoSOX fluorescence. **(C)** Fluorescent images of cells stained for nuclei of all (Hoechst) and dead (Propidium Iodide, PI) cells. Scale bar: 125 µM. **(D)** Mean ± SEM of percent of cell death. Mean data were obtained from three independent experiments n = 3, ** indicates $p < 0.01$; *** indicates $p < 0.001$; NS, not significant; one-way Anova with post-hoc Tukey test.

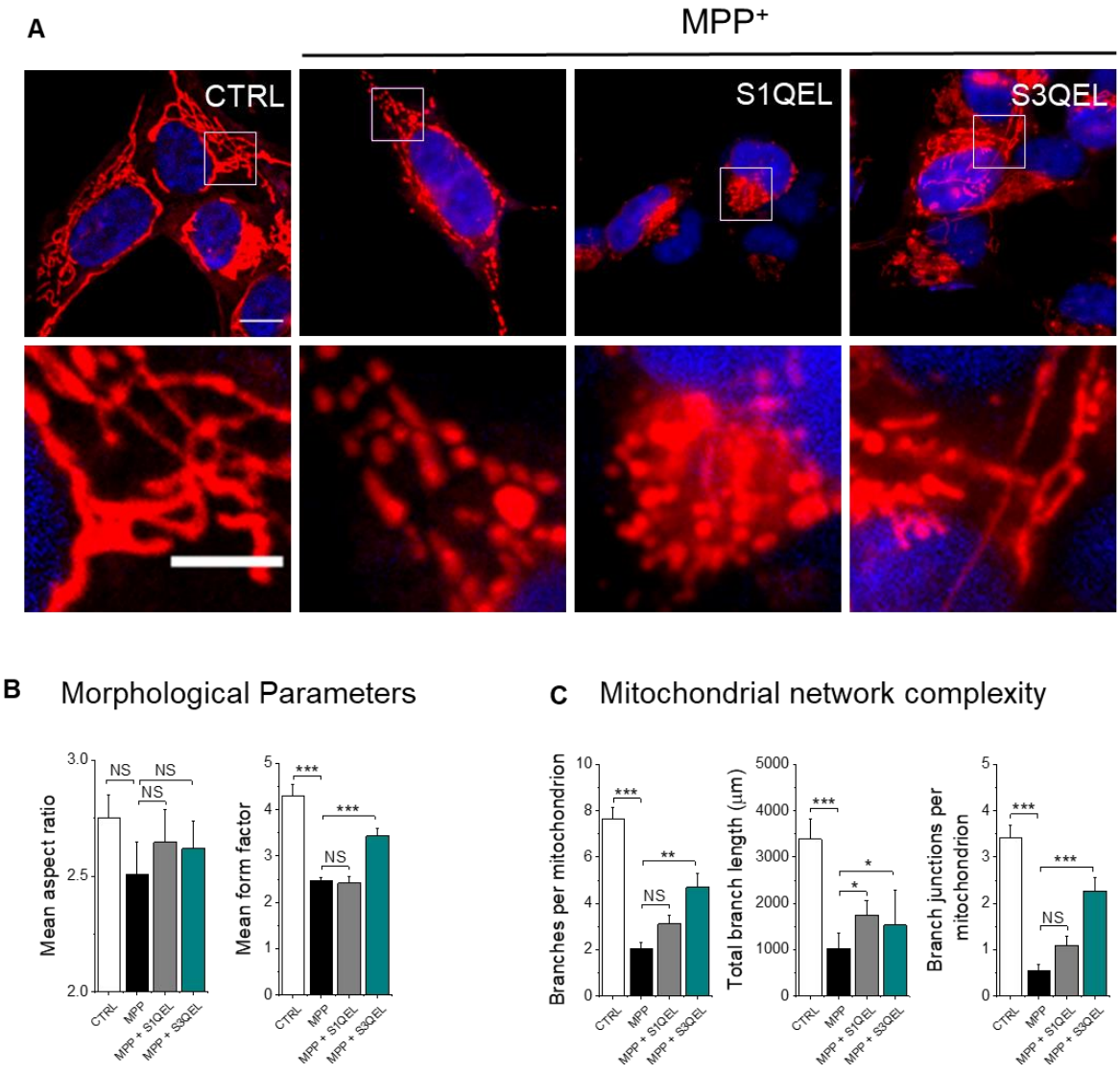

Figure 4.19 Effects of S1QEL and S3QEL on mitochondrial fission in SH-SY5Y cells.

SH-SY5Y cells were pretreated with either S1QEL (10 µM) or S3QEL (5 µM) for 1 hour, then they were incubated with 1 mM MPP^+ for 24 hours at 37 ºC. After treatment, cells were stained for mitochondria using MitoTracker™ Red. **(A)** Fluorescent images showing the mitochondrial morphology of untreated (CTRL) and treated cells. Scale bars: 10 µm, and 5 µm for expanded images. **(B)** Quantification of changes in mitochondrial morphology through estimation of form factor and aspect ratio. **(C)** Quantification of mitochondrial network complexity through estimation of branch length and number per mitochondrion, and number of branch junctions per mitochondrion. Data presented as normalized mean ±

SEM of mitochondrial parameters from three independent experiments n =3; N = 335 cells in total. * indicates $p < 0.05$; ** indicates $p < 0.01$; *** indicates $p < 0.001$; NS, not significant; one-way Anova with post-hoc Tukey test.

4.2.11 TRPM2 channels mediate MPP^+ induced changes in Zn^{2+} redistribution and Drp1 recruitment to mitochondria

The fission process of mitochondria is catalysed by dynamin-related protein 1 (Drp1). Drp1 mediates outer membrane fission in response to specific cellular signals that result in its translocation from the cytoplasm to the outer membrane of mitochondria causing a restriction and scission of the mitochondrial network leading to mitochondrial fragmentation (Archer, 2013, Chappie et al., 2009, Friedman et al., 2011). Since it was shown in the previous sections that increased intracellular Ca^{2+} and Zn^{2+} levels in response to TRPM2 activation caused mitochondrial fragmentation, the next question was whether TRPM2 mediated changes in Zn^{2+} can induce Drp1 recruitment to mitochondria during MPP^+ treatment.

To determine the role of TRPM2 activation in Drp1 recruitment to mitochondria, SH-SY5Y cells were transfected with GFP-tagged Drp1 and incubated for 48 hours at 37 °C; cells were then treated with medium alone (CTRL) or with 1 mM MPP^+ for 24 hours, before staining with MitoTracker™ Red. In normal cellular conditions, Drp1 proteins are mostly found in the cytosol, however, a study reported that around 3% of the total Drp1 is associated with mitochondria (Smirnova et al., 2001), where they promote mitochondrial fission via GTP-dependent conformational change (Chang and Blackstone, 2010). Results revealed that, in control cells, Drp1-GFP is uniformly distributed throughout the cytoplasm; no detectable Drp1-GFP association with mitochondria was found. After 24 hours of MPP^+ treatment, Drp1-GFP aggregated into puncta, which were observed at disparate areas along mitochondria tubules and in the cytosol (Figure 4.20). Compared to cells in the later stages of mitochondrial fission where the network is highly fragmented, cells in the early stages of mitochondrial fission showed a higher degree of localization to mitochondria. This is probably because following the fragmentation, Drp-1 dissociates from mitochondria. The TRPM2 inhibitor, 2-APB, reduced the mitochondrial localization of Drp1-GFP and mitochondrial fission (Figure 4.20).

Next, to investigate the role of Zn^{2+} directly in mitochondrial fission, effect of the Zn^{2+} ionophore (Zn-PTO) on Drp1 translocation from the cytosol to mitochondria was tested. SH-SY5Y Cells were transfected with GFP-tagged Drp1 and incubated for 48 hours at 37 °C, before exposing to Zn-PTO (2 µM) for 2 hours. The results showed that Zn^{2+} caused Drp1 to aggregate into puncta seen on the fragmented mitochondria and some in the cytosol (Figure 4.21), as was observed with MPP^+ treated cells (Figure 4.20). However, the extent of mitochondrial fission is too extensive to detect significant association of Drp1-GFP with mitochondria. Moreover, to confirm the Zn^{2+} redistribution to mitochondria, cells were exposed to Zn-PTO or MPP^+ and stained for Zn^{2+} using FluoZin-3. Both treatments induce Zn^{2+} accumulation in mitochondria causing mitochondrial fission (Figure 4.22 – 4.23)

Collectively, these findings suggest that MPP^+-induced mitochondrial fragmentation is mediated by TRPM2-dependent Zn^{2+} mediated Drp1 recruitment to mitochondria.

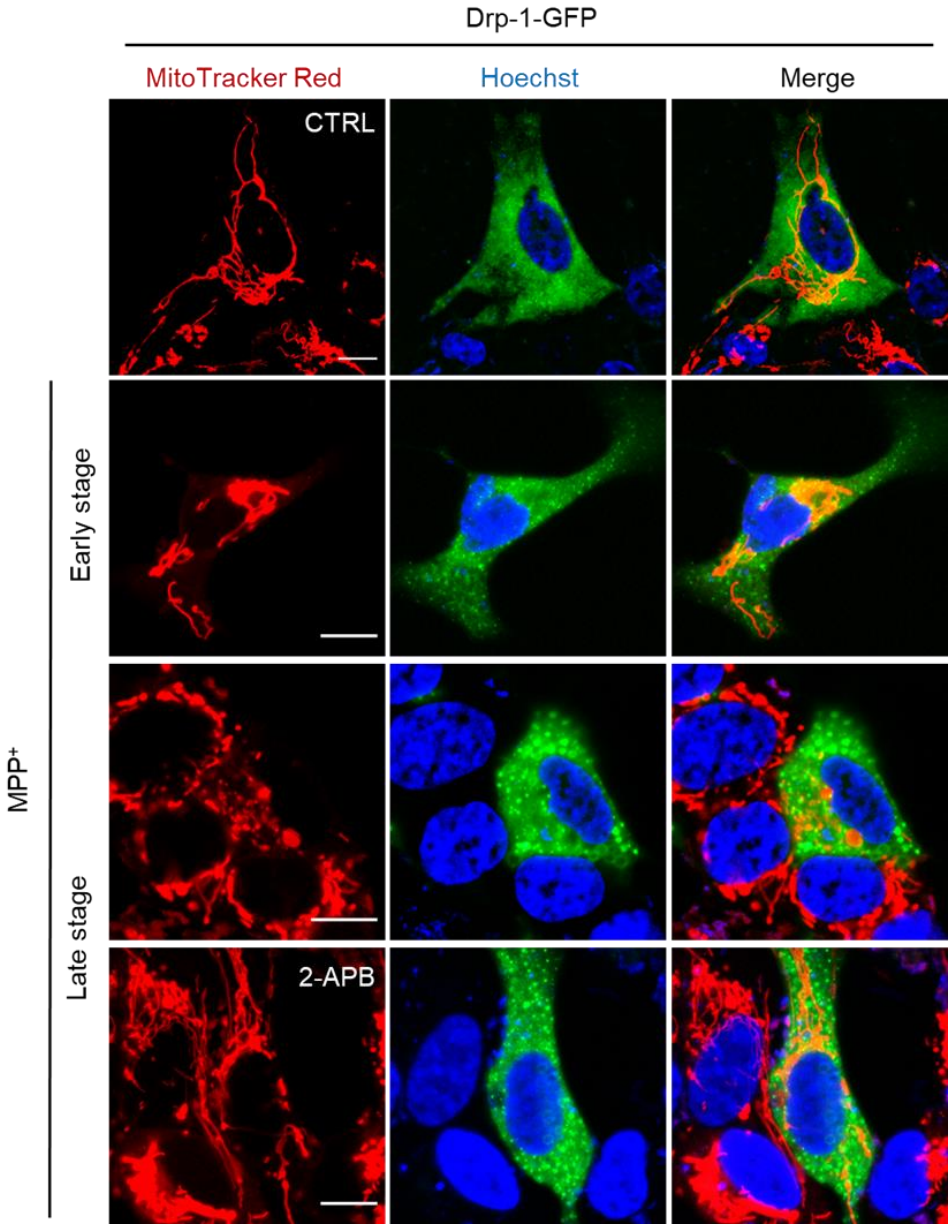

Figure 4.20 TRPM2 channels mediate MPP^+-induced mitochondrial Drp-1 recruitment.

Fluorescent images of SH-SY5Y cells transfected with Drp1-GFP and incubated for 48 hours at 37 ºC, then treated with medium alone (CTRL) or with 1 mM MPP^+ plus or minus the TRPM2 inhibitor (50 µM 2-APB) for 24 hours at 37 ºC. Following the treatment, cells were stained for mitochondria using MitoTracker™ Red and for cells nuclei with Hoechst. Scale bars: 10 µm.

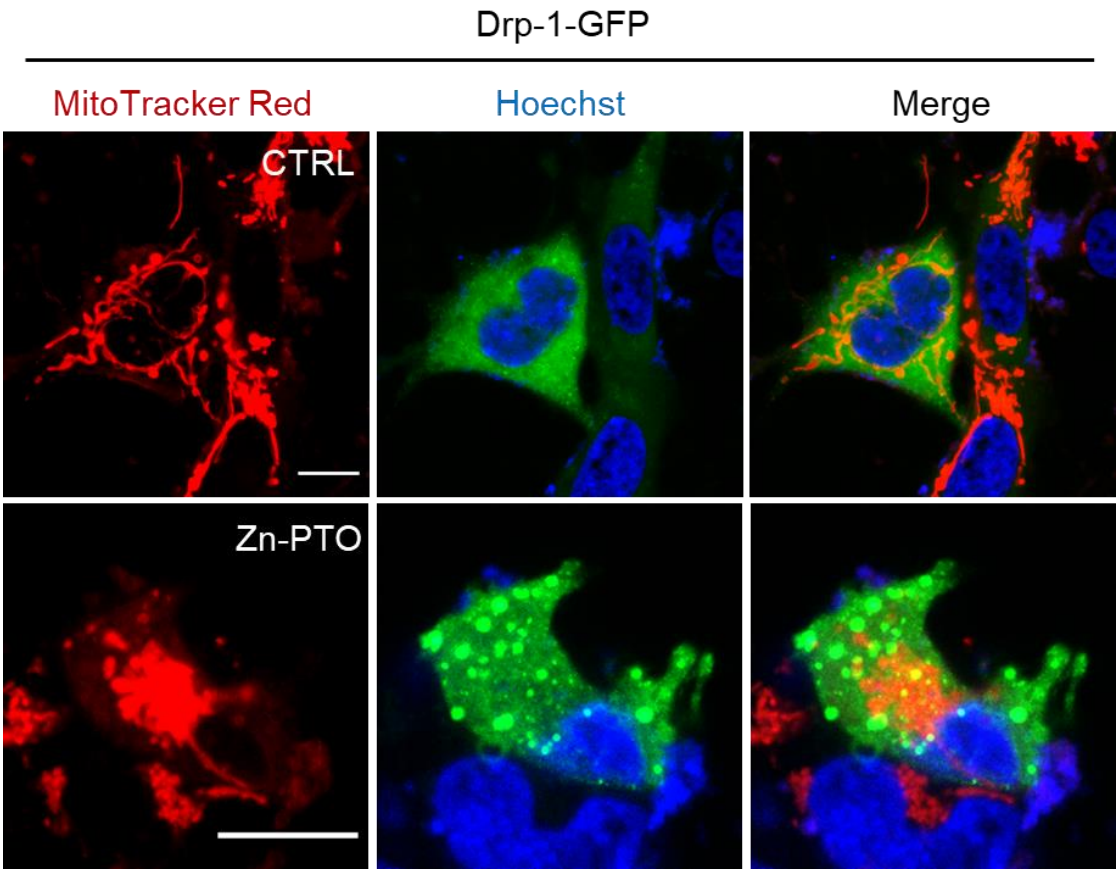

Figure 4.21 Rise in intracellular Zn^{2+} by Zn-ionophore (Zn-PTO) promotes mitochondrial Drp-1 recruitment.

Fluorescent images of SH-SY5Y cells transfected with Drp1-GFP and incubated for 48 hours at 37 ºC, then exposed to Ca^{2+} free medium alone (CTRL) or Ca^{2+} free medium containing the Zn^{2+} ionophore (Zn-PTO, 2µM) for 2 hours at 37 ºC. Following the treatment, cells were stained for mitochondria using MitoTracker™ Red and for cells nuclei with Hoechst. Scale bars: 10 µm.

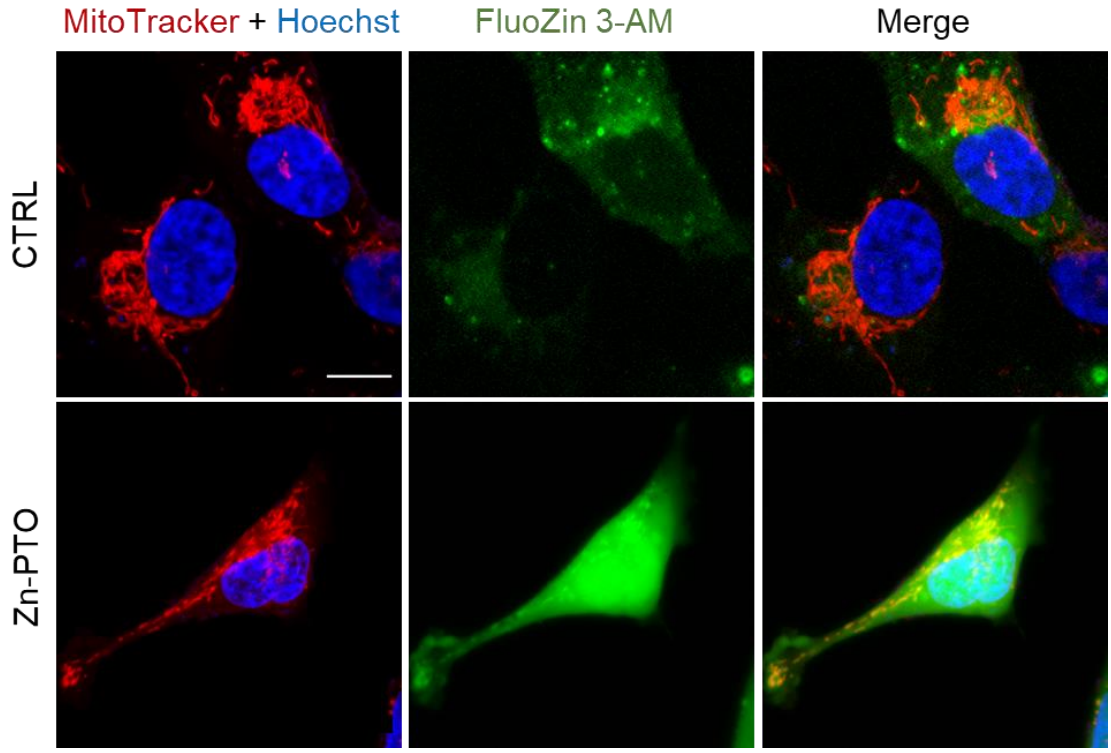

Figure 4.22 Rise in intracellular Zn^{2+} by Zn-ionophore (Zn-PTO) increases mitochondrial Zn^{2+} and mitochondrial fragmentation.

Fluorescent images of SH-SY5Y cells exposed to Ca^{2+} free medium alone (CTRL) or Ca^{2+} free medium containing the Zn^{2+} ionophore (Zn-PTO, 2µM) for 2 hours at 37 ºC. Following the treatment, cells were stained for mitochondria using MitoTracker™ Red, for nuclei with Hoechst, and for Zn^{2+} using FluoZin-3. The yellow spots represent the overlap of Zn^{2+} staining (FluoZin-3 green) with mitochondria staining (MitoTracker™ Red), indicating the localization of Zn^{2+} in mitochondria. Scale bars: 10 µm.

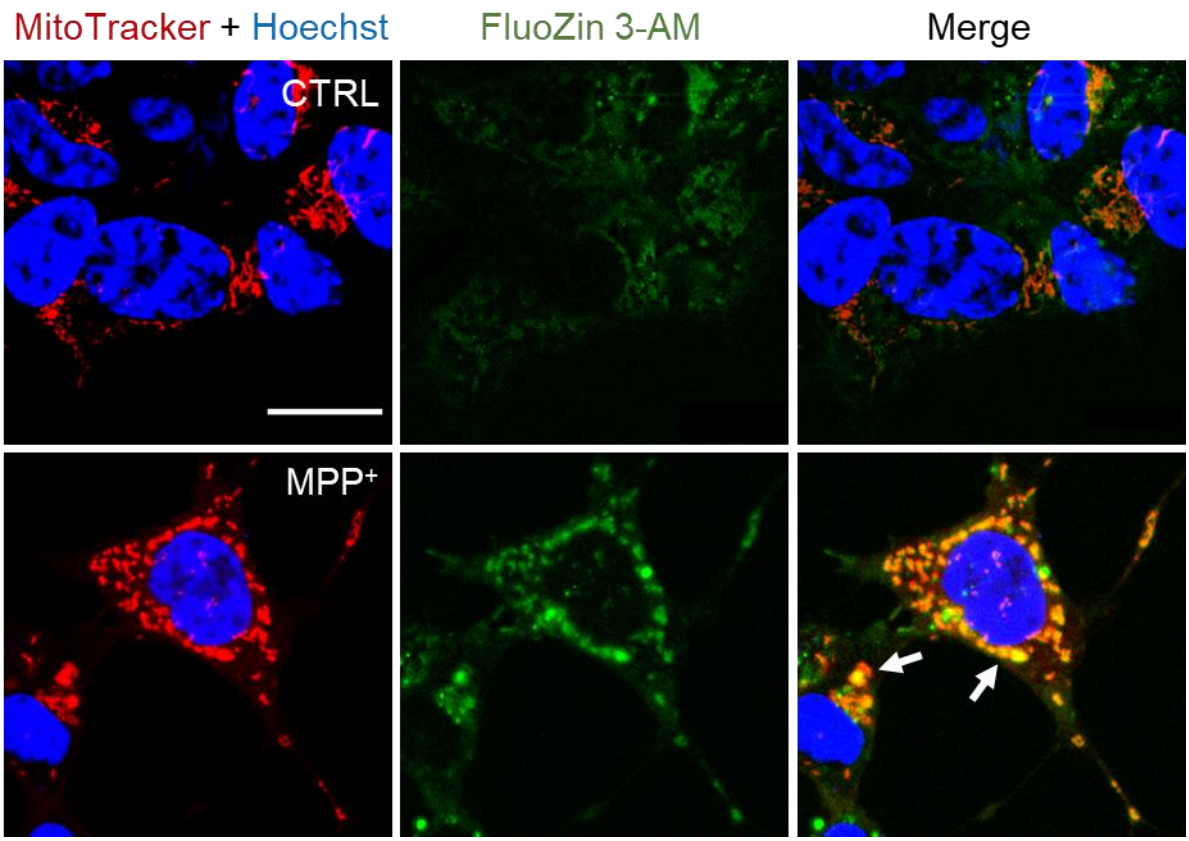

Figure 4.23 MPP^+ induces rise in mitochondrial Zn^{2+} and mitochondrial fragmentation.

Fluorescent images of SH-SY5Y cells treated with medium alone (CTRL) or with 1 mM MPP^+ for 24 hours at 37 ºC. Then, cells were stained for mitochondria using MitoTracker™ Red, for nuclei with Hoechst, and for Zn^{2+} using FluoZin-3. The arrows point to yellow spots representing the overlap of Zn^{2+} staining (FluoZin-3 green) with mitochondria staining (MitoTracker™ Red), indicating the localization of Zn^{2+} in mitochondria in cells treated with MPP^+. Scale bars: 10 µm.

4.3 Discussion

In the previous chapter, I have demonstrated that TRPM2-mediated Ca^{2+} and Zn^{2+} signals play a role in ROS generation. ROS are known to negatively impact the structure and function of lysosomes and mitochondria (Kurz et al., 2008a, Elfawy and Das, 2019, Abuarab et al., 2017, Li et al., 2017a, Lin and Beal, 2006). Given the fact that PD is characterized by the dysfunction of these organelles (Dehay et al., 2010, Kim et al., 2021, Mazzulli et al., 2016b, Deng et al., 2018, Balestrino and Schapira, 2020, Dias et al., 2013), the role of TRPM2-Ca^{2+}-Zn^{2+} signaling in lysosomal and mitochondrial biology was investigated. The results obtained using the MPP^+/SH-SY5Y cellular model of PD are presented in this Chapter (schematically depicted in Figure 4. 24). In summary, the results show: (i) inhibition of NOX2-generated ROS and TRPM2 mediated Ca^{2+} entry prevents MPP^+ induced mitochondrial fragmentation; (ii) extracellular Ca^{2+} entry leads to a marked decline in the number of functional lysosomes; (iii) elevation of cytosolic Ca^{2+} leads to the redistribution of lysosomal Zn^{2+} ions into mitochondria; (iv) the resultant increase in mitochondrial Zn^{2+} causes loss of mitochondrial membrane potential and the breakdown of mitochondrial network; (v) and, MPP^+ (via Zn^{2+}) induced mitochondrial fission can be inhibited by preventing the electron leak mainly from Complex III of the mitochondrial electron transport chain.

4.3.1 The functional interaction of NOX2 and TRPM2 channels in generating cytosolic ROS and Ca^{2+} signals

Apocynin, a pan inhibitor of NOX enzymes, and the NOX2 specific inhibitor Gp91ds-tat (Williams and Griendling, 2007), both completely inhibited mitochondrial fragmentation (Figure 4.2). These data are consistent the previous studies with neuronal cells where MPP^+ induced mitochondrial fragmentation and cell death were shown to be inhibited by NOX2 inhibition (Rastogi et al., 2017, Wu et al., 2006). Pharmacological inhibition (Figure 4.3) as well as siRNA mediated suppression (Figure 4.4) of TRPM2 channel expression prevented

mitochondrial fragmentation. Previous studies have reported that TRPM2 channels play an important role in oxidative stress induced mitochondrial fragmentation in endothelial and pancreatic β-cells (Abuarab et al., 2017, Li et al., 2017a, Li et al., 2017b). NOX2 generated ROS can stimulate TRPM2 channels. TRPM2 mediated extracellular Ca^{2+} entry, in turn, can promote the formation of functional NOX2 complex by recruiting the cytoplasmic p47phox subunit to plasma membrane NOX2. Ca^{2+} has been shown to activate protein kinase C and phosphorylate p47phox required for its recruitment to NOX2 (Fontayne et al., 2002, Belarbi et al., 2017). Thus MPP^+ likely promotes functional coupling between NOX2 and TRPM2 channels and such coupling could amplify both the mito-toxic Ca^{2+} and ROS signals. Although these observations were made using MPP^+, they are likely applicable to other forms of PD where NOX2 activation is involved. Therefore, disruption of NOX2-TRPM2 functional interaction may open up new avenues for treatment of PD.

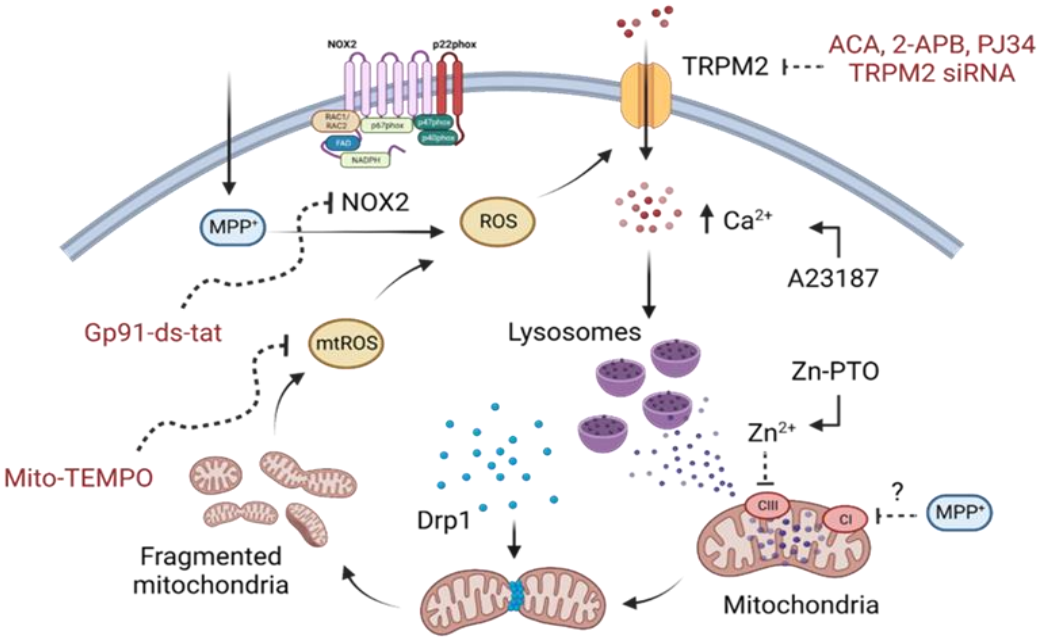

Figure 4.24 Schematic diagram summarizing the findings.

In SH-SY5Y cells, MPP^+ induces ROS generation via NOX2 and mitochondrial pathways. The pathway shows that MPP^+ induces ROS generation by NOX2, promoting TRPM2-mediated Ca^{2+} influx into the cells. Extracellular Ca^{2+} entry causes depletion of lysosomes and redistribution of lysosomal Zn^{2+} (purple dots) to mitochondria. In the mitochondria, Zn^{2+} inhibits mainly Complex III; this causes loss of mitochondrial membrane potential, and stimulates Drp1 recruitment (blue dots) from the cytosol to the mitochondria, leading to mitochondrial fragmentation. Mitochondrial dysfunction subsequently induces mitochondrial ROS (mtROS) overproduction. mtROS thus generated could further stimulate TRPM2 exacerbating the mitochondrial fission and dysfunction. Ca^{2+} and Zn^{2+} ionophores (A23187 and Zn-PTO) reproduce the effects of MPP^+ on mitochondria. NOX2 inhibition with gp91-ds-tat rescues mitochondria from MPP^+ effects. Blocking the TRPM2 channel using pharmacological inhibitors (ACA, 2-APB, PJ34) or TRPM2 siRNA prevents MPP^+-induced mitochondrial fragmentation. Figure created with BioRender.com

4.3.2 Dyshomeostasis of both Ca^{2+} and Zn^{2+} contributes to mitochondrial fragmentation

Multiple studies have shown that elevation of intracellular Ca^{2+} stimulates mitochondrial fission (Duchen, 2000a, Orrenius et al., 2015, Szabadkai et al., 2006). Inhibition of TRPM2 mediated Ca^{2+} entry (Figures 4.3, 4.4) as well as chelation of Ca^{2+} with BAPTA (Figure 4.5) were able to prevent MPP^+ induced mitochondrial fragmentation. These results are entirely consistent with the previous reports (Zhu et al., 2012, Wang et al., 2011). A time-dependence study of Ca^{2+} delivery through the Ca^{2+} ionophore, A23187 demonstrated a progressive loss of the normal mitochondrial network morphology (Figure 4.6 and 4.7), further supporting the role of Ca^{2+} in mitochondrial fragmentation.

However, besides Ca^{2+}, Zn^{2+} is implicated in neurodegeneration including in PD (Dexter et al., 1991). Indeed, chelation of Zn^{2+} with TPEN has been shown to prevent oxidative stress induced neuronal cell death (Medvedeva et al., 2009) including in PD (Sikora and Ouagazzal, 2021). Consistent with the role of Zn^{2+}, chelation of Zn^{2+} alone was sufficient to prevent MPP^+-induced mitochondria fragmentation (Figure 4.5) and the consequent cell death (Figure 3.12). The importance of Zn^{2+} was further confirmed through direct intracellular delivery of Zn^{2+} using the Zn^{2+} ionophore, Zn-PTO. Elevation of intracellular Zn^{2+} with Zn-PTO led to extensive mitochondrial fragmentation (Figure 4.9). A similar role for Zn^{2+} in oxidative stress induced mitochondrial fragmentation has been reported with human endothelial cells (Abuarab et al., 2017) and pancreatic β-cells (Li et al., 2017a).

Interestingly, chelation of Zn^{2+} with TPEN prevented A23187 induced mitochondrial fragmentation effectively as BAPTA (Figure 4.8). This result supports the idea that Ca^{2+} induced mitochondrial fragmentation during oxidative stress is likely mediated by Zn^{2+}.

4.3.3 TRPM2 mediated Ca^{2+} influx promotes lysosomal dysfunction

Studies presented in the preceding chapter demonstrated that MPP^+ activation of NOX2 generates ROS that stimulates Ca^{2+} influx through the TRPM2 channel. In this Chapter, I sought to understand how the ROS and Ca^{2+} signals generated at the plasma membrane are transmitted to mitochondrial network, causing the network to break down and the cells to die. Although it is known from various studies that ROS and Ca^{2+} can attack mitochondria directly resulting in mitochondrial damage (Camello-Almaraz et al., 2006, Pinton et al., 2008, Nicholls, 2005), recent studies with endothelial and pancreatic β-cells from this laboratory demonstrated that the Ca^{2+} signals generated at the plasma membrane first act on the lysosomes to release lysosomal Zn^{2+} that then causes mitochondrial damage (Abuarab et al., 2017, Li et al., 2017a). Similar results were obtained with SH-SY5Y cells. MPP^+ caused LMP and the loss of lysosomes (Figure 4.11). The Ca^{2+} ionophore, A23187 replicated the effect of MPP^+ on lysosomes; these effects were prevented by the chelation of Ca^{2+} with BAPTA confirming the role of cytosolic Ca^{2+} elevation in LMP and decline of lysosomal numbers (Figure 4.12). Importantly, preventing Ca^{2+} influx through MPP^+-induced TRPM2 channels with the TRPM2 blocker (2-APB) also rescued the loss of lysosomes in SH-SY5Y cells (Figure 4.11). Taken together, these data support the fact that MPP^+ induced TRPM2 mediated extracellular Ca^{2+} entry leads to LMP and a decline in lysosomal numbers. Whether TRPM2 induced NOX2 activation and NOX2 derived ROS also affect lysosomal integrity was not examined. Nevertheless, these findings provide a cell biological explanation for the previous reports that lysosomal dysfunction precedes mitochondrial dysfunction (Boya et al., 2003, Zhao et al., 2003, Cirman et al., 2004, Leist and Jäättelä, 2001, Mitrofan et al., 2010).

It is still unclear exactly how the increase in cytosolic Ca^{2+} level leads to LMP. However, it was found that high Ca^{2+} can activate calpain, a Ca^{2+}-dependent cytosolic protease, that has been attributed to promote LMP through degrading the lysosomal-associated membrane protein, LAMP-2 (Rodriguez and Torriglia,

2013, Khorchid and Ikura, 2002). Also, lysosomes are capable of transporting ions across their membrane in a bi-directional way, which is necessary for lysosomal function and the initiation of downstream signaling pathways (Udayar et al., 2022). Saposin, a Ca^{2+} binding protein, is another possible potential factor that might explain the association between increased cytosolic Ca^{2+} and the lysosomal dysfunction. It is suggested that Saposin has a suppressive effect on lysosomal hydrolase β-glucocerebrosidase (GCase) that is encoded by *GBA1* gene, which is thought to be a prevalent genetic risk factor for PD (Udayar et al., 2022). The mechanism by which *GBA1* is associated to PD is yet not known. However, it is believed that GCase dysfunction can cause buildup of lipid in the lysosomes, resulting in structural and functional alterations at the organelle level (Udayar et al., 2022). Additionally, in *GBA1*-related PD, it has been shown that contact between mitochondria and lysosomes is prolonged to cause mitochondria dysfunction, which may be avoided by increasing GCase activity in dopaminergic neuronal cells (Kim et al., 2021). Thus, collectively, these findings point to an upstream regulation of mitochondria activity involving mitochondrial-lysosomal interactions, and Ca^{2+}.

Although the majority of earlier studies, including genetic, cell biological and clinical studies have implicated mitochondria in PD pathology (Deng et al., 2018, Balestrino and Schapira, 2020, Dias et al., 2013, Tretter et al., 2004), recent studies have reported a significant role for lysosomal dysfunction in PD (Dehay et al., 2010, Kim et al., 2021, Mazzulli et al., 2016a, Sidransky and Lopez, 2012, Klein and Mazzulli, 2018). Lysosomal proteins are among the most important targets for several genetic mutations linked to PD. For instance, mutations in *GBA1*, *LRRK2* and *PARK9* genes have all been implicated with the development of PD (Udayar et al., 2022). An *in vivo* study using a mouse model of PD has shown a decrease in lysosomal numbers in the brain (Dehay et al., 2010). Lysosomal dysfunction in both glial and neuronal cells has been shown to be a trigger the progression of the pathological markers of neurodegenerative diseases, such as alpha-synuclein in PD (Choi et al., 2020, Udayar et al., 2022).

4.3.4 Ca^{2+} induced LMP is accompanied by the redistribution of Zn^{2+} to mitochondria leading to the fragmentation of mitochondrial network

Lysosomal damage is followed by the release of cytotoxic enzymes such as cathepsins (Nagakannan et al., 2020, Wang et al., 2018a) and metal ions including Ca^{2+} and Zn^{2+}. Given chelation of free Zn^{2+} with TPEN was able to prevent MPP^+ and calcium ionophore induced mitochondrial fission, we asked whether Zn^{2+} released from the lysosomes could induce mitochondrial damage. Consistent with this possibility, both MPP^+ and the calcium ionophore treatments led to a marked decline in lysosomal Zn^{2+} (Figures 4.10 - 4.12) and the redistribution of Zn^{2+} to mitochondria (Figure 4.7 and 4.22 – 4.23). Elevation of mitochondrial Zn^{2+} was accompanied by the fragmentation of mitochondrial network (Figure 4.8 - 4.9 and 4.22 – 4.23). These results are in agreement with the previous studies on endothelial (Abuarab et al., 2017) and pancreatic β-cells (Li et al., 2017a).

A previous study has demonstrated that lysosomal depletion precedes dopaminergic cell death in a mouse model of PD (Dehay et al., 2010). The authors suggested that restoring normal lysosomal level and function may constitute a potential neuroprotective therapy in PD (Dehay et al., 2010). Inhibition of Ca^{2+} entry via TRPM2 channel significantly rescued MPP^+-induced lysosomal depletion in SH-SY5Y cells (Figure 4.11). This suggests that the TRPM2 channel could be therapeutically targeted to prevent lysosomal loss in PD.

How Zn^{2+} enters mitochondria is uncertain. Several candidate mechanisms have been reported. These include mitochondrial calcium uniporter (MCU) (Malaiyandi et al., 2005), and Zip1 (Cho HM et al., 2019). Studies with *C-elegans* reported that ZnT9 (SLC-30A9), a Zn^{2+} exporter and SLC-25A25, a Zn^{2+} importer regulate mitochondrial Zn^{2+} levels to maintain mitochondrial homeostasis (Ma et al., 2022). As mentioned above, recent studies have reported close physical contacts

between mitochondria and lysosomes (Wong et al., 2018, Kim et al., 2021, Wong et al., 2019b). Such proximity between the two organelles might facilitate the efficient redistribution of Zn^{2+} from lysosomes to mitochondria during oxidative stress. Indeed, disruption of mitochondrial-lysosome contacts has been implicated in the regulation of mitochondrial dynamics (Wong et al., 2018).

Studies of human genetic mutations have provided support for the role of lysosomes in Zn^{2+} homeostasis. Genetic mutations in *ATP13A2*/*PARK9*, which encodes lysosomal P-type ATPase (type5) have been shown to be disrupt lysosomal function, leading to Zn^{2+} dyshomeostasis, that in turn affects mitochondrial function (Park et al., 2014, Tsunemi and Krainc, 2013). *PARK9* expression was found to be high in the brains of sporadic PD patients, suggesting a role for *PARK9* in the pathophysiology of PD (Tsunemi and Krainc, 2013). It has been found that a loss of function mutation in this gene might cause lysosomal dysfunction, which can then lead to an accumulation of α-Syn. Although the association between *PARK9* and lysosomal dysfunction is uncertain, it has been shown that Zn^{2+} sequestration by lysosomes was reduced in *PARK9*-deficient neurons and the expression of Zn^{2+} transporters increased (Tsunemi and Krainc, 2013). Moreover, reduced capacity of lysosomes to buffer cytosolic Zn^{2+} results in the accumulation of Zn^{2+} in mitochondria leading to the loss of ΔΨm and mitochondria dysfunction (Park et al., 2014).

Moreover, the data of this study also showed an association between increased mitochondria Zn^{2+} and Drp1 recruitment from the cytosol to mitochondria to initiate mitochondrial fission. Zn-PTO results suggest a role of Zn^{2+} in Drp-1 recruitment. Notably, inhibition of TRPM2 seems to attenuate MPP^{+}-induced Drp1 translocation to mitochondria (Figure 4.20), however, this aspect of the study requires further investigations. On the whole, these findings suggest that the recruitment of Drp-1 protein and subsequent mitochondria fragmentation is facilitated by the transfer of Zn^{2+} from lysosomes to mitochondria via TRPM2-mediated pathway. These findings are in agreement with other studies using endothelial and pancreatic β-cells (Abuarab et al., 2017, Li et al., 2017a).

4.3.5 MPP^+ induced loss of ΔΨm and mitochondrial ROS generation are mediated by Zn^{2+}

It has been suggested that mitochondrial Zn^{2+} uptake provides a way of excess Zn^{2+} clearance from the cytosol of neurons undergoing excitotoxicity (Dineley et al., 2005, Sensi et al., 2009). However, elevated mitochondrial Zn^{2+} levels induce loss of ΔΨm (an indicator of loss of mitochondrial function) and ROS generation, causing neuronal cell death (Dineley et al., 2005). Thus, there is some evidence that rise in mitochondrial Zn^{2+} is associated with the loss of ΔΨm and ROS production. Consistent with these reports, MPP^+ and Zn-PTO caused a rise in mitochondrial Zn^{2+} leading to the loss of ΔΨm and an increase in mtROS production, the effects being rescued by the TPEN pretreatment (Figure 3.12, 3.14, 4.9 and 4.14).

It is generally believed that MPP^+ impacts mitochondria by direct inhibition of mitochondrial ETC complexes (Cleeter et al., 1992, Nakamura et al., 2000, Smeyne and Jackson-Lewis, 2005). However, the data presented in this study suggested that the effect of MPP^+ might be rather indirect, being mediated by the Zn^{2+} inhibition of mitochondrial complexes. Previous studies have shown that Zn^{2+} is capable of inhibiting complex I and III (Sensi et al., 2009, Liu et al., 2021, Sharpley and Hirst, 2006, LORUSSO et al., 1991, Link and von Jagow, 1995, Dineley et al., 2003). Employing specific suppressors of mitochondrial complexes that prevent mtROS generation without altering forward electron transport (Wong et al., 2019a, Orr et al., 2015), data demonstrated that S3QEL (complex III suppressor) was capable of rescuing MPP^+ induced mtROS production (Figure 4.18 A-B) and mitochondrial fragmentation (Figures 4.19). These results are in line with the previous studies conducted on isolated mitochondria, where the authors of the study found that Zn^{2+} inhibits complex III more effectively than other sites in mitochondrial ETC including complex I (Kleiner, 1974, Link and von Jagow, 1995, LORUSSO et al., 1991). The S1/S3QEL compounds also prevented MPP^+-induced SH-SY5Y cell death (Figure 4.18 C-D). Impairments in mitochondrial complex I and III have been linked to a number of

neurodegenerative conditions (Cerri and Valente, 2020, Zorov et al., 2014, Liu et al., 2021).

Interestingly, Mito-TEMPO, a quencher of mtROS, was able to fully rescue MPP^+ induced mitochondrial dysfunction and fragmentation (Figure 4.16 and 4.17). Although MPP^+ stimulates ROS production by activating NOX2, NOX2 generated ROS appear to be not enough to cause mitochondrial damage. It appears that TRPM2 generated calcium signals need to mobilize lysosomal Zn^{2+} to mitochondria in order to trigger loss of ΔΨm (by inhibiting Complexes I and III), and subsequent mtROS production and mitochondrial fission. It is likely that mtROS would join the pool of ROS to further increase TRPM2 activation, NOX2 activation, and lysosomal dysfunction, thereby setting a vicious cycle of events that ultimately increase the rate of cell death.

To conclude, the findings presented in this chapter suggest that ROS, Ca^{2+} and Zn^{2+} serve as feedforward positive regulatory signals that promote cytotoxic communication between the plasma membrane, lysosomes, and mitochondria. This results in the dysfunction of lysosomes and mitochondria that ultimately causes neuronal cell death. Therefore, in order to develop safe drugs, a deeper understanding of the complexity of these pathways is required.

4.3.6 Experimental limitations

This study investigated the upstream (ROS and Ca^{2+}) and downstream (mitochondrial fission and cell death) effects of MPP^+ treatment by measuring events at a single time point. One limitation of single time point measurements is that it is possible to miss some of the events. A time-course study of these events will provide a dynamic picture of the events. The experiments in this chapter might have some limitations associated with used of non-specific fluorescents probes for cellular organelles and ions. The limitations of Ca^{2+} probes and chelators have already been discussed in the previous chapter.

LysoBrite™ Deep Red is a fluorescent probe that accumulates in acidic organelles and is commonly used to stain lysosomes. However, cells have other acidic organelles, such as endosomes that could also be stained with this probe. This could affect quantification data.

MitoTracker™ Red is a positively charged ΔΨm-sensitive fluorescent dye. It is rapidly taken up into the negatively charged mitochondria. However, during oxidative stress, mitochondrial network loses its potential (more depolarised). This is expected to limit the uptake of the dye and underestimate the effects that treatments have on mitochondrial dynamics (Poot and Pierce, 1999, Buckman et al., 2001). One potential solution is to mark the mitochondria by expressing mitochondria-targeted fluorescent proteins, such as Mito-GFP and Mito-Cherry.

Another point to be considered is the extent to which FluoZin3-AM can accumulate in mitochondria. At present there are no systematic studies demonstrating entry of FluoZin3-AM into organelles, but the finding that lysosomes which contain significant amounts of Zn^{2+} can be labelled with FluoZin-3 suggests that the AM- ester of FluoZin-3 likely accumulates in these organelles before it is hydrolysed by the cytoplasmic esterases.

Chapter 5
TRPM2 pore-blocking antibodies inhibit death signaling in a cellular model of Parkinson's disease

5.1 Introduction

Ion channels are complex transmembrane proteins that regulate the electrical signals required for maintaining cellular homeostasis and tissue functions, including cardiovascular and nervous systems (Kleopa, 2011). Ion channels are the target of approximately 18% of small-molecule drugs that are reported in ChEMBL database (Santos et al., 2017, Hutchings et al., 2019). Numerous therapies target ion channels for diseases ranging from cardiovascular diseases, type II diabetes to neurological conditions (Krafte, 2016). Due to paucity of knowledge on structure and function, the majority of drugs targeted to ion channels are small molecules and peptide modulators which have been identified from studies of naturally occurring substances, for instance, plant and animal toxins (Hutchings et al., 2019). For over past two decades, there has been a growing interest in therapeutic monoclonal antibodies (mAbs) (Reichert et al., 2005).

Currently, it is acknowledged that antibodies offer several potential therapeutic advantages (Hutchings et al., 2019), since they have greater approval success rate than small molecule drugs (Reichert et al., 2005). This is because unlike small molecule drugs, which may have more off-target interactions, antibodies offer the benefit of higher target specificity. Furthermore, there is less variability in patient pharmacokinetics in antibody-based therapies and longer duration of action, resulting in lower dose requirements (Hutchings et al., 2019).

To date, most of the antibody-based therapies for PD are focused on targeting α-synuclein since aggregation of α-synuclein in the brain is a primary hallmark of the disease. In animal models of PD, immunotherapy targeting α-synuclein has

yielded promising outcomes (Nimmo et al., 2020). However, recent two phase 2 clinical trials of anti- α-synuclein monoclonal antibodies showed no patient benefit (Whone, 2022). Accordingly, it is important to target other PD associated protein targets.

One example is the TRPM2 channel. The role of TRPM2 channel in PD and other neurodegenerative disorders has recently received a lot of interest because it is highly expressed in brain (Faouzi and Penner, 2014, Sun et al., 2018, Chung et al., 2011, Lee et al., 2013). Based on the findings in pervious chapters and on what has been earlier reported in other studies, the TRPM2 channel plays a role in dopaminergic neuronal death and hence in the development of PD (Hermosura and Garruto, 2007, Xie et al., 2010b, Vaidya and Sharma, 2020, Belrose and Jackson, 2018). Various small molecules have been shown to block TRPM2 channel activity. These include flufenamic acid (FFA), 2-(3-methylphenyl) aminobenzoic acid (3-MFA), anthranilic acid (ACA), and 2-aminoethoxydiphenyl borate (2-APB), N-(5,6-Dihydro-6-oxo-2-phenanthridinyl)-2-acetamide hydrochloride (PJ34), econazole and clotrimazole (Luo et al., 2018, Togashi et al., 2008, Kraft et al., 2006, Hill et al., 2004b, Hill et al., 2004a, Fonfria et al., 2004). The majority of TRPM2 channel inhibitors, however, are non-specific and can affect other channels and proteins (Luo et al., 2018). Because of the lack of specific and efficient TRPM2 inhibitors, it is challenging to study and validate TRPM2 channel as a therapeutic target (Luo et al., 2018).

Generating an effective antibody targeting the function of an ion channel is quite challenging since several important hurdles might be involved, such as the short binding site and the limited number of potential epitopes in the target region (Hutchings et al., 2019). Furthermore, ion channels within the same family generally have significant sequence homology, especially in the pore region, where most channel blockers act (Hutchings et al., 2019). As a result, the available epitopes either lack the immunogenicity necessary to generate strong antibody responses in mammalian hosts or produce antibodies with cross-reactivity. In some cases even when the extracellular regions are large enough,

protein synthesis cannot reliably produce high-quality products as a result of poor expression or difficulty in purification (Hutchings et al., 2019).

The mechanisms of antibody action involve direct blockage of the ion permeation route, modulation of the gating, and internalization and degradation of the channel following surface aggregation clustering (Sun and Li, 2013). Ion channels have several functionally important regions that could be targeted by antibodies for channel modulation. One such region is the outer mouth of the channel pore because binding of an antibody to this region potentially blocks ion conductance through the channel (Sun and Li, 2013). In the case of channels with six transmembrane domains, antibodies were generated against the short extracellular loop N-terminal to the pore-forming region, known as E3, which exhibits substantial sequences variation (Sun and Li, 2013). E3 was initially investigated in voltage-gated potassium channels. Anti-peptide antibodies targeted to E3 segments of two channel proteins, K_v1.2 and K_v3.1, suppressed more than 70% of neuronal cell currents (Zhou et al., 1998, Sun and Li, 2013). Later, E3 targeting has been expanded to include other voltage-gated cation channels, such as Nav 1.5 and TRPC5, which also yielded considerable inhibition of whole cell currents (50-60%) in transfected cells (Xu et al., 2005, Sun and Li, 2013). Antibody could target other channel regions that are not directly close to the pore-forming domains, such as the S4 voltage sensor region of sodium channels expressed in dorsal root ganglion (DRG) neurons (Schwartz et al., 1990). Although antibodies are often targeted to the extracellular domains of voltage sensing and pore domains, as mentioned above, they may not be able to distinguish between the closely related subtypes due to considerable degree of structural conservation (Colecraft and Trimmer, 2022). Although many voltage-gated ion channels have relatively small accessible extracellular pore-forming parts, they have a significant portion of their structure on the intracellular side, providing an opportunity to generate antibodies that target the intracellular sites of ion channels. However, these regions need to be involved in channel regulation (Colecraft and Trimmer, 2022).

Currently, there is no antibody-based therapeutic available on the market that targets the function of an ion channel (Sun and Li, 2013, Colecraft and Trimmer, 2022). However, function-blocking antibodies have been successfully used in a variety of experimental contexts to establish the specificity of an effect.

This chapter aims to develop an antibody against the extracellular region of the TRPM2 channel and examine its ability to recognize the channel using immunological methods, and to inhibit the channel function by measuring Ca^{2+} influx. A further aim of the study was to test the ability of the antibody to prevent MPP^{+} induced mitochondrial and lysosomal damage, and cell death using SH-SY5Y cells.

5.2 Results

5.2.1 Antibody production

To generate an antibody capable of blocking the TRPM2 channel activity, an extracellular epitope (ECE) of the human TRPM2 channel was chosen as an antigen. The ECE was identified by the bioinformatic analysis of the channel, involving sequence alignment with other related members and the 3D structure of the channel. Potential glycosylation sites were excluded. The details of the sequence and its location in the channel was not explained in this thesis for confidentiality reasons due to its potential for intellectual property rights (the commercialisation unit of Leeds University is currently assessing our application for IPR). The ECE chosen has low sequence similarity to other members of the channel family.

Two approaches were used to generate antibodies against the ECE. First is the traditional approach, where the synthetic ECE peptide, conjugated to the keyhole limpet hemocyanin protein was used to raise antibodies (named anti-TRPM2-

ECE) in the rabbit (outsourced). The second approach, adopted from a paper published by Ottonolle and colleagues (Canali et al., 2014), involved grafting a tandem construct of ECE sequence into the His6-tagged *Pyrococcus furiosus* thioredoxin (His6-pTRX) scaffold protein. In the tandem construct, three ECE peptide sequences were separated by the flexible GSG (glycine-serine-glycine) sequences. The resulting ECE concatemer, ECE3x, was back translated into DNA sequence. The custom synthesized ECE3x DNA sequence was cloned into surface exposed loop of His6-pTRX and the resulting construct, His6-pTRX-ECE3x, was expressed in *E.coli* (Figure 5.1). This part of the work has been carried out in our lab by my supervisor, Professor Asipu Sivaprasadarao, and Anthony Chan. The expressed protein was purified by Ni^{2+}-affinity chromatography and used as an antigen to generate antibodies in rabbit (outsourced).

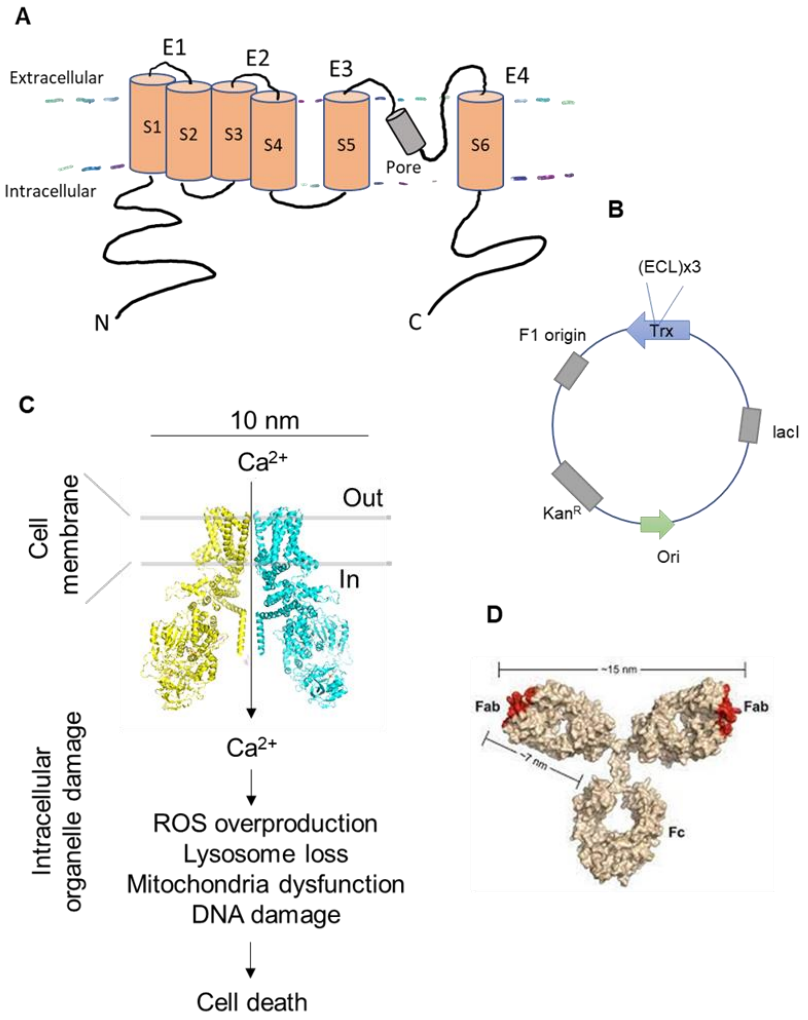

Figure 5.1 Antibody generated against the extracellular epitope (ECE) of TRPM2 channel.

(A) Membrane topology of one subunit of TRPM2, depicting the S1-S6 transmembrane segments and the extracellular loops. **(B)** Schematic of the plasmid construct used to express the tandem (triple) repeat of an ECE inserted into the thioredoxin (Trx) scaffold. The Trx-ECE3x was expressed in *E.coli* and the purified protein was used to raise antibodies in rabbit. **(C)** Structure of human TRPM2 channel showing the Ca^{2+} entry pathway. Only two diagonally placed subunits are shown for clarity (PDB: 6PUR, Pymol was used to generate this figure). The diameter of the channel is 10 nm. Ca^{2+} entry leads to intracellular organelle dysfunction as explained in previous chapters. **(D)** 3D structure of IgG which has a diameter of 15 nm (Klein and Bjorkman, 2010), is shown for size comparison with TRPM2. Precisely how the antibody binds the channel is unclear but is expected to block the entrance of the pore.

5.2.2 Anti-ECE3x antibody purification

ECE3x-targeted antibody was purified from the crude serum by using AminoLink® Coupling Resin (from Thermo Fisher Scientific Lot # 20381), which enables efficient covalent immobilization of proteins to a beaded agarose, making it an effective method for affinity purification of antibodies and antigens (Thermo fisher Scientific, user guide). The His6-pTRX-ECE3x fusion antigen was coupled to AminoLink® Coupling Resin using cyanoborohydride solution (NaCNBH3) as for the manufacturer's instructions. The purification procedure involved two chromatography steps. First, His6-pTrx scaffold protein was immobilized on a Talon (metal-affinity) resin and the crude antiserum was run through this resin to remove any potential antibodies against this scaffold protein. Second, the unbound flow-through fractions were collected and run on a resin coupled to His6-pTRX-ECE3x fusion antigen. After that, the bound anti-ECE3x antibody was released by applying elution buffer (0.1 M glycine-HCl, pH 2.5). The eluted fractions were collected and the absorbance at 280 nm was recorded for each fraction. The fractions with peak absorbance were pooled and dialyzed against 50 mM Tris-HCl, pH 7.5 buffer at 4 ºC. Finally, an equal volume of glycerol was added, and the sample was aliquoted and stored at -20 ºC.

5.2.3 Immunochemical and functional characterisation of anti-TRPM2 antibodies

The purified anti-TRPM2-ECE3x and anti-TRPM2-ECE antibodies were first subjected to immunochemical (Western blotting and immunocytochemistry) and functional testing. For this, two cell lines were used, HEK-293 cells stably expressing the recombinant human TRPM2 channels under the control of a tetracycline promoter (HEK-TRPM2^{tet}) and the SH-SY5Y neuroblastoma cell line, which expresses TRPM2 channels natively (Chen et al., 2013, Sun et al., 2018). The HEK-TRPM2^{tet} cells were treated with tetracycline (1 µg/ml) for 48 hours to

induce TRPM2 expression prior to immunochemical analysis, control cells being left untreated.

The specificity of anti-TRPM2-ECE3x antibodies for TRPM2 was examined by Western blotting of the lysates of HEK-TRPM2^{tet} cells (tetracycline induced and non-induced) and SH-SY5Y cells. The results of immunoblotting revealed that ECE3x antibody can recognize the ~170 KDa corresponding to the theoretical size of TRPM2 protein in the extracts of tetracycline-induced HEK-TRPM2^{+tet} cells, whereas the corresponding band was absent in non-induced cells (Figure 5.2 A). However, there are significant number of nonspecific bands (with the exception of a ~80 KDa band) that are common to both induced and non-induced extracts. The ~80 KDa is likely a proteolytic product of TRPM2. As for SH-SY5Y, the anti-TRPM2-ECE3x antibody was able to detect the native TRPM2 protein, but the band is rather faint (Figure 5.3 A). This could be explained by the low expression level of TRPM2 protein in these cells relative to the recombinant HEK-TRPM2^{tet} cells. Like the anti-TRPM2-ECE3x antibody, the anti-ECE antibody was also able to detect the ~170 KDa TRPM2 band in the induced cells but not in uninduced HEK-TRPM2^{tet} cells (data not shown, work performed by Jinmiao Qu in Professor Sivaprasadarao's lab).

The ability of the two anti-TRPM2 antibodies to recognize surface expressed TRPM2 was also examined using immunocytochemical staining. HEK-TRPM2^{tet} (both tetracycline induced and non-induced cells) and SH-SY5Y cells were allowed to bind the anti-TRPM2-ECE3x antibodies, and then stained with the Cy3 conjugated donkey anti-Rabbit IgG secondary antibody. Fluorescent images show intense staining of tetracycline-induced HEK-TRPM2^{+tet} cells compared to non-induced cells (Figure 5.2 B). Anti-TRPM2-ECE3x antibody was also able to detect TRPM2 in SH-SY5Y cells, but the TRPM2 staining was weak when compared with HEK-TRPM2^{+tet} cells; this is consistent with the reported low-level expression of the channel in SH-SY5Y cells (An et al., 2019). However, pre-treatment of cells with MPP^+ led to a marked increase in TRPM2 expression (Figure 5.3 B). These latter data are in agreement with the previous report that

MPP^+ stimulates surface expression of the channel in SH-SY5Y cells (Sun et al., 2018, Yildizhan et al., 2022).

The next question to address was whether the binding of anti-TRPM2-ECE3x antibody to TRPM2 can prevent extracellular Ca^{2+} entry into the cells. For this, as reported previously (Price and Lummis, 2005), cells were preloaded with the cell permeable Fura-2-AM Ca^{2+} reporter, and changes in intracellular Ca^{2+} in response to H_2O_2 stimulus was recorded. To determine the effect of the anti-TRPM2-ECE3x antibody, tetracycline-induced HEK-$TRPM2^{tet}$ cells, as well as SH-SY5Y cells, were treated with PBS (control) or the purified anti-ECE3x antibody for 2 hours at 37 ºC and then changes in intracellular Ca^{2+} were recorded. The results show that addition of H_2O_2 caused a marked increase in Ca^{2+} entry in tetracycline treated HEK-$TRPM2^{tet}$ cells, but not in uninduced cells (Figure 5.2 C-D), as well as in SH-SY5Y cells (Figure 5.3 C-D). The anti-TRPM2-ECE3x antibody was able to inhibit the Ca^{2+} rise as effectively as the 2-APB, a chemical inhibitor of TRPM2, in both cell lines.

The effect of anti-ECE antibody on MPP^+-induced changes in intracellular Ca^{2+} in SH-SY5Y cells was investigated using fluorescent microscopy instead of Flexstation because, unlike H_2O_2, the effect of MPP^+ on Ca^{2+} rise is slow and less robust. SH-SY5Y cells were exposed to medium only (CTRL), or medium containing MPP^+ (1 mM) for 24 hours to stimulate TRPM2 expression. Cells were pre-treated with either anti-TRPM2-ECE antibody or preimmune serum for 2 hours, before staining for Ca^{2+} using Fluo-4-AM. Figure 5.4 shows that compared to the control, MPP^+ treatment caused a significant increase in Fluo-4 fluorescence. No such increase was observed in cells pre-treated with the anti-TRPM2-ECE antibody, whereas preimmune serum failed to prevent the MPP^+-induced rise in Ca^{2+} (Figure 5.4). These results confirm that the anti-ECE antibody can prevent MPP^+-induced, TRPM2 mediated Ca^{2+} influx in SH-SY5Y cells.

Together, these data demonstrate that both the anti-TRPM2 antibodies may serve as useful tools to determine the cell biological roles of the TRPM2 channel in native cells.

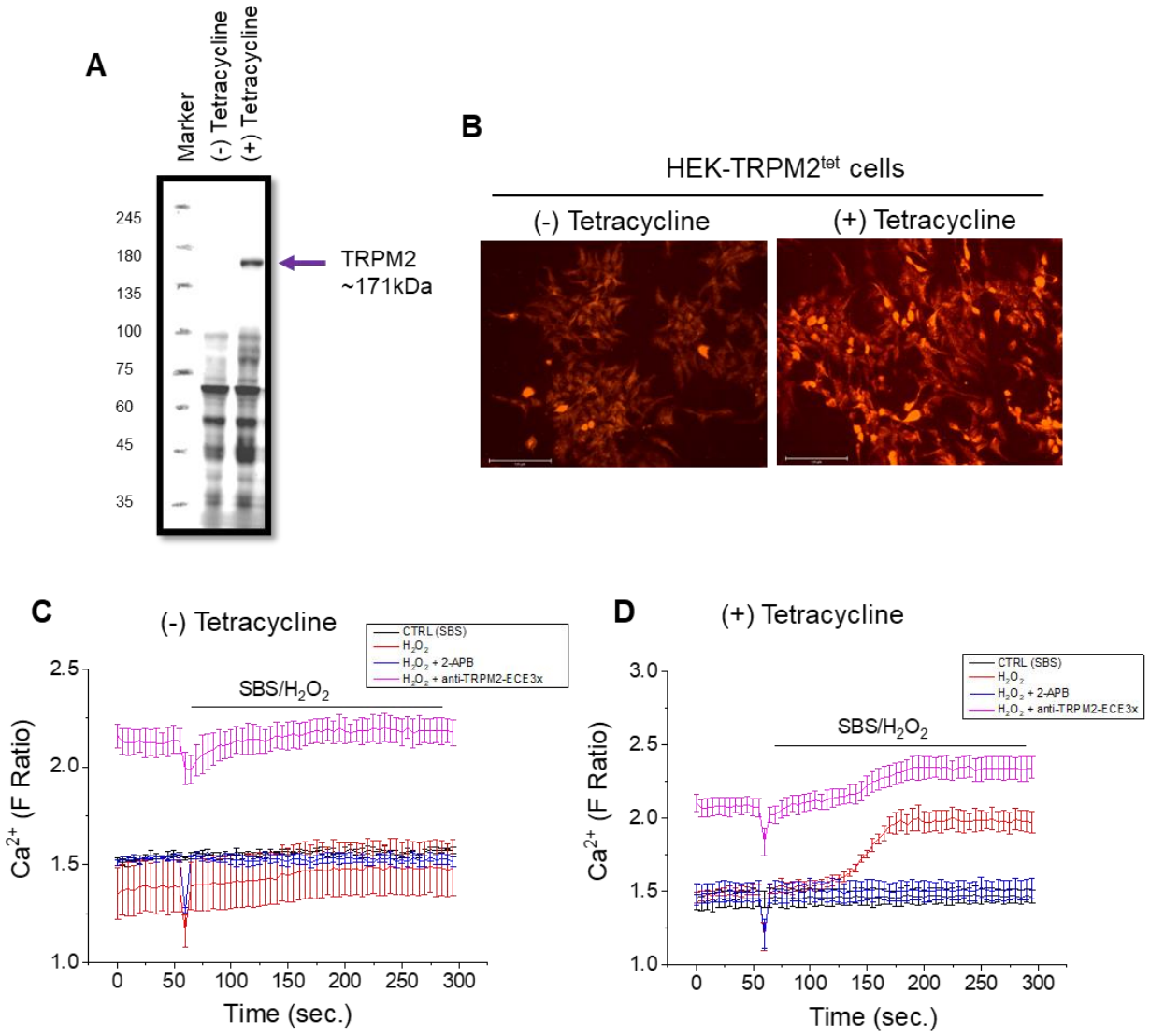

Figure 5.2 Immunochemical and functional characterization of the anti-TRPM2 -ECE3x antibody in HEK-TRPM2^{tet} cells.

(A) Immunoblot showing the expression of TRPM2 (~170 KDa band) using the anti-TRPM2-ECE3x antibody in tetracycline-induced ($^{+}$tet) and non-induced ($^{-}$tet) HEK-TRPM2^{tet} cells. **(B)** Fluorescent images show surface immunostaining of TRPM2 in the induced, but not uninduced HEK-TRPM2^{tet} cells. These cells were fixed in 4% PFA and incubated with ECE3x antibody (1:200 dilution) for 2 hours, then stained with Cy3 conjugated donkey anti-Rabbit IgG (1:500 dilution) for 1 hour. Scale bar: 125 µm. **(C-D)** Functional analysis of TRPM2 expression by measurement of Ca^{2+} influx in non-induced **(C)** and in tetracycline-induced **(D)** HEK-TRPM2^{tet} cells. Cells were pre-treated with the anti-TRPM2-ECE3x antibody (~35 µg/ml, 2 hours) or a TRPM2 inhibitor (150 µM 2-APB,10 min).

Then, cells were washed with SBS. After loading the cells with the Ca^{2+} indicator, Fura-2-AM, they were stimulated with 3 mM H_2O_2 at the 60 second time point. Changes in cytosolic Ca^{2+} were measured using Flexstation III. Results show the F ratio (340 nm/ 380 nm) representing the Ca^{2+} levels at different time points. Inset shows treatments used on the cells; data points with the error bars (SEM) are colored according to the inset.

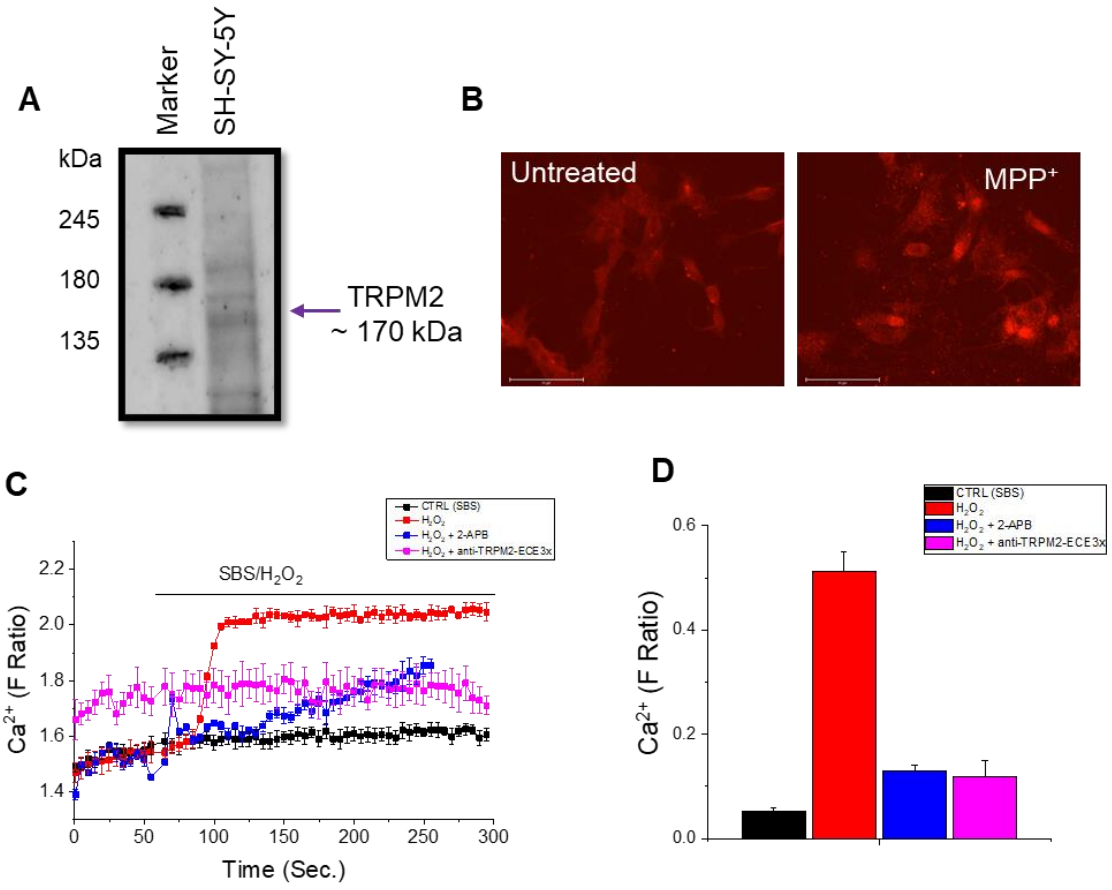

Figure 5.3 Immunochemical and functional characterization of the anti-TREM2-ECE3x antibody using SH-SY5Y cells.

(A-B) Immunodetection of TRPM2 using anti-ECE3x antibody. **(A)** Western blot shows ~ 170 kDa band most likely corresponding to TRPM2 protein. **(B)** Fluorescent images of SH-SY5Y cells show immunostaining of TRPM2 using ECE3x antibody in cells either untreated or treated with 1 mM MPP^+ for 24 hours. Cells were fixed in 4% PFA and incubated with the anti-TRPM2-ECE4x antibody (1:200 dilution) for 2 hours, then stained with Cy3 conjugated donkey anti-Rabbit IgG (1:500 dilution) for 1 hour. Scale bar: 75 µm. **(C)** Functional analysis of TRPM2 expression by measurement of Ca^{2+} influx in SH-SY5Y cells which were first pre-treated with ECE3x antibody (35 µg/ml, 2 hours) or TRPM2 inhibitor (150 µM 2-APB, 10 min). FlexStation recordings and analysis were performed as for Figure 5.2. **(D)** Mean ± SEM of F ratio from (C).

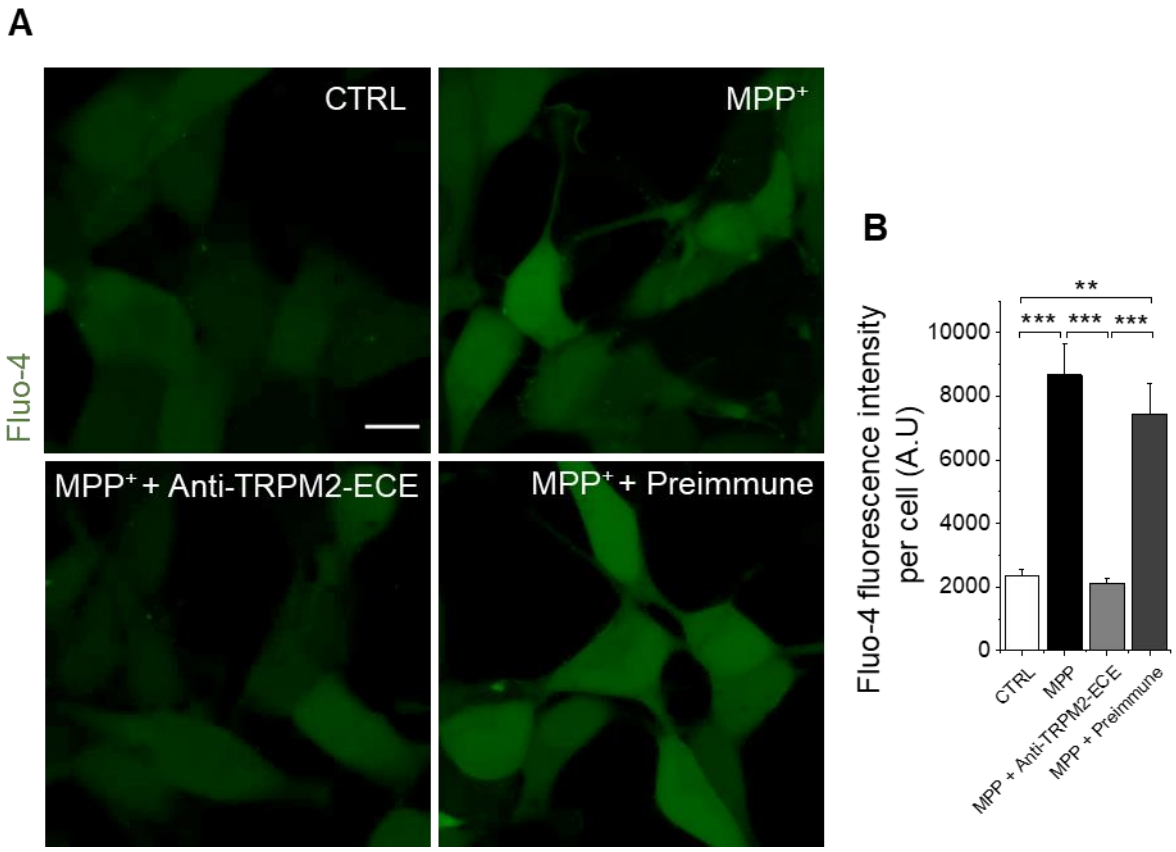

Figure 5.4 Functional characterization of the anti-TRPM2-ECE antibody.

(A) Fluorescent images of SH-SY5Y cells stained for cytosolic Ca^{2+} using Fluo-4-AM; cells were either untreated (CTRL) or treated with 1 mM MPP^+ for 24 hours; in the bottom two panels, MPP^+ treated cells were pre-treated with the anti-TRPM2-ECE antibody or preimmune serum. Scale bar: 10 µM. **(B)** Mean ± SEM of data from (A) expressed as mean Fluo-4 fluorescence per cell from two independent experiments; n = 2; N = 376 cells. ** indicates $p < 0.01$, *** indicates $p < 0.001$; one-way ANOVA with post-hoc Tukey test.

5.2.4 The anti-TRPM2-ECE antibody attenuates cellular and mitochondrial ROS production

Data presented in Chapter 3 of this thesis have shown that MPP^+ induces a rise in cytosolic and mitochondrial ROS levels in SH-SY5Y cells. The studies have also suggested that activation of TRPM2 channels underlies MPP^+-induced rise in intracellular ROS. Thus, the ability of anti-TRPM2-ECE antibody to prevent MPP^+-induced rise in total intracellular and mitochondrial ROS generation was next investigated.

To test the effect of the anti-TRPM2-ECE antibody on cytosolic and mitochondrial ROS levels in SH-SY5Y cells, cells were first incubated with the anti-TRPM2-ECE antibody for 2 hours. Cells were then treated with 1 mM MPP^+ at 37 °C for 24 hours, before staining for the total and mitochondrial ROS. As has been shown in Chapter 3, MPP^+ caused a significant increase in the production of total ROS (DHE signal) and mitochondrial ROS (MitoSOX signal) in control cells. In cells pre-treated with the anti-TRPM2-ECE antibody, however, the fluorescence signals were significantly reduced (Figures 5.5 and 5.6). Interestingly, the inhibitory effect of anti-TRPM2-ECE antibodies on total ROS ($p < 0.01$) appears to be greater than that on mitochondrial ROS generation ($p < 0.05$).

To conclude, these findings suggest that targeting TRPM2 channels using the specific anti-TRPM2-ECE antibody attenuates cytosolic and mitochondrial ROS production (see Chapter 3).

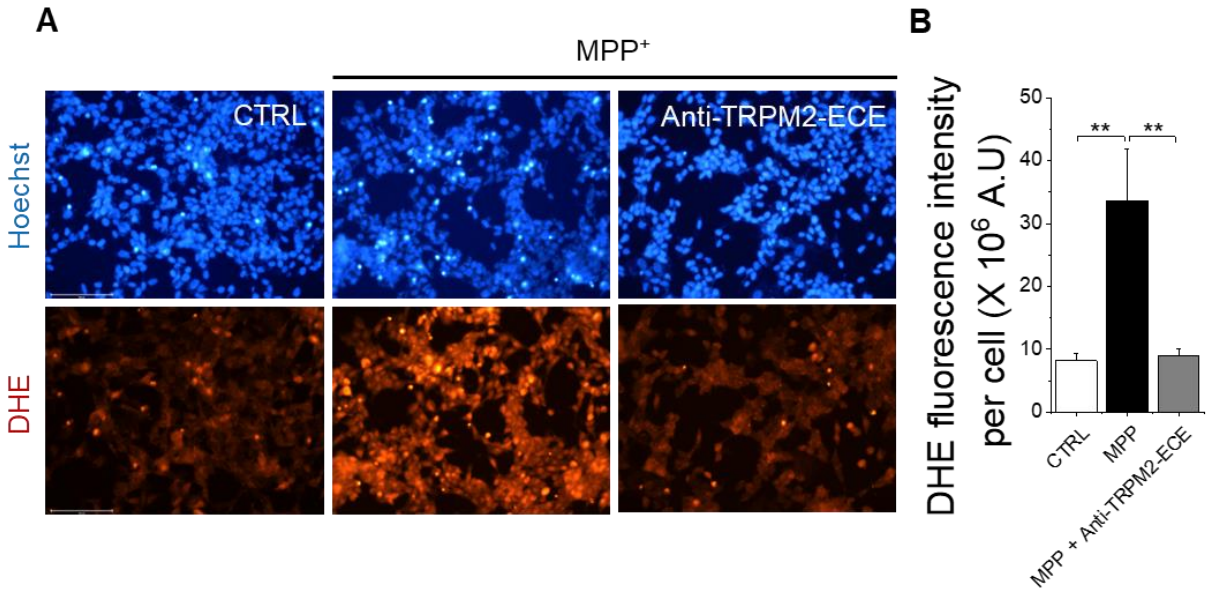

Figure 5.5 The anti-TRPM2-ECE antibody attenuates cytosolic ROS level in MPP^+-treated SH-SY5Y cells.

SH-SY5Y cells were untreated (CTRL) or pretreated for 2 hours with the anti-TRPM2-ECE antibody. The cells were then exposed to the 1 mM MPP^+ for 24 hours at 37 °C. CTRL represents cells not exposed to MPP^+. **(A)** Fluorescent images of SH-SY5Y cells stained with Hoechst 33342 for nuclei and with dihydroethidium (DHE), for total ROS. Scale bar: 100 µM. **(B)** Mean ± SEM of data from (A) expressed as mean of DHE signal per cell from four independent experiments n = 4; N = 38,147 cells. ** indicates $p < 0.01$; one-way ANOVA with post-hoc Tukey test.

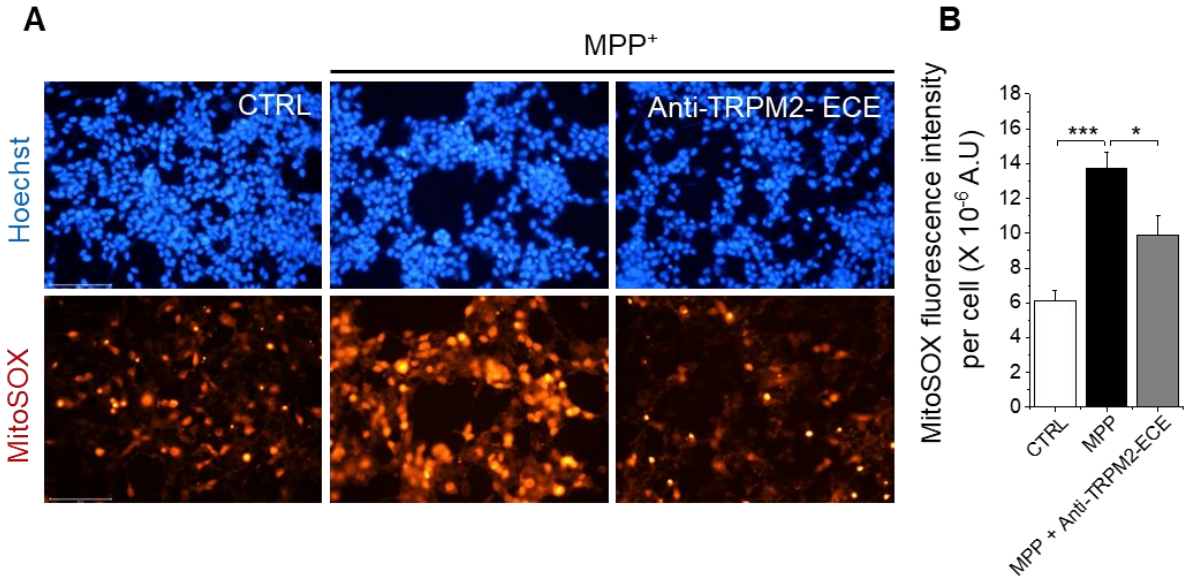

Figure 5.6 The anti-TRPM2-ECE antibody attenuates MPP^+-induced mitochondrial ROS production in SH-SY5Y cells.

SH-SY5Y cells were untreated (CTRL) or pretreated for 2 hours with the anti-TRPM2-ECE antibody. The cells were then exposed to the 1 mM MPP^+ for 24 hours at 37 °C. CTRL represents cells not exposed to MPP^+. **(A)** Fluorescent images of SH-SY5Y cells stained with Hoechst 33342 for nuclei and with MitoSOX for mitochondrial ROS. Scale bar: 100 µM. **(B)** Mean ± SEM of data from (A) expressed as mean of MitoSOX per cell from four independent experiments n = 4; N = 51,478 cells. * indicates $p < 0.05$, *** indicates $p < 0.001$; one-way ANOVA with post-hoc Tukey test.

5.2.5 The anti-TRPM2-ECE antibody prevents MPP^+-induced mitochondrial fragmentation

The role of TRPM2 in mitochondrial fission during oxidative stress has been demonstrated in pancreatic β-cells and endothelial cells (Li et al., 2017a, Abuarab et al., 2017, Wang et al., 2012). Results presented in Chapter 4, have shown that pharmacological inhibition and silencing of TRPM2 channel expression with siRNA can rescue SH-SY5Y cells from MPP^+-induced mitochondrial fission. Accordingly, the ability of the anti-TRPM2-ECE antibody to prevent MPP^+-induced mitochondrial fission was examined. For this, cells were treated with the medium (control), MPP^+ alone, and MPP^+ with either anti-TRPM2-ECE antibody or preimmune serum and stained with MitoTracker™ Red. Results show that in the control cells, mitochondria appear mostly filamentous with long branched network, whereas with in MPP^+-treated cells, mitochondria lose their branched network and appear fragmented with the majority of mitochondria being spherical (Figure 5.7 A). The anti-TRPM2-ECE antibody, but not the preimmune serum, was able to fully prevent the effect of MPP^+ on mitochondrial network in SH-SY5Y cells (Figure 5.7).

Various parameters were analysed to quantify the mitochondria morphology from 2D and 3D data sets of images acquired from confocal microscope (Figure 5.7 B-L). For each single mitochondrion of SH-SY5Y cell, the morphological characteristics were analysed. By 2D analysis of images, parameters such as the length (represented as aspect ratio) and the mitochondrial connectively or branching (represented by form factor) were calculated. The results showed that the anti-TRPM2-ECE antibody, but not the preimmune serum, rescued the MPP^+ induced decrease in the aspect ratio and the form factor (Figure 5.7 B-C). Analysis of 3D data demonstrated the ability of the anti-TRPM2-ECE antibody, but not the preimmune serum, to rescue the effect of MPP^+ on other mitochondrial parameters, including the sphericity, volume, surface area, branch length, and the number of mitochondrial branches and branch junctions (Figure 5.7 D-L). These data imply that anti-TRPM2-ECE antibody can overcome the damaging effect of MPP^+ on mitochondrial structure.

These findings not only provide further support for the role of TRPM2 mediated Ca^{2+} entry in mitochondrial dynamics, but more importantly, they demonstrate the ability of anti-TRPM2-ECE antibody to preserve the mitochondrial integrity in the face of MPP^{+} insult.

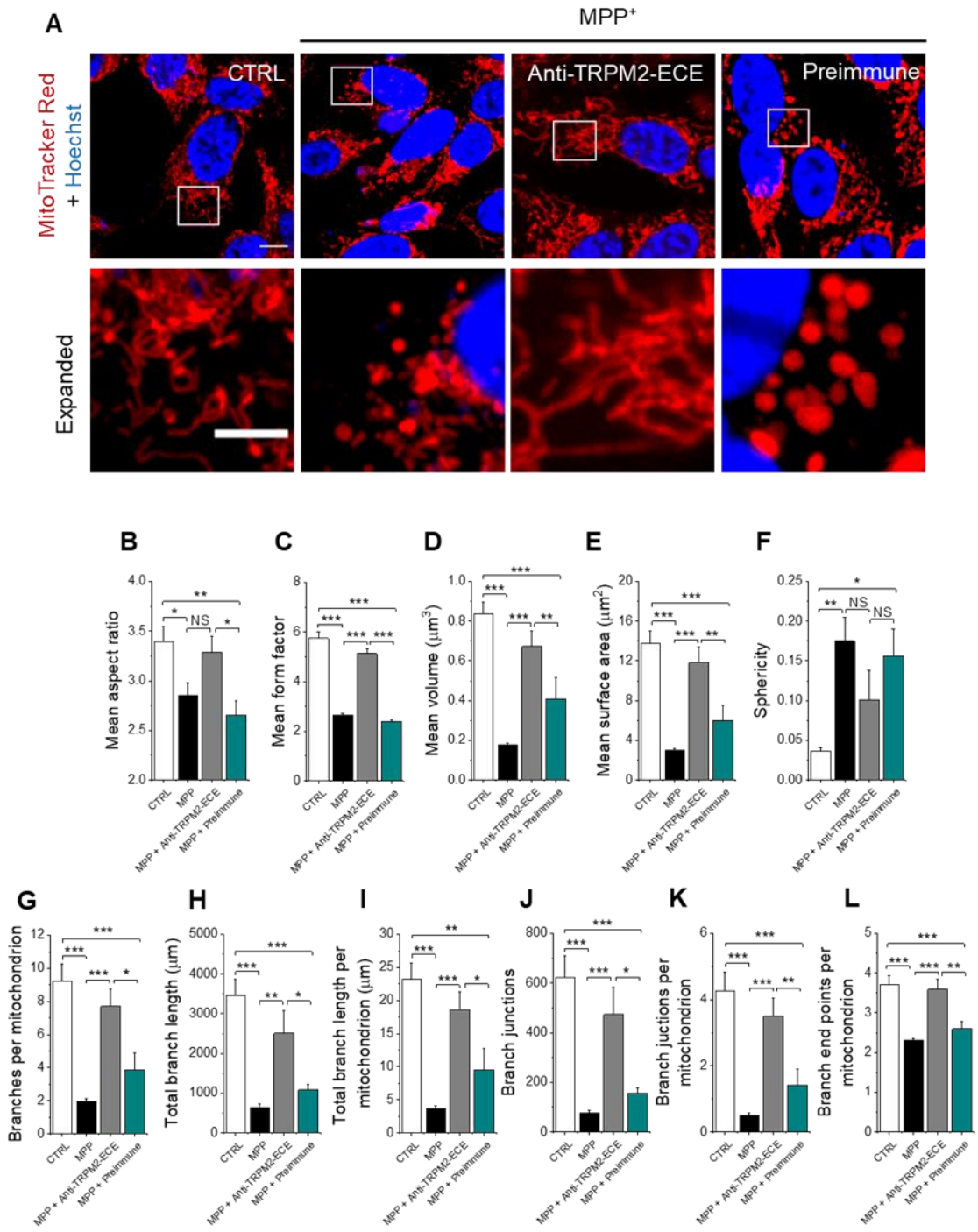

Figure 5.7 The anti-TRPM2-ECE antibody rescues MPP⁺ induced mitochondrial fragmentation in SH-SY5Y cells.

SH-SY5Y cells were untreated (CTRL) or pretreated for 2 hours with either anti-TRPM2-ECE antibody or preimmune serum. The cells were then exposed to the 1 mM MPP^+ for 24 hours at 37 °C. CTRL represents cells not exposed to MPP^+. **(A)** Fluorescent images of SH-SY5Y cells stained for mitochondria with MitoTracker™ Red. Scale bars: 10 µM, and 5 µM for expanded images. **(B-L)**

Quantification of changes in mitochondrial morphology through estimation of mean aspect ratio **(B)**, mean form factor **(C)**, mean volume **(D)**, mean surface area **(E)**, sphericity **(F)**, branches per mitochondrion **(G)**, total branch length **(H)**, total branch length per mitochondrion **(I)**, branch junctions **(J)**, and branch junctions per mitochondrion **(K)**, branch end points per mitochondrion **(L)**. Data represent mean ± SEM of mitochondrial parameters from five independent experiments n = 5; N = 281 cells for 2D analysis, and N = 394 cells for 3D analysis. * indicates $p < 0.05$, ** indicates $p < 0.01$, *** indicates $p < 0.001$; NS, not significant; one-way ANOVA with post-hoc Tukey test.

5.2.6 The anti-TRPM2-ECE antibody restores lysosomal depletion that occurs in MPP^+-treated SH-SY5Y cells

Studies have shown that MPP^+ treatment leads to lysosomal depletion (Chapter 4) (Dehay et al., 2010). Therefore, the ability of anti-TRPM2-ECE antibody to rescue MPP^+ induced lysosomal decline was next examined.

For this, SH-SY5Y cells were exposed to medium alone (control) or to MPP^+ for 24 hours at 37 °C in the presence or absence of either anti-TRPM2-ECE antibody or preimmune serum. After treatment, cells were stained for lysosomes using LysoBrite Red, and the images acquired using the confocal microscope. As noted in Chapter 4, MPP^+ treatment caused a significant decrease in the number of lysosomes (Figure 5.8). The anti-TRPM2-ECE antibody, but not the preimmune serum, rescued the MPP^+ induced loss of lysosomes. These results indicate that anti-TRPM2-ECE antibody is capable of preventing MPP^+-induced lysosomal depletion.

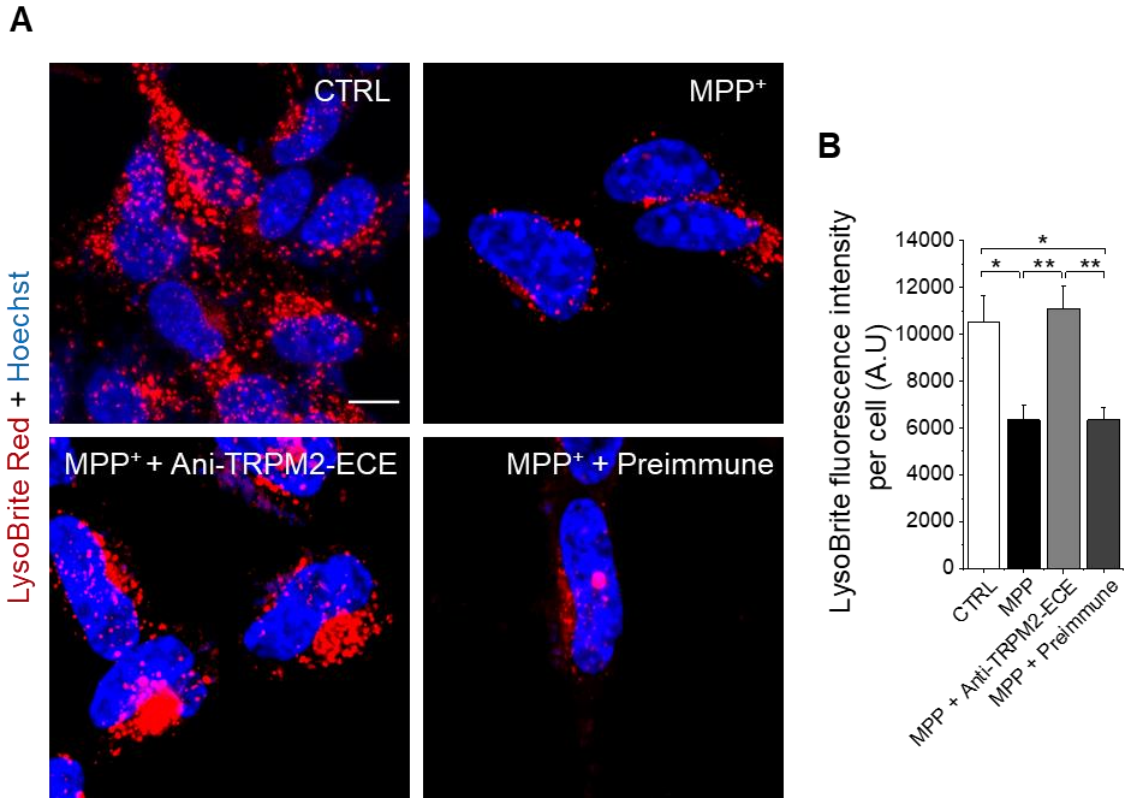

Figure 5.8 The anti-TRPM2-ECE antibody rescues MPP$^+$-induced lysosomal loss in SH-SY5Y cells.

SH-SY5Y cells were untreated (CTRL) or pretreated for 2 hours with either anti-TRPM2-ECE antibody or preimmune serum. The cells were then exposed to the 1 mM MPP$^+$ for 24 hours at 37 °C. CTRL represents cells not exposed to MPP$^+$. **(A)** Fluorescent images of SH-SY5Y cells stained for lysosomes using LysoBrite Red. Scale bars: 10 µM, and 5 µM for expanded images. **(B)** Mean ± SEM of data from (A) expressed as mean of LysoBrite Red fluorescence per cell from three independent experiments n = 3; N = 400 cells. * indicates $p < 0.05$, ** indicates $p < 0.01$, NS, not significant; one-way ANOVA with post-hoc Tukey test.

5.2.7 The anti-TRPM2-ECE antibody inhibits the MPP^+-induced SH-SY5Y cell death

Data presented in Chapter 3 of this thesis, as well as previous published studies (Sun et al., 2018, Yildizhan et al., 2022) have shown that MPP^+ kills neuronal cells by stimulating TRPM2-mediated Ca^{2+} influx. Following the demonstration that anti-TRPM2-ECE antibody inhibits MPP^+ induced TRPM2 mediated Ca^{2+} influx, excessive ROS production and mitochondrial fragmentation, I examined the ability of the antibody to prevent MPP^+-induced SH-SY5Y cell death. To investigate this, SH-SY5Y cells were pre-treated with the anti-TRPM2-ECE antibody and then exposed to MPP^+ for 24 hours before staining to assess cell death. MPP^+ treatment caused significant death ($p < 0.001$) of SH-SY5Y cells (Figure 5.9), which was remarkably rescued by the anti-TRPM2-ECE antibody ($p < 0.001$) (Figure 5.9 B).

These data demonstrate that the anti-TRPM2-ECE antibody is capable of inhibiting MPP^+-induced SH-SY5Y cells death.

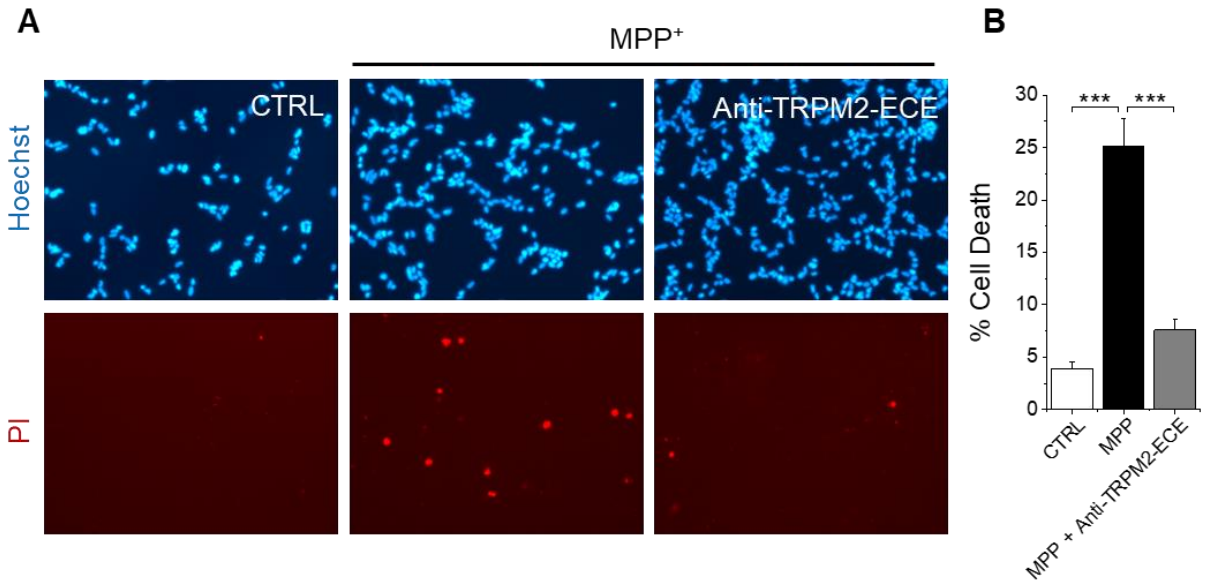

Figure 5.9 The anti-TRPM2-ECE antibody inhibits MPP^+-induced SH-SY5Y cell death.

SH-SY5Y cells were untreated or pretreated for 2 hours with the anti-TRPM2-ECE antibody. The cells were then exposed to the 1 mM MPP^+ for 24 hours at 37 °C. CTRL represents cells not exposed to MPP^+. **(A)** Fluorescent images of SH-SY5Y cells stained for nuclei of all (Hochest 33342) and dead (Propidium iodide, PI) cells. **(B)** Mean ± SEM of percent cell death from five independent experiments n = 5; N = 54,326 cells. *** indicates $p < 0.001$; one-way ANOVA with post-hoc Tukey test.

5.3 Discussion

In this Chapter, I have described the production of novel antibodies against an extracellular loop of TRPM2 channel. The aim was to test whether targeting this loop, predicted to block the pore, would prevent the toxic effect of MPP^+ on SH-SY5Y cells by blocking the extracellular Ca^{2+} entry.

The results demonstrate that anti-TRPM2-ECE antibodies can (i) recognise the channel protein in western blotting and immunostaining, (ii) prevent H_2O_2- and MPP^+-induced TRPM2 mediated Ca^{2+} influx, and (iii) prevent MPP^+ induced ROS production, lysosomal decline, mitochondrial fragmentation, and cell death.

Two different antibodies targeted to an extracellular loop were developed. Anti-TRPM2-ECE was raised against the ECE peptide sequence, whereas the anti-TRPM2-ECE3x was raised against the tandem triple repeat of ECE inserted into the *Pyrococcus* thioredoxin scaffold protein produced in *E.coli* (Canali et al., 2014). Both antibodies were characterized by western blotting and immunocytochemistry using HEK-$TRPM2^{tet}$ cells and SH-SY5Y cells. While the HEK cell data showed clear staining, the signal to noise ratio was high in SH-SY5Y cells, presumably because of low level of channel expression in comparison to the recombinant HEK-$TRPM2^{tet}$ cells.

Most research commonly used function blocking antibodies are produced against extracellular domains of ion channels. These include 6-transmembrane domain containing channels, including voltage gated ion channels and TRP channels (Sun et al., 2012, Xu et al., 2005). Antibodies have also been raised against the E3 peptide sequence of the mouse TRPM2 channel (Sun et al., 2012, Ru et al., 2015, Zhang et al., 2022). The authors reported that the TRPM2E3 antibody (TM2E3) was able to specifically recognise TRPM2 in immunostaining and immunoblotting, and recue of H_2O_2 induced loss of metabolic activity of H5V mouse endothelial cells. The authors have also reported inhibition of Ca^{2+} currents in HEK-293 cells overexpressing TRPM2 channels (Sun et al., 2012).

With H5V cells, however, the inhibition of Ca^{2+} currents is partial. The authors attributed this to the presence of TRPM2-independent Ca^{2+} entry via other ROS-sensitive Ca^{2+}-permeable channels such as TRPC1,TRPC3, TRPC4, TRPM5, TRPC6, TRPM7 (Sun et al., 2012).

The authors have not presented the details of how their antibodies have been raised. Crucial information about the sequence of the peptide used to raise the antibodies is missing in the paper by Sun et al. (2012). Interestingly, the E3 loop of TRPM2 channels is short (9 amino acid long) in TRPM2 channels of most species, including the human, zebrafish, mouse and nematode. We presume that the authors have used the entire sequence of the E3 loop to raise antibodies. Despite being short, the TM2E3 antibody was able to display function blocking effects. There is one amino acid difference between the mouse TRPM2-E3 and human TRPM2-E3. There were no data on whether the TM2E3 antibody can recognize the human TRPM2 in the paper by Sun et al. As our group is planning to protect the intellectual property rights of our antigenic peptide, I am unable to present details of how our antigen differs from TM2E3.

The anti-TRPM2-ECE and ECE3x antibodies detected a band at ~170 KDa, corresponding to the theoretical size of TRPM2 by western blotting; the band was present in HEK-$TRPM2^{tet}$ cell extracts engineered to express the TRPM2 channel, but not in uninduced cells. However, western blotting of SH-SY5Y cell extracts with both the antibodies showed a high level of background bands, making the identification of TRPM2 band difficult. This could be attributed to the low expression level of TRPM2 protein in these cells. Further optimization needs to be done to reduce background staining in western blotting and to improve the signal noise ratio in native cell extracts. However, both antibodies were able to prevent MPP^+ induced Ca^{2+} influx in SH-SY5Y cells (Figures 5.3 and 5.4), as well as the H_2O_2 induced Ca^{2+} entry in tetracycline induced HEK-$TRPM2^{+tet}$ cells (Figure 5.2). These data suggest that both the anti-TRPM2-antibodies bind the surface expressed TRPM2 channels in SH-SY5Y cells and have the potential to counter the toxic effects of this toxin on the downstream signaling in neuronal cells.

Consistent with this possibility, anti-TRPM2-ECE was able to effectively prevent MPP^+-induced SH-SY5Y cell death (Figure 5.9). Furthermore, at the organelle level, the antibodies were able to rescue the lysosomes and mitochondrial network from the damaging effects of MPP^+, including the loss of lysosomes and the breakdown of the mitochondrial network (Figure 5.7 and 5.8). In addition, the antibodies attenuated MPP^+ induced ROS production (Figure 5.5 and 5.6). Given loss of lysosomes (Dehay et al., 2010) and mitochondrial fragmentation and dysfunction, and excess ROS production (Deng et al., 2018, Dias et al., 2013, Tretter et al., 2004, Balestrino and Schapira, 2020) are well established features of both genetic and idiopathic PD, the results provide compelling evidence that the ECE targeted anti-TRPM2 antibodies can serve as useful cell biological tools to investigate Parkinson's disease. More importantly, from the medical point of view, they provide the proof-of-principle for therapeutic potential of ECE targeted antibodies in the treatment of PD. Although not tested, they are likely to prove useful in investigations into the cell biological basis of a number of other diseases where oxidative stress and TRPM2 channels have been implicated. The diseases where TRPM2 channels have been implicated include diabetes, cardiovascular diseases, cancer, and neurodegenerative diseases such as Alzheimer's and Parkinson's (Yamamoto and Shimizu, 2016, Yamamoto et al., 2007, Ye et al., 2014, Zeng et al., 2010b, Zhang et al., 2012, Manna et al., 2015, Malko and Jiang, 2020, Hiroi et al., 2013, Hermosura and Garruto, 2007).

Although there is a rapidly growing list of therapeutic antibodies that have been approved by the FDA, there are no anti-ion channel antibodies that are currently being used in clinical practice (Colecraft and Trimmer, 2022). This is presumably due to the technical difficulties in developing antibodies against ion channels and the relative paucity of mechanistic information on how they work. The present work not only provided evidence for the ability of anti-TRPM2 antibodies to prevent neurotoxin-induced cell death, but provided the cell biological mechanism by which this protective effect was achieved.

Chapter 6
General discussion and summary

6.1 Discussion and summary of key findings

Parkinson's disease (PD) is the world's second most prevalent neurodegenerative disease following Alzheimer's disease. The loss of dopaminergic neurons in the substantia nigra pars compacta (SNpc) and accumulation/aggregation of α-synuclein in Lewy bodies (LBs) are major defining features of PD. Approximately 15% of patients with PD have a family history of genetic mutations associated with the disease, whereas the remaining cases are sporadic with uncertain aetiology and likely to be caused by a combination of genetic and environmental risk factor (such as, exposure to toxins) (Deng et al., 2018). Oxidative stress is an important factor contributing to dopaminergic cell death because of excessive ROS production (Choi et al., 2012). It is commonly known that elevated ROS levels have harmful effects on cellular organelles including mitochondria and lysosomes (Lin and Beal, 2006, Kurz et al., 2008a, Elfawy and Das, 2019, Abuarab et al., 2017, Li et al., 2017a). The dysfunctions of mitochondria and lysosomes have been linked to PD in several studies (Kim et al., 2021, Dehay et al., 2010, Deng et al., 2018, Mazzulli et al., 2016b, Zhu and Chu, 2010). Considering that ROS influence Ca^{2+} homeostasis and disrupt organelles' function, in this thesis, I have investigated how the Parkinson's disease-causing toxin, MPP^{+} affects TRPM2 channel dependent Ca^{2+} and ROS signaling to impact organelle function to eventually cause dopaminergic neuronal cell death (Chapters 3 and 4). The last part of the thesis (Chapter 5) describes the ability of antibodies raised against an extracellular epitope of the TRPM2 channel to attenuate all these subcellular cytotoxic events to protect the cells from death.

The rationale for focusing on the TRPM2 ion channel is as follows: (i) it is a ROS-sensitive ion channel which, by permeating Ca^{2+}, affects intracellular Zn^{2+} homeostasis; (ii) both Ca^{2+} and Zn^{2+} are cytotoxic signaling ions; and (iii) studies

have reported TRPM2 association with a number of diseases including neurodegenerative disorders, such as Alzheimer's and Parkinson's diseases (Jiang et al., 2010, Yamamoto and Shimizu, 2016, Yamamoto et al., 2007, Malko and Jiang, 2020). This channel is natively expressed in the neuroblastoma SH-SY5Y cells which are commonly used as human neuronal cellular model to study the mechanisms of neurodegeneration because of their neuronal properties (An et al., 2019, Xicoy et al., 2017). Also, this cell line along with the neurotoxin, MPP^+, is a widely used model that mimics PD (Xicoy et al., 2017). In this study, it was hypothesized that MPP^+ generated ROS activate the TRPM2 channel to generate ionic signals that, by affecting the crosstalk between the various intracellular organelles, causes neuronal cell death. A combination of biochemical, molecular and cell biological approaches were used to test this hypothesis.

The experiments reported in Chapter 3 investigated the role of TRPM2 channels in MPP^+-induced oxidative stress and cell death in SH-SY5Y cells. In agreement with previous findings (Yang et al., 2018, Lee et al., 2011, Wang and Liu, 2022), MPP^+ was found to stimulate ROS generation in SH-SY5Y cells. Quenching the total cytosolic ROS with antioxidants was shown to prevent MPP^+-induced ROS overproduction and cell death. Interestingly, quenching mitochondrial ROS alone with Mito-TEMPO was sufficient to prevent MPP^+ induced cell death. These data suggested that NOX2-derived ROS promote mitochondria to produce mtROS, which has been further supported by the ability of gp91ds-tat (NOX2 inhibitor) to prevent mtROS production and SH-SY5Y cell death. These findings lend credence to the developing concept that ROS produced at one location might act as a positive feedback signal to stimulate ROS production at another location, a phenomenon termed "ROS-induced ROS production" (RIRP) (Daiber, 2010, Dikalov, 2011).

NOX2 overexpression and subsequent increase in ROS generation have been reported in both animal models (Wu et al., 2003) and *in vitro* cellular models of PD (Keeney et al., 2021, Zawada et al., 2011). Increased intracellular Ca^{2+} is involved in both NOX2 activation and the production of mtROS (Rada and Leto,

2008, Bréchard et al., 2005, Schenten et al., 2008, Schenten et al., 2010, Camello-Almaraz et al., 2006, Görlach et al., 2015, Feissner et al., 2009, Kowaltowski et al., 1998). Therefore, Ca^{2+} dyshomeostasis has been linked to the production of ROS and the subsequent cell death seen in degenerative diseases.

It is well established that ROS activates the TRPM2 channel to stimulate Ca^{2+} influx that, in turn, triggers cell death. Results showed that MPP^+ caused an increase in intracellular Ca^{2+} in SH-SY5Y cells by activating the TRPM2 channel. Furthermore, the data from this study suggested that MPP^+-induced Ca^{2+} influx through TRPM2, stimulates NOX2 activation at the plasma membrane to generate ROS that, in turn, promotes mtROS production. Also, these results suggest that ROS required for TRPM2 activation might be generated through activation of NOX2 by MPP^+ treatment. Taken together, these findings suggest functional coupling between NOX2 and TRPM2 channels at the plasma membrane that help amplify the intracellular Ca^{2+} and ROS to toxic levels.

Inhibition of TRPM2 channels with siRNA and pharmacological blockers significantly prevented the effect of MPP^+ on cytosolic and mitochondrial ROS generation as well as on cell death. These results question the commonly held belief that MPP^+ acts directly on complex I of mitochondria to produce ROS to cause cell death (Cleeter et al., 1992, Ramsay et al., 1991, Yang et al., 2018). On the other hand, it is hard to understand how the inhibition of TRPM2 could attenuate the reported MPP^+'s ability to impact complex I directly. To address this ambiguous effect of MPP^+ on mitochondria, the role of Ca^{2+} in this pathway was investigated. The data demonstrate that chelation of cytosolic Ca^{2+} can significantly prevent MPP^+-induced cytosolic and mitochondrial ROS generation and cell death. It is known that increased cytosolic Ca^{2+} level is associated with increased Ca^{2+} influx into the mitochondria, affecting mitochondrial complexes (Pandya et al., 2013, Pan et al., 2013, Bravo-Sagua et al., 2017). Interestingly, data from this study have also shown that increased cytosolic Ca^{2+} is accompanied by increased Zn^{2+} and mtROS levels in SH-SY5Y cells. Recent evidence has linked Zn^{2+} to neuronal cell death caused by oxidative stress (Li et

al., 2017b, Kim et al., 1999). This has been further supported in other cell types, including endothelial cells (Abuarab et al., 2017) and pancreatic β-cells (Li et al., 2017a), where the authors revealed that TRPM2-mediated Ca^{2+} influx leads to a rise in mitochondrial Zn^{2+}, resulting in mitochondrial dysfunction and fission. Direct elevation of Zn^{2+} by using a Zn^{2+} ionophore (Zn-PTO) was sufficient to increase mtROS production and cell death, thus reproducing the effects of both MPP^+ and elevated cytosolic Ca^{2+}. Collectively, these findings suggest that Zn^{2+} mediates Ca^{2+}-induced mtROS production and cell death and indicate that Zn^{2+} has the primary detrimental influence on mitochondria.

Mitochondria play an important role in apoptosis; therefore, the effect of MPP^+ and TRPM2-Ca^{2+}-Zn^{2+} signaling on mitochondria morphology in SH-SY5Y cells was examined in chapter 4. In particular how the ROS and Ca^{2+} signals generated at the plasma membrane are transmitted to mitochondria, causing mitochondrial fragmentation and cell death was investigated. First, the results confirm that mitochondria undergo extensive fragmentation in response to MPP^+, which is consistent with previous studies (Zhu et al., 2012, Wang et al., 2011). Second, the data demonstrate that inhibition of NOX2-generated ROS and TRPM2-mediated Ca^{2+} influx, and chelation of Ca^{2+}, prevent MPP^+-induced mitochondria fragmentation. Third, in addition to mitochondria fragmentation, MPP^+ caused a marked reduction in the lysosome number and loss of $\Delta\Psi m$. The Ca^{2+} ionophore, A23187, has shown a similar effect on lysosomes as MPP^+, indicating the role of elevated cytosolic Ca^{2+} in lysosomal membrane permeabilization (LMP) and a decline in the number of lysosomes. The results also show that preventing Ca^{2+} influx through MPP^+-stimulated TRPM2 channel with a TRPM2 blocker (2-APB) rescued the lysosomes from the MPP^+ effect. Importantly, along with the decrease in the number of lysosomes, there was a redistribution of Zn^{2+} from lysosomes into mitochondria. Fourth, the resultant rise in mitochondrial Zn^{2+} was accompanied by the loss of $\Delta\Psi m$ and the breakdown of the mitochondrial network.

Zn^{2+} chelation has been shown to prevent oxidative stress-induced neuronal cell death (Medvedeva et al., 2009). The data in this study clearly demonstrate that

the chelation of Zn^{2+} alone was sufficient to prevent MPP^+-induced mitochondrial fragmentation and cell death, which is confirmed further through direct delivery of Zn^{2+} using Zn-PTO. These results and the role of Zn^{2+} in oxidative stress-induced mitochondria fission are in agreement with other studies that reported similar effects of Zn^{2+} in endothelial cells (Abuarab et al., 2017) and pancreatic β-cells (Li et al., 2017a). Thus, the data of this study provide evidence that Zn^{2+} acts downstream to Ca^{2+} in oxidative stress-induced mitochondrial fragmentation pathways in neuronal cells. Moreover, MPP^+ and Zn-PTO caused an increase in mitochondrial Zn^{2+} leading to a loss of ΔΨm and mtROS generation. This could be explained by the effects of Zn^{2+} on mitochondrial ETC complexes (Sensi et al., 2009, Link and von Jagow, 1995, Liu et al., 2021, Sharpley and Hirst, 2006, LORUSSO et al., 1991, Dineley et al., 2003). Therefore, specific suppressors of mitochondrial complexes (I and III) were used to determine the relative contribution of these two complexes in mtROS production and mitochondrial fragmentation. The data revealed that mitochondrial complex III suppression prevents MPP^+-induced mtROS production, mitochondrial fragmentation, and the death of SH-SY5Y cells more effectively than complex I. Collectively, these findings suggest that MPP^+-induced mtROS production is an indirect effect and might be mediated by Zn^{2+} inhibiting mitochondrial complex III. Finally, data also demonstrate that Zn^{2+} accumulation in mitochondria promotes Drp-1 protein recruitment to mitochondria initiating the fission process in a pathway mediated by TRPM2.

In chapter 5, two antibodies, targeted an extracellular epitope of the TRPM2 channel, named anti-TRPM2-ECE and -ECE3x, have been developed. The data demonstrate that anti-TRPM2-ECE3x successfully recognized TRPM2 in western blotting and or immunostaining assays in HEK293 cells engineered to overexpress the TRPM2 when induced with tetracycline. Both antibodies were able to prevent H_2O_2- and MPP^+-induced Ca^{2+} influx indicating their ability to block the Ca^{2+}-permeating pore in the TRPM2 channel and prevent its function. Notably, the anti-TRPM2-ECE antibody has been found to protect cells from the damaging effects of MPP^+ and oxidative stress on their organelles and viability. Data from this study show that anti-TRPM2-ECE antibody significantly prevents MPP^+-induced ROS production and loss of lysosomes. Moreover, the

effectiveness of the anti-TRPM2-ECE antibody in preventing MPP^+-induced mitochondrial fragmentation and cell death was remarkable in SH-SY5Y cells. Thus, these function blocking anti-TRPM2 antibodies serve as a useful biological tool to investigate intracellular events that are affected during oxidative stress. Furthermore, they might guide development of novel therapeutic approaches for the treatment of PD and other diseases where TRPM2 have been implicated.

The findings of this study could have significant implications for understanding the pathology of PD as well as possible therapeutic approaches. The data show that the TRPM2 channel deploys Ca^{2+} and Zn^{2+} signals to promote harmful communication between different cellular compartments during oxidative stress. This novel signaling pathway may prove to be a promising therapeutic target not just for PD, but many other oxidative stress-linked disorders which share similar pathways. Supporting this idea is the fact that the TRPM2 channel has a role in many ROS-associated diseases (Yamamoto and Shimizu, 2016). In addition, recent studies have implicated TRPM2 in oxidative stress-induced mitochondrial fragmentation in endothelial and pancreatic β-cells (Abuarab et al., 2017, Li et al., 2017a), which is a common feature of many ROS-associated diseases. Thus, the findings reported in this thesis likely have implications for a wide spectrum of diseases.

To conclude, the findings presented in this thesis reveal a mechanistic link between NOX2, TRPM2, ROS, Ca^{2+} and Zn^{2+} in the PD-toxin induced cytotoxic signaling associated with neuronal cell death. Furthermore, they report the development and potential use of TRPM2 function-blocking antibodies to interrogate cellular and molecular mechanisms of cell death in systems where TRPM2 channels have been implicated. It is also hoped that this novel signaling pathway will guide development of novel therapeutic approaches to diseases for which there are currently no cure, including Parkinson’s disease.

6.2 Future work

Results presented in this thesis reveal a novel signalling circuit, comprising NOX2, TRPM2, Ca^{2+}, and Zn^{2+}, that underlies neurotoxin-mediated dopaminergic cell death. Since the experiments have been carried out using the SH-SY5Y cell line, it would be important to examine this pathway in primary cells and brain tissue. Whether a similar mechanism occurs in other models of PD remains to be determined. The effects of MPP^+ on ROS production, lysosome function and mitochondrial dynamics could be investigated in dopaminergic neurons expressing disease causing mutants of α-synuclein gene. In addition, whether other neurotoxins, including pesticides (Rotenone and Paraquat) use similar mechanisms to impact mitochondrial dynamics and cell death should be examined. Such studies will provide mechanistic insights into both genetic and sporadic forms of PD.

The data presented in chapter 3 suggested functional coupling between NOX2 and TRPM2. It would be important to confirm these findings using other biochemical and microscopy-based studies including coimmunoprecipitation and colocalization methods, such as the Proximity Ligation Assay (PLA) for protein-protein interactions.

In chapter 4, it was found that MPP^+ causes a decline in lysosomes number and cause mitochondrial fragmentation. An *in vivo* study has reported the effect of MPP^+ on lysosome function (Dehay et al., 2010), however, similar *in vivo* studies should be carried on mitochondria dynamics. Furthermore, it would be interesting to test if NOX2 and TRPM2 inhibitors, and Zn^{2+} chelators, can prevent MPP^+-induced mitochondria fission in animal models.

List of References

ABUARAB, N., MUNSEY, T. S., JIANG, L. H., LI, J. & SIVAPRASADARAO, A. 2017. High glucose-induced ROS activates TRPM2 to trigger lysosomal membrane permeabilization and Zn^{2+}-mediated mitochondrial fission. *Sci Signal,* 10.

ADRAIN, C. & MARTIN, S. J. 2001. The mitochondrial apoptosome: a killer unleashed by the cytochrome seas. *Trends Biochem Sci,* 26**,** 390-7.

AHMAD, W., IJAZ, B., SHABBIRI, K., AHMED, F. & REHMAN, S. 2017. Oxidative toxicity in diabetes and Alzheimer's disease: mechanisms behind ROS/ RNS generation. *Journal of Biomedical Science,* 24**,** 76.

ALEXANDER, G. E. 2004. Biology of Parkinson's disease: pathogenesis and pathophysiology of a multisystem neurodegenerative disorder. *Dialogues in clinical neuroscience,* 6**,** 259-280.

ALTENHÖFER, S., RADERMACHER, K. A., KLEIKERS, P. W., WINGLER, K. & SCHMIDT, H. H. 2015. Evolution of NADPH Oxidase Inhibitors: Selectivity and Mechanisms for Target Engagement. *Antioxid Redox Signal,* 23**,** 406-27.

ALVES-LOPES, R., NEVES, K. B., ANAGNOSTOPOULOU, A., RIOS, F. J., LACCHINI, S., MONTEZANO, A. C. & TOUYZ, R. M. 2020. Crosstalk between vascular redox and calcium signaling in hypertension involves TRPM2 (transient receptor potential melastatin 2) cation channel. *Hypertension,* 75**,** 139-149.

AN, X., FU, Z., MAI, C., WANG, W., WEI, L., LI, D., LI, C. & JIANG, L.-H. 2019. Increasing the TRPM2 channel expression in human neuroblastoma SH-SY5Y cells augments the susceptibility to ROS-induced cell death. *Cells,* 8**,** 28.

ANANTHARAM, V., KAUL, S., SONG, C., KANTHASAMY, A. & KANTHASAMY, A. G. 2007. Pharmacological inhibition of neuronal NADPH oxidase protects against 1-methyl-4-phenylpyridinium (MPP^+)-induced oxidative stress and apoptosis in mesencephalic dopaminergic neuronal cells. *NeuroToxicology,* 28**,** 988-997.

ANGELOVA, P. R. & ABRAMOV, A. Y. 2018. Role of mitochondrial ROS in the brain: from physiology to neurodegeneration. *FEBS letters,* 592**,** 692-702.

ANNUNZIATO, L., AMOROSO, S., PANNACCIONE, A., CATALDI, M., PIGNATARO, G., D'ALESSIO, A., SIRABELLA, R., SECONDO, A., SIBAUD, L. & DI RENZO, G. F. 2003. Apoptosis induced in neuronal cells by oxidative stress: role played by caspases and intracellular calcium ions. *Toxicol Lett,* 139**,** 125-33.

ARCHER, S. L. 2013. Mitochondrial Dynamics — Mitochondrial Fission and Fusion in Human Diseases. *New England Journal of Medicine,* 369**,** 2236-2251.

AYUB, K. & HALLETT, M. B. 2004. The mitochondrial ADPR link between Ca^{2+} store release and Ca^{2+} influx channel opening in immune cells. *FASEB journal : official publication of the Federation of American Societies for Experimental Biology,* 18**,** 1335-1338.

BAGKOS, G., KOUFOPOULOS, K. & PIPERI, C. 2014. A new model for mitochondrial membrane potential production and storage. *Med Hypotheses,* 83**,** 175-81.

BAI, S., SONG, Y., HUANG, X., PENG, L., JIA, J., LIU, Y. & LU, H. 2016. Statin use and the risk of Parkinson's disease: an updated meta-analysis. *PLoS One,* 11**,** e0152564.

BALABAN, R. S., NEMOTO, S. & FINKEL, T. 2005. Mitochondria, oxidants, and aging. *Cell,* 120**,** 483-95.

BALESTRINO, R. & SCHAPIRA, A. H. V. 2020. Parkinson disease. *Eur J Neurol,* 27**,** 27-42.

BALLARD, P. A., TETRUD, J. W. & LANGSTON, J. W. 1985. Permanent human parkinsonism due to 1-methyl-4-phenyl-1,2,3,6-tetrahydropyridine (MPTP): seven cases. *Neurology,* 35**,** 949-56.

BÁNSÁGHI, S., GOLENÁR, T., MADESH, M., CSORDÁS, G., RAMACHANDRARAO, S., SHARMA, K., YULE, D. I., JOSEPH, S. K. & HAJNÓCZKY, G. 2014. Isoform-and species-specific control

of inositol 1, 4, 5-trisphosphate (IP_3) receptors by reactive oxygen species. *Journal of Biological Chemistry,* 289**,** 8170-8181.

BARNHAM, K. J., MASTERS, C. L. & BUSH, A. I. 2004. Neurodegenerative diseases and oxidative stress. *Nature Reviews Drug Discovery,* 3**,** 205-214.

BARSOUM, M. J., YUAN, H., GERENCSER, A. A., LIOT, G., KUSHNAREVA, Y., GRÄBER, S., KOVACS, I., LEE, W. D., WAGGONER, J. & CUI, J. 2006. Nitric oxide-induced mitochondrial fission is regulated by dynamin-related GTPases in neurons. *The EMBO journal,* 25**,** 3900-3911.

BAUMGARTNER, H. K., GERASIMENKO, J. V., THORNE, C., FERDEK, P., POZZAN, T., TEPIKIN, A. V., PETERSEN, O. H., SUTTON, R., WATSON, A. J. M. & GERASIMENKO, O. V. 2009. Calcium Elevation in Mitochondria Is the Main Ca^{2+} Requirement for Mitochondrial Permeability Transition Pore (mPTP) Opening*. *Journal of Biological Chemistry,* 284**,** 20796-20803.

BEAL, M. F. 2002. Oxidatively modified proteins in aging and disease1, 2 1Guest Editor: Earl Stadtman 2This article is part of a series of reviews on "Oxidatively Modified Proteins in Aging and Disease." The full list of papers may be found on the homepage of the journal. *Free Radical Biology and Medicine,* 32**,** 797-803.

BEDARD, K. & KRAUSE, K.-H. 2007. The NOX family of ROS-generating NADPH oxidases: physiology and pathophysiology. *Physiological reviews,* 87**,** 245-313.

BELARBI, K., CUVELIER, E., DESTÉE, A., GRESSIER, B. & CHARTIER-HARLIN, M.-C. 2017. NADPH oxidases in Parkinson's disease: a systematic review. *Molecular Neurodegeneration,* 12**,** 84.

BELROSE, J. C. & JACKSON, M. F. 2018. TRPM2: a candidate therapeutic target for treating neurological diseases. *Acta Pharmacologica Sinica,* 39**,** 722-732.

BENTERS, J., FLÖGEL, U., SCHÄFER, T., LEIBFRITZ, D., HECHTENBERG, S. & BEYERSMANN, D. 1997. Study of the interactions of cadmium and zinc ions with cellular calcium homoeostasis using 19F-NMR spectroscopy. *Biochemical Journal,* 322**,** 793-799.

BERRIDGE, M. J., BOOTMAN, M. D. & RODERICK, H. L. 2003. Calcium signalling: dynamics, homeostasis and remodelling. *Nature reviews Molecular cell biology,* 4**,** 517-529.

BIDO, S., SORIA, F. N., FAN, R. Z., BEZARD, E. & TIEU, K. 2017. Mitochondrial division inhibitor-1 is neuroprotective in the A53T-α-synuclein rat model of Parkinson's disease. *Scientific reports,* 7**,** 1-13.

BLAKE, R. & TROUNCE, I. A. 2014. Mitochondrial dysfunction and complications associated with diabetes. *Biochim Biophys Acta,* 1840**,** 1404-12.

BOGESKI, I., KILCH, T. & NIEMEYER, B. A. 2012. ROS and SOCE: recent advances and controversies in the regulation of STIM and Orai. *The Journal of physiology,* 590**,** 4193-4200.

BOGESKI, I., KUMMEROW, C., AL-ANSARY, D., SCHWARZ, E. C., KOEHLER, R., KOZAI, D., TAKAHASHI, N., PEINELT, C., GRIESEMER, D. & BOZEM, M. 2010. Differential redox regulation of ORAI ion channels: a mechanism to tune cellular calcium signaling. *Science signaling,* 3**,** ra24-ra24.

BONET-PONCE, L., BEILINA, A., WILLIAMSON, C. D., LINDBERG, E., KLUSS, J. H., SAEZ-ATIENZAR, S., LANDECK, N., KUMARAN, R., MAMAIS, A. & BLECK, C. K. 2020. LRRK2 mediates tubulation and vesicle sorting from lysosomes. *Science advances,* 6**,** eabb2454.

BONIFATI, V., RIZZU, P., VAN BAREN, M. J., SCHAAP, O., BREEDVELD, G. J., KRIEGER, E., DEKKER, M. C., SQUITIERI, F., IBANEZ, P., JOOSSE, M., VAN DONGEN, J. W., VANACORE, N., VAN SWIETEN, J. C., BRICE, A., MECO, G., VAN DUIJN, C. M., OOSTRA, B. A. & HEUTINK, P. 2003. Mutations in the *DJ-1* gene associated with autosomal recessive early-onset parkinsonism. *Science,* 299**,** 256-9.

BOOTMAN, M. D., RODERICK, H. L., O'CONNOR, R. & BERRIDGE, M. J. 2003. CHAPTER 131 - Intracellular Calcium Signaling. *In:* BRADSHAW, R. A. & DENNIS, E. A. (eds.) *Handbook of Cell Signaling.* Burlington: Academic Press.

BORDT, E. A., CLERC, P., ROELOFS, B. A., SALADINO, A. J., TRETTER, L., ADAM-VIZI, V., CHEROK, E., KHALIL, A., YADAVA, N. & SHEALINNA, X. G. 2017. The putative Drp1 inhibitor mdivi-1 is a reversible mitochondrial complex I inhibitor that modulates reactive oxygen species. *Developmental cell,* 40**,** 583-594. e6.

BOVO, E., LIPSIUS, S. L. & ZIMA, A. V. 2012. Reactive oxygen species contribute to the development of arrhythmogenic Ca^{2+} waves during β-adrenergic receptor stimulation in rabbit cardiomyocytes. *The Journal of Physiology,* 590**,** 3291-3304.

BOWERS, K. & SRAI, S. K. S. 2018. The trafficking of metal ion transporters of the Zrt- and Irt-like protein family. *Traffic,* 19**,** 813-822.

BOYA, P., GONZALEZ-POLO, R.-A., PONCET, D., ANDREAU, K., VIEIRA, H. L. A., ROUMIER, T., PERFETTINI, J.-L. & KROEMER, G. 2003. Mitochondrial membrane permeabilization is a critical step of lysosome-initiated apoptosis induced by hydroxychloroquine. *Oncogene,* 22**,** 3927-3936.

BRAAK, H., DEL TREDICI, K., RÜB, U., DE VOS, R. A., STEUR, E. N. J. & BRAAK, E. 2003. Staging of brain pathology related to sporadic Parkinson's disease. *Neurobiology of aging,* 24**,** 197-211.

BRAND, M. D. 2010. The sites and topology of mitochondrial superoxide production. *Experimental gerontology,* 45**,** 466-472.

BRANDES, R. P., WEISSMANN, N. & SCHRÖDER, K. 2014. Nox family NADPH oxidases: Molecular mechanisms of activation. *Free Radical Biology and Medicine,* 76**,** 208-226.

BRANDT, T., CAVELLINI, L., KÜHLBRANDT, W. & COHEN, M. M. 2016. A mitofusin-dependent docking ring complex triggers mitochondrial fusion *in vitro*. *Elife,* 5.

BRAR, S. S., KENNEDY, T. P., STURROCK, A. B., HUECKSTEADT, T. P., QUINN, M. T., WHORTON, A. R. & HOIDAL, J. R. 2002. An NADPH oxidase regulates growth and transcription in melanoma cells. *American Journal of Physiology-Cell Physiology,* 282**,** C1212-C1224.

BRAVO-SAGUA, R., PARRA, V., LÓPEZ-CRISOSTO, C., DÍAZ, P., QUEST, A. & LAVANDERO, S. 2017. Calcium transport and signaling in mitochondria. *Compr Physiol,* 7**,** 623-634.

BRÉCHARD, S., BUEB, J.-L. & TSCHIRHART, E. 2005. Interleukin-8 primes oxidative burst in neutrophil-like HL-60 through changes in cytosolic calcium. *Cell Calcium,* 37**,** 531-540.

BRÉCHARD, S., MELCHIOR, C., PLANÇON, S., SCHENTEN, V. & TSCHIRHART, E. 2008. Store-operated Ca^{2+} channels formed by TRPC1, TRPC6 and Orai1 and non-store-operated channels formed by TRPC3 are involved in the regulation of NADPH oxidase in HL-60 granulocytes. *Cell calcium,* 44**,** 492-506.

BRECKENRIDGE, C. B., BERRY, C., CHANG, E. T., SIELKEN JR, R. L. & MANDEL, J. S. 2016. Association between Parkinson's disease and cigarette smoking, rural living, well-water consumption, farming and pesticide use: systematic review and meta-analysis. *PloS one,* 11**,** e0151841.

BRIEGER, K., SCHIAVONE, S., MILLER, F. J., JR. & KRAUSE, K. H. 2012. Reactive oxygen species: from health to disease. *Swiss Med Wkly,* 142**,** w13659.

BRINI, M. & CARAFOLI, E. 2011. The plasma membrane Ca^{2+} ATPase and the plasma membrane sodium calcium exchanger cooperate in the regulation of cell calcium. *Cold Spring Harb Perspect Biol,* 3.

BUCKMAN, J. F., HERNÁNDEZ, H., KRESS, G. J., VOTYAKOVA, T. V., PAL, S. & REYNOLDS, I. J. 2001. MitoTracker labeling in primary neuronal and astrocytic cultures: influence of mitochondrial membrane potential and oxidants. *J Neurosci Methods,* 104**,** 165-76.

BUGGER, H. & ABEL, E. D. 2010. Mitochondria in the diabetic heart. *Cardiovascular research,* 88**,** 229-240.

BURGOYNE, R. D. 2007. Neuronal calcium sensor proteins: generating diversity in neuronal Ca^{2+} signalling. *Nat Rev Neurosci,* 8**,** 182-93.

CADENAS, E. & BOVERIS, A. 1980. Enhancement of hydrogen peroxide formation by protophores and ionophores in antimycin-supplemented mitochondria. *Biochemical Journal,* 188**,** 31-37.

CALKINS, M. J., MANCZAK, M. & REDDY, P. H. 2012. Mitochondria-targeted antioxidant SS31 prevents amyloid beta-induced mitochondrial abnormalities and synaptic degeneration in Alzheimer's disease. *Pharmaceuticals,* 5**,** 1103-1119.

CALVO-RODRIGUEZ, M. & BACSKAI, B. J. 2021. Mitochondria and Calcium in Alzheimer's Disease: From Cell Signaling to Neuronal Cell Death. *Trends Neurosci,* 44**,** 136-151.

CAMELLO-ALMARAZ, C., GOMEZ-PINILLA, P. J., POZO, M. J. & CAMELLO, P. J. 2006. Mitochondrial reactive oxygen species and Ca^{2+} signaling. *Am J Physiol Cell Physiol,* 291**,** C1082-8.

CANALI, E., BOLCHI, A., SPAGNOLI, G., SEITZ, H., RUBIO, I., PERTINHEZ, T. A., MÜLLER, M. & OTTONELLO, S. 2014. A high-performance thioredoxin-based scaffold for peptide immunogen construction: proof-of-concept testing with a human papillomavirus epitope. *Scientific Reports,* 4**,** 4729.

CASAS, A. I., DAO, V. T.-V., DAIBER, A., MAGHZAL, G. J., DI LISA, F., KALUDERCIC, N., LEACH, S., CUADRADO, A., JAQUET, V., SEREDENINA, T., KRAUSE, K. H., LÓPEZ, M. G., STOCKER, R., GHEZZI, P. & SCHMIDT, H. H. H. W. 2015. Reactive Oxygen-Related Diseases: Therapeutic Targets and Emerging Clinical Indications. *Antioxidants & redox signaling,* 23**,** 1171-1185.

CASE, A. J., LI, S., BASU, U., TIAN, J. & ZIMMERMAN, M. C. 2013. Mitochondrial-localized NADPH oxidase 4 is a source of superoxide in angiotensin II-stimulated neurons. *Am J Physiol Heart Circ Physiol,* 305**,** H19-28.

CARRASCO, E. & WERNER, P. 2002. Selective destruction of dopaminergic neurons by low concentrations of 6-OHDA and MPP^+: protection by acetylsalicylic acid (aspirin). *Parkinsonism & Related Disorders,* 8**,** 407-411.

CASSARINO, D. S., PARKS, J. K., PARKER, W. D. & BENNETT, J. P. 1999. The parkinsonian neurotoxin MPP^+ opens the mitochondrial permeability transition pore and releases cytochrome *c* in isolated mitochondria via an oxidative mechanism. *Biochimica et Biophysica Acta (BBA) - Molecular Basis of Disease,* 1453**,** 49-62.

CASTELLI, V., BENEDETTI, E., ANTONOSANTE, A., CATANESI, M., PITARI, G., IPPOLITI, R., CIMINI, A. & D'ANGELO, M. 2019. Neuronal cells rearrangement during aging and neurodegenerative disease: metabolism, oxidative stress and organelles dynamic. *Frontiers in molecular neuroscience,* 12**,** 132.

CEREGHETTI, G. M., COSTA, V. & SCORRANO, L. 2010. Inhibition of Drp1-dependent mitochondrial fragmentation and apoptosis by a polypeptide antagonist of calcineurin. *Cell Death & Differentiation,* 17**,** 1785-1794.

CEREGHETTI, G. M., STANGHERLIN, A., MARTINS DE BRITO, O., CHANG, C. R., BLACKSTONE, C., BERNARDI, P. & SCORRANO, L. 2008. Dephosphorylation by calcineurin regulates translocation of Drp1 to mitochondria. *Proc Natl Acad Sci U S A,* 105**,** 15803-8.

CERIELLO, A. 2006. Oxidative stress and diabetes-associated complications. *Endocr Pract,* 12 Suppl 1**,** 60-2.

CERRI, S. & VALENTE, E. M. 2020. Mitochondria and Parkinson's disease: a complex (III) liaison. *Brain,* 143**,** 3175-3178.

CHAKRABARTI, R., JI, W. K., STAN, R. V., DE JUAN SANZ, J., RYAN, T. A. & HIGGS, H. N. 2018. INF2-mediated actin polymerization at the ER stimulates mitochondrial calcium uptake, inner membrane constriction, and division. *J Cell Biol,* 217**,** 251-268.

CHALMERS, S. & MCCARRON, J. G. 2008. The mitochondrial membrane potential and Ca^{2+} oscillations in smooth muscle. *J Cell Sci,* 121**,** 75-85.

CHAN, P., DELANNEY, L. E., IRWIN, I., LANGSTON, J. W. & DI MONTE, D. 1991. Rapid ATP loss caused by 1-methyl-4-phenyl-1, 2, 3, 6-tetrahydropyridine in mouse brain. *Journal of neurochemistry,* 57**,** 348-351.

CHANG, C.-R. & BLACKSTONE, C. 2010. Dynamic regulation of mitochondrial fission through modification of the dynamin-related protein Drp1. *Annals of the New York Academy of Sciences,* 1201**,** 34-39.

CHANG, G. D. & RAMIREZ, V. D. 1987. Effects of dopamine metabolism of MPTP and MPP^+ infused through a push-pull cannula into the caudate nucleus of awake adult male rats. *Brain Research,* 424**,** 49-57.

CHAPPIE, J. S., ACHARYA, S., LIU, Y. W., LEONARD, M., PUCADYIL, T. J. & SCHMID, S. L. 2009. An intramolecular signaling element that modulates dynamin function *in vitro* and *in vivo*. *Mol Biol Cell,* 20**,** 3561-71.

CHATURVEDI, R. K. & FLINT BEAL, M. 2013. Mitochondrial Diseases of the Brain. *Free Radical Biology and Medicine,* 63**,** 1-29.

CHAUDHRY, A. 2019. Mitochondria Analyzer (online). *http:github.com/AhsenChaudhry/Mitochondria-Analyzer.*

CHAUDHRY, A., SHI, R. & LUCIANI, D. S. 2020. A pipeline for multidimensional confocal analysis of mitochondrial morphology, function, and dynamics in pancreatic β-cells. *American Journal of Physiology-Endocrinology and Metabolism,* 318**,** E87-E101.

CHEN, H., DETMER, S. A., EWALD, A. J., GRIFFIN, E. E., FRASER, S. E. & CHAN, D. C. 2003. Mitofusins Mfn1 and Mfn2 coordinately regulate mitochondrial fusion and are essential for embryonic development. *J Cell Biol,* 160**,** 189-200.

CHEN, S. J., ZHANG, W., TONG, Q., CONRAD, K., HIRSCHLER-LASZKIEWICZ, I., BAYERL, M., KIM, J. K., CHEUNG, J. Y. & MILLER, B. A. 2013. Role of TRPM2 in cell proliferation and susceptibility to oxidative stress. *Am J Physiol Cell Physiol,* 304**,** C548-60.

CHEN, T. S., KOUTSILIERI, E. & RAUSCH, W. D. 1995. MPP^+ selectively affects calcium homeostasis in mesencephalic cell cultures from embryonal C57/Bl6 mice. *J Neural Transm Gen Sect,* 100**,** 153-63.

CHENG, G., CAO, Z., XU, X., VAN MEIR, E. G. & LAMBETH, J. D. 2001. Homologs of gp91phox: cloning and tissue expression of Nox3, Nox4, and Nox5. *Gene,* 269**,** 131-40.

CHO, B., CHO, H. M., JO, Y., KIM, H. D., SONG, M., MOON, C., KIM, H., KIM, K., SESAKI, H., RHYU, I. J., KIM, H. & SUN, W. 2017. Constriction of the mitochondrial inner compartment is a priming event for mitochondrial division. *Nat Commun,* 8**,** 15754.

CHO, H. M., RYU, J. R., JO, Y., SEO, T. W., CHOI, Y. N., KIM, J. H., CHUNG, J. M., CHO, B., KANG, H. C., YU, S. W., YOO, S. J., KIM, H. & SUN, W. 2019. Drp1-Zip1 Interaction Regulates Mitochondrial Quality Surveillance System. *Mol Cell,* 73**,** 364-376.e8.

CHOI, D. H., CRISTÓVÃO, A. C., GUHATHAKURTA, S., LEE, J., JOH, T. H., BEAL, M. F. & KIM, Y. S. 2012. NADPH oxidase 1-mediated oxidative stress leads to dopamine neuron death in Parkinson's disease. *Antioxid Redox Signal,* 16**,** 1033-45.

CHOI, I., ZHANG, Y., SEEGOBIN, S. P., PRUVOST, M., WANG, Q., PURTELL, K., ZHANG, B. & YUE, Z. 2020. Microglia clear neuron-released α-synuclein via selective autophagy and prevent neurodegeneration. *Nat Commun,* 11**,** 1386.

CHOI, W.-S., KRUSE, S. E., PALMITER, R. D. & XIA, Z. 2008. Mitochondrial complex I inhibition is not required for dopaminergic neuron death induced by rotenone, MPP^+, or paraquat. *Proceedings of the National Academy of Sciences,* 105**,** 15136-15141.

CHOI, W. S., YOON, S. Y., OH, T. H., CHOI, E. J., O'MALLEY, K. L. & OH, Y. J. 1999. Two distinct mechanisms are involved in 6-hydroxydopamine-and MPP^+-induced dopaminergic neuronal cell death: role of caspases, ROS, and JNK. *Journal of neuroscience research,* 57**,** 86-94.

CHOUCHANI, E. T., PELL, V. R., JAMES, A. M., WORK, L. M., SAEB-PARSY, K., FREZZA, C., KRIEG, T. & MURPHY, M. P. 2016. A Unifying Mechanism for Mitochondrial Superoxide Production during Ischemia-Reperfusion Injury. *Cell Metab,* 23**,** 254-63.

CHUNG, K. K., FREESTONE, P. S. & LIPSKI, J. 2011. Expression and functional properties of TRPM2 channels in dopaminergic neurons of the substantia nigra of the rat. *Journal of Neurophysiology,* 106**,** 2865-2875.

CIRMAN, T., OREŠIĆ, K., MAZOVEC, G. D., TURK, V., REED, J. C., MYERS, R. M., SALVESEN, G. S. & TURK, B. 2004. Selective disruption of lysosomes in HeLa cells triggers apoptosis mediated by cleavage of Bid by multiple papain-like lysosomal cathepsins. *Journal of Biological Chemistry,* 279**,** 3578-3587.

CLAPHAM, D. E. 2007. Calcium signaling. *Cell,* 131**,** 1047-58.
CLEETER, M. W., COOPER, J. M. & SCHAPIRA, A. H. 1992. Irreversible inhibition of mitochondrial complex I by 1-methyl-4-phenylpyridinium: evidence for free radical involvement. *J Neurochem,* 58**,** 786-9.
COLECRAFT, H. M. & TRIMMER, J. S. 2022. Controlling ion channel function with renewable recombinant antibodies. *J Physiol,* 600**,** 2023-2036.
COLLATZ, M. B., RÜDEL, R. & BRINKMEIER, H. 1997. Intracellular calcium chelator BAPTA protects cells against toxic calcium overload but also alters physiological calcium responses. *Cell Calcium,* 21**,** 453-9.
COLLINS, T. J., LIPP, P., BERRIDGE, M. J. & BOOTMAN, M. D. 2001. Mitochondrial Ca^{2+} uptake depends on the spatial and temporal profile of cytosolic Ca^{2+} signals. *J Biol Chem,* 276**,** 26411-20.
COLVIN, R. A., HOLMES, W. R., FONTAINE, C. P. & MARET, W. 2010. Cytosolic zinc buffering and muffling: their role in intracellularzinc homeostasis. *Metallomics,* 2**,** 306-317.
COLVIN, R. A., LAI, B., HOLMES, W. R. & LEE, D. 2015. Understanding metal homeostasis in primary cultured neurons. Studies using single neuron subcellular and quantitative metallomics. *Metallomics,* 7**,** 1111-1123.
COOKSON, M. R. & SHAW, P. J. 1999. Oxidative stress and motor neurone disease. *Brain pathology,* 9**,** 165-186.
CROWLEY, L. C., CHRISTENSEN, M. E. & WATERHOUSE, N. J. 2016. Measuring Mitochondrial Transmembrane Potential by TMRE Staining. *Cold Spring Harb Protoc,* 2016.
DAIBER, A. 2010. Redox signaling (cross-talk) from and to mitochondria involves mitochondrial pores and reactive oxygen species. *Biochimica et Biophysica Acta (BBA) - Bioenergetics,* 1797**,** 897-906.
DANIEL, N. H., ARAVIND, A. & THAKUR, P. 2021. Are ion channels potential therapeutic targets for Parkinson's disease? *NeuroToxicology,* 87**,** 243-257.
DE BRITO, O. M. & SCORRANO, L. 2008. Mitofusin 2 tethers endoplasmic reticulum to mitochondria. *Nature,* 456**,** 605-10.
DE RIJK, M. C., BRETELER, M. M., GRAVELAND, G. A., OTT, A., GROBBEE, D. E., VAN DER MECHÉ, F. G. & HOFMAN, A. 1995. Prevalence of Parkinson's disease in the elderly: the Rotterdam Study. *Neurology,* 45**,** 2143-6.
DEHAY, B., BOVE, J., RODRIGUEZ-MUELA, N., PERIER, C., RECASENS, A., BOYA, P. & VILA, M. 2010. Pathogenic lysosomal depletion in Parkinson's disease. *J Neurosci,* 30**,** 12535-44.
DENG, H., DODSON, M. W., HUANG, H. & GUO, M. 2008. The Parkinson's disease genes *pink1* and *parkin* promote mitochondrial fission and/or inhibit fusion in Drosophila. *Proceedings of the National Academy of Sciences,* 105**,** 14503-14508.
DENG, H., WANG, P. & JANKOVIC, J. 2018. The genetics of Parkinson disease. *Ageing Res Rev,* 42**,** 72-85.
DESOUKI, M. M., KULAWIEC, M., BANSAL, S., DAS, G. C. & SINGH, K. K. 2005. Cross talk between mitochondria and superoxide generating NADPH oxidase in breast and ovarian tumors. *Cancer biology & therapy,* 4**,** 1367-1373.
DEXTER, D., CARAYON, A., JAVOY-AGID, F., AGID, Y., WELLS, F., DANIEL, S., LEES, A., JENNER, P. & MARSDEN, C. 1991. Alterations in the levels of iron, ferritin and other trace metals in Parkinson's disease and other neurodegenerative diseases affecting the basal ganglia. *Brain,* 114**,** 1953-1975.
DEXTER, D. T., WELLS, F. R., LEE, A. J., AGID, F., AGID, Y., JENNER, P. & MARSDEN, C. D. 1989. Increased nigral iron content and alterations in other metal ions occurring in brain in Parkinson's disease. *Journal of neurochemistry,* 52**,** 1830-1836.
DI, A., GAO, X. P., QIAN, F., KAWAMURA, T., HAN, J., HECQUET, C., YE, R. D., VOGEL, S. M. & MALIK, A. B. 2012. The redox-sensitive cation channel TRPM2 modulates phagocyte ROS production and inflammation. *Nat Immunol,* 13**,** 29-34.
DIAS, V., JUNN, E. & MOURADIAN, M. M. 2013. The role of oxidative stress in Parkinson's disease. *J Parkinsons Dis,* 3**,** 461-91.

DICKSON, D. W. 2018. Neuropathology of Parkinson disease. *Parkinsonism & related disorders,* 46**,** S30-S33.
DIKALOV, S. 2011. Cross talk between mitochondria and NADPH oxidases. *Free radical biology & medicine,* 51**,** 1289-1301.
DINELEY, K. E., RICHARDS, L. L., VOTYAKOVA, T. V. & REYNOLDS, I. J. 2005. Zinc causes loss of membrane potential and elevates reactive oxygen species in rat brain mitochondria. *Mitochondrion,* 5**,** 55-65.
DINELEY, K. E., VOTYAKOVA, T. V. & REYNOLDS, I. J. 2003. Zinc inhibition of cellular energy production: implications for mitochondria and neurodegeneration. *Journal of neurochemistry,* 85**,** 563-570.
DRÖGE, W. 2002. Free radicals in the physiological control of cell function. *Physiol Rev,* 82**,** 47-95.
DU, J., XIE, J. & YUE, L. 2009a. Intracellular calcium activates TRPM2 and its alternative spliced isoforms. *Proceedings of the National Academy of Sciences,* 106**,** 7239-7244.
DU, J., XIE, J. & YUE, L. 2009b. Modulation of TRPM2 by acidic pH and the underlying mechanisms for pH sensitivity. *The Journal of general physiology,* 134**,** 471-488.
DUCHEN, M. R. 2000a. Mitochondria and Ca^{2+} in cell physiology and pathophysiology. *Cell Calcium,* 28**,** 339-348.
DUCHEN, M. R. 2000b. Mitochondria and calcium: from cell signalling to cell death. *J Physiol,* 529 Pt 1**,** 57-68.
DUDA, J., PÖTSCHKE, C. & LISS, B. 2016. Converging roles of ion channels, calcium, metabolic stress, and activity pattern of Substantia nigra dopaminergic neurons in health and Parkinson's disease. *Journal of neurochemistry,* 139**,** 156-178.
DUDKINA, N. V., KOUŘIL, R., PETERS, K., BRAUN, H.-P. & BOEKEMA, E. J. 2010. Structure and function of mitochondrial supercomplexes. *Biochimica et Biophysica Acta (BBA) - Bioenergetics,* 1797**,** 664-670.
EL-AGNAF, O. M., JAKES, R., CURRAN, M. D., MIDDLETON, D., INGENITO, R., BIANCHI, E., PESSI, A., NEILL, D. & WALLACE, A. 1998. Aggregates from mutant and wild-type α-synuclein proteins and NAC peptide induce apoptotic cell death in human neuroblastoma cells by formation of β-sheet and amyloid-like filaments. *FEBS letters,* 440**,** 71-75.
ELFAWY, H. A. & DAS, B. 2019. Crosstalk between mitochondrial dysfunction, oxidative stress, and age related neurodegenerative disease: Etiologies and therapeutic strategies. *Life Sciences,* 218**,** 165-184.
ELMORE, S. 2007. Apoptosis: a review of programmed cell death. *Toxicol Pathol,* 35**,** 495-516.
EREJUWA, O. O. 2012. Oxidative stress in diabetes mellitus: is there a role for hypoglycemic drugs and/or antioxidants. *Oxidative stress and diseases,* 217**,** 246.
ERMAK, G. & DAVIES, K. J. 2002. Calcium and oxidative stress: from cell signaling to cell death. *Mol Immunol,* 38**,** 713-21.
ETHELL, D. W. & BUHLER, L. A. 2003. Fas ligand-mediated apoptosis in degenerative disorders of the brain. *J Clin Immunol,* 23**,** 439-46.
EURA, Y., ISHIHARA, N., YOKOTA, S. & MIHARA, K. 2003. Two mitofusin proteins, mammalian homologues of FZO, with distinct functions are both required for mitochondrial fusion. *J Biochem,* 134**,** 333-44.
FAOUZI, M. & PENNER, R. 2014. TRPM2. *Handb Exp Pharmacol,* 222**,** 403-26.
FAVARO, G., ROMANELLO, V., VARANITA, T., ANDREA DESBATS, M., MORBIDONI, V., TEZZE, C., ALBIERO, M., CANATO, M., GHERARDI, G., DE STEFANI, D., MAMMUCARI, C., BLAAUW, B., BONCOMPAGNI, S., PROTASI, F., REGGIANI, C., SCORRANO, L., SALVIATI, L. & SANDRI, M. 2019. DRP1-mediated mitochondrial shape controls calcium homeostasis and muscle mass. *Nature Communications,* 10**,** 2576.
FEDERICO, A., CARDAIOLI, E., DA POZZO, P., FORMICHI, P., GALLUS, G. N. & RADI, E. 2012. Mitochondria, oxidative stress and neurodegeneration. *Journal of the neurological sciences,* 322**,** 254-262.

FEISSNER, R. F., SKALSKA, J., GAUM, W. E. & SHEU, S. S. 2009. Crosstalk signaling between mitochondrial Ca2+ and ROS. *Front Biosci (Landmark Ed),* 14**,** 1197-218.
FENG, S.-T., WANG, Z.-Z., YUAN, Y.-H., WANG, X.-L., SUN, H.-M., CHEN, N.-H. & ZHANG, Y. 2020. Dynamin-related protein 1: A protein critical for mitochondrial fission, mitophagy, and neuronal death in Parkinson's disease. *Pharmacological research,* 151**,** 104553.
FENG, X. & YANG, J. 2016. Lysosomal Calcium in Neurodegeneration. *Messenger (Los Angeles, Calif. : Print),* 5**,** 56-66.
FEUERSTEIN, T., HEDLER, L., JACKISCH, R. & HERTTING, G. 1988. An *in vitro* model of 1-methyl-4-phenyl-pyridinium MPP^+ toxicity: incubation of rabbit caudate nucleus slices with MPP^+ followed by biochemical and functional analysis. *British journal of pharmacology,* 95**,** 449-458.
FISHER, A. B. 2009. Redox signaling across cell membranes. *Antioxid Redox Signal,* 11**,** 1349-56.
FISHMAN, P. S. & OYLER, G. A. 2002. Significance of the *parkin* gene and protein in understanding Parkinson's disease. *Curr Neurol Neurosci Rep,* 2**,** 296-302.
FONFRIA, E., MARSHALL, I. C. B., BENHAM, C. D., BOYFIELD, I., BROWN, J. D., HILL, K., HUGHES, J. P., SKAPER, S. D. & MCNULTY, S. 2004. TRPM2 channel opening in response to oxidative stress is dependent on activation of poly(ADP-ribose) polymerase. *British journal of pharmacology,* 143**,** 186-192.
FONFRIA, E., MURDOCK, P. R., CUSDIN, F. S., BENHAM, C. D., KELSELL, R. E. & MCNULTY, S. 2006. Tissue distribution profiles of the human TRPM cation channel family. *Journal of Receptors and Signal Transduction,* 26**,** 159-178.
FONG, K.-L., MCCAY, P. B., POYER, J. L., KEELE, B. B. & MISRA, H. 1973. Evidence that peroxidation of lysosomal membranes is initiated by hydroxyl free radicals produced during flavin enzyme activity. *Journal of Biological Chemistry,* 248**,** 7792-7797.
FONTAYNE, A., DANG, P. M.-C., GOUGEROT-POCIDALO, M.-A. & EL BENNA, J. 2002. Phosphorylation of p47 p hox Sites by PKC α, βII, δ, and ζ: Effect on Binding to p22phox and on NADPH Oxidase Activation. *Biochemistry,* 41**,** 7743-7750.
FORRESTER, S. J., KIKUCHI, D. S., HERNANDES, M. S., XU, Q. & GRIENDLING, K. K. 2018. Reactive Oxygen Species in Metabolic and Inflammatory Signaling. *Circ Res,* 122**,** 877-902.
FRAGKOULI, A. & DOXAKIS, E. 2014. miR-7 and miR-153 protect neurons against MPP^+-induced cell death via upregulation of mTOR pathway. *Front Cell Neurosci,* 8**,** 182.
FRANCO, R., SCHONEVELD, O., GEORGAKILAS, A. G. & PANAYIOTIDIS, M. I. 2008. Oxidative stress, DNA methylation and carcinogenesis. *Cancer letters,* 266**,** 6-11.
FRIEDMAN, J. R., LACKNER, L. L., WEST, M., DIBENEDETTO, J. R., NUNNARI, J. & VOELTZ, G. K. 2011. ER tubules mark sites of mitochondrial division. *Science,* 334**,** 358-62.
FRIEDMAN, J. R. & NUNNARI, J. 2014. Mitochondrial form and function. *Nature,* 505**,** 335-343.
FRÖHLICH, C., GRABIGER, S., SCHWEFEL, D., FAELBER, K., ROSENBAUM, E., MEARS, J., ROCKS, O. & DAUMKE, O. 2013. Structural insights into oligomerization and mitochondrial remodelling of dynamin 1-like protein. *Embo j,* 32**,** 1280-92.
FULTON, D. J. R., LI, X., BORDAN, Z., HAIGH, S., BENTLEY, A., CHEN, F. & BARMAN, S. A. 2017. Reactive Oxygen and Nitrogen Species in the Development of Pulmonary Hypertension. *Antioxidants,* 6**,** 54.
GALLUZZI, L., VITALE, I., AARONSON, S. A., ABRAMS, J. M., ADAM, D., AGOSTINIS, P., ALNEMRI, E. S., ALTUCCI, L., AMELIO, I., ANDREWS, D. W., ANNICCHIARICO-PETRUZZELLI, M., ANTONOV, A. V., ARAMA, E., BAEHRECKE, E. H., BARLEV, N. A., BAZAN, N. G., BERNASSOLA, F., BERTRAND, M. J. M., BIANCHI, K., BLAGOSKLONNY, M. V., BLOMGREN, K., BORNER, C., BOYA, P., BRENNER, C., CAMPANELLA, M., CANDI, E., CARMONA-GUTIERREZ, D., CECCONI, F., CHAN, F. K. M., CHANDEL, N. S., CHENG, E. H., CHIPUK, J. E., CIDLOWSKI, J. A., CIECHANOVER, A., COHEN, G. M., CONRAD, M., CUBILLOS-RUIZ, J. R., CZABOTAR, P. E., D'ANGIOLELLA, V., DAWSON, T. M., DAWSON, V. L., DE LAURENZI, V., DE MARIA, R., DEBATIN, K.-M., DEBERARDINIS, R. J., DESHMUKH, M., DI DANIELE, N., DI VIRGILIO, F., DIXIT, V. M., DIXON, S. J., DUCKETT, C.

S., DYNLACHT, B. D., EL-DEIRY, W. S., ELROD, J. W., FIMIA, G. M., FULDA, S., GARCÍA-SÁEZ, A. J., GARG, A. D., GARRIDO, C., GAVATHIOTIS, E., GOLSTEIN, P., GOTTLIEB, E., GREEN, D. R., GREENE, L. A., GRONEMEYER, H., GROSS, A., HAJNOCZKY, G., HARDWICK, J. M., HARRIS, I. S., HENGARTNER, M. O., HETZ, C., ICHIJO, H., JÄÄTTELÄ, M., JOSEPH, B., JOST, P. J., JUIN, P. P., KAISER, W. J., KARIN, M., KAUFMANN, T., KEPP, O., KIMCHI, A., KITSIS, R. N., KLIONSKY, D. J., KNIGHT, R. A., KUMAR, S., LEE, S. W., LEMASTERS, J. J., LEVINE, B., LINKERMANN, A., LIPTON, S. A., LOCKSHIN, R. A., LÓPEZ-OTÍN, C., LOWE, S. W., LUEDDE, T., LUGLI, E., MACFARLANE, M., MADEO, F., MALEWICZ, M., MALORNI, W., MANIC, G., et al. 2018. Molecular mechanisms of cell death: recommendations of the Nomenclature Committee on Cell Death 2018. *Cell Death & Differentiation,* 25**,** 486-541.

GAO, H.-M., LIU, B., ZHANG, W. & HONG, J.-S. 2003. Critical role of microglial NADPH oxidase-derived free radicals in the *in vitro* MPTP model of Parkinson's disease. *The FASEB Journal,* 17**,** 1-22.

GAO, L. & MANN, G. E. 2009. Vascular NADPH oxidase activation in diabetes: a double-edged sword in redox signalling. *Cardiovasc Res,* 82**,** 9-20.

GE, W., LI, D., GAO, Y. & CAO, X. 2015. The roles of lysosomes in inflammation and autoimmune diseases. *International Reviews of Immunology,* 34**,** 415-431.

GEE, K. R., ZHOU, Z.-L., TON-THAT, D., SENSI, S. & WEISS, J. 2002. Measuring zinc in living cells: A new generation of sensitive and selective fluorescent probes. *Cell calcium,* 31**,** 245-251.

GEORGE, J. M., JIN, H., WOODS, W. S. & CLAYTON, D. F. 1995. Characterization of a novel protein regulated during the critical period for song learning in the zebra finch. *Neuron,* 15**,** 361-72.

GHOSH, S., SULISTYONINGRUM, D. C., GLIER, M. B., VERCHERE, C. B. & DEVLIN, A. M. 2011. Altered glutathione homeostasis in heart augments cardiac lipotoxicity associated with diet-induced obesity in mice. *J Biol Chem,* 286**,** 42483-42493.

GIACHINI, L., FRANCIA, F., VERONESI, G., LEE, D. W., DALDAL, F., HUANG, L. S., BERRY, E. A., COCCO, T., PAPA, S., BOSCHERINI, F. & VENTUROLI, G. 2007. X-Ray absorption studies of Zn^{2+} binding sites in bacterial, avian, and bovine cytochrome *bc1* complexes. *Biophys J,* 93**,** 2934-51.

GIBSON, G. E. 2002. Interactions of oxidative stress with cellular calcium dynamics and glucose metabolism in Alzheimer's disease. *Free Radical Biology and Medicine,* 32**,** 1061-1070.

GITLER, A. D., CHESI, A., GEDDIE, M. L., STRATHEARN, K. E., HAMAMICHI, S., HILL, K. J., CALDWELL, K. A., CALDWELL, G. A., COOPER, A. A., ROCHET, J.-C. & LINDQUIST, S. 2009. Alpha-synuclein is part of a diverse and highly conserved interaction network that includes PARK9 and manganese toxicity. *Nature genetics,* 41**,** 308-315.

GOMEZ-LAZARO, M., BONEKAMP, N. A., GALINDO, M. F., JORDÁN, J. & SCHRADER, M. 2008. 6-Hydroxydopamine (6-OHDA) induces Drp1-dependent mitochondrial fragmentation in SH-SY5Y cells. *Free Radical Biology and Medicine,* 44**,** 1960-1969.

GOMEZ-SUAGA, P., PAILLUSSON, S., STOICA, R., NOBLE, W., HANGER, D. P. & MILLER, C. C. J. 2017. The ER-Mitochondria Tethering Complex VAPB-PTPIP51 Regulates Autophagy. *Curr Biol,* 27**,** 371-385.

GÖRLACH, A., BERTRAM, K., HUDECOVA, S. & KRIZANOVA, O. 2015. Calcium and ROS: A mutual interplay. *Redox biology,* 6**,** 260-271.

GOTTLIEB, E., ARMOUR, S. M., HARRIS, M. H. & THOMPSON, C. B. 2003. Mitochondrial membrane potential regulates matrix configuration and cytochrome *c* release during apoptosis. *Cell Death & Differentiation,* 10**,** 709-717.

GRIPARIC, L., VAN DER WEL, N. N., OROZCO, I. J., PETERS, P. J. & VAN DER BLIEK, A. M. 2004. Loss of the intermembrane space protein Mgm1/OPA1 induces swelling and localized constrictions along the lengths of mitochondria. *J Biol Chem,* 279**,** 18792-8.

GROHM, J., KIM, S., MAMRAK, U., TOBABEN, S., CASSIDY-STONE, A., NUNNARI, J., PLESNILA, N. & CULMSEE, C. 2012. Inhibition of Drp1 provides neuroprotection *in vitro* and *in vivo*. *Cell Death & Differentiation,* 19**,** 1446-1458.

GRÜNEWALD, A., ARNS, B., SEIBLER, P., RAKOVIC, A., MÜNCHAU, A., RAMIREZ, A., SUE, C. M. & KLEIN, C. 2012. ATP13A2 mutations impair mitochondrial function in fibroblasts from patients with Kufor-Rakeb syndrome. *Neurobiol Aging,* 33**,** 1843.e1-7.

GRUPE, M., MYERS, G., PENNER, R. & FLEIG, A. 2010. Activation of store-operated ICRAC by hydrogen peroxide. *Cell calcium,* 48**,** 1-9.

GUDALA, K., KANUKULA, R. & BANSAL, D. 2015. Reduced risk of Parkinson's disease in users of calcium channel blockers: a meta-analysis. *International journal of chronic diseases,* 2015.

GULCIN, İ. & ALWASEL, S. H. 2022. Metal ions, metal chelators and metal chelating assay as antioxidant method. *Processes,* 10**,** 132.

GUO, X., DISATNIK, M.-H., MONBUREAU, M., SHAMLOO, M., MOCHLY-ROSEN, D. & QI, X. 2013. Inhibition of mitochondrial fragmentation diminishes Huntington's disease–associated neurodegeneration. *The Journal of clinical investigation,* 123**,** 5371-5388.

HALLIWELL, B. 1989. Oxidants and the central nervous system: some fundamental questions. Is oxidant damage relevant to Parkinson's disease, Alzheimer's disease, traumatic injury or stroke? *Acta Neurologica Scandinavica,* 80**,** 23-33.

HAN, Y., GOLDBERG, J. M., LIPPARD, S. J. & PALMER, A. E. 2018. Superiority of SpiroZin2 Versus FluoZin-3 for monitoring vesicular Zn^{2+} allows tracking of lysosomal Zn^{2+} pools. *Scientific Reports,* 8**,** 15034.

HANSEN, L. L., IKEDA, Y., OLSEN, G. S., BUSCH, A. K. & MOSTHAF, L. 1999. Insulin Signaling Is Inhibited by Micromolar Concentrations of H_2O_2: EVIDENCE FOR A ROLE OF H_2O_2 IN TUMOR NECROSIS FACTOR α-MEDIATED INSULIN RESISTANCE*. *Journal of Biological Chemistry,* 274**,** 25078-25084.

HARA, Y., WAKAMORI, M., ISHII, M., MAENO, E., NISHIDA, M., YOSHIDA, T., YAMADA, H., SHIMIZU, S., MORI, E., KUDOH, J., SHIMIZU, N., KUROSE, H., OKADA, Y., IMOTO, K. & MORI, Y. 2002. LTRPC2 Ca^{2+}-permeable channel activated by changes in redox status confers susceptibility to cell death. *Mol Cell,* 9**,** 163-73.

HARRIS, J. J. & ATTWELL, D. 2012. The energetics of CNS white matter. *Journal of Neuroscience,* 32**,** 356-371.

HARVEY, R. A. A. F., D.R. 2011. *Biochemistry, Lippincott illustrated reviews*, Philadelphia : Wolters Kluwer Health/Lippincott Williams & Wilkins, ©2011.

HASEGAWA, E., TAKESHIGE, K., OISHI, T., MURAI, Y. & MINAKAMI, S. 1990. 1-Methyl-4-phenylpyridinium MPP^+ induces NADH-dependent superoxide formation and enhances NADH-dependent lipid peroxidation in bovine heart submitochondrial particles. *Biochemical and Biophysical Research Communications,* 170**,** 1049-1055.

HASTINGS, T. G. 2009. The role of dopamine oxidation in mitochondrial dysfunction: implications for Parkinson's disease. *J Bioenerg Biomembr,* 41**,** 469-72.

HEATHER, L. C., CARR, C. A., STUCKEY, D. J., POPE, S., MORTEN, K. J., CARTER, E. E., EDWARDS, L. M. & CLARKE, K. 2010. Critical role of complex III in the early metabolic changes following myocardial infarction. *Cardiovascular research,* 85**,** 127-136.

HECQUET, C. M., AHMMED, G. U. & MALIK, A. B. 2010. TRPM2 channel regulates endothelial barrier function. *Adv Exp Med Biol,* 661**,** 155-67.

HEMPEL, N. & TREBAK, M. 2017. Crosstalk between calcium and reactive oxygen species signaling in cancer. *Cell Calcium,* 63**,** 70-96.

HENGARTNER, M. O. 2000. The biochemistry of apoptosis. *Nature,* 407**,** 770-6.

HERMOSURA, M. C. & GARRUTO, R. M. 2007. TRPM7 and TRPM2—Candidate susceptibility genes for Western Pacific ALS and PD? *Biochimica et Biophysica Acta (BBA)-Molecular Basis of Disease,* 1772**,** 822-835.

HERNANDES, M. S. & BRITTO, L. R. 2012. NADPH oxidase and neurodegeneration. *Curr Neuropharmacol,* 10**,** 321-7.

HIDALGO, C., SÁNCHEZ, G., BARRIENTOS, G. & ARACENA-PARKS, P. 2006. A transverse tubule NADPH oxidase activity stimulates calcium release from isolated triads via ryanodine receptor type 1 S-glutathionylation. *Journal of Biological Chemistry,* 281**,** 26473-26482.
HILL, K., BENHAM, C. D., MCNULTY, S. & RANDALL, A. D. 2004a. Flufenamic acid is a pH-dependent antagonist of TRPM2 channels. *Neuropharmacology,* 47**,** 450-460.
HILL, K., MCNULTY, S. & RANDALL, A. 2004b. Inhibition of TRPM2 channels by the antifungal agents clotrimazole and econazole. *Naunyn-Schmiedeberg's archives of pharmacology,* 370**,** 227-237.
HILL, K., TIGUE, N. J., KELSELL, R. E., BENHAM, C. D., MCNULTY, S., SCHAEFER, M. & RANDALL, A. D. 2006. Characterisation of recombinant rat TRPM2 and a TRPM2-like conductance in cultured rat striatal neurones. *Neuropharmacology,* 50**,** 89-97.
HIROI, T., WAJIMA, T., NEGORO, T., ISHII, M., NAKANO, Y., KIUCHI, Y., MORI, Y. & SHIMIZU, S. 2013. Neutrophil TRPM2 channels are implicated in the exacerbation of myocardial ischaemia/reperfusion injury. *Cardiovascular research,* 97**,** 271-281.
HOCHHAUSER, E., KIVITY, S., OFFEN, D., MAULIK, N., OTANI, H., BARHUM, Y., PANNET, H., SHNEYVAYS, V., SHAINBERG, A., GOLDSHTAUB, V., TOBAR, A. & VIDNE, B. A. 2003. Bax ablation protects against myocardial ischemia-reperfusion injury in transgenic mice. *Am J Physiol Heart Circ Physiol,* 284**,** H2351-9.
HOM, J. R., GEWANDTER, J. S., MICHAEL, L., SHEU, S. S. & YOON, Y. 2007. Thapsigargin induces biphasic fragmentation of mitochondria through calcium-mediated mitochondrial fission and apoptosis. *J Cell Physiol,* 212**,** 498-508.
HOOL, L. C. & CORRY, B. 2007. Redox control of calcium channels: from mechanisms to therapeutic opportunities. *Antioxidants and Redox Signaling,* 9**,** 409-435.
HOUSTIS, N., ROSEN, E. D. & LANDER, E. S. 2006. Reactive oxygen species have a causal role in multiple forms of insulin resistance. *Nature,* 440**,** 944-948.
HÜBNER, C. & HAASE, H. 2021. Interactions of zinc- and redox-signaling pathways. *Redox Biology,* 41**,** 101916.
HULSMANS, M., VAN DOOREN, E. & HOLVOET, P. 2012. Mitochondrial reactive oxygen species and risk of atherosclerosis. *Curr Atheroscler Rep,* 14**,** 264-76.
HUTCHINGS, C. J., COLUSSI, P. & CLARK, T. G. 2019. Ion channels as therapeutic antibody targets. *MAbs,* 11**,** 265-296.
ICHIMIYA, M., CHANG, S. H., LIU, H., BEREZESKY, I. K., TRUMP, B. F. & AMSTAD, P. A. 1998. Effect of Bcl-2 on oxidant-induced cell death and intracellular Ca^{2+} mobilization. *Am J Physiol,* 275**,** C832-9.
ISHIHARA, N., JOFUKU, A., EURA, Y. & MIHARA, K. 2003. Regulation of mitochondrial morphology by membrane potential, and DRP1-dependent division and FZO1-dependent fusion reaction in mammalian cells. *Biochem Biophys Res Commun,* 301**,** 891-8.
ISHIHARA, N., NOMURA, M., JOFUKU, A., KATO, H., SUZUKI, S. O., MASUDA, K., OTERA, H., NAKANISHI, Y., NONAKA, I. & GOTO, Y.-I. 2009. Mitochondrial fission factor Drp1 is essential for embryonic development and synapse formation in mice. *Nature cell biology,* 11**,** 958-966.
ISLAM, M. T. 2017. Oxidative stress and mitochondrial dysfunction-linked neurodegenerative disorders. *Neurological research,* 39**,** 73-82.
IWAI, A., MASLIAH, E., YOSHIMOTO, M., GE, N., FLANAGAN, L., DE SILVA, H. R., KITTEL, A. & SAITOH, T. 1995. The precursor protein of non-Aβ component of Alzheimer's disease amyloid is a presynaptic protein of the central nervous system. *Neuron,* 14**,** 467-475.
JACKSON-LEWIS, V., VILA, M., TIEU, K., TEISMANN, P., VADSETH, C., CHOI, D.-K., ISCHIROPOULOS, H. & PRZEDBORSKI, S. 2002. Blockade of microglial activation is neuroprotective in the 1-methyl-4-phenyl-1, 2, 3, 6-tetrahydropyridine mouse model of Parkinson disease. *Journal of Neuroscience,* 22**,** 1763-1771.

JANG, Y., LEE, M. H., LEE, J., JUNG, J., LEE, S. H., YANG, D. J., KIM, B. W., SON, H., LEE, B., CHANG, S., MORI, Y. & OH, U. 2014. TRPM2 mediates the lysophosphatidic acid-induced neurite retraction in the developing brain. *Pflugers Arch,* 466**,** 1987-98.

JAVITCH, J. A. & SNYDER, S. H. 1984. Uptake of MPP^+ by dopamine neurons explains selectivity of parkinsonism-inducing neurotoxin, MPTP. *Eur J Pharmacol,* 106**,** 455-6.

JENNER, P. 2003. The contribution of the MPTP-treated primate model to the development of new treatment strategies for Parkinson's disease. *Parkinsonism & related disorders,* 9**,** 131-137.

JENNER, P. & OLANOW, C. W. 1998. Understanding cell death in Parkinson's disease. *Annals of neurology,* 44**,** S72-S84.

JIANG, D., SULLIVAN, P. G., SENSI, S. L., STEWARD, O. & WEISS, J. H. 2001. Zn^{2+} induces permeability transition pore opening and release of pro-apoptotic peptides from neuronal mitochondria. *J Biol Chem,* 276**,** 47524-9.

JIANG, L. H., YANG, W., ZOU, J. & BEECH, D. J. 2010. TRPM2 channel properties, functions and therapeutic potentials. *Expert Opin Ther Targets,* 14**,** 973-88.

JIN, C., KUMAR, P., GRACIA-SANCHO, J. & DUFOUR, J.-F. 2021. Calcium transfer between endoplasmic reticulum and mitochondria in liver diseases. *FEBS Letters,* 595**,** 1411-1421.

JOHANSSON, A.-C., APPELQVIST, H., NILSSON, C., KÅGEDAL, K., ROBERG, K. & ÖLLINGER, K. 2010. Regulation of apoptosis-associated lysosomal membrane permeabilization. *Apoptosis,* 15**,** 527-540.

JONCKHEERE, A. I., SMEITINK, J. A. & RODENBURG, R. J. 2012. Mitochondrial ATP synthase: architecture, function and pathology. *J Inherit Metab Dis,* 35**,** 211-25.

KAISER, C. A., MARTIN, K. C., AMON, A., YAFFE, M., PLOEGH, H., BRETSCHER, A., KRIEGER, M., BERK, A. & LODISH, H. 2020. Molecular Cell Biology (International Edition). 9 ed. New York: Macmillan Learning.

KANEKO, S., KAWAKAMI, S., HARA, Y., WAKAMORI, M., ITOH, E., MINAMI, T., TAKADA, Y., KUME, T., KATSUKI, H., MORI, Y. & AKAIKE, A. 2006. A critical role of TRPM2 in neuronal cell death by hydrogen peroxide. *J Pharmacol Sci,* 101**,** 66-76.

KASHIO, M., SOKABE, T., SHINTAKU, K., UEMATSU, T., FUKUTA, N., KOBAYASHI, N., MORI, Y. & TOMINAGA, M. 2012. Redox signal-mediated sensitization of transient receptor potential melastatin 2 (TRPM2) to temperature affects macrophage functions. *Proceedings of the National Academy of Sciences,* 109**,** 6745-6750.

KASHIO, M. & TOMINAGA, M. 2017. The TRPM2 channel: A thermo-sensitive metabolic sensor. *Channels (Austin),* 11**,** 426-433.

KASS, G. E., WRIGHT, J. M., NICOTERA, P. & ORRENIUS, S. 1988. The mechanism of 1-methyl-4-phenyl-1,2,3,6-tetrahydropyridine toxicity: role of intracellular calcium. *Arch Biochem Biophys,* 260**,** 789-97.

KATTOOR, A. J., POTHINENI, N. V. K., PALAGIRI, D. & MEHTA, J. L. 2017. Oxidative Stress in Atherosclerosis. *Curr Atheroscler Rep,* 19**,** 42.

KATZENSCHLAGER, R., HEAD, J., SCHRAG, A., BEN-SHLOMO, Y., EVANS, A., LEES, A. J. & PARKINSON'S DISEASE RESEARCH GROUP OF THE UNITED, K. 2008. Fourteen-year final report of the randomized PDRG-UK trial comparing three initial treatments in PD. *Neurology,* 71**,** 474-480.

KAWAHARA, T., QUINN, M. T. & LAMBETH, J. D. 2007. Molecular evolution of the reactive oxygen-generating NADPH oxidase (Nox/Duox) family of enzymes. *BMC Evol Biol,* 7**,** 109.

KEENEY, M. T., HOFFMAN, E. K., FARMER, K., BODLE, C. R., FAZZARI, M., ZHARIKOV, A., CASTRO, S. L., KOFLER, J. K., CIFUENTES-PAGANO, E., PAGANO, P. J., BURTON, E. A., HASTINGS, T. G., GREENAMYRE, J. T. & DI MAIO, R. 2021. Neuronal NADPH oxidase 2 in Parkinson's disease pathogenesis. *bioRxiv***,** 2021.05.13.443999.

KERR, J. F., WINTERFORD, C. M. & HARMON, B. V. 1994. Apoptosis. Its significance in cancer and cancer therapy. *Cancer,* 73**,** 2013-26.

KHANDRIKA, L., KUMAR, B., KOUL, S., MARONI, P. & KOUL, H. K. 2009. Oxidative stress in prostate cancer. *Cancer Lett,* 282**,** 125-36.
KHORCHID, A. & IKURA, M. 2002. How calpain is activated by calcium. *Nature Structural Biology,* 9**,** 239-241.
KIM, S., WONG, Y. C., GAO, F. & KRAINC, D. 2021. Dysregulation of mitochondria-lysosome contacts by GBA1 dysfunction in dopaminergic neuronal models of Parkinson's disease. *Nat Commun,* 12**,** 1807.
KIM, Y. H., KIM, E. Y., GWAG, B. J., SOHN, S. & KOH, J. Y. 1999. Zinc-induced cortical neuronal death with features of apoptosis and necrosis: mediation by free radicals. *Neuroscience,* 89**,** 175-82.
KINOSHITA, K., TADA, Y., MUROI, Y., UNNO, T. & ISHII, T. 2015. Selective loss of dopaminergic neurons in the substantia nigra pars compacta after systemic administration of MPTP facilitates extinction learning. *Life Sci,* 137**,** 28-36.
KIRKINEZOS, I. G. & MORAES, C. T. 2001. Reactive oxygen species and mitochondrial diseases. *Semin Cell Dev Biol,* 12**,** 449-57.
KITADA, T., ASAKAWA, S., HATTORI, N., MATSUMINE, H., YAMAMURA, Y., MINOSHIMA, S., YOKOCHI, M., MIZUNO, Y. & SHIMIZU, N. 1998. Mutations in the *parkin* gene cause autosomal recessive juvenile parkinsonism. *Nature,* 392**,** 605-8.
KLEIN, A. D. & MAZZULLI, J. R. 2018. Is Parkinson's disease a lysosomal disorder? *Brain,* 141**,** 2255-2262.
KLEIN, J. S. & BJORKMAN, P. J. 2010. Few and far between: how HIV may be evading antibody avidity. *PLoS pathogens,* 6**,** e1000908.
KLEINER, D. 1974. The effect of Zn^{2+} ions on mitochondrial electron transport. *Archives of Biochemistry and Biophysics,* 165**,** 121-125.
KLEINER, D. & VON JAGOW, G. 1972. On the inhibition of mitochondrial electron transport by Zn^{2+} ions. *FEBS letters,* 20**,** 229-232.
KLEOPA, K. A. 2011. Autoimmune channelopathies of the nervous system. *Curr Neuropharmacol,* 9**,** 458-67.
KNARYAN, V. H., SAMANTARAY, S., PARK, S., AZUMA, M., INOUE, J. & BANIK, N. L. 2014. SNJ-1945, a calpain inhibitor, protects SH-SY 5Y cells against MPP^+ and rotenone. *Journal of neurochemistry,* 130**,** 280-290.
KNOWLES, H., LI, Y. & PERRAUD, A.-L. 2013. The TRPM2 ion channel, an oxidative stress and metabolic sensor regulating innate immunity and inflammation. *Immunologic research,* 55**,** 241-248.
KOPIN, I. J. 1987. MPTP: an industrial chemical and contaminant of illicit narcotics stimulates a new era in research on Parkinson's disease. *Environmental health perspectives,* 75**,** 45-51.
KOVALEVICH, J. & LANGFORD, D. 2013. Considerations for the use of SH-SY5Y neuroblastoma cells in neurobiology. *Neuronal cell culture: methods and protocols***,** 9-21.
KOWALTOWSKI, A. J., NAIA-DA-SILVA, E. S., CASTILHO, R. F. & VERCESI, A. E. 1998. Ca^{2+}-stimulated mitochondrial reactive oxygen species generation and permeability transition are inhibited by dibucaine or Mg^{2+}. *Archives of biochemistry and biophysics,* 359**,** 77-81.
KRAFT, R., GRIMM, C., FRENZEL, H. & HARTENECK, C. 2006. Inhibition of TRPM2 cation channels by N-(p-amylcinnamoyl) anthranilic acid. *British journal of pharmacology,* 148**,** 264-273.
KRAFTE, D. 2016. increasingly enticing targets for drug discovery. *Drug Discovery***,** 65.
KRISTAL, B. S., CONWAY, A. D., BROWN, A. M., JAIN, J. C., ULLUCI, P. A., LI, S. W. & BURKE, W. J. 2001. Selective dopaminergic vulnerability: 3, 4-dihydroxyphenylacetaldehyde targets mitochondria. *Free Radical Biology and Medicine,* 30**,** 924-931.
KROEMER, G., GALLUZZI, L., VANDENABEELE, P., ABRAMS, J., ALNEMRI, E. S., BAEHRECKE, E. H., BLAGOSKLONNY, M. V., EL-DEIRY, W. S., GOLSTEIN, P., GREEN, D. R., HENGARTNER, M., KNIGHT, R. A., KUMAR, S., LIPTON, S. A., MALORNI, W., NUÑEZ, G., PETER, M. E.,

TSCHOPP, J., YUAN, J., PIACENTINI, M., ZHIVOTOVSKY, B., MELINO, G. & NOMENCLATURE COMMITTEE ON CELL, D. 2009. Classification of cell death: recommendations of the Nomenclature Committee on Cell Death 2009. *Cell death and differentiation,* 16**,** 3-11.

KRÜGER, R., KUHN, W., MÜLLER, T., WOITALLA, D., GRAEBER, M., KÖSEL, S., PRZUNTEK, H., EPPLEN, J. T., SCHOLS, L. & RIESS, O. 1998. AlaSOPro mutation in the gene encoding α-synuclein in Parkinson's disease. *Nature genetics,* 18**,** 106-108.

KUKIC, I., KELLEHER, S. L. & KISELYOV, K. 2014. Zn^{2+} efflux through lysosomal exocytosis prevents Zn^{2+}-induced toxicity. *Journal of cell science,* 127**,** 3094-3103.

KURZ, T., TERMAN, A., GUSTAFSSON, B. & BRUNK, U. T. 2008a. Lysosomes and oxidative stress in aging and apoptosis. *Biochimica et Biophysica Acta (BBA)-General Subjects,* 1780**,** 1291-1303.

KURZ, T., TERMAN, A., GUSTAFSSON, B. & BRUNK, U. T. 2008b. Lysosomes in iron metabolism, ageing and apoptosis. *Histochemistry and cell biology,* 129**,** 389-406.

LAFERLA, F. M. 2002. Calcium dyshomeostasis and intracellular signalling in Alzheimer's disease. *Nature Reviews Neuroscience,* 3**,** 862-872.

LAN, A. P., CHEN, J., CHAI, Z. F. & HU, Y. 2016. The neurotoxicity of iron, copper and cobalt in Parkinson's disease through ROS-mediated mechanisms. *Biometals,* 29**,** 665-678.

LANGE, I., YAMAMOTO, S., PARTIDA-SANCHEZ, S., MORI, Y., FLEIG, A. & PENNER, R. 2009. TRPM2 functions as a lysosomal Ca^{2+}-release channel in β cells. *Science signaling,* 2**,** ra23-ra23.

LANGSTON, J. W. & BALLARD JR, P. A. 1983. Parkinson's disease in a chemist working with l-methyl-4-phenyl-l, 2, 5, 6-tetrahydropyridine. *New England Journal of Medicine,* 309.

LANGSTON, J. W., BALLARD, P., TETRUD, J. W. & IRWIN, I. 1983. Chronic Parkinsonism in humans due to a product of meperidine-analog synthesis. *Science,* 219**,** 979-980.

LANGSTON, J. W., IRWIN, I. & RICAURTE, G. A. 1987. Neurotoxins, parkinsonism and Parkinson's disease. *Pharmacology & therapeutics,* 32**,** 19-49.

LAUNAY, P., BESSMAN, M. J., KINET, J.-P., SCHARENBERG, A. M., STOKES, A. J., BAGLEY, L. A., PERRAUD, A.-L., ZHU, Q., DUNN, C. A., FLEIG, A., PENNER, R. & SCHMITZ, C. 2001. ADP-ribose gating of the calcium-permeable LTRPC2 channel revealed by Nudix motif homology. *Nature,* 411**,** 595-599.

LEE, A. & GILBERT, R. M. 2016. Epidemiology of Parkinson disease. *Neurologic clinics,* 34**,** 955-965.

LEE, C. R., MACHOLD, R. P., WITKOVSKY, P. & RICE, M. E. 2013. TRPM2 channels are required for NMDA-induced burst firing and contribute to H_2O_2-dependent modulation in substantia nigra pars reticulata GABAergic neurons. *Journal of Neuroscience,* 33**,** 1157-1168.

LEE, D. H., KIM, C. S. & LEE, Y. J. 2011. Astaxanthin protects against MPTP/MPP^+-induced mitochondrial dysfunction and ROS production *in vivo* and *in vitro*. *Food Chem Toxicol,* 49**,** 271-80.

LEE, J. E., WESTRATE, L. M., WU, H., PAGE, C. & VOELTZ, G. K. 2016a. Multiple dynamin family members collaborate to drive mitochondrial division. *Nature,* 540**,** 139-143.

LEE, P.-C., LIU, L.-L., SUN, Y., CHEN, Y.-A., LIU, C.-C., LI, C.-Y., YU, H.-L. & RITZ, B. 2016b. Traffic-related air pollution increased the risk of Parkinson's disease in Taiwan: a nationwide study. *Environment international,* 96**,** 75-81.

LEGROS, F., LOMBÈS, A., FRACHON, P. & ROJO, M. 2002. Mitochondrial fusion in human cells is efficient, requires the inner membrane potential, and is mediated by mitofusins. *Mol Biol Cell,* 13**,** 4343-54.

LEIST, M. & JÄÄTTELÄ, M. 2001. Four deaths and a funeral: from caspases to alternative mechanisms. *Nature reviews Molecular cell biology,* 2**,** 589-598.

LENZEN, S., DRINKGERN, J. & TIEDGE, M. 1996. Low antioxidant enzyme gene expression in pancreatic islets compared with various other mouse tissues. *Free Radic Biol Med,* 20**,** 463-6.

LEWEN, A., MATZ, P. & CHAN, P. H. 2000. Free radical pathways in CNS injury. *Journal of neurotrauma,* 17**,** 871-890.

LI, C., ZHANG, Y., LIU, R. & MAI, Y. 2021. Ramelteon ameliorated 1-methyl-4-phenylpyridinium MPP^+-induced neurotoxicity in neuronal cells in a mitochondrial-dependent pathway. *Bioengineered,* 12**,** 4868-4877.

LI, C. J., FRIEDMAN, D. J., WANG, C., METELEV, V. & PARDEE, A. B. 1995. Induction of apoptosis in uninfected lymphocytes by HIV-1 Tat protein. *Science,* 268**,** 429-431.

LI, F., ABUARAB, N. & SIVAPRASADARAO, A. 2016. Reciprocal regulation of actin cytoskeleton remodelling and cell migration by Ca^{2+} and Zn^{2+}: role of TRPM2 channels. *Journal of cell science,* 129**,** 2016-2029.

LI, F., MUNSEY, T. S. & SIVAPRASADARAO, A. 2017a. TRPM2-mediated rise in mitochondrial Zn^{2+} promotes palmitate-induced mitochondrial fission and pancreatic β-cell death in rodents. *Cell Death & Differentiation,* 24**,** 1999-2012.

LI, X. & JIANG, L. H. 2019. A critical role of the transient receptor potential melastatin 2 channel in a positive feedback mechanism for reactive oxygen species-induced delayed cell death. *J Cell Physiol,* 234**,** 3647-3660.

LI, X., YANG, W. & JIANG, L.-H. 2017b. Alteration in Intracellular Zn^{2+} Homeostasis as a Result of TRPM2 Channel Activation Contributes to ROS-Induced Hippocampal Neuronal Death. *Frontiers in molecular neuroscience,* 10**,** 414-414.

LIN, M. T. & BEAL, M. F. 2006. Mitochondrial dysfunction and oxidative stress in neurodegenerative diseases. *Nature,* 443**,** 787-95.

LINK, T. A. & VON JAGOW, G. 1995. Zinc Ions Inhibit the Qp Center of Bovine Heart Mitochondrial *bc1* Complex by Blocking a Protonatable Group. *Journal of Biological Chemistry,* 270**,** 25001-25006.

LIU, H. Y., GALE, J. R., REYNOLDS, I. J., WEISS, J. H. & AIZENMAN, E. 2021. The Multifaceted Roles of Zinc in Neuronal Mitochondrial Dysfunction. *Biomedicines,* 9.

LIU, L., SUN, X., GUO, Y. & GE, K. 2022. Evodiamine induces ROS-Dependent cytotoxicity in human gastric cancer cells via TRPV1/Ca^{2+} pathway. *Chemico-Biological Interactions,* 351**,** 109756.

LIU, X. & HAJNÓCZKY, G. 2009. Ca^{2+}-dependent regulation of mitochondrial dynamics by the Miro-Milton complex. *Int J Biochem Cell Biol,* 41**,** 1972-6.

LIU, Z., ZHOU, T., ZIEGLER, A. C., DIMITRION, P. & ZUO, L. 2017. Oxidative stress in neurodegenerative diseases: from molecular mechanisms to clinical applications. *Oxidative medicine and cellular longevity,* 2017.

LOCKSHIN, R. A. & ZAKERI, Z. 2004. Apoptosis, autophagy, and more. *International Journal of Biochemistry and Cell Biology,* 36**,** 2405-2419.

LORENZO, O., RAMÍREZ, E., PICATOSTE, B., EGIDO, J. & TUÑÓN, J. 2013. Alteration of Energy Substrates and ROS Production in Diabetic Cardiomyopathy. *Mediators of Inflammation,* 2013**,** 461967.

LORUSSO, M., COCCO, T., SARDANELLI, A. M., MINUTO, M., BONOMI, F. & PAPA, S. 1991. Interaction of Zn^{2+} with the bovine-heart mitochondrial *bc1* complex. *European Journal of Biochemistry,* 197**,** 555-561.

LOTHARIUS, J., DUGAN, L. L. & O'MALLEY, K. L. 1999. Distinct mechanisms underlie neurotoxin-mediated cell death in cultured dopaminergic neurons. *Journal of Neuroscience,* 19**,** 1284-1293.

LU, Q., HARAGOPAL, H., SLEPCHENKO, K. G., STORK, C. & LI, Y. V. 2016. Intracellular zinc distribution in mitochondria, ER and the Golgi apparatus. *International journal of physiology, pathophysiology and pharmacology,* 8**,** 35-43.

LUO, X., LI, M., ZHAN, K., YANG, W., ZHANG, L., WANG, K., YU, P. & ZHANG, L. 2018. Selective inhibition of TRPM2 channel by two novel synthesized ADPR analogues. *Chem Biol Drug Des,* 91**,** 552-566.

MA, T., ZHAO, L., ZHANG, J., TANG, R., WANG, X., LIU, N., ZHANG, Q., WANG, F., LI, M., SHAN, Q., YANG, Y., YIN, Q., YANG, L., GAN, Q. & YANG, C. 2022. A pair of transporters

controls mitochondrial Zn^{2+} levels to maintain mitochondrial homeostasis. *Protein & Cell,* 13**,** 180-202.
MAGNANI, F., NENCI, S., FANANAS, E. M., CECCON, M., ROMERO, E., FRAAIJE, M. W. & MATTEVI, A. 2017. Crystal structures and atomic model of NADPH oxidase. *Proceedings of the National Academy of Sciences,* 114**,** 6764-6769.
MALAIYANDI, L. M., VERGUN, O., DINELEY, K. E. & REYNOLDS, I. J. 2005. Direct visualization of mitochondrial zinc accumulation reveals uniporter-dependent and -independent transport mechanisms. *J Neurochem,* 93**,** 1242-50.
MALKO, P. & JIANG, L.-H. 2020. TRPM2 channel-mediated cell death: An important mechanism linking oxidative stress-inducing pathological factors to associated pathological conditions. *Redox Biology,* 37**,** 101755.
MANCZAK, M., ANEKONDA, T. S., HENSON, E., PARK, B. S., QUINN, J. & REDDY, P. H. 2006. Mitochondria are a direct site of A beta accumulation in Alzheimer's disease neurons: implications for free radical generation and oxidative damage in disease progression. *Hum Mol Genet,* 15**,** 1437-49.
MANCZAK, M., PARK, B. S., JUNG, Y. & REDDY, P. H. 2004. Differential expression of oxidative phosphorylation genes in patients with Alzheimer's disease. *NeuroMolecular Medicine,* 5**,** 147-162.
MANNA, P. T., MUNSEY, T. S., ABUARAB, N., LI, F., ASIPU, A., HOWELL, G., SEDO, A., YANG, W., NAYLOR, J., BEECH, D. J., JIANG, L. H. & SIVAPRASADARAO, A. 2015. TRPM2-mediated intracellular Zn2+ release triggers pancreatic β-cell death. *Biochem J,* 466**,** 537-46.
MARAMBAUD, P., DRESES-WERRINGLOER, U. & VINGTDEUX, V. 2009. Calcium signaling in neurodegeneration. *Molecular Neurodegeneration,* 4**,** 20.
MARAZITA, M. C., DUGOUR, A., MARQUIONI-RAMELLA, M. D., FIGUEROA, J. M. & SUBURO, A. M. 2016. Oxidative stress-induced premature senescence dysregulates VEGF and CFH expression in retinal pigment epithelial cells: implications for age-related macular degeneration. *Redox biology,* 7**,** 78-87.
MARET, W. 2014. Analyzing free zinc ion concentrations in cell biology with fluorescent chelating molecules. *Metallomics,* 7**,** 202-211.
MARREIRO, D. D., CRUZ, K. J., MORAIS, J. B., BESERRA, J. B., SEVERO, J. S. & DE OLIVEIRA, A. R. 2017. Zinc and Oxidative Stress: Current Mechanisms. *Antioxidants (Basel),* 6.
MARSHALL, I. C., BOYFIELD, I. & MCNULTY, S. 2005. Ratiometric Ca^{2+} measurements using the FlexStation® Scanning Fluorometer. *Methods Mol Biol,* 312**,** 119-24.
MARTYN, K. D., FREDERICK, L. M., VON LOEHNEYSEN, K., DINAUER, M. C. & KNAUS, U. G. 2006. Functional analysis of Nox4 reveals unique characteristics compared to other NADPH oxidases. *Cellular signalling,* 18**,** 69-82.
MASSULLO, P., SUMOZA-TOLEDO, A., BHAGAT, H. & PARTIDA-SÁNCHEZ, S. TRPM channels, calcium and redox sensors during innate immune responses. 2006. Elsevier, 654-666.
MATTSON, M. P. 2000. Apoptosis in neurodegenerative disorders. *Nature Reviews Molecular Cell Biology,* 1**,** 120-130.
MAZO, N. A., ECHEVERRIA, V., CABEZAS, R., ÁVILA-RODRIGUEZ, M., TARASOV, V. V., YARLA, N. S., ALIEV, G. & BARRETO, G. E. 2017. Medicinal plants as protective strategies against Parkinson's disease. *Current pharmaceutical design,* 23**,** 4180-4188.
MAZZULLI, J. R., ZUNKE, F., TSUNEMI, T., TOKER, N. J., JEON, S., BURBULLA, L. F., PATNAIK, S., SIDRANSKY, E., MARUGAN, J. J., SUE, C. M. & KRAINC, D. 2016a. Activation of beta-Glucocerebrosidase Reduces Pathological alpha-Synuclein and Restores Lysosomal Function in Parkinson's Patient Midbrain Neurons. *J Neurosci,* 36**,** 7693-706.
MAZZULLI, J. R., ZUNKE, F., TSUNEMI, T., TOKER, N. J., JEON, S., BURBULLA, L. F., PATNAIK, S., SIDRANSKY, E., MARUGAN, J. J., SUE, C. M. & KRAINC, D. 2016b. Activation of β-Glucocerebrosidase Reduces Pathological α-Synuclein and Restores Lysosomal Function in Parkinson's Patient Midbrain Neurons. *J Neurosci,* 36**,** 7693-706.
MCMANUS, M. J., MURPHY, M. P. & FRANKLIN, J. L. 2011. The mitochondria-targeted antioxidant MitoQ prevents loss of spatial memory retention and early

neuropathology in a transgenic mouse model of Alzheimer's disease. *Journal of Neuroscience,* 31**,** 15703-15715.

MEDVEDEVA, Y. V., LIN, B., SHUTTLEWORTH, C. W. & WEISS, J. H. 2009. Intracellular Zn^{2+} Accumulation Contributes to Synaptic Failure, Mitochondrial Depolarization, and Cell Death in an Acute Slice Oxygen–Glucose Deprivation Model of Ischemia. *The Journal of Neuroscience,* 29**,** 1105-1114.

MEISSNER, G. 2010. Regulation of ryanodine receptor ion channels through posttranslational modifications. *Current topics in membranes.* Elsevier.

METODIEWA, D. & KOŚKA, C. 1999. Reactive oxygen species and reactive nitrogen species: relevance to cyto neuro-toxic events and neurologic disorders. An overview. *Neurotoxicity Research,* 1**,** 197-233.

MEUER, K., SUPPANZ, I. E., LINGOR, P., PLANCHAMP, V., GÖRICKE, B., FICHTNER, L., BRAUS, G. H., DIETZ, G. P. H., JAKOBS, S. & BÄHR, M. 2007. Cyclin-dependent kinase 5 is an upstream regulator of mitochondrial fission during neuronal apoptosis. *Cell death and differentiation,* 14**,** 651.

MINKE, B., WU, C.-F. & PAK, W. L. 1975. Induction of photoreceptor voltage noise in the dark in Drosophila mutant. *Nature,* 258**,** 84-87.

MIQUEL, E., CASSINA, A., MARTÍNEZ-PALMA, L., SOUZA, J. M., BOLATTO, C., RODRÍGUEZ-BOTTERO, S., LOGAN, A., SMITH, R. A., MURPHY, M. P. & BARBEITO, L. 2014. Neuroprotective effects of the mitochondria-targeted antioxidant MitoQ in a model of inherited amyotrophic lateral sclerosis. *Free Radical Biology and Medicine,* 70**,** 204-213.

MITROFAN, L. M., CASTELLS, F. B., PELKONEN, J. & MÖNKKÖNEN, J. 2010. Lysosomal-mitochondrial axis in zoledronic acid-induced apoptosis in human follicular lymphoma cells. *J Biol Chem,* 285**,** 1967-79.

MITTAL, S., BJØRNEVIK, K., IM, D. S., FLIERL, A., DONG, X., LOCASCIO, J. J., ABO, K. M., LONG, E., JIN, M. & XU, B. 2017. β2-Adrenoreceptor is a regulator of the α-synuclein gene driving risk of Parkinson's disease. *Science,* 357**,** 891-898.

MIZUNO, Y., SAITOH, T. & SONE, N. 1987. Inhibition of mitochondrial alpha-ketoglutarate dehydrogenase by 1-methyl-4-phenylpyridinium ion. *Biochemical and biophysical research communications,* 143**,** 971-976.

MONTEZANO, A. C., DULAK-LIS, M., TSIROPOULOU, S., HARVEY, A., BRIONES, A. M. & TOUYZ, R. M. 2015. Oxidative stress and human hypertension: vascular mechanisms, biomarkers, and novel therapies. *Can J Cardiol,* 31**,** 631-41.

MOUSTAFA, A. A., CHAKRAVARTHY, S., PHILLIPS, J. R., GUPTA, A., KERI, S., POLNER, B., FRANK, M. J. & JAHANSHAHI, M. 2016. Motor symptoms in Parkinson's disease: A unified framework. *Neuroscience & Biobehavioral Reviews,* 68**,** 727-740.

MURPHY, M. P. 2009a. How mitochondria produce reactive oxygen species. *Biochemical journal,* 417**,** 1-13.

MURPHY, M. P. 2009b. How mitochondria produce reactive oxygen species. *The Biochemical journal,* 417**,** 1-13.

MURPHY, M. P., BAYIR, H., BELOUSOV, V., CHANG, C. J., DAVIES, K. J. A., DAVIES, M. J., DICK, T. P., FINKEL, T., FORMAN, H. J., JANSSEN-HEININGER, Y., GEMS, D., KAGAN, V. E., KALYANARAMAN, B., LARSSON, N.-G., MILNE, G. L., NYSTRÖM, T., POULSEN, H. E., RADI, R., VAN REMMEN, H., SCHUMACKER, P. T., THORNALLEY, P. J., TOYOKUNI, S., WINTERBOURN, C. C., YIN, H. & HALLIWELL, B. 2022. Guidelines for measuring reactive oxygen species and oxidative damage in cells and *in vivo*. *Nature Metabolism,* 4**,** 651-662.

MURPHY, M. P. & HARTLEY, R. C. 2018. Mitochondria as a therapeutic target for common pathologies. *Nature Reviews Drug Discovery,* 17**,** 865-886.

NAGAKANNAN, P., IQBAL, M. A., YEUNG, A., THLIVERIS, J. A., RASTEGAR, M., GHAVAMI, S. & EFTEKHARPOUR, E. 2016. Perturbation of redox balance after thioredoxin reductase deficiency interrupts autophagy-lysosomal degradation pathway and enhances cell

death in nutritionally stressed SH-SY5Y cells. *Free Radical Biology and Medicine,* 101**,** 53-70.

NAGAKANNAN, P., TABESHMEHR, P. & EFTEKHARPOUR, E. 2020. Oxidative damage of lysosomes in regulated cell death systems: Pathophysiology and pharmacologic interventions. *Free Radic Biol Med,* 157**,** 94-127.

NAGAMINE, K., KUDOH, J., MINOSHIMA, S., KAWASAKI, K., ASAKAWA, S., ITO, F. & SHIMIZU, N. 1998. Molecular cloning of a novel putative Ca^{2+} channel protein (TRPC7) highly expressed in brain. *Genomics,* 54**,** 124-31.

NAGANO, T., MIZUNO, M., MORITA, K. & NAWA, H. 2015. Pathological implications of oxidative stress in patients and animal models with schizophrenia: the role of epidermal growth factor receptor signaling. *Neurotoxin Modeling of Brain Disorders—Life-long Outcomes in Behavioral Teratology***,** 429-446.

NAKAMURA, K., BINDOKAS, V. P., MARKS, J. D., WRIGHT, D. A., FRIM, D. M., MILLER, R. J. & KANG, U. J. 2000. The selective toxicity of 1-methyl-4-phenylpyridinium to dopaminergic neurons: the role of mitochondrial complex I and reactive oxygen species revisited. *Mol Pharmacol,* 58**,** 271-8.

NAKAMURA, K., NEMANI, V. M., AZARBAL, F., SKIBINSKI, G., LEVY, J. M., EGAMI, K., MUNISHKINA, L., ZHANG, J., GARDNER, B. & WAKABAYASHI, J. 2011. Direct Membrane Association Drives Mitochondrial Fission by the Parkinson Disease-associated Protein α-Synuclein*♦. *Journal of Biological Chemistry,* 286**,** 20710-20726.

NAOI, M. & MARUYAMA, W. 1999. Cell death of dopamine neurons in aging and Parkinson's disease. *Mechanisms of ageing and development,* 111**,** 175-188.

NAZIROGLU, M. 2011. TRPM2 cation channels, oxidative stress and neurological diseases: where are we now? *Neurochem Res,* 36**,** 355-66.

NEGRE-SALVAYRE, A., GUERBY, P., GAYRAL, S., LAFFARGUE, M. & SALVAYRE, R. 2020. Role of reactive oxygen species in atherosclerosis: Lessons from murine genetic models. *Free Radic Biol Med,* 149**,** 8-22.

NEILL, S., DESIKAN, R. & HANCOCK, J. 2002. Hydrogen peroxide signalling. *Current opinion in plant biology,* 5**,** 388-395.

NEVES CARVALHO, A., FIRUZI, O., JOAO GAMA, M., VAN HORSSEN, J. & SASO, L. 2017. Oxidative stress and antioxidants in neurological diseases: is there still hope? *Current drug targets,* 18**,** 705-718.

NICHOLLS, D. G. 2005. Mitochondria and calcium signaling. *Cell Calcium,* 38**,** 311-317.

NICKEL, A., KOHLHAAS, M. & MAACK, C. 2014. Mitochondrial reactive oxygen species production and elimination. *J Mol Cell Cardiol,* 73**,** 26-33.

NILIUS, B. 2007. TRP channels in disease. *Biochimica et Biophysica Acta (BBA) - Molecular Basis of Disease,* 1772**,** 805-812.

NIMMO, J. T., VERMA, A., DODART, J.-C., WANG, C. Y., SAVISTCHENKO, J., MELKI, R., CARARE, R. O. & NICOLL, J. A. R. 2020. Novel antibodies detect additional α-synuclein pathology in synucleinopathies: potential development for immunotherapy. *Alzheimer's Research & Therapy,* 12**,** 159.

NOJIRI, H., SHIMIZU, T., FUNAKOSHI, M., YAMAGUCHI, O., ZHOU, H., KAWAKAMI, S., OHTA, Y., SAMI, M., TACHIBANA, T., ISHIKAWA, H., KUROSAWA, H., KAHN, R. C., OTSU, K. & SHIRASAWA, T. 2006. Oxidative stress causes heart failure with impaired mitochondrial respiration. *J Biol Chem,* 281**,** 33789-801.

NORBERG, E., ORRENIUS, S. & ZHIVOTOVSKY, B. 2010. Mitochondrial regulation of cell death: processing of apoptosis-inducing factor (AIF). *Biochem Biophys Res Commun,* 396**,** 95-100.

NÚÑEZ, M. T., URRUTIA, P., MENA, N., AGUIRRE, P., TAPIA, V. & SALAZAR, J. 2012. Iron toxicity in neurodegeneration. *Biometals,* 25**,** 761-76.

OLAH, M. E., JACKSON, M. F., LI, H., PEREZ, Y., SUN, H. S., KIYONAKA, S., MORI, Y., TYMIANSKI, M. & MACDONALD, J. F. 2009. Ca^{2+}-dependent induction of TRPM2 currents in hippocampal neurons. *The Journal of physiology,* 587**,** 965-979.

ONA, V. O., LI, M., VONSATTEL, J. P. G., ANDREWS, L. J., KHAN, S. Q., CHUNG, W. M., FREY, A. S., MENON, A. S., LI, X.-J. & STIEG, P. E. 1999. Inhibition of caspase-1 slows disease progression in a mouse model of Huntington's disease. *Nature,* 399**,** 263-267.

ONG, S.-B., KWEK, X.-Y., KATWADI, K., HERNANDEZ-RESENDIZ, S., CRESPO-AVILAN, G. E., ISMAIL, N. I., LIN, Y.-H., YAP, E. P., LIM, S.-Y. & JA, K. M. M. 2019. Targeting mitochondrial fission using Mdivi-1 in a clinically relevant large animal model of acute myocardial infarction: a pilot study. *International journal of molecular sciences,* 20**,** 3972.

ONYANGO, I. G., KHAN, S. M. & BENNETT JR, J. P. 2017. Mitochondria in the pathophysiology of Alzheimer's and Parkinson's diseases. *Front Biosci (Landmark Ed),* 22**,** 854-872.

ORR, A. L., VARGAS, L., TURK, C. N., BAATEN, J. E., MATZEN, J. T., DARDOV, V. J., ATTLE, S. J., LI, J., QUACKENBUSH, D. C. & GONCALVES, R. L. 2015. Suppressors of superoxide production from mitochondrial complex III. *Nature chemical biology,* 11**,** 834-836.

ORRENIUS, S., GOGVADZE, V. & ZHIVOTOVSKY, B. 2015. Calcium and mitochondria in the regulation of cell death. *Biochemical and Biophysical Research Communications,* 460**,** 72-81.

ORRENIUS, S., ZHIVOTOVSKY, B. & NICOTERA, P. 2003. Regulation of cell death: the calcium–apoptosis link. *Nature reviews Molecular cell biology,* 4**,** 552-565.

OWSIANIK, G., TALAVERA, K., VOETS, T. & NILIUS, B. 2006. Permeation and selectivity of TRP channels. *Annu Rev Physiol,* 68**,** 685-717.

PAN, X., LIU, J., NGUYEN, T., LIU, C., SUN, J., TENG, Y., FERGUSSON, M. M., ROVIRA, I. I., ALLEN, M. & SPRINGER, D. A. 2013. The physiological role of mitochondrial calcium revealed by mice lacking the mitochondrial calcium uniporter. *Nature cell biology,* 15**,** 1464-1472.

PANDYA, J. D., NUKALA, V. N. & SULLIVAN, P. G. 2013. Concentration dependent effect of calcium on brain mitochondrial bioenergetics and oxidative stress parameters. *Frontiers in neuroenergetics,* 5**,** 10.

PARK, J.-S., KOENTJORO, B., VEIVERS, D., MACKAY-SIM, A. & SUE, C. M. 2014. Parkinson's disease-associated human ATP13A2 (*PARK9*) deficiency causes zinc dyshomeostasis and mitochondrial dysfunction. *Human molecular genetics,* 23**,** 2802-2815.

PARK, J., CHOI, H., MIN, J. S., PARK, S. J., KIM, J. H., PARK, H. J., KIM, B., CHAE, J. I., YIM, M. & LEE, D. S. 2013. Mitochondrial dynamics modulate the expression of pro-inflammatory mediators in microglial cells. *Journal of neurochemistry,* 127**,** 221-232.

PARK, J. S., MEHTA, P., COOPER, A. A., VEIVERS, D., HEIMBACH, A., STILLER, B., KUBISCH, C., FUNG, V. S., KRAINC, D., MACKAY-SIM, A. & SUE, C. M. 2011. Pathogenic effects of novel mutations in the P-type ATPase ATP13A2 (*PARK9*) causing Kufor-Rakeb syndrome, a form of early-onset parkinsonism. *Hum Mutat,* 32**,** 956-64.

PARK, L., ZHOU, P., PITSTICK, R., CAPONE, C., ANRATHER, J., NORRIS, E. H., YOUNKIN, L., YOUNKIN, S., CARLSON, G. & MCEWEN, B. S. 2008. Nox2-derived radicals contribute to neurovascular and behavioral dysfunction in mice overexpressing the amyloid precursor protein. *Proceedings of the National Academy of Sciences,* 105**,** 1347-1352.

PERIER, C., TIEU, K., GUÉGAN, C., CASPERSEN, C., JACKSON-LEWIS, V., CARELLI, V., MARTINUZZI, A., HIRANO, M., PRZEDBORSKI, S. & VILA, M. 2005. Complex I deficiency primes Bax-dependent neuronal apoptosis through mitochondrial oxidative damage. *Proceedings of the National Academy of Sciences,* 102**,** 19126-19131.

PERRAUD, A.-L., FLEIG, A., DUNN, C. A., BAGLEY, L. A., LAUNAY, P., SCHMITZ, C., STOKES, A. J., ZHU, Q., BESSMAN, M. J. & PENNER, R. 2001. ADP-ribose gating of the calcium-permeable LTRPC2 channel revealed by Nudix motif homology. *Nature,* 411**,** 595-599.

PERRAUD, A.-L., SHEN, B., DUNN, C. A., RIPPE, K., SMITH, M. K., BESSMAN, M. J., STODDARD, B. L. & SCHARENBERG, A. M. 2003. NUDT9, a member of the Nudix hydrolase family, is an evolutionarily conserved mitochondrial ADP-ribose pyrophosphatase. *Journal of Biological Chemistry,* 278**,** 1794-1801.

PFEIFFER, R. F. 2016. Non-motor symptoms in Parkinson's disease. *Parkinsonism & Related Disorders,* 22**,** S119-S122.

PICARD, M., WHITE, K. & TURNBULL, D. M. 2013. Mitochondrial morphology, topology, and membrane interactions in skeletal muscle: a quantitative three-dimensional electron microscopy study. *J Appl Physiol (1985),* 114**,** 161-71.

PINTON, P., GIORGI, C., SIVIERO, R., ZECCHINI, E. & RIZZUTO, R. 2008. Calcium and apoptosis: ER-mitochondria Ca^{2+} transfer in the control of apoptosis. *Oncogene,* 27**,** 6407-18.

PLOTNIKOV, E. Y., VASILEVA, A. K., ARKHANGELSKAYA, A. A., PEVZNER, I. B., SKULACHEV, V. P. & ZOROV, D. B. 2008. Interrelations of mitochondrial fragmentation and cell death under ischemia/reoxygenation and UV-irradiation: protective effects of SkQ1, lithium ions and insulin. *FEBS Lett,* 582**,** 3117-24.

POLYMEROPOULOS, M. H., LAVEDAN, C., LEROY, E., IDE, S. E., DEHEJIA, A., DUTRA, A., PIKE, B., ROOT, H., RUBENSTEIN, J., BOYER, R., STENROOS, E. S., CHANDRASEKHARAPPA, S., ATHANASSIADOU, A., PAPAPETROPOULOS, T., JOHNSON, W. G., LAZZARINI, A. M., DUVOISIN, R. C., DI IORIO, G., GOLBE, L. I. & NUSSBAUM, R. L. 1997. Mutation in the alpha-synuclein gene identified in families with Parkinson's disease. *Science,* 276**,** 2045-7.

POOT, M. & PIERCE, R. H. 1999. Detection of changes in mitochondrial function during apoptosis by simultaneous staining with multiple fluorescent dyes and correlated multiparameter flow cytometry. *Cytometry: The Journal of the International Society for Analytical Cytology,* 35**,** 311-317.

PORTBURY, S. D. & ADLARD, P. A. 2017. Zinc Signal in Brain Diseases. *Int J Mol Sci,* 18.

PRATT, E. P. S., DAMON, L. J., ANSON, K. J. & PALMER, A. E. 2021. Tools and techniques for illuminating the cell biology of zinc. *Biochimica et Biophysica Acta (BBA) - Molecular Cell Research,* 1868**,** 118865.

PRICE, K. L. & LUMMIS, S. C. R. 2005. FlexStation examination of 5-HT3 receptor function using Ca^{2+}- and membrane potential-sensitive dyes: Advantages and potential problems. *Journal of Neuroscience Methods,* 149**,** 172-177.

PRZEDBORSKI, S., TIEU, K., PERIER, C. & VILA, M. 2004. MPTP as a Mitochondrial Neurotoxic Model of Parkinson's Disease. *Journal of Bioenergetics and Biomembranes,* 36**,** 375-379.

QIAN, C. & COLVIN, R. A. 2016. Zinc flexes its muscle: Correcting a novel analysis of calcium for zinc interference uncovers a method to measure zinc. *J Gen Physiol,* 147**,** 95-102.

RADA, B. & LETO, T. L. 2008. Oxidative innate immune defenses by Nox/Duox family NADPH oxidases. *Trends in Innate Immunity,* 15**,** 164-187.

RAHIMMI, A., KHOSROBAKHSH, F., IZADPANAH, E., MOLOUDI, M. R. & HASSANZADEH, K. 2015. N-acetylcysteine prevents rotenone-induced Parkinson's disease in rat: An investigation into the interaction of parkin and Drp1 proteins. *Brain research bulletin,* 113**,** 34-40.

RAMSAY, R. R., KRUEGER, M. J., YOUNGSTER, S. K., GLUCK, M. R., CASIDA, J. E. & SINGER, T. P. 1991. Interaction of 1-methyl-4-phenylpyridinium ion MPP^+ and its analogs with the rotenone/piericidin binding site of NADH dehydrogenase. *Journal of neurochemistry,* 56**,** 1184-1190.

RAPPOLD, P. M., CUI, M., GRIMA, J. C., FAN, R. Z., DE MESY-BENTLEY, K. L., CHEN, L., ZHUANG, X., BOWERS, W. J. & TIEU, K. 2014. Drp1 inhibition attenuates neurotoxicity and dopamine release deficits *in vivo*. *Nature communications,* 5**,** 5244.

RASTOGI, R., GENG, X., LI, F. & DING, Y. 2017. NOX Activation by Subunit Interaction and Underlying Mechanisms in Disease. *Frontiers in Cellular Neuroscience,* 10.

RECZEK, C. R. & CHANDEL, N. S. 2015. ROS-dependent signal transduction. *Curr Opin Cell Biol,* 33**,** 8-13.

REDDY, P. H., MANCZAK, M. & YIN, X. 2017. Mitochondria-division inhibitor 1 protects against amyloid-β induced mitochondrial fragmentation and synaptic damage in Alzheimer's Disease. *Journal of Alzheimer's Disease,* 58**,** 147-162.

REICHERT, J. M., ROSENSWEIG, C. J., FADEN, L. B. & DEWITZ, M. C. 2005. Monoclonal antibody successes in the clinic. *Nature Biotechnology,* 23**,** 1073-1078.

REPNIK, U. & TURK, B. 2010. Lysosomal–mitochondrial cross-talk during cell death. *Mitochondrion,* 10**,** 662-669.

REY, F., CIFUENTES, M., KIARASH, A., QUINN, M. & PAGANO, P. 2001. Novel competitive inhibitor of NADPH oxidase assembly attenuates vascular O_2 and systolic blood pressure in mice. *Circulation research,* 89**,** 408-414.

RIZZUTO, R., GIORGI, C., ROMAGNOLI, A. & PINTON, P. 2008. Ca^{2+} signaling, mitochondria and cell death. *Current molecular medicine,* 8**,** 119-130.

RIZZUTO, R., PINTON, P., CARRINGTON, W., FAY, F. S., FOGARTY, K. E., LIFSHITZ, L. M., TUFT, R. A. & POZZAN, T. 1998. Close contacts with the endoplasmic reticulum as determinants of mitochondrial Ca^{2+} responses. *Science,* 280**,** 1763-6.

ROBERTS, C. K. & SINDHU, K. K. 2009. Oxidative stress and metabolic syndrome. *Life Sci,* 84**,** 705-12.

RODRIGUEZ-OROZ, M. C., JAHANSHAHI, M., KRACK, P., LITVAN, I., MACIAS, R., BEZARD, E. & OBESO, J. A. 2009. Initial clinical manifestations of Parkinson's disease: features and pathophysiological mechanisms. *The Lancet Neurology,* 8**,** 1128-1139.

RODRIGUEZ, G. E. V. & TORRIGLIA, A. 2013. Calpain 1 induce lysosomal permeabilization by cleavage of lysosomal associated membrane protein 2. *Biochimica et Biophysica Acta (BBA)-Molecular Cell Research,* 1833**,** 2244-2253.

ROH, HYUN C., COLLIER, S., GUTHRIE, J., ROBERTSON, J. D. & KORNFELD, K. 2012. Lysosome-Related Organelles in Intestinal Cells: Are a Zinc Storage Site. elegans. *Cell Metabolism,* 15**,** 88-99.

ROLLEMA, H., KUHR, W. G., KRANENBORG, G., DE VRIES, J. & VAN DEN BERG, C. 1988. MPP^+-induced efflux of dopamine and lactate from rat striatum have similar time courses as shown by *in vivo* brain dialysis. *Journal of Pharmacology and Experimental Therapeutics,* 245**,** 858-866.

ROSENBAUM, T. 2015. Activators of TRPM2: Getting it right. *The Journal of general physiology,* 145**,** 485-487.

ROSSI, F. & ZATTI, M. 1964. Biochemical aspects of phagocytosis in polymorphonuclear leucocytes. NADH and NADPH oxidation by the granules of resting and phagocytizing cells. *Experientia,* 20**,** 21-3.

RU, X., ZHENG, C., ZHAO, Q., LAN, H.-Y., HUANG, Y., WAN, S., MORI, Y. & YAO, X. 2015. Transient receptor potential channel M2 contributes to neointimal hyperplasia in vascular walls. *Biochimica et Biophysica Acta (BBA) - Molecular Basis of Disease,* 1852**,** 1360-1371.

SABHARWAL, S. S. & SCHUMACKER, P. T. 2014. Mitochondrial ROS in cancer: initiators, amplifiers or an Achilles' heel? *Nat Rev Cancer,* 14**,** 709-21.

ŞAHIN, M. & AYBEK, E. 2019. Jamovi: an easy to use statistical software for the social scientists. *International Journal of Assessment Tools in Education,* 6**,** 670-692.

SAHOO, S., MEIJLES, D. N. & PAGANO, P. J. 2016. NADPH oxidases: key modulators in aging and age-related cardiovascular diseases? *Clin Sci (Lond),* 130**,** 317-35.

SANCHEZ-RAMOS, J., BARRETT, J. N., GOLDSTEIN, M., WEINER, W. J. & HEFTI, F. 1986. 1-Methyl-4-phenylpyridinium (MPP^+) but not 1-methyl-4-phenyl-1, 2, 3, 6-tetrahydropyridine (MPTP) selectively destroys dopaminergic neurons in cultures of dissociated rat mesencephalic neurons. *Neuroscience letters,* 72**,** 215-220.

SANO, Y., INAMURA, K., MIYAKE, A., MOCHIZUKI, S., YOKOI, H., MATSUSHIME, H. & FURUICHI, K. 2001. Immunocyte Ca^{2+} influx system mediated by LTRPC2. *Science,* 293**,** 1327-1330.

SANTEL, A. & FRANK, S. 2008. Shaping mitochondria: The complex posttranslational regulation of the mitochondrial fission protein DRP1. *IUBMB Life,* 60**,** 448-55.

SANTEL, A. & FULLER, M. T. 2001. Control of mitochondrial morphology by a human mitofusin. *J Cell Sci,* 114**,** 867-74.

SANTIAGO, M., GRANERO, L., MACHADO, A. & CANO, J. 1995. Complex I inhibitor effect on the nigral and striatal release of dopamine in the presence and absence of nomifensine. *Eur J Pharmacol,* 280**,** 251-6.

SANTO-DOMINGO, J. & DEMAUREX, N. 2010. Calcium uptake mechanisms of mitochondria. *Biochimica et Biophysica Acta (BBA) - Bioenergetics,* 1797**,** 907-912.

SANTOS, R., URSU, O., GAULTON, A., BENTO, A. P., DONADI, R. S., BOLOGA, C. G., KARLSSON, A., AL-LAZIKANI, B., HERSEY, A., OPREA, T. I. & OVERINGTON, J. P. 2017. A comprehensive map of molecular drug targets. *Nat Rev Drug Discov,* 16**,** 19-34.

SAVICA, R., GROSSARDT, B. R., ROCCA, W. A. & BOWER, J. H. 2018. Parkinson disease with and without Dementia: A prevalence study and future projections. *Mov Disord,* 33**,** 537-543.

SAWA, A., WIEGAND, G. W., COOPER, J., MARGOLIS, R. L., SHARP, A. H., LAWLER, J. F., JR., GREENAMYRE, J. T., SNYDER, S. H. & ROSS, C. A. 1999. Increased apoptosis of Huntington disease lymphoblasts associated with repeat length-dependent mitochondrial depolarization. *Nat Med,* 5**,** 1194-8.

SCHAPIRA, A. H. V., MANN, V. M., COOPER, J. M., KRIGE, D., JENNER, P. J. & MARSDEN, C. D. 1992. Mitochondrial function in Parkinson's disease. *Annals of Neurology: Official Journal of the American Neurological Association and the Child Neurology Society,* 32**,** S116-S124.

SCHENTEN, V., BRÉCHARD, S., MELCHIOR, C., PLANÇON, S., SALSMANN, A. & TSCHIRHART, E. 2008. Ca^{2+}-dependent regulation of NOX2 activity via MRP proteins in HL-60 granulocytes. *Calcium Binding Proteins,* 3**,** 25-30.

SCHENTEN, V., BRÉCHARD, S., PLANÇON, S., MELCHIOR, C., FRIPPIAT, J.-P. & TSCHIRHART, E. J. 2010. iPLA2, a novel determinant in Ca^{2+}- and phosphorylation-dependent S100A8/A9 regulated NOX2 activity. *Biochimica et Biophysica Acta (BBA) - Molecular Cell Research,* 1803**,** 840-847.

SCHWARTZ, A., PALTI, Y. & MEIRI, H. 1990. Structural and developmental differences between three types of Na channels in dorsal root ganglion cells of newborn rats. *J Membr Biol,* 116**,** 117-28.

SEIFERT, E. 2014. OriginPro 9.1: scientific data analysis and graphing software-software review. *Journal of Chemical Information and Modeling,* 54**,** 1552.

SENSI, S. L., PAOLETTI, P., BUSH, A. I. & SEKLER, I. 2009. Zinc in the physiology and pathology of the CNS. *Nat Rev Neurosci,* 10**,** 780-91.

SHARMA, N., KAPOOR, M. & NEHRU, B. 2016. Apocyanin, NADPH oxidase inhibitor prevents lipopolysaccharide induced α-synuclein aggregation and ameliorates motor function deficits in rats: possible role of biochemical and inflammatory alterations. *Behavioural brain research,* 296**,** 177-190.

SHARPLEY, M. S. & HIRST, J. 2006. The Inhibition of Mitochondrial Complex I (NADH:Ubiquinone Oxidoreductase) by Zn^{2+}. *Journal of Biological Chemistry,* 281**,** 34803-34809.

SHEEHAN, J. P., SWERDLOW, R. H., MILLER, S. W., DAVIS, R. E., PARKS, J. K., PARKER, W. D. & TUTTLE, J. B. 1997. Calcium homeostasis and reactive oxygen species production in cells transformed by mitochondria from individuals with sporadic Alzheimer's disease. *Journal of Neuroscience,* 17**,** 4612-4622.

SHELINE, C. T., ZHU, J., ZHANG, W., SHI, C. & CAI, A. L. 2013. Mitochondrial inhibitor models of Huntington's disease and Parkinson's disease induce zinc accumulation and are attenuated by inhibition of zinc neurotoxicity *in vitro* or *in vivo*. *Neurodegener Dis,* 11**,** 49-58.

SHEN, B. W., PERRAUD, A.-L., SCHARENBERG, A. & STODDARD, B. L. 2003. The crystal structure and mutational analysis of human NUDT9. *Journal of molecular biology,* 332**,** 385-398.

SHIMIZU, N., ASAKAWA, S., MINOSHIMA, S., KITADA, T., HATTORI, N., MATSUMINE, H., YOKOCHI, M., YAMAMURA, Y. & MIZUNO, Y. 2000. *PARKIN* as a pathogenic gene for autosomal recessive juvenile parkinsonism. *J Neural Transm Suppl***,** 19-30.

SIDRANSKY, E. & LOPEZ, G. 2012. The link between the *GBA* gene and parkinsonism. *The Lancet Neurology,* 11**,** 986-998.
SIKLÓS, L., ENGELHARDT, J., HARATI, Y., SMITH, R. G., JOÓ, F. & APPEL, S. H. 1996. Ultrastructural evidence for altered calcium in motor nerve terminals in amyotrophc lateral sclerosis. *Annals of neurology,* 39**,** 203-216.
SIKORA, J. & OUAGAZZAL, A.-M. 2021. Synaptic Zinc: An Emerging Player in Parkinson's Disease. *International Journal of Molecular Sciences,* 22**,** 4724.
SINGH, N., PILLAY, V. & CHOONARA, Y. E. 2007. Advances in the treatment of Parkinson's disease. *Progress in Neurobiology,* 81**,** 29-44.
SKULACHEV, V., CHISTYAKOV, V., JASAITIS, A. & SMIRNOVA, E. 1967. Inhibition of the respiratory chain by zinc ions. *Biochemical and biophysical research communications,* 26**,** 1-6.
SLUPE, A. M., MERRILL, R. A., FLIPPO, K. H., LOBAS, M. A., HOUTMAN, J. C. & STRACK, S. 2013. A calcineurin docking motif (LXVP) in dynamin-related protein 1 contributes to mitochondrial fragmentation and ischemic neuronal injury. *J Biol Chem,* 288**,** 12353-65.
SMEYNE, R. J. & JACKSON-LEWIS, V. 2005. The MPTP model of Parkinson's disease. *Brain Res Mol Brain Res,* 134**,** 57-66.
SMIRNOVA, E., GRIPARIC, L., SHURLAND, D. L. & VAN DER BLIEK, A. M. 2001. Dynamin-related protein Drp1 is required for mitochondrial division in mammalian cells. *Molecular biology of the cell,* 12**,** 2245-2256.
SNOW, B. J., ROLFE, F. L., LOCKHART, M. M., FRAMPTON, C. M., O'SULLIVAN, J. D., FUNG, V., SMITH, R. A., MURPHY, M. P., TAYLOR, K. M. & GROUP, P. S. 2010. A double-blind, placebo-controlled study to assess the mitochondria-targeted antioxidant MitoQ as a disease-modifying therapy in Parkinson's disease. *Movement Disorders,* 25**,** 1670-1674.
SONG, K., WANG, H., KAMM, G. B., POHLE, J., DE CASTRO REIS, F., HEPPENSTALL, P., WENDE, H. & SIEMENS, J. 2016. The TRPM2 channel is a hypothalamic heat sensor that limits fever and can drive hypothermia. *Science,* 353**,** 1393-1398.
SORCE, S. & KRAUSE, K.-H. 2009. NOX enzymes in the central nervous system: from signaling to disease. *Antioxidants & redox signaling,* 11**,** 2481-2504.
SOSA, V., MOLINÉ, T., SOMOZA, R., PACIUCCI, R., KONDOH, H. & LLEONART, M. E. 2013. Oxidative stress and cancer: an overview. *Ageing research reviews,* 12**,** 376-390.
SRINIVASAN, S., GUHA, M., KASHINA, A. & AVADHANI, N. G. 2017. Mitochondrial dysfunction and mitochondrial dynamics-The cancer connection. *Biochim Biophys Acta Bioenerg,* 1858**,** 602-614.
SUMOZA-TOLEDO, A. & PENNER, R. 2011. TRPM2: a multifunctional ion channel for calcium signalling. *The Journal of physiology,* 589**,** 1515-1525.
SUN, H. & LI, M. 2013. Antibody therapeutics targeting ion channels: are we there yet? *Acta Pharmacologica Sinica,* 34**,** 199-204.
SUN, L., YAU, H. Y., WONG, W. Y., LI, R. A., HUANG, Y. & YAO, X. 2012. Role of TRPM2 in H_2O_2-induced cell apoptosis in endothelial cells. *PLoS One,* 7**,** e43186.
SUN, Y., SUKUMARAN, P., SCHAAR, A. & SINGH, B. B. 2015. TRPM7 and its role in neurodegenerative diseases. *Channels,* 9**,** 253-261.
SUN, Y., SUKUMARAN, P., SELVARAJ, S., CILZ, N. I., SCHAAR, A., LEI, S. & SINGH, B. B. 2018. TRPM2 Promotes Neurotoxin MPP^+/MPTP-Induced Cell Death. *Mol Neurobiol,* 55**,** 409-420.
SURMEIER, D. J., GUZMAN, J. N., SANCHEZ-PADILLA, J. & SCHUMACKER, P. T. 2011. The role of calcium and mitochondrial oxidant stress in the loss of substantia nigra pars compacta dopaminergic neurons in Parkinson's disease. *Neuroscience,* 198**,** 221-231.
SULZER, D. & SURMEIER, D. J. 2013. Neuronal vulnerability, pathogenesis, and Parkinson's disease. *Movement Disorders,* 28**,** 715-724.
SUZUKI, K., MIZUNO, Y., YAMAUCHI, Y., NAGATSU, T. & MITSUO, Y. 1992. Selective inhibition of complex I by N-methylisoquinolinium ion and N-methyl-1, 2, 3, 4-

tetrahydroisoquinoline in isolated mitochondria prepared from mouse brain. *Journal of the neurological sciences,* 109**,** 219-223.

SUZUKI, Y. J., FORMAN, H. J. & SEVANIAN, A. 1997. Oxidants as stimulators of signal transduction. *Free Radical Biology and Medicine,* 22**,** 269-285.

SWERDLOW, R. H., PARKS, J. K., MILLER, S. W., DAVIS, R. E., TUTTLE, J. B., TRIMMER, P. A., SHEEHAN, J. P., BENNETT JR, J. P. & PARKER JR, W. D. 1996. Origin and functional consequences of the complex I defect in Parkinson's disease. *Annals of Neurology: Official Journal of the American Neurological Association and the Child Neurology Society,* 40**,** 663-671.

SZABADKAI, G., SIMONI, A. M., BIANCHI, K., DE STEFANI, D., LEO, S., WIECKOWSKI, M. R. & RIZZUTO, R. 2006. Mitochondrial dynamics and Ca^{2+} signaling. *Biochimica et Biophysica Acta (BBA) - Molecular Cell Research,* 1763**,** 442-449.

TAKAHASHI, N., KOZAI, D., KOBAYASHI, R., EBERT, M. & MORI, Y. 2011. Roles of TRPM2 in oxidative stress. *Cell Calcium,* 50**,** 279-87.

TAN, J., ZHANG, T., JIANG, L., CHI, J., HU, D., PAN, Q., WANG, D. & ZHANG, Z. 2011. Regulation of intracellular manganese homeostasis by Kufor-Rakeb syndrome-associated ATP13A2 protein. *The Journal of biological chemistry,* 286**,** 29654-29662.

TAN, S., SCHUBERT, D. & MAHER, P. 2001. Oxytosis: a novel form of programmed cell death. *Current topics in medicinal chemistry,* 1**,** 497-506.

TARAFDAR, A. & PULA, G. 2018. The Role of NADPH Oxidases and Oxidative Stress in Neurodegenerative Disorders. *International Journal of Molecular Sciences,* 19**,** 3824.

TILOKANI, L., NAGASHIMA, S., PAUPE, V. & PRUDENT, J. 2018. Mitochondrial dynamics: overview of molecular mechanisms. *Essays Biochem,* 62**,** 341-360.

TOGASHI, K., HARA, Y., TOMINAGA, T., HIGASHI, T., KONISHI, Y., MORI, Y. & TOMINAGA, M. 2006. TRPM2 activation by cyclic ADP-ribose at body temperature is involved in insulin secretion. *Embo j,* 25**,** 1804-15.

TOGASHI, K., INADA, H. & TOMINAGA, M. 2008. Inhibition of the transient receptor potential cation channel TRPM2 by 2-aminoethoxydiphenyl borate (2-APB). *British journal of pharmacology,* 153**,** 1324-1330.

TRETTER, L., SIPOS, I. & ADAM-VIZI, V. 2004. Initiation of neuronal damage by complex I deficiency and oxidative stress in Parkinson's disease. *Neurochemical research,* 29**,** 569-577.

TSIEN, R. Y. 1980. New calcium indicators and buffers with high selectivity against magnesium and protons: design, synthesis, and properties of prototype structures. *Biochemistry,* 19**,** 2396-2404.

TSUNEMI, T. & KRAINC, D. 2013. Zn^{2+} dyshomeostasis caused by loss of ATP13A2/PARK9 leads to lysosomal dysfunction and alpha-synuclein accumulation. *Human Molecular Genetics,* 23**,** 2791-2801.

TSUTSUI, H., KINUGAWA, S. & MATSUSHIMA, S. 2011. Oxidative stress and heart failure. *Am J Physiol Heart Circ Physiol,* 301**,** H2181-90.

TU, B. P. & WEISSMAN, J. S. 2004. Oxidative protein folding in eukaryotes: mechanisms and consequences. *J Cell Biol,* 164**,** 341-6.

TWELVES, D., PERKINS, K. S. M. & COUNSELL, C. 2003. Systematic review of incidence studies of Parkinson's disease. *Movement disorders: official journal of the Movement Disorder Society,* 18**,** 19-31.

TYMIANSKI, M., WALLACE, M. C., SPIGELMAN, I., UNO, M., CARLEN, P. L., TATOR, C. H. & CHARLTON, M. P. 1993. Cell-permeant Ca^{2+} chelators reduce early excitotoxic and ischemic neuronal injury *in vitro* and *in vivo*. *Neuron,* 11**,** 221-35.

UDAYAR, V., CHEN, Y., SIDRANSKY, E. & JAGASIA, R. 2022. Lysosomal dysfunction in neurodegeneration: emerging concepts and methods. *Trends Neurosci,* 45**,** 184-199.

VAIDYA, B. & SHARMA, S. S. 2020. Transient Receptor Potential Channels as an Emerging Target for the Treatment of Parkinson's Disease: An Insight Into Role of Pharmacological Interventions. *Front Cell Dev Biol,* 8**,** 584513.

VALENTE, E. M., ABOU-SLEIMAN, P. M., CAPUTO, V., MUQIT, M. M., HARVEY, K., GISPERT, S., ALI, Z., DEL TURCO, D., BENTIVOGLIO, A. R., HEALY, D. G., ALBANESE, A., NUSSBAUM, R., GONZÁLEZ-MALDONADO, R., DELLER, T., SALVI, S., CORTELLI, P., GILKS, W. P., LATCHMAN, D. S., HARVEY, R. J., DALLAPICCOLA, B., AUBURGER, G. & WOOD, N. W. 2004. Hereditary early-onset Parkinson's disease caused by mutations in *PINK1*. *Science,* 304**,** 1158-60.

VALENTIN, F., BUEB, J.-L., CAPDEVILLE-ATKINSON, C. & TSCHIRHART, E. 2001. Rac-1-mediated O_2 secretion requires Ca^{2+} influx in neutrophil-like HL-60 cells. *Cell Calcium,* 29**,** 409-415.

VAN LAAR, V. S. & BERMAN, S. B. 2009. Mitochondrial dynamics in Parkinson's disease. *Experimental neurology,* 218**,** 247-256.

VENDROV, A. E., STEVENSON, M. D., ALAHARI, S., PAN, H., WICKLINE, S. A., MADAMANCHI, N. R. & RUNGE, M. S. 2017. Attenuated Superoxide Dismutase 2 Activity Induces Atherosclerotic Plaque Instability During Aging in Hyperlipidemic Mice. *Journal of the American Heart Association,* 6**,** e006775.

VERMA, S., QUILLINAN, N., YANG, Y. F., NAKAYAMA, S., CHENG, J., KELLEY, M. H. & HERSON, P. S. 2012. TRPM2 channel activation following *in vitro* ischemia contributes to male hippocampal cell death. *Neurosci Lett,* 530**,** 41-6.

VILA, M. & PRZEDBORSKI, S. 2003. Targeting programmed cell death in neurodegenerative diseases. *Nature Reviews Neuroscience,* 4**,** 365-375.

WAI, T. & LANGER, T. 2016. Mitochondrial Dynamics and Metabolic Regulation. *Trends Endocrinol Metab,* 27**,** 105-117.

WAKABAYASHI, J., ZHANG, Z., WAKABAYASHI, N., TAMURA, Y., FUKAYA, M., KENSLER, T. W., IIJIMA, M. & SESAKI, H. 2009. The dynamin-related GTPase Drp1 is required for embryonic and brain development in mice. *J Cell Biol,* 186**,** 805-16.

WAKABAYASHI, K., TANJI, K., ODAGIRI, S., MIKI, Y., MORI, F. & TAKAHASHI, H. 2013. The Lewy body in Parkinson's disease and related neurodegenerative disorders. *Mol Neurobiol,* 47**,** 495-508.

WANG, F., GOMEZ-SINTES, R. & BOYA, P. 2018a. Lysosomal membrane permeabilization and cell death. *Traffic,* 19**,** 918-931.

WANG, L., FU, T.-M., ZHOU, Y., XIA, S., GREKA, A. & WU, H. 2018b. Structures and gating mechanism of human TRPM2. *Science,* 362**,** eaav4809.

WANG, Q., HUANG, L. & YUE, J. 2017. Oxidative stress activates the TRPM2-Ca^{2+}-CaMKII-ROS signaling loop to induce cell death in cancer cells. *Biochimica et Biophysica Acta (BBA) - Molecular Cell Research,* 1864**,** 957-967.

WANG, Q., LIU, N., NI, Y.-S., YANG, J.-M., MA, L., LAN, X.-B., WU, J., NIU, J.-G. & YU, J.-Q. 2021. TRPM2 in ischemic stroke: Structure, molecular mechanisms, and drug intervention. *Channels,* 15**,** 136-154.

WANG, Q. & LIU, Y. 2022. Cryptotanshinone ameliorates MPP^+-induced oxidative stress and apoptosis of SH-SY5Y neuroblastoma cells: the role of STAT3 in Parkinson's disease. *Metabolic Brain Disease,* 37**,** 1477-1485.

WANG, Q., TOMPKINS, K. D., SIMONYI, A., KORTHUIS, R. J., SUN, A. Y. & SUN, G. Y. 2006. Apocynin protects against global cerebral ischemia–reperfusion-induced oxidative stress and injury in the gerbil hippocampus. *Brain research,* 1090**,** 182-189.

WANG, T., PEI, Z., ZHANG, W., LIU, B., LANGENBACH, R., LEE, C., WILSON, B., REECE, J. M., MILLER, D. S. & HONG, J. S. 2005. MPP^+-induced COX-2 activation and subsequent dopaminergic neurodegeneration. *The FASEB journal,* 19**,** 1134-1136.

WANG, X., PETRIE, T. G., LIU, Y., LIU, J., FUJIOKA, H. & ZHU, X. 2012. Parkinson's disease-associated *DJ-1* mutations impair mitochondrial dynamics and cause mitochondrial dysfunction. *J Neurochem,* 121**,** 830-9.

WANG, X., SU, B., LIU, W., HE, X., GAO, Y., CASTELLANI, R. J., PERRY, G., SMITH, M. A. & ZHU, X. 2011. DLP1-dependent mitochondrial fragmentation mediates 1-methyl-4-

phenylpyridinium toxicity in neurons: implications for Parkinson's disease. *Aging Cell,* 10**,** 807-23.
WHONE, A. 2022. Monoclonal Antibody Therapy in Parkinson's Disease—The End? : Mass Medical Soc.
WILLIAMS, H. C. & GRIENDLING, K. K. 2007. NADPH oxidase inhibitors: new antihypertensive agents? *Journal of cardiovascular pharmacology,* 50**,** 9-16.
WONG, H.-S., MONTERNIER, P.-A. & BRAND, M. D. 2019a. S1QELs suppress mitochondrial superoxide/hydrogen peroxide production from site *IQ* without inhibiting reverse electron flow through Complex I. *Free Radical Biology and Medicine,* 143**,** 545-559.
WONG, Y. C., KIM, S., PENG, W. & KRAINC, D. 2019b. Regulation and Function of Mitochondria-Lysosome Membrane Contact Sites in Cellular Homeostasis. *Trends Cell Biol,* 29**,** 500-513.
WONG, Y. C., YSSELSTEIN, D. & KRAINC, D. 2018. Mitochondria-lysosome contacts regulate mitochondrial fission via RAB7 GTP hydrolysis. *Nature,* 554**,** 382-386.
WU, D.-C., TEISMANN, P., TIEU, K., VILA, M., JACKSON-LEWIS, V., ISCHIROPOULOS, H. & PRZEDBORSKI, S. 2003. NADPH oxidase mediates oxidative stress in the 1-methyl-4-phenyl-1, 2, 3, 6-tetrahydropyridine model of Parkinson's disease. *Proceedings of the National Academy of Sciences,* 100**,** 6145-6150.
WU, D. C., RÉ, D. B., NAGAI, M., ISCHIROPOULOS, H. & PRZEDBORSKI, S. 2006. The inflammatory NADPH oxidase enzyme modulates motor neuron degeneration in amyotrophic lateral sclerosis mice. *Proc Natl Acad Sci U S A,* 103**,** 12132-7.
XIA, S., WANG, L., FU, T. M. & WU, H. 2019. Mechanism of TRPM2 channel gating revealed by cryo-EM. *Febs j,* 286**,** 3333-3339.
XICOY, H., WIERINGA, B. & MARTENS, G. J. 2017. The SH-SY5Y cell line in Parkinson's disease research: a systematic review. *Molecular neurodegeneration,* 12**,** 1-11.
XIE, H.-R., HU, L.-S. & LI, G.-Y. 2010a. SH-SY5Y human neuroblastoma cell line: *in vitro* cell model of dopaminergic neurons in Parkinson's disease. *Chinese medical journal,* 123**,** 1086-1092.
XIE, Y. F., MACDONALD, J. F. & JACKSON, M. F. 2010b. TRPM2, calcium and neurodegenerative diseases. *Int J Physiol Pathophysiol Pharmacol,* 2**,** 95-103.
XU, S. Z., ZENG, F., LEI, M., LI, J., GAO, B., XIONG, C., SIVAPRASADARAO, A. & BEECH, D. J. 2005. Generation of functional ion-channel tools by E3 targeting. *Nat Biotechnol,* 23**,** 1289-93.
YAMAMOTO, S. & SHIMIZU, S. 2016. Targeting TRPM2 in ROS-Coupled Diseases. *Pharmaceuticals (Basel),* 9.
YAMAMOTO, S., WAJIMA, T., HARA, Y., NISHIDA, M. & MORI, Y. 2007. Transient receptor potential channels in Alzheimer's disease. *Biochim Biophys Acta,* 1772**,** 958-67.
YAN, L.-J. 2014. Positive oxidative stress in aging and aging-related disease tolerance. *Redox Biology,* 2**,** 165-169.
YANG, S. J., YANG, J. W., NA, J. M., HA, J. S., CHOI, S. Y. & CHO, S. W. 2018. 3-(Naphthalen-2-yl(propoxy)methyl)azetidine hydrochloride attenuates MPP^+-induced cytotoxicity by regulating oxidative stress and mitochondrial dysfunction in SH-SY5Y cells. *BMB Rep,* 51**,** 590-595.
YE, M., YANG, W., AINSCOUGH, J. F., HU, X. P., LI, X., SEDO, A., ZHANG, X. H., ZHANG, X., CHEN, Z., LI, X. M., BEECH, D. J., SIVAPRASADARAO, A., LUO, J. H. & JIANG, L. H. 2014. TRPM2 channel deficiency prevents delayed cytosolic Zn^{2+} accumulation and CA1 pyramidal neuronal death after transient global ischemia. *Cell Death Dis,* 5**,** e1541.
YI, F., HE, X. & WANG, D. 2013. Lycopene protects against MPP^+-induced cytotoxicity by maintaining mitochondrial function in SH-SY5Y cells. *Neurochem Res,* 38**,** 1747-57.
YILDIZHAN, K., ÇINAR, R. & NAZIROĞLU, M. 2022. The involvement of TRPM2 on the MPP^+-induced oxidative neurotoxicity and apoptosis in hippocampal neurons from neonatal mice: protective role of resveratrol. *Neurological Research,* 44**,** 636-644.

YILDIZHAN, K. & NAZIROĞLU, M. 2020. Glutathione Depletion and Parkinsonian Neurotoxin MPP^+-Induced TRPM2 Channel Activation Play Central Roles in Oxidative Cytotoxicity and Inflammation in Microglia. *Mol Neurobiol,* 57**,** 3508-3525.

YOSHIKAWA, T. 1993. Free radicals and their scavengers in Parkinson's disease. *European neurology,* 33**,** 60-68.

YSSELSTEIN, D., NGUYEN, M., YOUNG, T. J., SEVERINO, A., SCHWAKE, M., MERCHANT, K. & KRAINC, D. 2019a. LRRK2 kinase activity regulates lysosomal glucocerebrosidase in neurons derived from Parkinson's disease patients. *Nature communications,* 10**,** 1-9.

YSSELSTEIN, D., SHULMAN, J. M. & KRAINC, D. 2019b. Emerging links between pediatric lysosomal storage diseases and adult parkinsonism. *Movement Disorders,* 34**,** 614-624.

YUAN, H., ZHANG, X., HUANG, X., LU, Y., TANG, W., MAN, Y., WANG, S., XI, J. & LI, J. 2010. NADPH oxidase 2-derived reactive oxygen species mediate FFAs-induced dysfunction and apoptosis of β-cells via JNK, p38 MAPK and p53 pathways. *PLoS One,* 5**,** e15726.

ZAIDI, A. 2010. Plasma membrane Ca^{2+}-ATPases: Targets of oxidative stress in brain aging and neurodegeneration. *World journal of biological chemistry,* 1**,** 271.

ZARRANZ, J. J., ALEGRE, J., GÓMEZ-ESTEBAN, J. C., LEZCANO, E., ROS, R., AMPUERO, I., VIDAL, L., HOENICKA, J., RODRIGUEZ, O. & ATARÉS, B. 2004. The new mutation, E46K, of α-synuclein causes parkinson and Lewy body dementia. *Annals of Neurology: Official Journal of the American Neurological Association and the Child Neurology Society,* 55**,** 164-173.

ZAWADA, W. M., BANNINGER, G. P., THORNTON, J., MARRIOTT, B., CANTU, D., RACHUBINSKI, A. L., DAS, M., GRIFFIN, W. S. & JONES, S. M. 2011. Generation of reactive oxygen species in 1-methyl-4-phenylpyridinium MPP^+ treated dopaminergic neurons occurs as an NADPH oxidase-dependent two-wave cascade. *J Neuroinflammation,* 8**,** 129.

ZAWADA, W. M., MRAK, R. E., BIEDERMANN, J., PALMER, Q. D., GENTLEMAN, S. M., ABOUD, O. & GRIFFIN, W. S. 2015. Loss of angiotensin II receptor expression in dopamine neurons in Parkinson's disease correlates with pathological progression and is accompanied by increases in Nox4- and 8-OH guanosine-related nucleic acid oxidation and caspase-3 activation. *Acta Neuropathol Commun,* 3**,** 9.

ZENG, X., SIKKA, S. C., HUANG, L., SUN, C., XU, C., JIA, D., ABDEL-MAGEED, A. B., POTTLE, J. E., TAYLOR, J. T. & LI, M. 2010a. Novel role for the transient receptor potential channel TRPM2 in prostate cancer cell proliferation. *Prostate cancer and prostatic diseases,* 13**,** 195-201.

ZENG, X., SIKKA, S. C., HUANG, L., SUN, C., XU, C., JIA, D., ABDEL-MAGEED, A. B., POTTLE, J. E., TAYLOR, J. T. & LI, M. 2010b. Novel role for the transient receptor potential channel TRPM2 in prostate cancer cell proliferation. *Prostate Cancer Prostatic Dis,* 13**,** 195-201.

ZHANG, W., WANG, T., QIN, L., GAO, H. M., WILSON, B., ALI, S. F., ZHANG, W., HONG, J. S. & LIU, B. 2004. Neuroprotective effect of dextromethorphan in the MPTP Parkinson's disease model: role of NADPH oxidase. *The FASEB journal,* 18**,** 589-591.

ZHANG, Y., YING, F., TIAN, X., LEI, Z., LI, X., LO, C.-Y., LI, J., JIANG, L. & YAO, X. 2022. TRPM2 Promotes Atherosclerotic Progression in a Mouse Model of Atherosclerosis. *Cells,* 11**,** 1423.

ZHANG, Z., ZHANG, W., JUNG, D. Y., KO, H. J., LEE, Y., FRIEDLINE, R. H., LEE, E., JUN, J., MA, Z., KIM, F., TSITSILIANOS, N., CHAPMAN, K., MORRISON, A., COOPER, M. P., MILLER, B. A. & KIM, J. K. 2012. TRPM2 Ca^{2+} channel regulates energy balance and glucose metabolism. *Am J Physiol Endocrinol Metab,* 302**,** E807-16.

ZHAO, M., ANTUNES, F., EATON, J. W. & BRUNK, U. T. 2003. Lysosomal enzymes promote mitochondrial oxidant production, cytochrome *c* release and apoptosis. *European Journal of Biochemistry,* 270**,** 3778-3786.

ZHAO, R. Z., JIANG, S., ZHANG, L. & YU, Z. B. 2019. Mitochondrial electron transport chain, ROS generation and uncoupling (Review). *Int J Mol Med,* 44**,** 3-15.

ZHOU, B. Y., MA, W. & HUANG, X. Y. 1998. Specific antibodies to the external vestibule of voltage-gated potassium channels block current. *J Gen Physiol,* 111**,** 555-63.

ZHU, J. & CHU, C. T. 2010. Mitochondrial dysfunction in Parkinson's disease. *J Alzheimers Dis,* 20 Suppl 2**,** S325-34.

ZHU, M., ZHOU, M., SHI, Y. & LI, W.-W. 2012. Effects of echinacoside on MPP^+-induced mitochondrial fragmentation, mitophagy and cell apoptosis in SH-SY5Y cells. *Zhong xi yi jie he xue bao = Journal of Chinese integrative medicine,* 10**,** 1427-1432.

ZIMA, A. V. & BLATTER, L. A. 2006. Redox regulation of cardiac calcium channels and transporters. *Cardiovascular research,* 71**,** 310-321.

ZOROV, D. B., JUHASZOVA, M. & SOLLOTT, S. J. 2014. Mitochondrial reactive oxygen species (ROS) and ROS-induced ROS release. *Physiological reviews,* 94**,** 909-950.